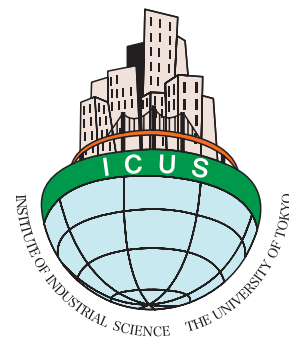
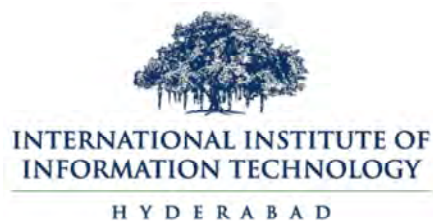


USMCA 2018

17th International Symposium on
NEW TECHNOLOGIES FOR URBAN SAFETY OF MEGA CITIES IN ASIA

12-14 December 2018

International Institute of Information Technology, Hyderabad, India



USMCA 2018

KEYNOTES

TOWARDS DISASTER RESILIENT SOCIETY IN URBAN AREA

K. MEGURO¹

¹ Director/Professor, ICUS, IIS, the University of Tokyo, Japan, meguro@iis.u-tokyo.ac.jp

Keywords: Disaster Resilience, Disaster Imagination, Comprehensive Disaster Management System, Comprehensive Disaster Management Matrix

1. INTRODUCTION

Why do many people live in disaster-prone areas? The reason is that hazards bringing damage to a community can be benefitted at the same time if the community has high disaster resilience. Then, how can we build a disaster resilient community? The most important thing is to improve disaster imagination capability of the people from decision making a level to the general public. This is because people cannot prepare and respond well to an unimaginable situation.

In my lecture, I will introduce what disaster imagination is and a concept of "comprehensive disaster management system" which can effectively improve the disaster resilience of society in the urban area.

2. COMPREHENSIVE DISASTER MANAGEMENT SYSTEM

In order to minimize the negative impact due to hazard, I have proposed "Comprehensive disaster management system" as shown in Figure 1. The system is down into seven stages, starting with "damage mitigation", "preparedness", and "prediction and early warning" as pre-disaster countermeasures and "damage assessment", "disaster response", "recovery", and "build back better" in the post-disaster countermeasures. Information and communication play an essential role in all seven stages.

By combining these seven measures properly considering natural and social characteristics of the target region, the negative impact due to hazard can be minimized. Moreover, considering disaster as an important opportunity to solve potential problems of the affected region, we can create a better region and community than before.

3. PROCEDURE FOR DISASTER RESILIENT SOCIETY

3.1 Comprehensive Disaster Management Matrix

At all seven stages of disaster management, it is necessary to understand that the government is not the only actor in disaster management but the collaboration among local community and the residents' participation is vital. Therefore, there are three forms of effort described as public support (PS), mutual assistance (MA) and self-help effort (SE). Although there are differences in weights in each countermeasure, there are structural (H: Hard) and non-structural (S: Soft) measures. Further, a comprehensive disaster management matrix (CDMM) shown in Figure 2 can be prepared. A CDMM is composed of two kinds of the matrix; ideal situation matrix (ISM) and current situation matrix (CSM). The ISM, which includes all measures by three efforts, should be prepared

by filling up all columns with possible countermeasures and it should be standardized by specialists in the field of disaster management. The CSM, which shows all countermeasures already implemented in the target area, should be prepared by local governmental officials.

After the 1995 Kobe Earthquake, the importance of MA and SE has been recognized, however during the 2011 Great East Japan Earthquake and Tsunami Disaster, the involvement of private companies in MA and SE was recognized as important, collaborating with the local people in activities such as rescue and firefighting.

The countermeasure by three types of effort is often complementary to each other and it must be well-balanced. In other words, if the work is concentrated in PS part, the cost could be enormous while, if each individual puts an effort while cooperating with each other, it could be much more effective with lesser cost. PS should promote MA and SE rather than enhancing people's dependency on PS. In order to realize this situation, the disclosure of

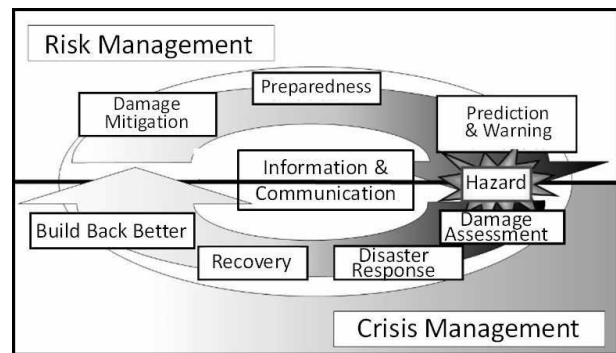


Figure 1: Comprehensive disaster management system

↓ Event

	Damage Mitigation	Preparedness	Prediction and Early Warning	Damage Assessment	Emergency Disaster Response	Recovery and Reconstruction
SE (Self-help Effort)	H					
	S					
MA (Mutual Assistance)	H					
	S					
PS (Public Support)	H					
	S					

Two kinds of matrices :
Ideal and current situations

Figure 2: Comprehensive disaster management matrix

information about the disaster risk to the general public becomes important.

3.2 Promotion method for comprehensive disaster management

In order to efficiently conduct disaster management countermeasures, it is essential to make appropriate combinations of countermeasures at seven stages by three efforts considering regional characteristics, target disaster types, current disaster preparedness, available time and budget at each stage. Figure 3 shows the specific procedure to find appropriate combinations of countermeasures. The difference between ISM and CSM indicates the action item matrix (AIM) that shows the necessary countermeasures have to be taken. To all countermeasures (action items) written in the AIM, information on responsible section/person, necessary time and budget, and the effect when completed will be added. This approach could be applied to all possible hazards in the target area. However, the contents will differ based on the type of hazard, and thus Disaster Management Matrix for each type of disaster needs to be created, and all necessary disaster matrices should be integrated as shown in Figure 4.

Subjected to the available time and budget, it is possible to determine realistically, the countermeasures that can achieve maximum effect within the given condition. By practicing this process over several years,

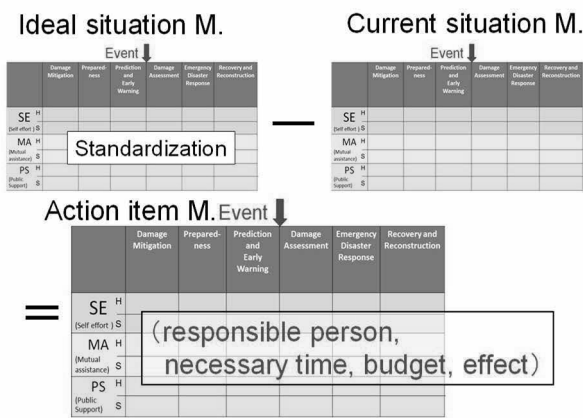


Figure 3: How to obtain action item matrix

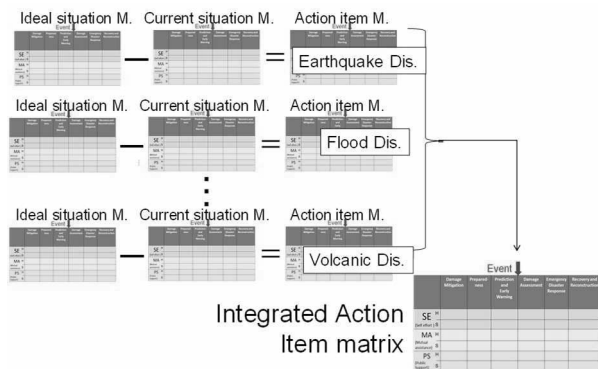


Figure 4: How to obtain integrated action item matrix

PDCA management cycle is put into practice and effective progress management is realized as shown in Figure 5.

3.3 Relation among national, prefectural and municipality governments

According to the Disaster Countermeasures Basic Act in Japan, the mayor of the municipality, such as city, town, and the village has responsibility for disaster operation and response. Therefore, when they discuss the disaster management plan and countermeasures, they tend to consider hazard, which can be managed by themselves, as a scenario hazard. Then, it becomes very difficult, or practically impossible for them to consider a much larger-scale disaster that they could not manage. This situation was observed in many affected areas due to the 2011 Great East Japan Earthquake and Tsunami. One of the main causes was that they put only themselves, the municipality level government, in disaster countermeasure matrix when they discussed disaster management plan and countermeasures as shown in the upper sub figure in Figure 6. In order to solve this problem, they should put prefectural and national governments besides them in PS column as shown in the bottom subfigure in Figure 6.

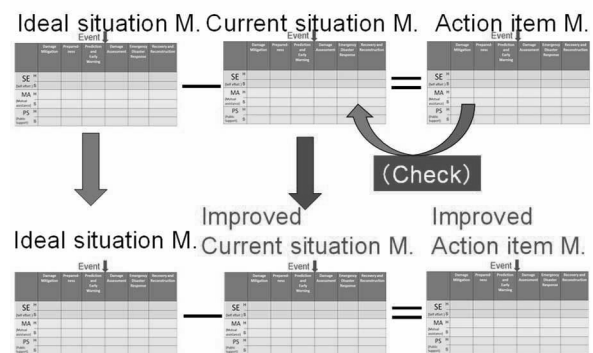
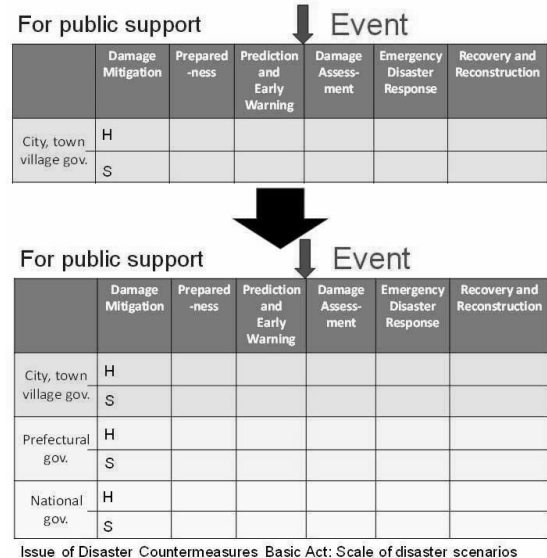


Figure 5: PDCA cycle for implementation of efficient countermeasures



Issue of Disaster Countermeasures Basic Act: Scale of disaster scenarios

Figure 6: Relations among national, prefectural and municipality governments

Then, they can write what they cannot do in the columns of prefectural and national governments. By combining these seven measures properly considering natural and social characteristics of the target region, the negative impact due to hazard can be minimized. Moreover, also, considering disaster as an important opportunity to solve potential problems of the affected region, we can create a better region and community than before. From the prefectural governments' viewpoint, they considered that what they should do in case of the disaster was waiting for requests from municipalities and respond them. However, prefectural governments can recognize that when the affected municipalities cannot respond because of too large disaster for the municipalities to manage, without waiting for requests from the affected municipalities, prefectural governments should visit the affected sites and carry out operation and response of disaster instead of the affected municipalities. Moreover, when three-level governments fill all countermeasure items together that each government should do in the bottom matrix as shown in Figure 6, they can recognize spontaneously, the duplications and gap among different governments.

4. MISUNDERSTANDING ON DISASTER MANAGEMENT

As mentioned in chapter 3, the negative impact due to hazard can be minimized, and potential problems can also be solved by a proper combination of countermeasures at all seven stages. However, in many countries, especially in developing countries, disaster response is considered the most important measures of disaster management. Major activities of the disaster response stage are a supply of emergency goods, such as food, water, clothes, and search and rescue operation.

In case of the 1995 Kobe earthquake disaster in Japan, approximately 40,000 to 45,000 people were trapped under the damaged structures just after to a couple of days. Among them, as Figure 7 shows that 8,000 people were taken out by public sectors and local communities did 27,000. Survivor's ratio of the people taken out by local communities was much higher than that by public sectors. Figure 8 shows the number and survivor's ratio of people taken out under damaged structures by public sectors in Kobe City. The total number was getting bigger in the second, and the third days, however, survivor's ratio was getting smaller from approximately 70 % in the first day, 20% in the second day, and 10 % in the third day. Beside Japanese public sectors' teams, international search and rescue teams with rescue dogs visited from Switzerland, France, and the UK and they could rescue no survivor and find 13 dead bodies. In the case of the 2015 Gorkha Earthquake disaster in Nepal, over 9,000 people were killed mainly by the collapse of vulnerable structures. While over 22,000 people were rescued from under the damaged structures. Among them, over 80 % of them were saved by local communities but only less than 0.1 % were rescued by international search and rescue teams. Figure 10 shows 21 earthquakes causing over 5,000 fatalities in the last 100 years. Among 21 events, collapse of weak masonry structures was the primary cause of fatalities in 17 ones. There are three major reasons why

much more people are killed and injured by the collapse of masonry structures compared with another type of structures. First, as failure behavior of weak masonry structure is brittle, people cannot have time for their evacuation. Second, the size of bricks is small as a structural material and members, they fill the survival space during the collapse, and it becomes difficult to have survival space under the damaged structure. Third, heavy dust is generated during the collapse, and people cannot get fresh air under such condition.

Based on these facts, we should recognize that strengthening of weak structures is the most important measures for earthquake disaster reduction in the future.

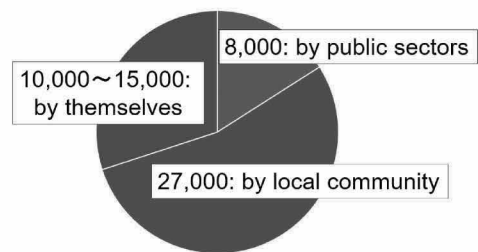


Figure 7: Who took out the people from under the damaged structures (1995 Kobe earthquake, Japan)

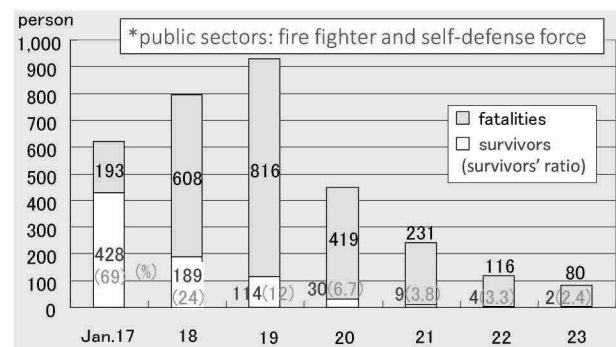


Figure 8: Number and Survivor's ratio of people taken out under damaged structures by public sectors* in Kobe City

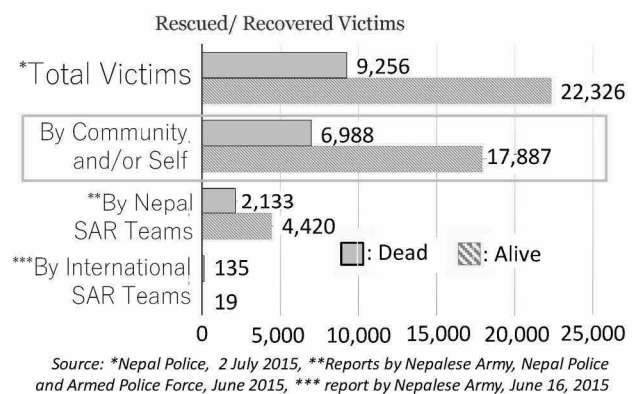


Figure 9: Result by Search and Rescue Operation (2015 Gorkha Earthquake, Nepal)



Figure 10: Earthquakes causing over 5,000 fatalities in the last 100 years

About search and rescue, the local community can contribute the most, and we should not expect too much on the contribution of international teams.

However, when we checked the disaster-related international projects in the past, many of them are focused on emergency and disaster response as shown in Figure 11. Main activities of “emergency response” are search and rescue operation, and emergency supply. However, both of these two activities cannot contribute to disaster reduction in the future. Also, as already mentioned, it is quite difficult to save people by search and rescue operation by international teams.

Then, what is the reason of concentration of projects on the phase of “emergency response”? I think that there are two major reasons. One is that it is relatively easier to carry out emergency response, such as rescue operation and emergency supply, compared with the other phase activities, especially mitigation and preparedness. The other reason is that responsible person of the project is always requested the high presence of the project by the sponsor organization. In order to raise the presence of the project, the most effective way is to get the press to report it. Mass media people report disaster-related activities only just after the big disaster.

To solve the problems introduced above, what should we do? We should pay attention to two issues below.

Besides the budget, it is necessary to establish proper indicator/index for the evaluation of real effects of the project for reducing human casualties and economic loss due to hazards in future. To let the public understand better the real effects of each disaster countermeasures, education of press to improve disaster imagination for better information dissemination is essential.

6. CONCLUSIONS

To build a disaster resilient community, I have introduced “comprehensive disaster management system” that consists of three pre-event measures and four post-event ones. “Damage mitigation”, “preparedness”, and

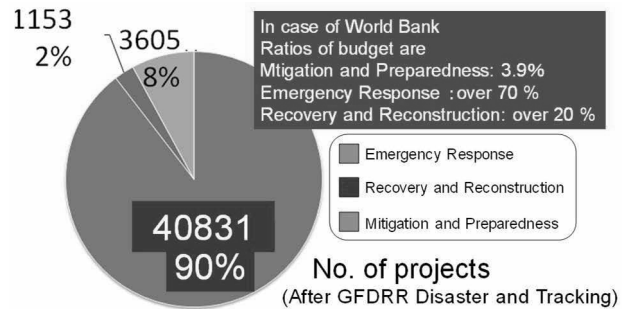


Figure 11: International projects on disaster management during 1990 - 2010

“prediction and early warning” are the elements of pre-event measures, and “damage assessment”, “(emergency) disaster response”, “recovery”, and “build back better” are those of post-event measures. Combining these seven countermeasures properly considering a natural and social characteristics of the target region, we can minimize the negative impact due to hazard. And also, considering disasters as an important opportunity to solve potential problems of the affected region, we can create a better community than before.

In each of the seven countermeasures, there are three efforts, namely, “self-help effort (SE)”, “mutual assistance (MA)” and “public support (PS)”. Based on the combination of above mentioned countermeasures and efforts, the “comprehensive disaster management matrix” was introduced.

In addition, based on the past earthquake disasters, I have pointed out some important lessons that are often misunderstood by many people. Due to the limitation of the space, a solution to improve seismic capacity of weak buildings and disaster information management were not explained in this manuscript, I will introduce them during my lecture at the conference.

USMCA 2018

SESSION 1

INFRASTRUCTURE MANAGEMENT

DEVELOPMENT AND PRACTICAL APPLICATION OF TRAIN OPERATION CONTROL METHOD AGAINST WIND GUST USING DOPPLER RADAR

H. SUZUKI¹, K. KUSUNOKI², C. FUJIWARA³ and H. INOUE⁴

¹ Director, Research and Development Center, East Japan Railway Company, Saitama, Japan, h-suzuki@jreast.co.jp
 (corresponding author)

² Head, Meteorological Research Institute, Ibaraki, Japan, kkusunok@mri-jma.go.jp

³ Researcher, Research and Development Center, East Japan Railway Company, Saitama, Japan, chusei-fujiwara@jreast.co.jp

⁴ Researcher, Meteorological Research Institute, Ibaraki, Japan, hainoue@mri-jma.go.jp

Keywords: Wind gust, Vortex, Doppler radar, Train operation control

1. Introduction

Wind gusts such as tornadoes are among natural disasters that can cause serious damage. On inland in Japan, approximately 25 tornadoes occur each year[1]. Railways also suffer damage from wind gusts. In Japan, train derailment accidents caused by wind gusts have occurred in 1970, 1978, 2005 and 2006[2],[3],[4] as shown in Table 1. Among these, an accident occurring in December 2005 on the Uetsu Line suffered casualties[3]. The cause of this accident is said to be winter wind gust on the Sea of Japan side[3]. We thus developed a train operation control method against such wind gusts using Doppler radar and this method was put to practical use from the 2017-18 winter.

Railway operators in Japan enforce train operation control such as speed reduction or suspension of operations based on wind velocity observed by anemometers, to ensure safe train operation in the times of strong winds. But it is difficult to detect wind gusts with anemometers arranged at intervals along the tracks, because the spatial scale of wind gusts is small. Doppler radars, which can make planar and continuous observation of wind velocity, are suitable for detecting such wind gusts.

In developing a train operation control method against wind gusts using Doppler radar, we started with observing and studying winter wind gusts themselves, as there have been many unexplained areas. We thus deployed a weather observation network, using Doppler radars and anemometers etc. on the Shonai Plain in Yamagata Prefecture. Based on the obtained knowledge regarding winter wind gusts, we developed a method suitable for detecting wind gusts with Doppler radar, and

train operation control method against wind gusts using Doppler radar.

By this method, the radar automatically detects and traces vortices in the air that accompany tornados on the ground surface. When it is predicted that vortices cross a rail line, a warning is issued to stop trains in that section. This method was put to practical use on the Uetsu Line and the Rikuusai Line in the Shonai area from December 19, 2017. This is the first case of practical use of such train operation control method against wind gusts using Doppler radar.

2. Observation network and obtained knowledge

There have been many unexplained areas in wind gusts. In particular, knowledge was scarce regarding winter wind gusts on the Sea of Japan side that caused the Uetsu line accident on 2005. We thus started with observing and studying winter wind gusts themselves. Therefore, from 2007, we deployed a weather observation network on the Shonai Plain in Yamagata Prefecture[5],[6].

Two X-band Doppler radars were installed with an observable range of a radius of over 30 km[5]. We set up 26 weather observation stations to measure wind direction and velocity, air pressure, temperature and humidity[5]. Furthermore, we also set up a linear array wind and pressure sensors system, with 12 anemometers at 100 m intervals and 25 barometers at 50 m intervals[6].

From those observations, we obtained following knowledge regarding winter wind gusts. (1) Wind gusts on the ground surface accompany precipitation and vortices in the air[7]. (2) Vortices form on the Sea of Japan, move straight east and make landfall[8].

Table 1: Outline of train derailment accidents caused by wind gusts in Japan

Date and time	Location	Type of wind gust	Outline of accidents		Source
2006.9.17 14:05	The premises of Minami-Nobeoka station on Nippo Line	Tornado	Overturn of two vehicles of express train in time of reducing speed	Two Injuries	Japan Transport Safety Board[4]
2005.12.25 19:14	Between Sagoshi station and Kita-Amarume station on Uetsu Line	Unknown	Overturn of 6 vehicles of express train	Five deaths and 32 injuries	Japan Transport Safety Board[3]
1978.2.28 21:34	Between Minami-Sunamati station and Kasai station on Touzai Line	Tornado	Overturn of one vehicle and derailment of two vehicles of passenger train	21 Injuries	Fujii et al.[2]
1970.2.5 10:10	The premises of Kamiyama station on Uetsu Line	Tornado	Overturn of one vehicle of freight train	Four Injuries	

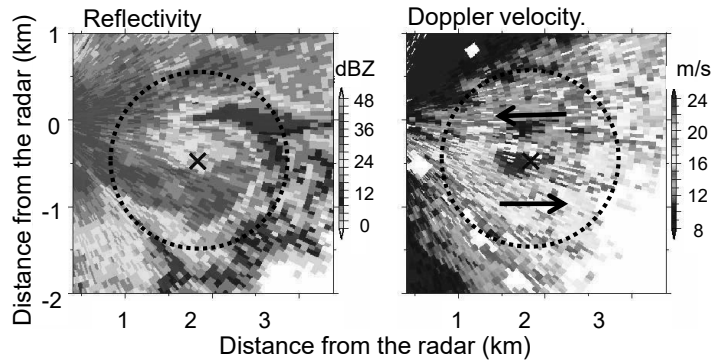


Figure 1: Radar image at time of wind gust observation.(December 5, 2007)

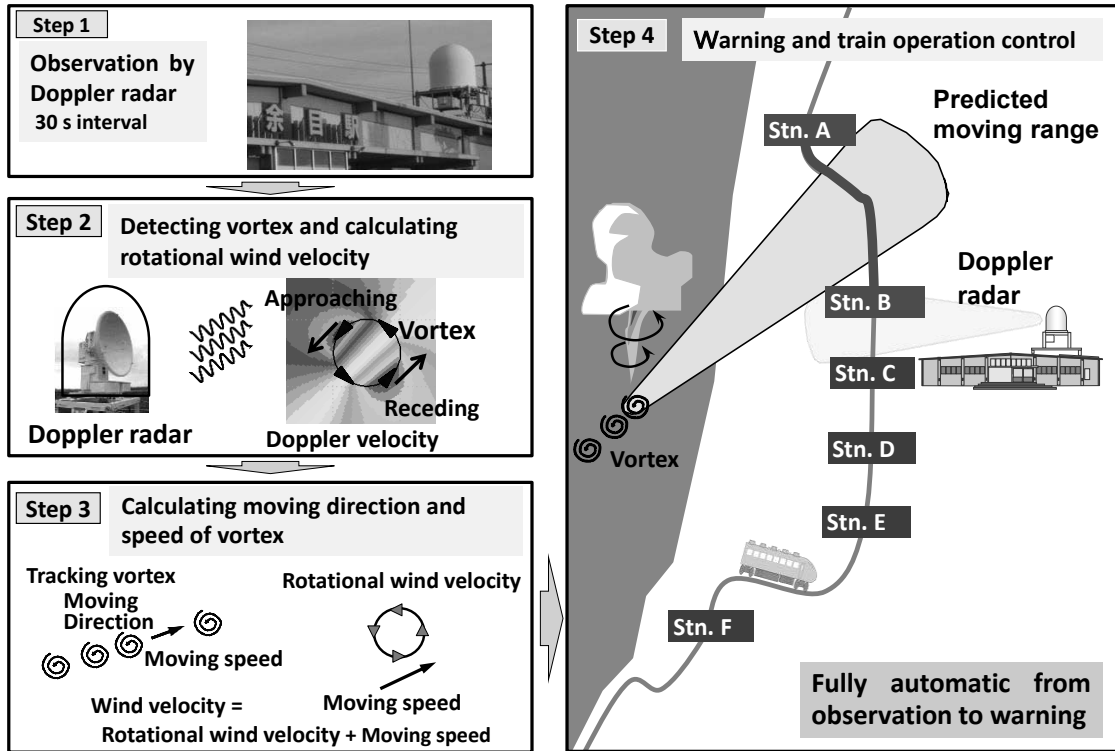


Figure 2: Procedure of the train operation control method against wind gusts using Doppler radar.

- (3) Multiple vortices sometimes occur simultaneously[9].
- (4) Vortices develop from lower layer to upper layer[10].
- (5) Wind velocity distribution of wind gust on the ground surface roughly agrees with the Rankine vortex model[11].
- (6) The maximum wind velocity of the vortex on the ground surface and the vortex in the air are roughly the same[12].

The following findings in regards to method of wind gust detection are obtained based on above knowledge.

- (1) Method of detecting vortices in the air using Doppler radar is effective to detect wind gusts on the ground surface.
- (2) The moving speed and direction of vortices in the air can be obtained by tracking vortices.
- (3) A wind gust detection system needs to simultaneously detect and track multiple vortices.
- (4) A detection method that frequently observes the lower layer is suitable.
- (5) It is considered that vortices in the air can be detected with the Rankine vortex model.
- (6) The maximum wind velocity of the vortex on the ground surface can be estimated from the maximum wind velocity of the vortex in the air.

3. Methods of detecting vortices

A Doppler radar is a meteorological observation device that can observe wind phenomena, in addition to its function as a conventional weather radar measuring precipitation. It can observe components of approaching and receding wind from radar in the air, using the Doppler effect of radio waves reflected from precipitation particles such as raindrops blown by the wind. In a Doppler radar, rotating winds such as vortices in the air that accompany tornados can be detected by extracting pairs of approaching and receding winds.

Figure 1 is a typical example of radar images when a wind gust on the ground surface is observed, and shows images of reflectivity and Doppler velocity of a wind gust on December 5, 2007. In this case, a hook-shaped echo was observed which is the characteristic pattern of a vortex, and a pair of approaching and receding winds was present in the Doppler velocity image.

Wind velocity distribution of vortex accompanied by wind gust on the ground surface roughly agrees with Rankine vortex model. From this knowledge, it is

Table 2: Wind velocity and Fujita scale of wind gusts that have caused train accidents in Japan.

Date and time	Location	Type of wind gust	Wind velocity of wind gust	Rank on Fujita scale	Source
2006.9.17 14:05	The premises of Minami-Nobeoka station on Nippo Line	Tornado	Over 51 ~ 53m/s	F-2	Japan Transport Safety Board[4]
2005.12.25 19:14	Between Sagoshi station and Kita-Amarume station on Uetsu Line	Unknown	About 40 m/s	F-1	Japan Transport Safety Board[3]
1978.2.28 21:34	Between Minami-Sunamati station and Kasai station on Touzai Line	Tornado	Over 80m/s	F-2 ~ 3	Shimamura[14]
1970.2.5 10:10	The premises of Kamiyama station on Uetsu Line	Tornado	Unknown	Unknown	

considered that vortices in the air can be extracted from the Doppler velocity data observed by Doppler radar using the Rankin vortex model. Therefore, to detect vortices in the air, we decided to use the algorithm improving the multi-scale meso-vortex/divergence detection algorithm for detecting mesoscale vortex/divergence signatures in Doppler radar observations proposed by Suzuki et al.[13].

4. Procedure for train operation control

Based on the above knowledge, we proposed a train operation control method against wind gusts using Doppler radar enforced by the procedure shown in Figure 2. There is single Doppler radar used in this method. This procedure is conducted fully automatically.

Step 1 is observation by Doppler radar. Observation by Doppler radar is conducted at 30 second intervals. Doppler radar observes low layer as possible. This is because vortex in the air develops from lower layer to upper layer. Quality control of the observed data is then carried out.

Step 2 is to detect vortex in the air and calculate its rotational wind velocity. Vortices are detected to find pairs of approaching and receding winds. This is because rotating winds such as vortices are observed as pairs of approaching and receding winds by Doppler radar. To detect vortices, the algorithm improving the multi-scale meso-vortex/divergence detection algorithm proposed by Suzuki et al.[13] is used. Furthermore, rotational wind velocity of vortices is calculated using that algorithm.

Step 3 is to calculate moving direction and wind velocity of vortex. When the vortex is under continuous observation, the moving direction and speed of the vortex can be obtained. Then the maximum wind velocity of vortex in the air can be obtained by adding rotational wind velocity of vortex and the moving speed of vortex. This wind velocity is recognized as the maximum wind velocity of wind gust on the ground surface. This is because the maximum wind velocity of the vortex on the ground surface and the vortex in the air are roughly the same. Therefore, train operation control against wind gust is issued based on the wind velocity of vortex in the air.

Step 4 is to issue warning and train operation control. When the vortex accompanied wind velocity above a train operation control value is detected, a warning is issued. Furthermore, in the case that vortex crosses a rail line, train operation control is issued in the section wind gusts are predicted to pass.

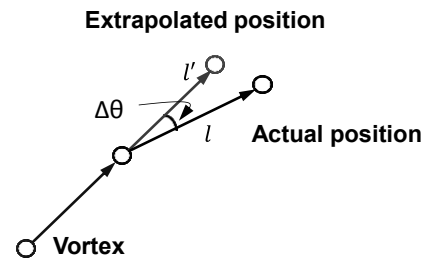


Figure 3: Schematic diagram of actual position of vortex and extrapolated prediction position of that.

5. Train operation standard

In putting this method into practical use, it is necessary to decide the train operation standard such as train operation control value of wind gust, the predicted moving range of that, operation control classification and section, and duration of train operation control.

5.1 Train operation control value

The train operation control value of wind gust is set based on wind gusts that have caused train accidents in Japan in the past. Table 2 shows the wind velocity and Fujita scale of wind gusts that have caused train accidents. Based on this table, the minimum wind velocity was about 40 m/s and the minimum rank of Fujita Scale was the F-1 scale. Therefore, the train operation control value is set at wind velocity of 33 m/s which is the minimum wind velocity of the F-1 scale.

5.2 Predicted moving range of wind gust

The predicted moving range of wind gust is set as the area where wind gusts are predicted to pass within ten minutes, because ten minutes is enough time to stop trains.

Specifically, this range is set as the extrapolated range based on the moving speed and direction of the vortex to the range plus the prediction error. Figure 3 schematically shows actual moving position of vortex and extrapolated prediction position of that. Figure 4 shows frequency distribution of difference between the actual moving position and the extrapolated predicted position of moving distance and direction. The range of the prediction error is set to be twice the standard deviation of the difference between them. Figure 5 shows the predicted moving range of wind gust.

5.3 Operation control classification and section

Baker and Sterling[15] showed that the reduction of

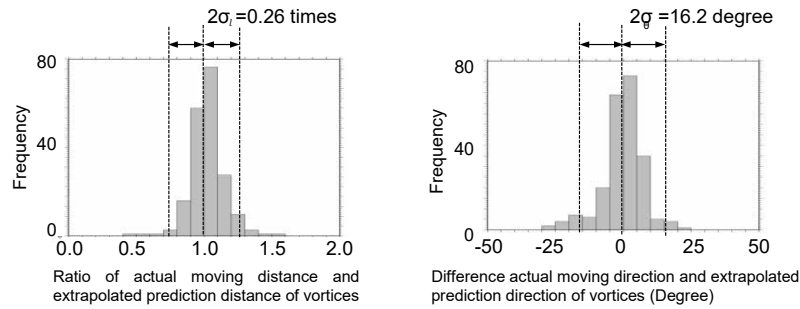


Figure 4: Frequency of difference between the actual moving position and the extrapolated predicted position. Right side is ratio of actual moving distance and extrapolated prediction distance. Left side is difference of actual moving direction and extrapolated predicted direction.

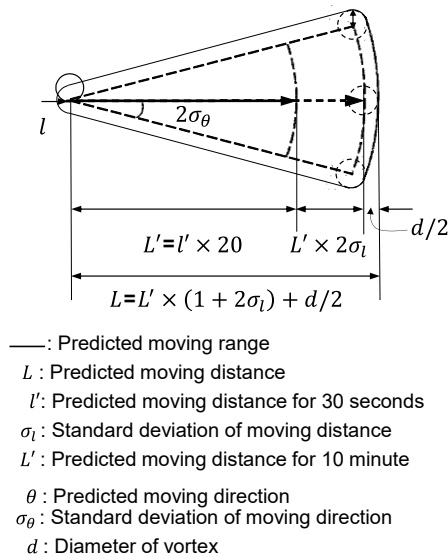


Figure 5: The predicted moving range of wind gust (wind gust).

train speed at times when tornadoes are expected would lead to a very significant reduction in accident risk. Therefore, operation control classification is decided to be stopped due to the lowest risk of accident. When a vortex accompanied wind velocity above the train operation control value is detected and that vortex crosses a rail line, suspension of operations is issued for the section where wind gusts are predicted to pass.

Suspension of operations is enforced between nearest stations outside the predicted moving range of wind gust.

5.4 Duration of suspension of operations

The predicted moving range of wind gust is set as the area where wind gusts accompanied wind velocity above the train operation control value are predicted to pass within ten minutes. Therefore, suspension of operations is continued for ten minutes after that vortex is detected.

6. Evaluation of this method

The evaluation of this method was conducted from the aspects of both safety and stability of train operation. Because, in railway, it is important to ensure sufficient safety, but in addition to this it is also important to ensure normal train operation as much as possible[16].

Safety was evaluated by the number of wind gust captured. This number is the number of wind gusts

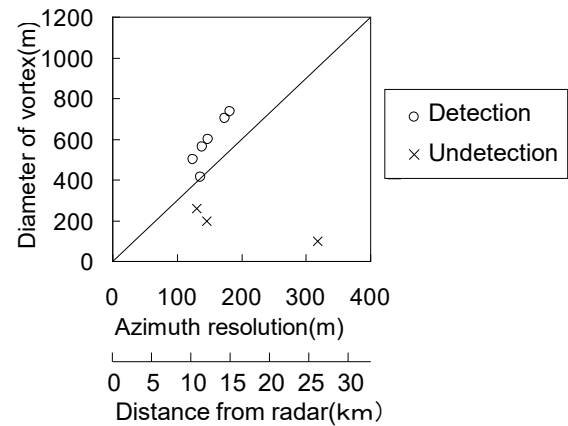


Figure 6: Propriety of detection of vortex, and relationship between diameter of vortex and azimuth resolution.

detected by Doppler radar. In the Shonai Plain, from the 2007-08 winter to the 2013-14 winter, there were no wind gusts that the Japan Metrological Agency (JMA) has certified as the F-1 scale or more. That is, no wind gusts exceeding the train operation regulation value have occurred. Therefore, evaluation was enforced using wind gusts certified as the F-0 scale or observed by anemometers on the ground surface. The F-0 scale is the lowest rank on Fujita scale. Wind gusts observed by anemometers were assumed to be the case where the wind velocity suddenly increased to a wind velocity of 30 m/s or more. The breakdown is as follows: three F-0 scale, and six wind gusts observed by anemometers. This method could detect six wind gusts out of those but could not detect three wind gusts as shown Table 3.

Figure 6 shows relationship between diameter of vortex and azimuth resolution of Doppler radar. Here, the azimuthal distance increases with distance from the radar. The straight line in this figure shows the value at which the azimuth resolution of the radar and the diameter of the vortex are 1: 3. From this figure, it is considered that it is divided into a region in which vortices in the air can be detected and a region in which vortices can be undetected, and the boundary is considered to be divided by that straight line in which the azimuth resolution of the radar and the diameter of the vortex are 1: 3.

Figure 7 shows Doppler velocity distribution map and the Doppler velocity at the center position of the meshes in the XY cross section in the case of vortex detected and

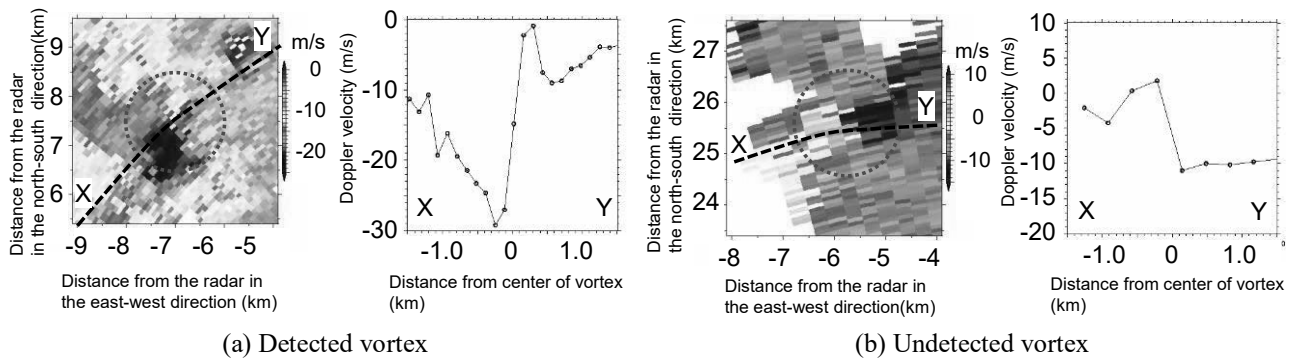


Figure 7: Right is Doppler velocity distribution and left is the Doppler velocity at the center position of the mesh in the XY cross section in the case of vortex detected and undetected by Doppler radar.

Table 3: Number of wind gust occurred and wind gust captured

Area	Scale of wind gust	Number of wind gust occurred	Number of wind gust captured
Shonai Plain	F-0 scale	9	6
Other areas	Over F-1 scale	4	4

Table 4: Predictive rate of wind gust, and number of detected wind gusts and actual wind gusts

Predictive rate	Detected wind gust	Actual wind gust
81.9%	99	81

Table 5: Rate of added time of suspension of operations, and hours of suspension of operation of wind gust (this method) and strong wind.

Rate of added time of suspension of operations	Hours of suspension of operations (per year)	
	Wind gust	Strong Wind
7.0%	2.2	31.2

undetected by Doppler radar. In Figure 7(a) where a vortex can be detected, there are three observed values between the maximum and the minimum of the Doppler velocity. On the other hand, in Figure 7(b) where the vortex could not be detected, there is no observed value between them. Although figures of other cases are omitted, in the case where vortex could be detected, there were one or more observed values between them. Therefore, if the diameter of vortices is more than three times the azimuth resolution of the radar, it is considered to be able to detect the vortex.

Furthermore, we analyzed the capture performance of our algorithm to detect vortices using four strong wind gusts occurred in other areas. The breakdown is as follows: one F-3 scale, one F-2 scale, and two F-1 scale. This algorithm was able to detect all these wind gusts as shown Table 3.

Stability was evaluated by the predictive rate of wind gusts. This rate is the ratio of the detected vortex to the actual vortex. The detected vortex is a case where the wind velocity of vortex in the air observed by Doppler radar is equal to or higher than the train operation control value of wind gust, and the rail line is included in the predicted movement range of wind gust. The actual vortex is the case where the detected vortex is actually a vortex. Table 4 shows number of detected wind gusts and actual wind gusts, and predictive rate of wind gust from



Figure 8: New Doppler radar used the train operation control against wind gusts

the 2007-08 winter to the 2013-14 winter. The predictive rate was high at 81.9%. In addition, we research the time of suspension of operations due to wind gust and strong winds. A train operation control against strong winds has been enforced conventionally. As a result, the time of suspension of operations due to wind gust was low at 7.0% of the time of suspension of operations due to strong winds as shown in Table 5.

Therefore, this method can secure both safety and stability of train operation. East Japan Railway Company (JR East) thus decided to adopt this method as a train operation control method against winter wind gusts that occur on the Sea of Japan side.

7. Practical application

For practical application of this method, a new X-band Doppler radar was built as shown in Figure 8. This Doppler radar has higher performance than the radar used in development and it was installed at a location more suitable for observation of wind gusts.

This method, as countermeasure of winter wind gusts on the Sea of Japan side, was put to practical use on the

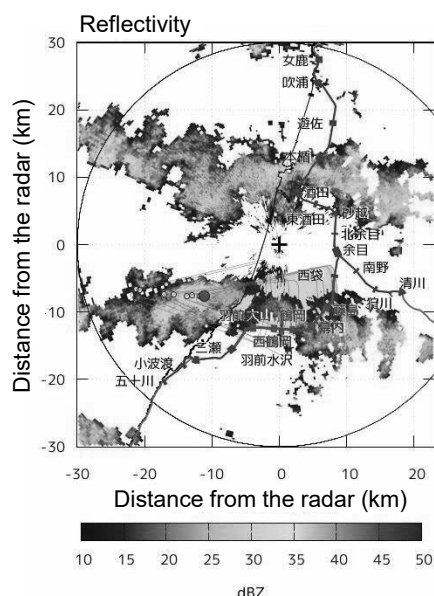


Figure 9: Example of reflectivity image of new Doppler radar and status at the time of issuing suspension of operations.

Uetsu Line and the Rikuusai Line in Shonai area from December 19, 2017.

Figure 9 shows example for reflectivity image of new Doppler radar and status at the time of issuing suspension of operations. Suspension of operations was issued 53 times by this method from its start to the end of March 2018. This was higher than the average times from the 2007-08 winter to the 2013-14 winter. This was due to severe weather condition of the 2017-18 winter. In addition, it is considered that the performance of new Doppler radar is higher than that of the radar used in development and predictive rate of wind gust is lowered.

8. Summary

We developed a train operation control method against winter wind gusts using a Doppler radar. In this method, when it is predicted that a wind gust at wind velocity of over 33m/s (lower limit of F-1 scale on Fujita scale) crosses a rail line within ten minutes, a warning is issued to stop trains in that section. This method was put to practical use on the Uetsu Line and the Rikuusai Line in the Shonai area from December 19, 2017. It is the first time in the world that such train operation control method against wind gusts using Doppler radar has been applied.

In the future, we will continue development to further improve the number of wind gust captured and the predictive rate of wind gusts, and expand the using area of this method.

REFERENCES

[1] Japan Meteorological Agency, Database of wind gusts such as tornadoes, <http://www.data.go.jp/obd/stats/data/bosai/tornado/index.html>.(in Japanese)
 [2] M. Fujii, T. Fujii and H. Muraishi, (1995), History of train operation control against strong winds, RTRI REPORT, Vol.9, pp.43-48.
 [3] Japan Transport Safety Board, (2008), Railway accident investigation report “Train derailment

accident between Sagoshi station and Kita-Amarume station on the Uetsu Line of East Japan Railway Company”, http://www.mlit.go.jp/jtsb/eng-rail_report/English/RA2008-4e.pdf, 1p.

- [4] Japan Transport Safety Board, (2008), Railway accident investigation report “Train derailment accident in the premises of Minami-Nobeoka on the Nippo Line of kyuushu Railway Company”, http://www.mlit.go.jp/jtsb/eng-rail_report/English/RA2008-6e.pdf, 1p.
 [5] K. Kusunoki, et al., (2008), An overview of the Shonai area railroad weather project and early outcomes, Preprints, 5th European Conf. on Radar in Meteorology and Hydrology, Eur. Meteor. Soc., p. 12.1.
 [6] K. Kusunoki, et al. (2012), A linear array of pressure and wind sensors for high resolution in situ measurements in winter tornadoes, Preprints, 7th European Conf. on Radar in Meteorology and Hydrology, Eur. Meteor. Soc.
 [7] K.Kusunoki, et al., (2009), Wind gust and storm evolutions observed during the Shonai Area Railroad Weather Project: A preliminary survey, Proc., 5th European Conf. on Severe Storms, Eur. Meteor. Soc., P09.16.
 [8] T. Ishitsu, et al., (2015), Statistical study of vortices landed in the Shonai plain in winter observed by Doppler radar, Proc. 108th Conf. Japan Meteor. Soc., 108, pp. 373. (in Japanese)
 [9] H. Inoue, et al. (2011), Finescale Doppler radar observation of a tornado and low-level misocyclones within a winter storm in the Japan Sea coastal region, Mon. Wea. Rev., Vol.139, pp.351-369.
 [10] K. Shimose, et al. (2011), Numerical simulation of weather disturbance caused wind gusts in the Shonai Plain, Proc. 100th Conf. Japan Meteor. Soc., pp.220. (in Japanese)
 [11] H. Inoue, et al.,(2013), Wind gust and weather disturbances observed in the Shonai Plain - Vortex and surface wind in the vortex II-, Proc. 104th Conf. Japan Meteor. Soc., pp.70. (in Japanese)
 [12] R. Kato, et al., (2015), Analysis of the horizontal two-dimensional near-surface structure of a winter tornadic vortex using high-resolution in situ wind and pressure measurements, J. Geophys. Res. Atmos, Vol.120, pp.5879–5894.
 [13] O. Suzuki, H. Yamauchi, M. Nakazato and K. Akaeda, (2007), A new multi-scale meso-vortex/divergence detection algorithm with modified Rankine combined vortex, Preprints, 33rd Conf. on Radar Meteor. P5.1.
 [14] M. Shimamura, (2006), Prevention from disasters and learn from disaster - Struggle of railway civil engineering maintenance department -, Japan Railway Civil Eng. Assoc., 271p. (in Japanese)
 [15] C. Baker and M. Sterling, (2018), The calculation of train stability in tornado winds, J. Wind Eng. Ind. Aerod., Vol.176, pp.158-164.
 [16] H. Muraishi, T. Sugiyama and S. Kagawa, (1995), Study on disaster prediction method by effective rainfall index, RTRI REPORT, Vol.9, pp.7-12. (in Japanese)

DEVELOPMENT OF BOND DETERIORATION MODEL IN CORRODED RC MEMBER FOR DISCRETE ANALYSIS MODEL

K. NAGAI¹, P. JIRADILOK², and K. MATSUMOTO³

¹ Associate Professor, Institute of Industrial Science, The University of Tokyo, Tokyo, Japan, nagai325@iis.u-tokyo.ac.jp

² Project researcher, Institute of Industrial Science, The University of Tokyo, Tokyo, Japan, punyawut@iis.u-tokyo.ac.jp

³ Project Assistant Professor, Institute of Industrial Science, The University of Tokyo, Tokyo, Japan, km312@iis.u-tokyo.ac.jp

Keywords: reinforced concrete, corrosion, bond deterioration, RBSM, discrete analysis

1. INTRODUCTION

For a maintenance of reinforced concrete (RC) structures, corrosion is the most serious problem that would lead to the collapse of the structures. For the appropriate maintenance, evaluating the precise residual capacity of corroded structures is necessary, although it is difficult due to the complicated damage patterns of local corrosion and cracking. Meso-scale simulation is one of the beneficial tools for analyzing the structure's member where the local damages are presented directly. In this study, a numerical model for simulating the spatial corrosion damage of reinforced concretes is developed based on a discrete analysis, Rigid Body Spring Model (RBSM). The corrosion model consists of rust expansion damage model, rebar effective-cross-section area reduction, and bond deterioration model. When the corrosion occurs, the corroded rebar losses its shape and creates corrosion product which changes the surface properties. However, in the typical discrete analysis model, the element is modeled as a rigid element which cannot deform. So, in this paper, the author focuses on the development of the bond deterioration model for representing the corrosion effect. Pull-out experiments are performed by using different corrosion degree and different reinforcement shape specimens. The data analysis is done for extracting the necessary information for developing the equivalent model for the bond deterioration in rigid element. Finally, the simulation results are compared with the previous experimental results for the validation of applicability of the model.

2. RIGID BODY SPRING MODEL (RBSM)

In this study, the corrosion model simulation is developed based on three-dimensional RBSM. In RBSM, a three-dimensional reinforced concrete model is meshed into polyhedral rigid elements whose phases are interconnected by a normal spring and two shear springs. Each rigid body consists of 6 degree of freedoms, i.e. 3 translational degrees of freedom and 3 rotational degrees of freedom at some points within its interior and connects with other rigid bodies by 3 springs, i.e. 2 shear springs and 1 normal spring [1,2]. Response of the spring provides the interaction between rigid elements.

This method simulates failure behavior by solving the equilibrium of forces of springs placed between rigid elements. Two types of elements, concrete and steel, are used to define the geometry of reinforced concrete. Since crack direction may affect crack patterns, the size of each

concrete element is approximately 1-2 cm³, referred to aggregate size, while the size of the steel element is set according to the geometric complexity of the reinforcement bar arrangement (Figure 1). To prevent the cracks propagated in a non-arbitrary direction, a random geometry, called Voronoi Diagram, is used for the element meshing.

The properties of the springs are determined so that the elements, when combined together, enable to predict the behavior as accurate as that of the experimental result. In this study, the 3D simulation system and original constitutive model were developed by Eddy et al., is used. [2]. The corrosion expansion model and spatial corrosion model used in this paper were developed in the previous studies by authors. [3,4]

3. EXPERIMENT

3.1 Concept of experiment

In this study, the changing of bond at interface when the corrosion occurs is investigated. In general, the bonding mechanism between rebar and concrete involves mechanical bond and frictional bond. By the pull-out test of concrete specimen reinforced with the round bar, the resistance force is only the friction bond which can be calculated by the rebar-concrete contact area and the maximum pull-out capacity. While, by the pull-out of deformed bar reinforced specimen, the resistance force is the contribution of both the friction bond and the mechanical bonds. Therefore, by performing the pull-out test on different corrosion degree specimens, the changing of these bonds due to the corrosion can be extracted (Figure 2).

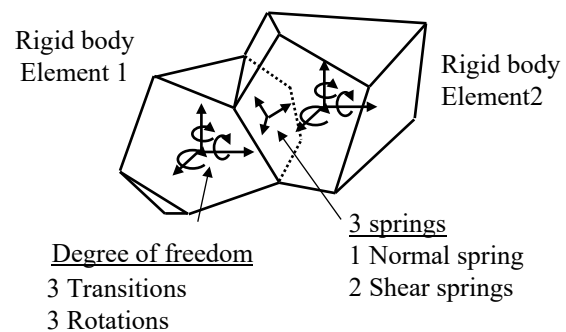


Figure 1: Elements in RBSM

3.2 Experiment sequence

In the experiment, the concrete specimens where the single round bar or deformed bar is placed are prepared. For each specimen, after around 28 days curing in wet condition, the electrical acceleration corrosion test was performed to accelerate the corrosion process at the rate of 0.11A

Figure 3 shows the corrosion acceleration test. The pull-out test is then performed for investigating the changing of the bond at different corrosion percentage. However, at this stage, the cover concrete has the corrosion cracking due to the rust expansion so that the pull-out capacity obtained here includes the effect of concrete damage. Therefore, in this study, second pull-out test of the specimen by casting new concrete is performed.

After the pull-out test on the cracked concrete specimen, the concrete cover is removed, and the corroded bar is taken. The rebar is placed again as a reinforcement in the casting of new specimen. After around 28 days of curing under wet condition, the specimen is tested by the pull-out test to investigate the changing of the bond without the effect of cracked concrete.

Figure 4 shows the form work of specimens that reinforced with a corroded rebar. Figure 5 shows the pull-out test experiment.

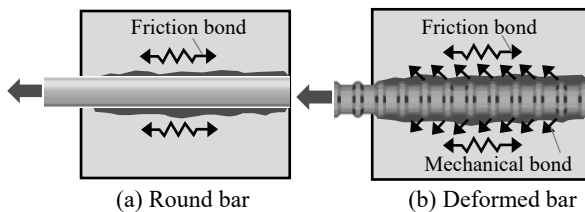


Figure 2: Resistance mechanism in pull out of round bar and deformed bar

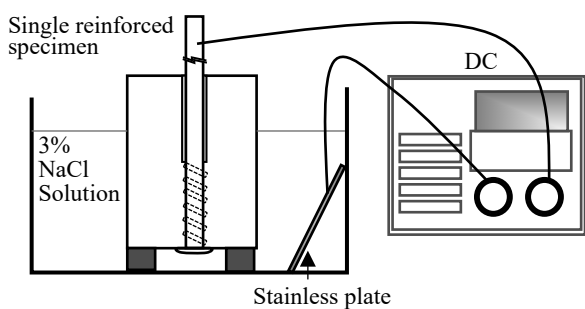


Figure 3: Corrosion acceleration test

3.3 Mix proportion of concrete

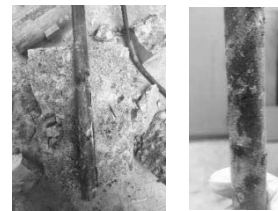
The mix proportion of concrete used for specimens is shown in Table 1.

3.4 Overview of specimens

Table 2 shows the list of specimens tested in this study. Figure 6 shows the specimen layout and the pull-out test condition of specimen reinforced with deformed bar (or round bar). Single reinforcement is embedded in each rectangular concrete specimen. The test specimen is basically a concrete cube $200\text{mm} \times 150\text{mm} \times 150\text{mm}$ with a bar embedded coaxially. Two types of 16 mm diameter rebars are prepared, plain bars and deformed bars with same embedment lengths. To achieve 100 mm embedment length at the free end of the specimen, plasticine is used to unbond the bars from the concrete over 100mm length from the pull-out end.

3.5 Steel corrosion acceleration experiment

Steel corrosion acceleration is conducted at 28 days after casting in order to create the corrosion along the longitudinal reinforcement. The specimens are provided electricity of 0.11A at different time to create different corrosion percentage along the rebar as show in Table 2. The steel weight loss of steel bar is obtained by measuring the unit weight loss of steel after the pull-out test.



(a) Removal of corroded bar



(b) Formwork of corroded reinforcement specimen

Figure 4: Preparation of corroded reinforcement specimen



Figure 5: Pull-out test

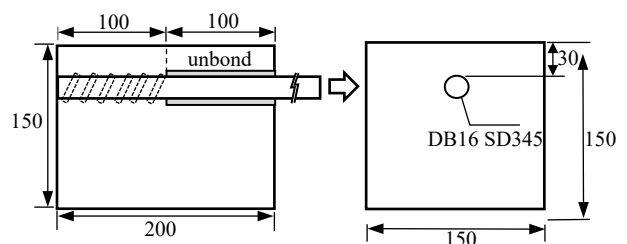


Figure 6: Specimen dimension (Unit:mm)

Table 1: Concrete mix proportion

G _{max} (mm)	Slump (cm)	W/C [%]	S/A [%]	Unit weight kg/m ³				AE [g/10L]
				water	cement	Fine aggregate	Coarse aggregate	
25	8±2	0.60	0.45	169	283	823	1023	13.3

Table 2: List of specimens

Name	Reinforcement	Current-time for corrosion (amp-hours)	Concrete condition	Corrosion level Weight loss (%)
RB-0W-NC	Round bar	0	No cracking	0
RB -1W-NC	Round bar	18.5		3.0
RB -2W-NC	Round bar	37		5.3
RB -4W-NC	Round bar	74		12.1
DB-0W-NC	Deformed	0		0
DB-2W-NC	Deformed	37		10.5
DB-4W-NC	Deformed	74		23.1

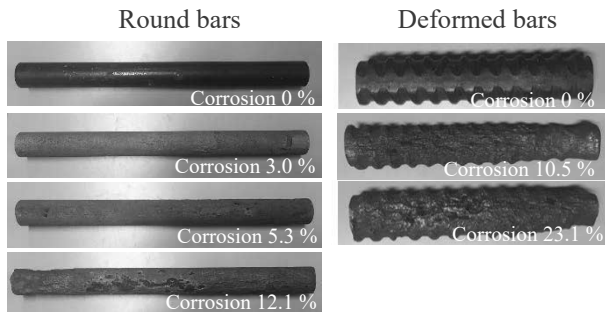


Figure 7: Corroded round bars and deformed bars from corrosion acceleration test

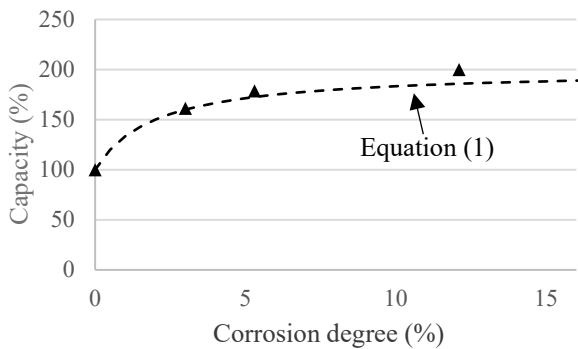


Figure 8: Pull-out capacity of corroded round bars

4. EXPERIMENTAL RESULTS AND MODELING OF INTERFACE

4.1 Round bar pull-out test results

Relationship between the steel weight loss percentage and the pull-out capacity obtained by tests is plotted in Figure 8. In the pull-out tests, all specimens fail by the slipping out at the interface between rebar and concrete, which means there is no cracking occurred in concrete phase. The pull-out capacity increases by the corrosion because the friction is increased by the rust and change of surface geometry.

From the results, the constitutive model for the shear spring in RBSM to present the change of friction is proposed by the following Equation (1). Where x is the

corrosion degree, M_{shear} is the modification factor of shear spring at the corroded interface in RBSM

$$M_{shear} = 200 - \frac{100}{0.5x+1} \quad (1)$$

4.2 Deformed bar Pull-out test results

Figure 9 shows the pull-out capacities of corroded deformed bar with non-crack concrete. In case of pull-out of corroded bar, it is obvious that even the corrosion degree increases up to 23.1%, the pull-out capacity has almost no change (less than 3% decreases comparing with the no corrosion condition). It can be assumed that the total bond of the pull out of the corroded deformed bar without concrete damage does not change.

To extract the mechanical bond changing from the total bond, super position theory was assumed. The frictional bond in Equation (1) was subtracted from the total bond. The remaining mechanical bond are shown in Figure 10. However, the reduction trend of mechanical bond shown in Figure 10 containing many local behaviors such as the knot deformation, the remaining of rust at interface, the sliding-opening effect and so on. Therefore, a simple linear Equation (2) is proposed to represent the reduction from these behaviors.

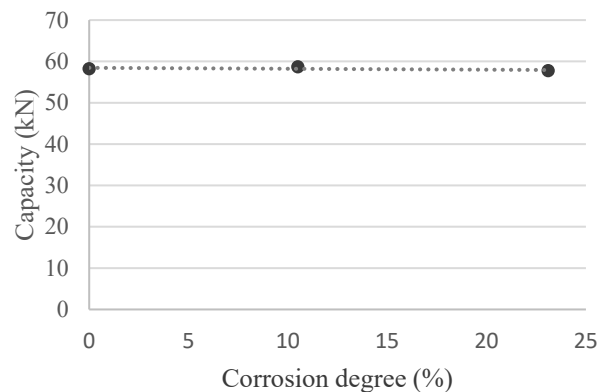


Figure 9: Pull-out capacities of corroded deformed bars

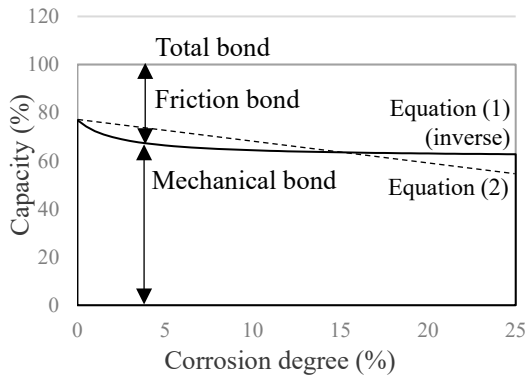


Figure 10: Modeling of mechanical bond reduction

$$M_{normal} = 100 - x \quad (2)$$

Where M_{normal} is the modification factor for the normal spring stiffness spring at the corroded interface in RBSM and, x is the corrosion percentage.

5. CORRODED BEAM SIMULATION

This chapter aims to validate the applicability of the numerical models proposed in this study. By the combination of the spatial corrosion model, the expansive strain model, and the bond deterioration model into RBSM simulation, it can consider the changing of steel properties and expansion damage on adjacent concrete based on steel weight loss, the bond deterioration and the non-uniformity of corrosion pattern [3,4]. In this study the corroded beam models are simulated. The loading test of corroded beam by S. Lim et al. [5] is referred. Reinforcements in the simulation are modified at every 5 mm based on corrosion profile obtained from the experiment.

Figure 11 shows the dimension of beam done by S. Lim et al. An experiment of corroded RC beam was conducted to study the effect of local corrosion condition on the capacity of the beam. After the corrosion acceleration test, the digital camera and X-ray technique were used to measure the corrosion profile along the rebar every 5 mm. Then, the corroded beams were subjected to the mechanical loading test to investigate the residual capacity.

Figure 13 shows the steel weight loss profile along the rebar of beam specimen by X-ray apparatus. The average corrosion degree is 25.54%.

5.1 Geometry of simulation model

The analysis model used in this study is formed up based on the experiment. The size of RC beam is $1,460 \times 140 \times 80 \text{ mm}^3$ reinforced with a DB13 rebar. Analysis model is meshed into meso-scale elements having average sizes approximately $10 \times 10 \times 10 \text{ mm}^3$. Two pin supports and two loading points are set at the same

location as in the experiment. The load is given at the two points above the beam. The friction of interface between the loading or support plate and the beam is removed. The model contains 62,458 elements. The input tensile strength of steel bar and concrete are 388 MPa and 3.24 MPa, respectively. Expansive strain is applied to the interface between rebar and concrete for generating the corrosion expansion. Subsequently, the mechanical loading is given in the same manner as experiment. Figure 12 shows the reinforced concrete beam simulation by RBSM in this study.

5.2 Corrosion patterns

In this study, the simulations of the models of non-corroded and corroded beams with different corrosion patterns are carried out for investigating the effect of spatial corrosion pattern on the capacity of RC beam.

Two different steel weight loss profile are set for the simulations. The first corrosion case is the uniform corrosion pattern at 25.5 percent along the bar. Second case is non-uniform corrosion obtained from 3D x-ray technique as shown in Figure 13 where the corrosion was measured every 5mm. The spatial variable steel weight loss is start from 250 mm to 1,090 mm in rebar length direction. The other zone, 0 to 250 and 1090 to 1490 mm, does not have information from the experiment, so the corrosion level is set as uniform corrosion pattern at 25.5 % in the simulation.

5.3 Analysis results

5.3.1 Load-displacement relationship

Load-displacement relationships of simulation results with the experimental data are shown in Figure 14. The load is defined as the total force acting at two pin points, while the displacement is the vertical displacement of loading point in the downward direction. The maximum capacity of each simulation case is 24.0 kN, 18.3 kN and 12.6 kN for the no corrosion case, the uniform corrosion case and the spatial corrosion case, respectively. In the experimental specimen, it was reported that the steel bar was yielded, and the specimen showed flexural behavior before the failure by reaching the shear capacity shown by the dot line in Figure 14. In case of simulation, beam with corrosions shows lower stiffness and capacity than the no corrosion case due to initial damage from corrosion which are bond deterioration and steel cross section reduction. Since the critical corrosion cross-section is located at the middle span, the stiffness of each beam is clearly different between no corrosion, uniform corrosion and non-uniform corrosion case. Comparing with the no corrosion case, the corroded beam's stiffness becomes close to the experimental result. In terms of the capacity, it reduces by the corrosion in the simulation. Non-uniform case shows the higher reduction because of the local severe corrosion in the model that indicates the necessity of considering the local corrosion to evaluate the residual capacity of the damaged reinforced concrete reasonably.

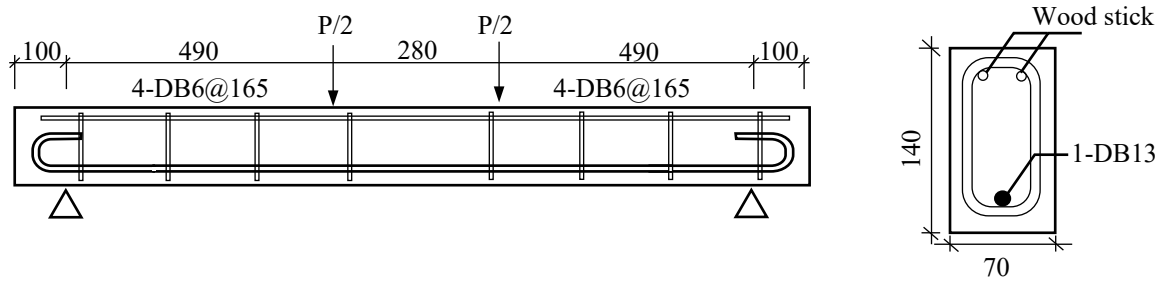


Figure 11: Dimension of beam in corrosion acceleration experiment

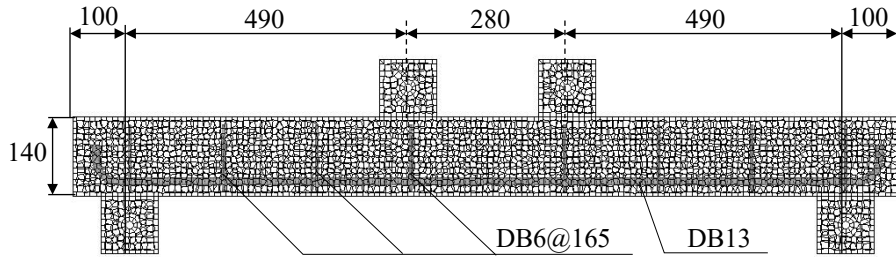


Figure 12: Geometry of numerical model by RBSM (Unit: mm)

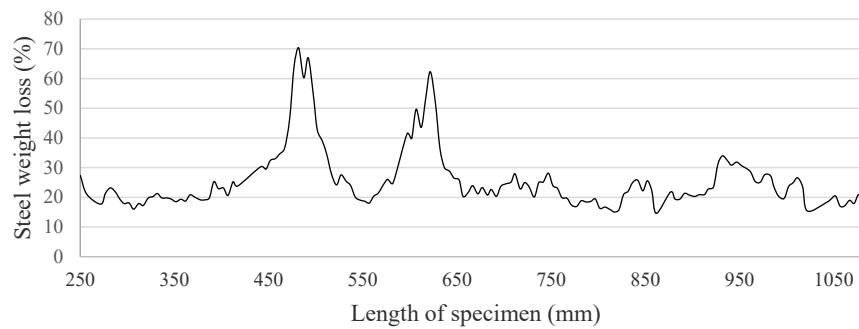


Figure 13: Local steel weight loss along the bar length

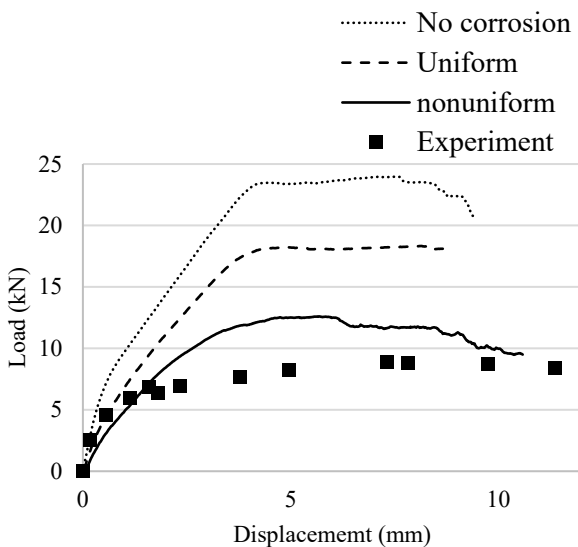


Figure 14: Load-displacement relationships

5.3.2 Crack patterns at failure

Figure 15 shows the internal crack pattern and the 3D surface overview crack of uniform and non-uniform corrosion simulations. For the corroded beam, corrosion crack along the longitudinal rebar length can be observed at the bottom of the beam. After the loading, in case of no corrosion and uniform corrosion case, the beam failure pattern indicated a flexural failure. Flexural cracks can be observed between the loading point pin location which is the maximum moment span. (Figure 15(a)) For the corroded beam with non-uniform corrosion pattern, a shear failure pattern can be observed as shown in Figure 15 (c). Shear crack occurred at the left shear span of the beam. This cracking is corresponding with the critical corroded cross-section. This result indicates that the initial crack damage from local corrosion can lead to the propagation of shear crack in the left span of the beam. Considering this effect, the beam simulation with non-uniform corrosion damage can present the similar failure pattern as the experiment correctly.

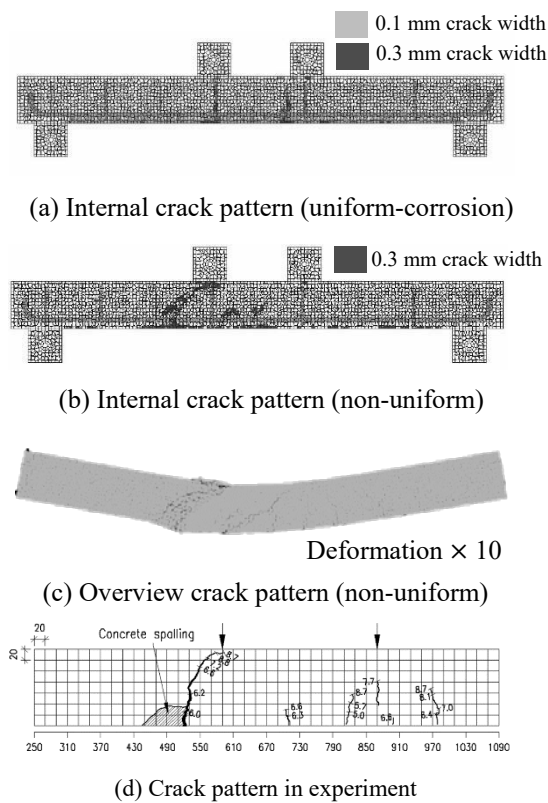


Figure 15: Failure patterns in simulations and experiment

6. CONCLUSIONS

1. The simulation system for evaluating the residual capacity of corroded RC beam considering the effects of the rust expansion, the bond deterioration, the rebar reduction, and the non-uniformity of corrosion pattern is developed.

2. The constitutive models of the bond deterioration by corrosion were reasonably developed based on the designed experiment. To extract the changing of the friction bond and the mechanical bond, the pull-out experiment program of concrete specimens reinforced with corroded round bar and corroded deformed bar at different corrosion percentage without corrosion cracking damage, were performed. The new constitutive model of shear spring and normal spring were proposed based on the changing of maximum pull-out capacities at different corrosion degree.

3. To validate the applicability of the new constitutive model, the corroded RC beam simulation were carried out using the new constitutive model. The simulation results show the reasonable results comparing with the experiment. The stiffness reduction and the residual capacity of corroded beam due to the initial damage from corrosion were simulated well. The non-uniform corrosion simulation showed the similar failure pattern as the experimental result.

REFERENCES

[1] K. Nagai, Y. Sato, T. Ueda, (2005) "Mesoscopic Simulation of Failure of Mortar and Concrete by 3D RBSM", *Journal of Advanced Concrete Technology*, Vol.3, pp.385–402

[2] L. Eddy, K. Nagai (2016) "Numerical Simulation of Beam-column Knee Joints with Mechanical Anchorages by 3D Rigid Body Spring Model", *Engineering Structures*, Vol. 126, pp.547-558

[3] P. Jiradilok, K. Nagai and K. Matsumoto, (2017), "Development of Spatial Corrosion Damage Simulation based on Rigid Body Spring Model.", The 6th International Doctoral Symposium, Hokkaido University, Hokkaido, Japan

[4] P. Jiradilok, K. Nagai and K. Matsumoto, (2018), "Development of non-uniform corroded RC member simulation based on Rigid Body Spring Model.", 12th fib International PhD-Symposium in Civil Engineering, Czech Technical University, Prague, Czech Republic

[5] S. Lim, M. Akiyama and D. M. Frangopol, (2016), "Assessment of the structural performance of corrosion-affected RC member based on experiment study and probabilistic modeling", *Engineering structures* 127, pp.189-205

NUMERICAL MODELLING OF RADIATING BOUNDARY CONDITIONS COMBINED FOR WAVE PROPAGATION IN NONLINEAR UNBOUNDED DOMAIN

R.S. Badry¹, P.K. Ramacharla²

¹ *Research Scholar, IIT Hyderabad, Ravishankar.Badry@research.iiit.ac.in (corresponding author)*

² *Professor and Registrar, IIT Hyderabad, ramacharla@iiit.ac.in*

Keywords: *Absorbing Boundary Conditions, Nonlinear material, Soil-Structure-Interaction, Finite Element Method, Explicit Time Integration*

1. INTRODUCTION

The effect of radiating boundary conditions on numerical simulations is one of the important aspects in soil structure interaction problems. As soil is a nonlinear medium, the boundary conditions have to consider the nonlinear behaviour to accurately resemble the wave propagation. To address the radiating boundary condition problem, researchers have developed various formulations, such as Local Absorbing Boundary Conditions [1], Absorbing Layers techniques (which includes Perfectly Matched Layers [2], Caughey Absorbing Layer Method [3] and Absorbing Layers by Increasing Damping [4]), Boundary element method [5] and Infinite elements [6]. With the exception of absorbing layer techniques, the above methods are not appropriate for simulating wave propagation through nonlinear material. Meanwhile, the absorbing layer methods require large number of layers or high computational complexity.

This paper presents a new radiating boundary condition for wave propagation in nonlinear material. The efficiency of the proposed methods has been verified for both 1D and 2D wave propagation problems and the accuracy is compared with extended meshed models. The study concludes that better responses can be obtained by using the proposed approach when compared with traditional Local Absorbing Boundary Conditions. The proposed method inherently considers the relaxation due to plastic deformation beyond the numerical domain boundary

2. METHODOLOGY

The proportionality relation between the incremental velocity $d\dot{u}$ and incremental strain $d\varepsilon_x$ is established by von Karman [7] for 1D nonlinear wave propagation problems

$$d\dot{u} = Cp(\varepsilon_x) d\varepsilon_x \quad (1)$$

where, $Cp(\varepsilon_x)$ is the p-wave velocity corresponding to instantaneous strain ε_x . Similar hypothesis can be applied for 3D wave propagation problem for developing local absorbing boundary condition assuming the waves impinge in normal direction.

$$d\dot{u} = Cp(\tilde{\varepsilon}) d\varepsilon_{xx} \quad (2a)$$

$$d\dot{v} = Cs(\tilde{\varepsilon}) d\varepsilon_{xy} \quad (2b)$$

$$d\dot{w} = Cs(\tilde{\varepsilon}) d\varepsilon_{xz} \quad \dots\dots \quad (2c)$$

where, $d\dot{u}$, $d\dot{v}$, and $d\dot{w}$ are the incremental particle velocities in x , y and z directions respectively. $d\varepsilon_{xx}$ is the axial strain. $d\varepsilon_{xy}$, and $d\varepsilon_{xz}$ are the shear strains. $Cp(\tilde{\varepsilon})$ and $Cs(\tilde{\varepsilon})$ are the p-wave and s-wave propagation velocities respectively. Let $d\dot{u}^{t+\Delta t}$, $d\dot{v}^{t+\Delta t}$, and $d\dot{w}^{t+\Delta t}$ are the known incremental particle velocities at time $t + \Delta t$ in boundary local x , y and z direction, then the incremental strains near the boundary can be obtained using equation (2)

$$d\varepsilon_{xx} = d\dot{u}^{t+\Delta t} / Cp(\tilde{\varepsilon})^t \quad (3a)$$

$$d\varepsilon_{xy} = d\dot{v}^{t+\Delta t} / Cs(\tilde{\varepsilon})^t \quad (3b)$$

$$d\varepsilon_{xz} = d\dot{w}^{t+\Delta t} / Cs(\tilde{\varepsilon})^t \quad (3c)$$

where, $Cp(\tilde{\varepsilon})^t$ and $Cs(\tilde{\varepsilon})^t$ are the p-wave and s-wave propagation velocities at the instantaneous strains $\tilde{\varepsilon}$ computed near the boundary at time t . The wave propagation velocities are estimated from the tangent material matrix computed at previous time step. When the waves impinge in normal direction to the boundary, the incremental strain $d\varepsilon_{yy}$, $d\varepsilon_{zz}$, and $d\varepsilon_{yz}$ due to wave propagation are assumed to be zero. Therefore, the incremental strain vector can be defined as

$$d\tilde{\varepsilon} = \{d\varepsilon_{xx}, 0, 0, d\varepsilon_{xy}, 0, d\varepsilon_{zx}\}^T \quad (4)$$

The strain vector can be updated to next time step $t + \Delta t$ using

$$\tilde{\varepsilon}^{t+\Delta t} = \tilde{\varepsilon}^t + d\tilde{\varepsilon} \quad (5)$$

The tangent material matrix C_{ij} and wave velocities for p-wave and s-wave can be estimated corresponding to instantaneous strain $\tilde{\varepsilon}^{t+\Delta t}$. The absorbing stresses at the boundary can be computed using

$$\tilde{\sigma}^{t+\Delta t} = \tilde{\sigma}^t + C_{ij} d\tilde{\varepsilon} \quad (6)$$

The above equation represents the local Absorbing Boundary Condition for nonlinear materials (NLABC). The procedure outlined can be applied for any nonlinear materials.

3. RESULTS AND DISCUSSIONS

In this section, the efficiency of the proposed method is verified with pure P-wave propagation as shown in Fig. 1. Two material models are selected to verify the applicability of the method.

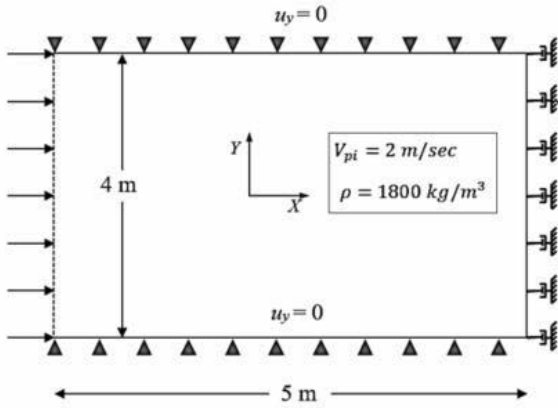


Figure 1. 2D Plane strain model for P-Wave propagation

3.1 Von-Mises elastic perfectly plastic material

Material properties chosen for the medium are initial modulus of elasticity $E_i = 4800\text{N/m}^2$, Poisson's Ration $\nu = 1/3$, density $\rho = 1800\text{kg/m}^3$ and ultimate yield stress $\sigma_{ulti} = 5\text{N/m}^2$. The analysis has been carried out for 10 seconds and time variation of load is considered using a Gaussian wavelet with time shift $t_s = 4$ seconds and peak frequency $f_p = 1\text{Hz}$. Stresses and displacements in the X-direction due to pure p-wave propagation in the medium are presented in Fig 2. The reflections are estimated as 10.71N/m^2 and 0.47N/m^2 respectively for ABC and NLABC. This concludes that the NLABC includes the energy due to plastic dissipation energy effectively.

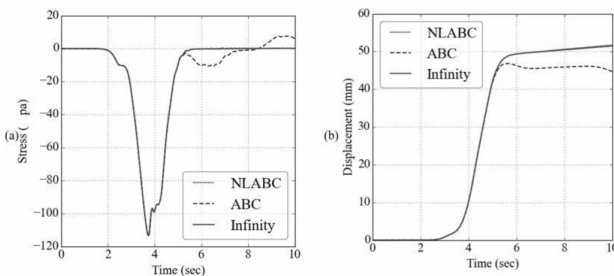


Figure 2: a) Stress at 2m and b) Displacement at 3m in the X-direction for elastic perfectly plastic material

3.2 Von-Mises Isotropic linear isotropic hardening material

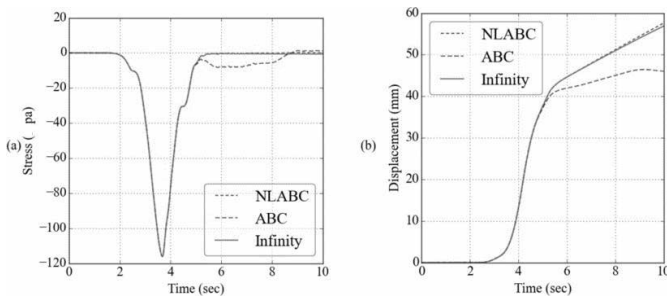


Figure 3: a) Stress at 2m and b) Displacement at 3m in the X-direction for linear isotropic hardening material

The model described for elastic perfectly plastic material including analysis time and loading is used by changing

the material to linear isotropic hardening material. The tangent modulus is taken as $E_T = 1200\text{N/m}^2$. Stresses and displacements in X-direction are presented in Fig 3. The reflections are estimated as 7.93N/m^2 and 0.82N/m^2 respectively for ABC and NLABC. The stress profile for NLABC deviates from the extended mesh model after 6 seconds. This indicates that current method cannot include the effect of plastic free energy dissipation i.e. energy dissipated due to loss of heat.

4. CONCLUSIONS

In this study, the framework to model radiating boundary conditions for wave propagation through nonlinear material is presented and the following conclusions are drawn from the study

1. The method requires additional computation cost to estimate the tangent material stress strain tensors and wave propagation velocities corresponding to instantaneous strains at the boundary.
2. The proposed method demonstrates that the effects of material nonlinearities i.e. tangent stress-strain tensor are accounted effectively.
3. The efficiency of the method is also analyzed for energy dissipation. Two types of energy dissipation are considered i.e. plastic deformation and plastic free dissipation. The proposed method does account for the energy dissipation due plastic deformation but not the plastic free energy dissipation. Therefore, this method produces reflection due to plastic free energy i.e. when isotropic hardening is present.
4. The method assumes that propagating wave impinge the boundary in normal direction. If the wave impinges any other direction, the performance is poor and needs further investigation.

REFERENCES

- [1] J. Lysmer., R.L. Kuhlemeyer., (1969). "Finite dynamic model for infinite media". *Journal of Engineering Mechanics*. Div ASCE 95(EM4):859–877.
- [2] J.P. Berenger., (1994) "A perfectly matched layer for the absorption of electromagnetic waves." *Journal of Computing in Physics*; 114(2):185–200.
- [3] J.F. Sembalt., L. Lenti., G. Ali., (2010) "A simple multi directional Absorbing Layer method to simulate elastic wave propagation in unbounded domains", *International Journal for Numerical methods in engineering*; 1: 1-22.
- [4] P. Rajagopal, M. Drozd, E.A. Skelton, M.J.S. Lowe, R.V. Craster, (2012) "On the use of absorbing layers to simulate the propagation of elastic waves in unbounded isotropic media using commercially available finite element packages", *NDT&E Int.* 51:30–40.
- [5] P.K. Banerjee., R. Butterfield., (1981). *Boundary element methods in engineering science*. McGraw-Hill Book Co.
- [6] P. Bettess., (1978) "Infinite elements", *International Journal for Numerical Methods in Engineering*; 11:54-64.
- [7] T. von Karman., and P. Duwez., (1950), "The propagation of plastic deformation in solids". *J. App. Phys.*, 21:987-994.

CAUSE ESTIMATION AND PROPOSAL OF INSPECTION METHOD FOR DAMAGED PC SLEEPERS OF INDIAN RAILWAYS

K. MATSUMOTO¹, K. NAGAI², R. SUNDARAM³, and A. AWASTHI⁴

¹ Project Assist. Prof., ICUS, IIS, The Univ. of Tokyo, Tokyo, Japan, km312@iis.u-tokyo.ac.jp (corresponding author)

² Associate Prof., ICUS, IIS, The Univ. of Tokyo, Tokyo, Japan, nagai325@iis.u-tokyo.ac.jp

³ Engineer, Sumitomo Mitsui Construction Co. Ltd., Tokyo, Japan, rajacz11@gmail.com

⁴ Deputy Chief Engineer, Construction Organization, Indian Railways, India, anupamawasthi1978@gmail.com

Keywords: Delayed Ettringite Formation (DEF), Alkali Silica Reaction (ASR), Sleepers, Prestressed Concrete

1. INTRODUCTION

Indian railways uses prestressed concrete (PC) sleepers made by pretension system in factories for its railway trucks. Sleepers are members which directly carry weight of train cars, therefore they are quite important for the safety transportation. Recently, a number of the PC sleepers are damaged by cracks after 6 to 9 years of production. These cracks are also seen in sleepers which are not used, even though any loads has not been applied to them. Figure 1 shows typical damages observed in the sleepers. According to the survey conducted in the central region of India, 45,000 of 128,000 sleepers in 100 km range of a train line are damaged by the cracks. This number corresponds to 35% of the total number sleepers. Consequently, Indian railways are facing to a problem related to passenger's safety transportation.

This study aims to determine the cause of damage in the sleepers, clarify mechanical performances of the sleepers in both material and structural level, and propose an inspection method for the existing sleepers. To determine the cause of the damage, Scanning Electron Microscope (SEM) for samples taken from the PC sleepers was carried out. To clarify mechanical performances of the damaged PC sleepers in material and structural level, compressive tests of core samples taken from the sleepers and loading tests of the damaged sleepers were conducted. In addition, an evaluation method for determining damage levels from crack patterns which can be seen on the outer surface of the sleepers was proposed based on the structural performances observed in the loading tests.

2. MANUFACTURING CONDITION OF SLEEPERS

To know the temperature rise inside the concrete during steam curing, field measurement of temperature using thermocouples and data-logger was performed in a concrete sleeper plant in India. For a sleeper, temperature was measured at two points, one inside the sleeper where maximum temperature is expected and one just outside that point.

Figures 2 shows the result of the temperature measurement. The measurement reveals that the maximum temperature reached inside concrete is over 80°C. Therefore, it is very well established that concrete temperature is beyond the critical temperature for the occurrence of Delayed Ettringite Formation (DEF) problem (as mentioned by Ghorab et al. [1], Heinz and Ludwig [2], Hanehara and Oyamada [3]). The temperature inside concrete generally follows the trend of temperature outside concrete but becomes more than the outside temperature after approximately 6 and 1/2 hours of casting. This depicts the effect of heat of hydration in addition to the outside curing temperature.

3. CLASSIFICATION OF DAMAGE LEVELS

Table 1 shows classifications of damage levels of the sleepers, which are expected to be used to evaluate inspection results in the field. The damage levels are determined according to the maximum crack width and number of cracks. There are four damage levels, which are "No damage", "Mild damage", "Moderate damage" and "Severe damage". The reason why the damage levels are

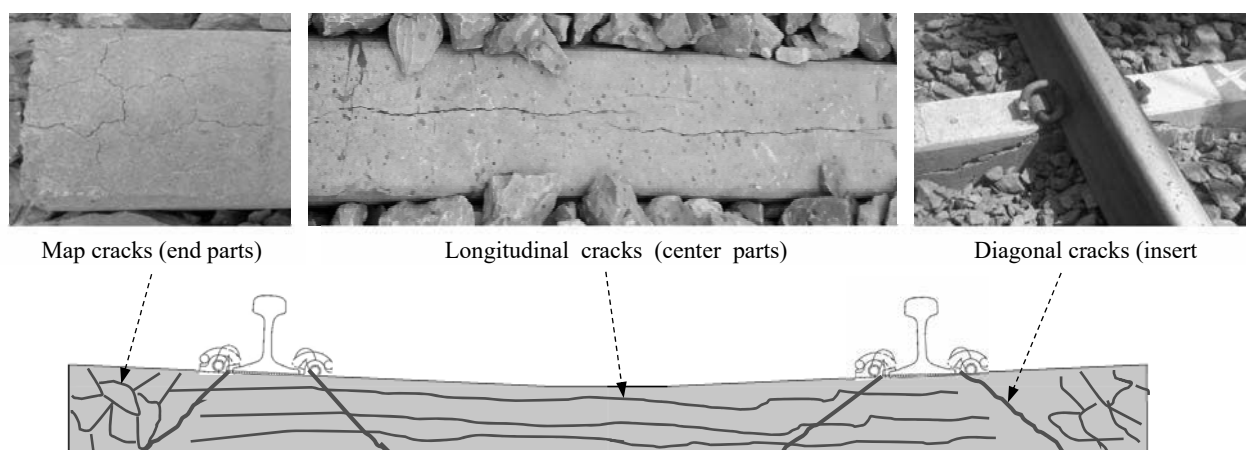


Figure 1: Typical crack patterns observed in the damaged PC sleepers of Indian Railways

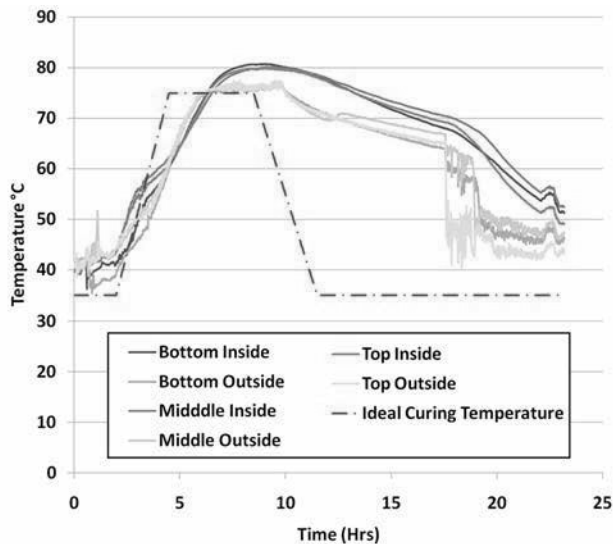


Figure 2: Temperature change during steam curing

Table 1: Classification of damage levels

Grade	Designation	Width and number of cracks
I	No damage	No cracks
II	Mild damage	Less than 1 mm max width
III	Moderate damage	Larger than 1 mm and less than 2 mm width, or single crack
IV	Severe damage	Larger than 2 mm width and multiple cracks

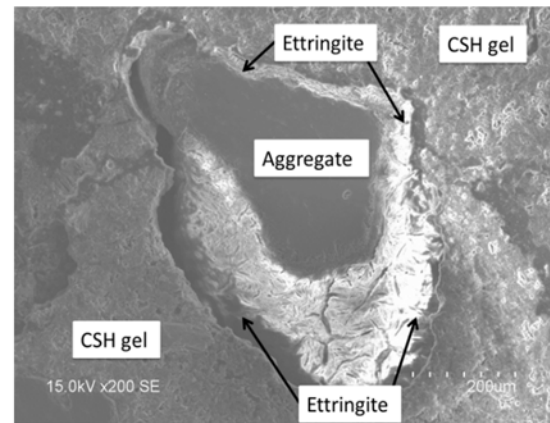
determined from width and number of cracks is that expansion strain of the concrete caused by DEF and Alkali Silica Reaction (ASR) seems has a correlation with them.

After several times of discussion with Indian Railways, by classifying the damage levels into four categories shown in Table 1, it was confirmed that they can consider a realistic replacement plan of the 45,000 pieces of sleepers.

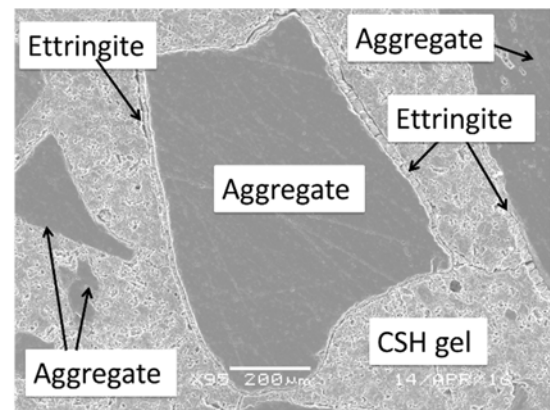
4. INVESTIGATION BY SCANNING ELECTRON MICROSCOPE (SEM)

To investigate cause of the premature cracking of sleepers, different damage levels of samples, “Moderate damage” and “No damage” were collected. The specimens are prepared by embedding small pieces of samples (approximately 1 cm x 1 cm x 1 cm) from each of the three categories into epoxy resin solution. Epoxy resin facilitate mounting of small pieces of concrete samples, which is polished to view the microstructure of concrete under SEM. After hardening of the epoxy resin, these specimens are cut and the exposed surface is grinded by using polishing abrasives. Then the polished surface is coated with platinum, which is needed to prevent the charging of specimen with the electron beam.

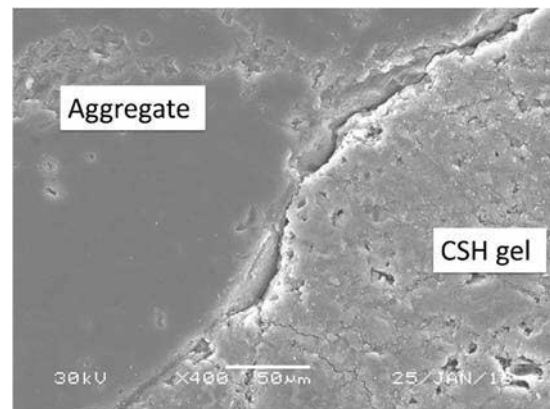
Figures 3(a), (b) and (c) show the typical SEM images of the specimen of “Severe damage”, “Moderate damage” and “No damage” sleepers, respectively. In the cases of



(a) Severe damage



(b) Moderate damage



(c) No damage

Figure 3: SEM images of samples

“Severe damage” and “Moderate damage” sleepers, it reveals that there is ettringite deposition around the interface of aggregate and paste. Also, ettringite could be noticed inside the paste. Few coarse aggregate also show some porosity and cracks inside them but ASR gel like substance is not noticed. On the other hand, in the case of “No damage” sleepers, it is observed that the interface of aggregate and paste seems to be intact and no ettringite formation has been noticed either in the C-S-H gel or at the interface of aggregate and paste. Apart from this, no ASR gel like substance is noticed.

Table 2: Damage level and manufacturing year of cut sleepers

No.	Damage level	Manufacturing year
1	I	2015
2	I	1986
3	II	2006
4	III	2006
5	IV	2002
6	IV	2006
7	IV	2002

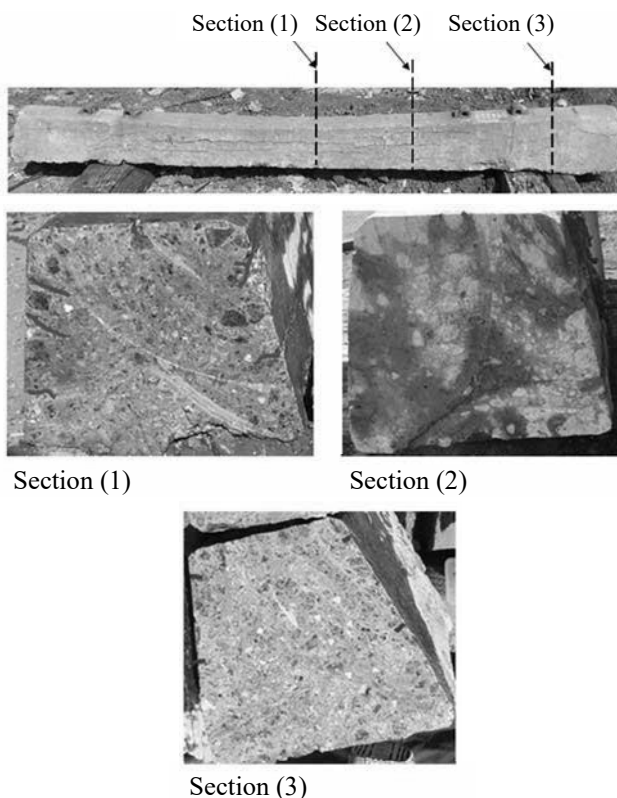


Figure 4: Inner crack patterns in cut cross sections

The results of SEM suggests that delayed ettringite formation might be the cause of premature damage in the concrete sleepers in India. However, occurrences of alkali-silica reaction also cannot be denied. ASR gel like product, in one of the “Severe damage” sleeper sample, suggests that ASR might have taken place. There are evidences that high early age temperature in concrete triggers both ASR and DEF ([4] and [5]).

5. CRACK PATTERNS AND MECHANICAL PROPERTIES OF CORE SAMPLES

5.1 Crack patterns in cut cross sections

To investigate inside crack progress, several locations of the PC sleepers were cut. Table 2 lists damage level and manufacturing year of the cut sleepers. Figure 4 shows typical inside crack patterns of “Severe damage” sleepers. In the cases of “No damage” sleepers, cracks are not observed in the cross sections.

Table 3: Damage level and manufacturing year of sleepers used for taking core samples

Damage level	Manufacturing year	Number of taken samples
I	2015	2
I	1986	2
II	2006	2
IV	2006	2



Figure 5: Core samples of "Severe damage" sleepers

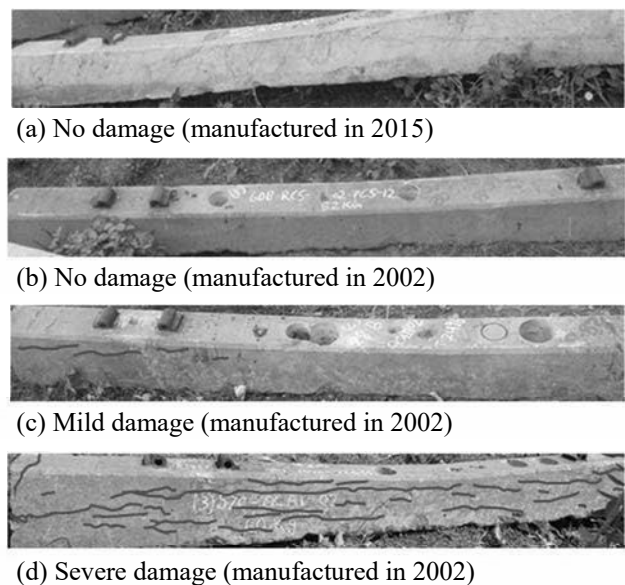


Figure 6: Damage conditions of sleepers for sample coring

In each damage level, depth of the cracks is about 20 to 30 mm. The cracks do not progress to the central part of the sleepers. Especially, crack width at the surface of “Severe damage” sleepers is larger than 2 mm, however, progress depth of the cracks is comparatively shallow. There is a tendency that inner macro cracks are not significant even though severe damage is observed on the surfaces. It can be considered that expansion of concrete caused by DEF and/or ASR is not uniform. Occurrence of DEF and ASR is affected by curing temperature and water content of the concrete. Cement hydration results the inner temperature to be higher than that near the surfaces. Also, depending on the environment condition around the structures, outside and inside water content becomes

different. From the above reasons, there is a possibility that the expansion strain occurred only in the inner part of the sleepers. When only the inner part is expanded, outer side of the concrete is subjected to tensile forces, as observed in the ring tension problem, resulting that cracks occur only in the outer part. Thus, crack patterns are affected by not only amount of expansion strain but also its spatial distribution.

5.2 Mechanical properties of core samples

Compressive loading tests of core samples taken from the sleepers were conducted. Table 3 lists damage levels

and manufacturing year of the core samples. Figure 5 shows a typical crack pattern of core sample taken from “Severe damage” sleepers. Figure 6 shows damage conditions of the sleepers used for taking core samples. Macro cracks were not observed in the core samples because cracks do not progress to the inner part of the sleepers as mentioned in 3.1. However, gaps can be noticed around the aggregates. It is because only the cement pastes are expanded by DEF as explained in the previous study [6].

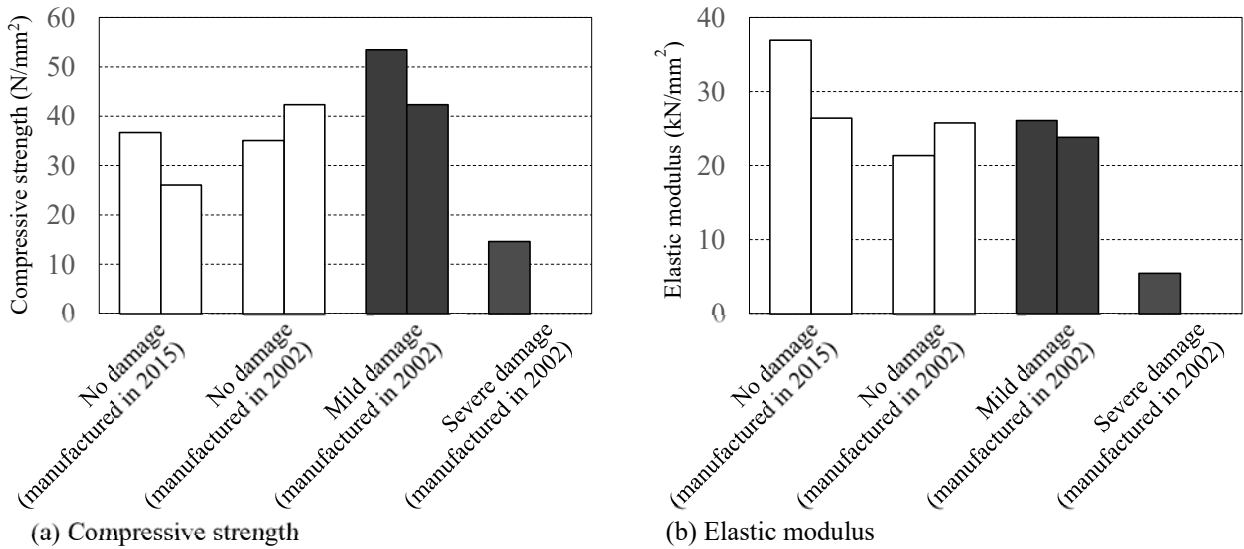


Figure 7: Results of compression tests of core samples

Table 4: Damage levels and manufacturing year of sleepers for loading tests

Damage level	Manufacturing year
I	2015
I	2015
I	2015
I	1986
I	1986
I	1986
II	2006
II	2002
III	2006
III	2006
III	2006
IV	2006
IV	2006
IV	2002
IV	2002

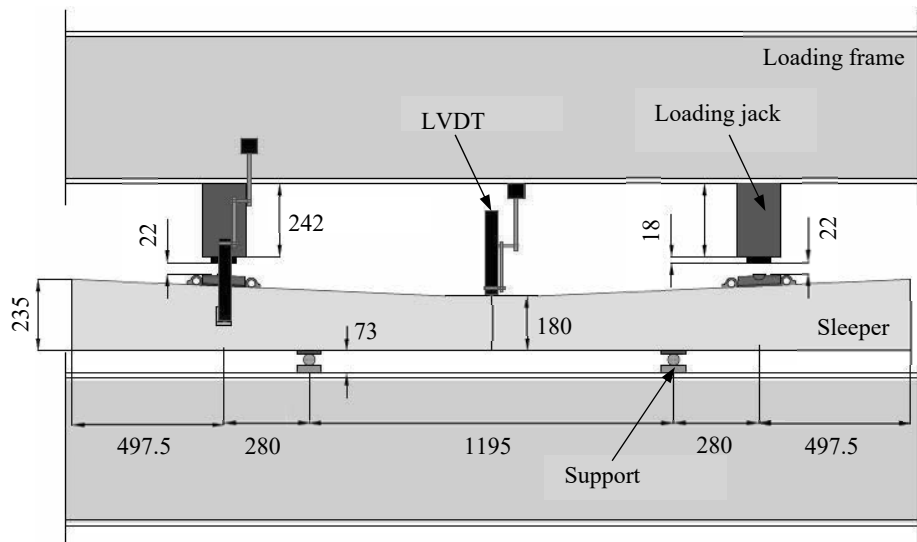


Figure 8: Apparatus of the loading test of sleepers (unit: mm)

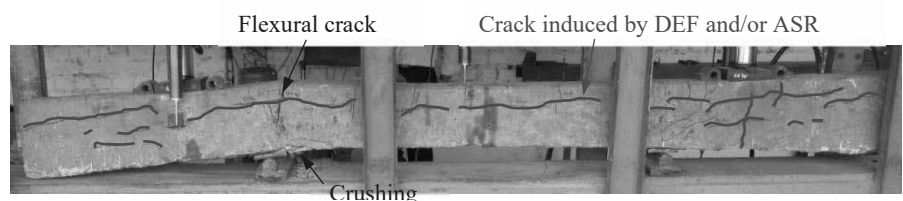


Figure 9: Failure pattern of “Severe damage” sleeper

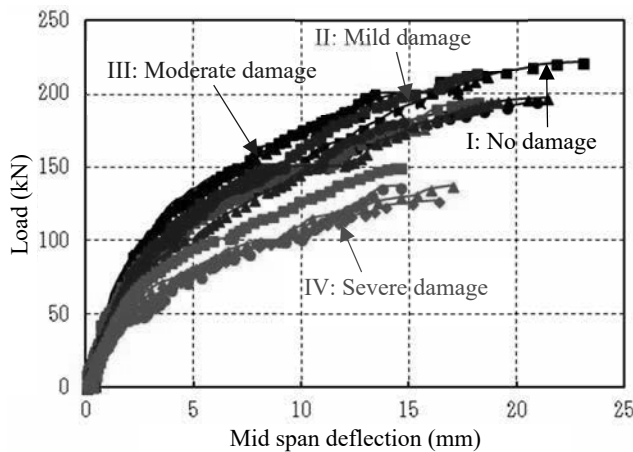


Figure 10: Load-mid span deflection relationships

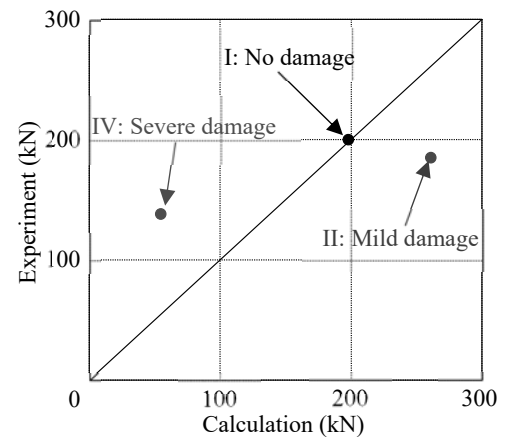


Figure 11: Comparison between calculated and experimental values of flexural capacities

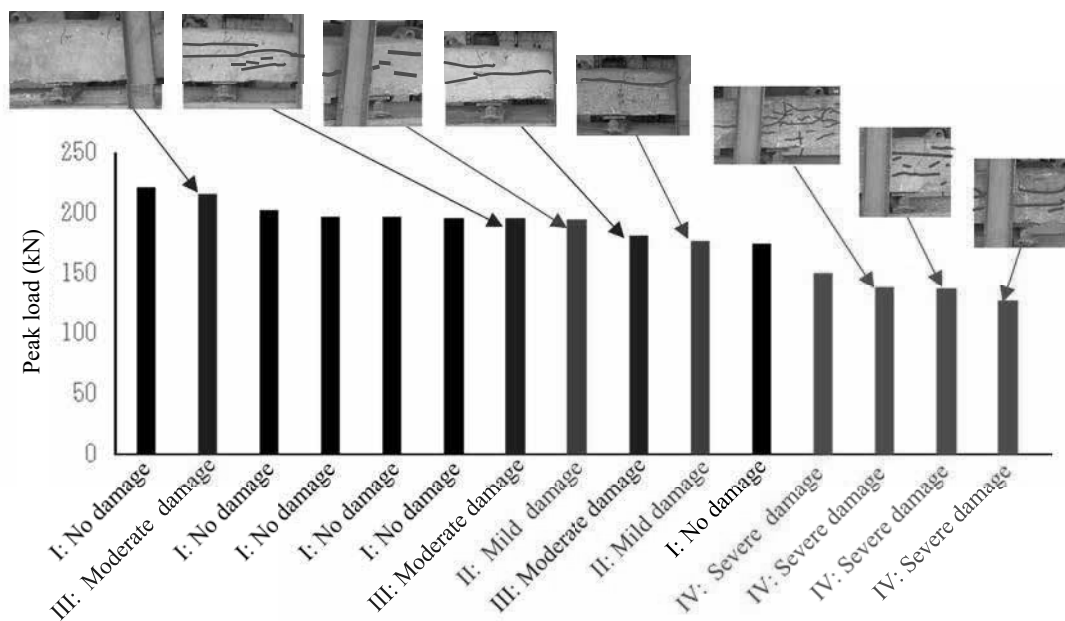


Figure 12: Peak loads versus crack patterns induced by DEF and/or ASR

Figure 7 shows the compressive strength and elastic modulus of the core samples. The elastic modulus was calculated based on Japanese Industrial Standard [7]. The results are slightly scattered, but there is a tendency that the elastic modulus decreases in the order of “No damage”, “Mild damage” and Moderate damage” while the compressive strength is almost constant. In the case of “Severe damage”, both compressive strength and elastic modulus significantly decreased. Compared to “No damage”, compressive strength and elastic modulus of “Severe damage” cases reduced by 42% and 17%, respectively. It reveals that mechanical properties of concrete decrease by gaps around the aggregates even if macro cracks do not occur.

6. INVESTIGATION OF STRUCTURAL PERFORMANCES OF DAMAGED PC SLEEPERS

6.1 Loading test

To investigate the structural performances of the damaged PC sleepers, two-point loading tests in the

simply supported condition were conducted. Table 4 lists damage levels and manufacturing years of the PC sleepers used for the loading tests. The tests were conducted by load control. The applied load was measured by load cells provided between the sleeper and the loading frame. The mid span deflection is calculated from displacements measured by Linear Variable Differential Transformers (LVDTs) installed at the mid span and supporting points. Figure 8 shows apparatus of the loading tests.

Figure 9 shows the failure pattern of “Severe damage” sleeper. After flexural cracks progressed, concrete was crushed at the compression fiber and the load suddenly decreased. The PC strands were not yielded, indicating that the failure mode was flexural compression failure. Figure 10 shows load-mid span deflection relationships. Especially in the case of “Severe damage” sleepers, both maximum load and member stiffness are reduced. Average of the maximum loads of “Severe damage” sleepers decreased to 69% of that of “No damage” sleepers.

Figure 11 shows the relationships between the maximum loads and crack patterns before the loading (that is, cracks caused by DEF and/or ASR). With wider crack width and larger number of cracks, the maximum load tends to decrease. It indicates that the damage levels determined by the method shown in Table 1 has a correlation with the structural performances. From this result, this study proposes classifications listed in Table 1 as an evaluation method for determining replacement priority of the damaged PC sleepers of Indian Railways.

6.2 Flexural capacity evaluation by macro equations

To investigate the possibility to evaluate flexural capacities of the existing damaged PC sleepers by using material test results of core samples, the flexural capacities are calculated by macro equations and compare them with the experimental results. In the calculation, a general method for calculating flexural capacities of PC members, in which plain strain distribution is assumed, is used. The test results of core samples (average values in Fig. 7) are used for compressive strength and elastic modulus of concrete. The equivalent stress block is assumed for stress distribution of concrete in the compression zone. In this calculation, the effect of concrete expansion and bond loss of PC strands on prestress is not considered.

Figure 12 shows comparison between the calculation and the experimental results. The calculated capacity almost agrees with the experimental result in the case of “No damage” sleeper. However, in the case of “Mild damage”, the calculation overestimates the capacity. It is considered that the compressive strength of the core samples in “Mild damage” cases is excessive. On the other hand, in the case of “Severe damage” sleeper, the calculation underestimates the capacity even though given compressive strength is obtained from the core samples which do not contain macro cracks. The failure mode in the calculation of “Severe damage” sleeper is almost near the compression failure of concrete just after the prestressing, however, such a behavior is not noticed in the experiment before the loading. One of the possible reasons is that prestress levels of the actual PC sleepers are decreased by bond loss of the PC strands after the concrete expansion. It is not easy to exactly predict the prestress loss due to expansion. However, this study confirmed that the macro equation can evaluate the decreasing tendency of flexural capacities according to the damage levels.

7. CONCLUSIONS

- 1) Temperature change during steam curing was measured in the factory of PC sleepers of Indian Railways. It revealed that the inner temperature of the concrete exceeds 80°C at the maximum. There is a high possibility of the occurrence of DEF.
- 2) Samples were taken from the damaged sleepers and SEM analysis was conducted. It was observed that gaps are formed around the aggregates and the gaps are filled with ettringite. It also indicates the occurrence of DEF.

- 3) An evaluation method for determining damage levels of PC sleepers of Indian Railways deteriorated by DEF and/or ASR was proposed. In the proposed method, damage levels are classified into “No damage”, “Mild damage”, “Moderate damage” and “Severe damage”.
- 4) The damaged PC sleepers were cut and inner crack patterns were investigated. Even “Severe damage” sleepers, cracks do not progress to the inner part. It is because the expansion strain occurs in only the inner part. Thus, not only amount of expansion strains but also spatial distributions of the expansion strain affects crack patterns.
- 5) Compression tests of core samples taken from the damaged sleepers revealed that compressive strength and elastic modulus significantly reduced in the case of “Severe damage” even though macro cracks are not observed. There is a possibility that mechanical properties of concrete affected by DEF decrease even though cracks on the surface are not visible.
- 6) According to the result of the loading tests of damaged PC sleepers, flexural capacities tend to decrease in the cases that DEF and ASR induce wider crack width and larger number of cracks. It indicates that the damage evaluation method proposed in study seems to be appropriate.

REFERENCES

- [1] H.Y. Ghorab., D. Heinz., U. Ludwig., T. Meskendahl. and A. Welter., (1980) “On the Stability of Calcium Aluminate Sulphate Hydrates in Pure Systems and in Cements,” *7th International Congress on Chemistry of Cement*, Vol. IV, pp. 496-503.
- [2] D. Heinz. and U. Ludwig., (1987) “Mechanism of Secondary Ettringite Formation in Mortars and Concretes subjected to Heat Treatment,” *American Concrete Institute, SP 100-105*, Detroit, pp. 2059-2071.
- [3] S. Hanehara. and T. Oyamada., (2010) “Reproduction of Delayed Ettringite Formation (DEF) in Concrete and Relationship between DEF and Alkali Silica Reaction,” *Monitoring and Retrofitting of Concrete Structures- B. H. Oh, et al. (eds) 2010 Korea Concrete Institute*, Seoul, ISBN 978-89-5708-181-5.
- [4] M. Thomas., K. Folliard., T. Drimalas. and T. Ramlochan., (2008) “Diagnosing Delayed Ettringite Formation in Concrete Structures,” *Cement and Concrete Research*, Vol. 38, pp. 841-847.
- [5] L. Baingam., W. Saengsoy., P. Choktaweekarn. and S. Tangtermsirikul., (2012) “Diagnosis of a Combined Alkali Silica Reaction and Delayed Ettringite Formation,” *Thammasat International Journal of Science and Technology*, Vol. 17, No. 4, pp. 22-35.
- [6] C. Famy., (1999) “Expansion of Heat-cured Mortar,” Ph.D Thesis, Imperial College of Science, Technology and Medicine.
- [7] Japanese Industrial Standards, (2017) “JIS A 1149: Method of Test for Static Modulus of Elasticity of Concrete.”

EFFECT OF SUB-STRATA LENGTH VARIATIONS ON SEISMIC PERFORMANCE OF MULTI-STOREY STRUCTURE WITH RAFT AND PILE FOUNDATION

M.S. ANU¹, V.S. VANI², R.R. RAJESWARA³, and M.NEERAJA⁴

¹ PG student, Civil Engineering Department, GITAM deemed to be University, Vizag, India, anuavanthika1@gmail.com

² Asst.Professor, Civil Engineering Department, GITAM deemed to be University, Vizag, India, drvsvani@gmail.com

³ Asst.Professor, Mechanical Department, GITAM deemed to be University, Vizag, India, r.resapu@gmail.com

⁴ Asst.Professor, Civil Department, GITAM deemed to be University, Vizag, India, medapatineeraja@gitam.edu

Keywords: L/D Ratio, ANSYS APDL, Soil structure-interaction, Raft, Pile Foundation, Seismic Performance

1. INTRODUCTION

Urbanization in the name of smart city is increasing day by day. These smart cities need to accommodate migrated people, resulting in growth of construction activities. The increased construction activities are imposing more loads on earth's crust especially in urban lands. Also deep foundations from the constructed multi-storey structures may also create disturbances on earth's crust changing profile of sub structure strata. This may result in movement of tectonic boundaries thereby increasing earthquake occurrences in recent past. During an earthquake lot of infra-structure damage is observed and the major damage is to structures. It is observed that interaction of surrounding sub-strata along with foundation plays a major role in response of structures during earthquake. The properties of surrounding soil to the structure and type of foundation also influence structural deformations and storey shears.

2. LAYOUT OF TEXT

PREVIOUSSTUDIES

Gaikwad M.V et.al[1], Sharmila Belkar et.al [2] etc., studied soil structure interaction considering seismic effects. Their studies concluded that the seismic parameters related to structure are affected by sub-strata that include type of soil, foundation.

METHODOLOGY

A G+5 RCC structure is modelled along with foundation (raft and pile), soil (marine clay) and bedrock (granite) considering Visakhapatnam sub-strata. It is modelled as continuum element using Ansys APDL. The dimensions of the model (Figure1) are given in Table 1.

Table 1: The details of the model

Structure Height	18 m
No. of floors & bays	G+5 & 4
Height of each floor	3 m
Area	23*23 m
Column & Beam size	0.5 m & 0.3 m (Beam 188 from Ansys library)
Soil dimensions	40 * 20 m, 80 * 20 m & 120*20 m (Drucker prager model)

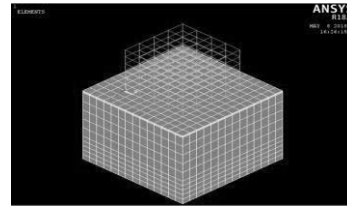


Figure 1: Model of G+5 Structure

The model with varying lengths (20, 40 and 120 m) with constant depth (20 m) is analyzed for using transient analysis by using El-Centro earthquake data [3]. The variations in seismic parameters like displacement and base shear is studied. An attempt has been made to correlate seismic parameters (peak displacement, maximum base shear) with length to depth (L/D) Ratios

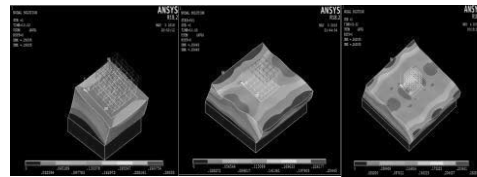


Figure 2: Total displacement of structure with varying lengths for raft foundation

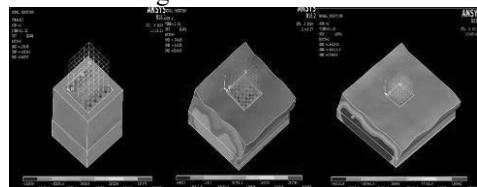


Figure 3: Total shear with varying lengths for raft Foundation

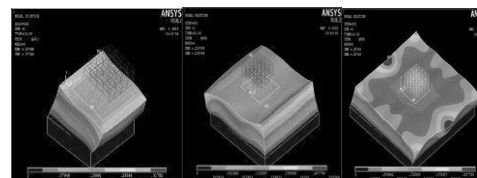


Figure 4: Total displacement of structure with varying lengths for pile foundation

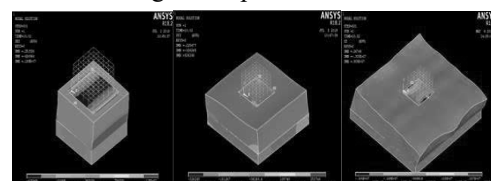


Figure 5: Total shear with varying lengths for pile Foundation

RESULTS AND DISCUSSIONS

The results obtained from the model structure after EI Centro Earthquake [3] is analyzed in terms displacement and shear for both raft and pile foundation.

It is observed from Figure 2 that the structure exhibited more deformations when compared to soil during earthquake in raft foundation. From the obtained results, graph (Figure 6) is plotted between total peak displacement and L/D ratio for nodes in structure and soil separately. An equation is obtained for deformation (structural nodes) using regression analysis is second degree polynomial as in (a) with $R^2 = 1$.

$$Y = 0.0016x^2 - 0.0379x + 0.359 \text{ -----}>(a)$$

The equation is tested for intermediate L/D ratio 3 for which it resulted peak displacement 0.2597. To simulate similar conditions the opted model length is 60 m for same constant depth 20 m. The model is analyzed and obtained peak displacement is 0.28961 for node 161. The error obtained from above model is 12% considering displacement in structure. Considering SSI (soil nodes) the L/D indicates only position of peak displacements i.e., shifting from structure to soil through foundation.

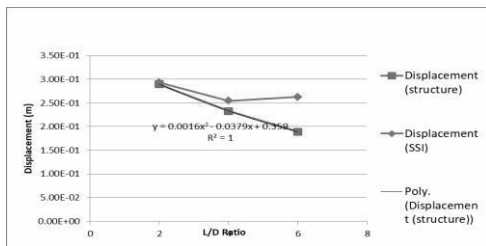


Figure 6: Variation of peak displacement for L/D for raft foundation

Figure 3 it is observed that the shear is more in soil structure junction at the structural base. From the obtained results, graph (Figure 7) is plotted between total base shear and L/D ratio.

From the Figure 7 it is observed that the variation of maximum shear shifted downward as L/D increased considering SSI

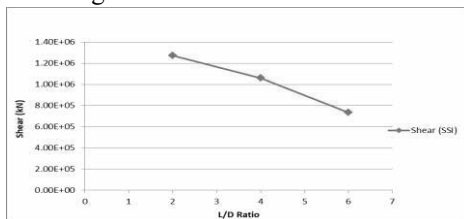


Figure 7: Variation of maximum shear for L/D in terms of varying lengths for raft foundation.

From the obtained results, graph is plotted between total peak displacement and L/D ratio for nodes in structure and soil separately for pile foundation (Figure 8). An equation is obtained for deformation considering structural nodes using regression analysis. It is a second degree polynomial as in (b) with $R^2 = 1$. A correlated equation cannot be obtained for nodes in soil.

$$Y = 0.0073x^2 - 0.1059x + 0.5402 \text{ -----}>(b)$$

Figure 9 shows variation of maximum shear for L/D in terms of varying lengths for raft foundation. The variation of maximum shear cannot be predicted using

L/D ratios.

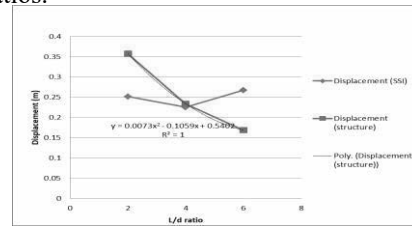


Figure 8: Variation of peak displacement for L/D in terms of varying lengths for pile foundation

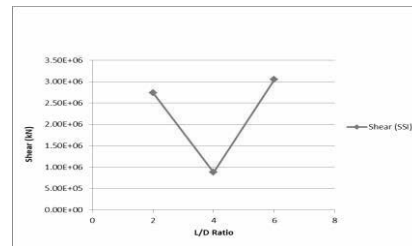


Figure 9: Variation of maximum shear for L/D in terms of varying length for pile foundation

Considering shear with the help of L/D ratio (Figure 9) neither position nor value can be predicted for intermediate values.

3. CONCLUSIONS

- For both raft and pile foundation, value of maximum shear at intermediate L/D ratios cannot be predicted. But the position of maximum shear can be predicted at intermediate L/D values which may occur on the plane of foundation and structure or soil.
- For both raft and pile foundation, value of maximum displacement at intermediate L/D ratios can be predicted for length variation (as per polynomial second degree). These values are shifting towards bottom storeys of structure as the length increased.
- For both foundations it is observed that adjacent buildings to the existing building will be affected within the range of 50 m from the adjacent building.

REFERENCES

References in the text should be numbers in square brackets like this [1]. The details of references are required to be provided in the following format given below.

Reference to a journal publication:

[1] Gaikwad M.V, Ghogare R.B and Vageesha S.Mathada, "Finite Element Analysis of Frame with Soil Structure Interaction", International Journal of Engineering Research and Technology, 2015, Volume 4 Issue 1, PP 91-95.

[2] Sharmila Belkar and Dr. Kiran Ladhane, "Dynamic Analysis of Soil Structure Interaction of Pile Supported Frame Structure", International Journal of Scientific & Engineering Research, 2015, Volume 6, Issue 10, pp 704-708.

AUTOMATIC AND HIGH-SPEED DAMAGE DETECTION OF REINFORCED CONCRETE BRIDGE SLAB BY GROUND PENETRATING RADAR

T. MIZUTANI¹, T. TAMAGUCHI²

¹ Project lecturer, Institute of Industrial Science, , The University of Tokyo, Tokyo, Japan, mizu-t@iis.u-tokyo.ac.jp

² Ph.D. Student, Department of Civil Engineering, The University of Tokyo, Tokyo, Japan, tyamaguchi@bridge.t.u-tokyo.ac.jp

Keywords: Ground Penetrating Radar, Bridge Deck, Damage, Crack, Segregation, Signal Processing

The costs of maintenance and replacement of highway in Japan are estimated about 4 trillion yen in 2015 which is equivalent to a few percent of Japanese national budget. The large percentage of the cost is for repair and replacement of reinforced concrete (RC) bridge slabs due to their deterioration. Countries other than Japan is considered to face with similar situation in present days or in the near future. In order to maintain transportation safety with a limited budget, inexpensive and reliable condition evaluation techniques of RC slab should be developed. Human-based inspection methods, such as dense hammering test on slab surface, have been conducted so far, however to conduct those inspection, pavements need to be removed beforehand and lane restrictions should be taken. As a result, those tests become time-consuming and costly. In addition, those inspection result have variation because the human-based test highly depends on the ability of inspectors.

Up to now, a variety of non-destructive testing techniques, for example Thermography, Impact-Echo method, Radar and etc., have been proposed and developed. As a particularly promising technique in these techniques to detect damages inside bridge slab automatically, radar technique which can realize non-contact and high-speed measurement is focused on in this research. Radar techniques are already practically used as “Ground Penetrating Radar (GPR)” to detect extraneous material, holes inside ground. There are some typical damages of bridge slab which can lead to serious damage such as holes. Horizontal cracks with width less than 1 mm can occur in the vicinity of upper reinforcement bar (rebar). If horizontal cracks deteriorate more, damage becomes “Sand-like” damage which is called “segregation”. To prevent the serious damage occurrence mentioned above, in the stage of horizontal crack or segregation, damage should be detected.

In present damage detection via GPR system, inspectors are just visually checking the image of reflected wave signal from slabs. However, the signal change at damage area are really slight because the wavelength of Ultra High Frequency (UHF) radio wave used in existing GPR system is several hundred times larger than the vertical scale of the damages. Thus, accurate damage detection is really difficult and the detection accuracy highly depends on the inspectors’ ability and expertise. In addition, the image-checking by inspectors are really time consuming and requires lots of effort. To increase the damage detection accuracy and realize automatic damage detection to decrease the



Figure 1: Ground Penetrating Radar-Mounted Vehicle



Figure 2: Example of Signal Processing Result

inspection time and the labor cost, the system should be improved from the both the sides of software and hardware.

To improve the software at first, the purpose of this research is set to develop the signal processing algorithm to detect damage of slab from radar signals. For hardware, GPR (Stepped Frequency-Continuous Wave (SF-CW) type, and 200 MHz-3.02 GHz range) which is already commercialized and which can realize on-vehicle measurement are utilized in this research[1], [2].

REFERENCES

Reference to a journal publication:

- [1] Tsukasa Mizutani, et al., “Bridge Slab Damage Detection by Signal Processing of UHF-Band Ground Penetrating Radar Data,” Journal of Disaster Research, Vol.12 No.3, pp. 415-421, 2017.
- [2] Takahiro Yamaguchi, Tsukasa Mizutani, “Sensitive Damage Detection of Reinforced Concrete Bridge Slab by “Time-Variant Deconvolution” of SHF-Band Radar Signal,” IEEE Transactions on Geoscience and Remote Sensing, 2018. (to appear)

USMCA 2018

SESSION 2

DISASTER MANAGEMENT I

Vulnerability Assessment of Soft Brick Unreinforced Masonry Walls: Study of 2001 Gujarat Earthquake

Jayaprakash Vemuri¹, Syed Ehteshamuddin², Kolluru V.L. Subramaniam^{3*}
^{1,2,3} Indian Institute of Technology Hyderabad

Abstract

Unreinforced soft-brick masonry structures comprise a large portion of buildings in seismic prone regions of India. Recent earthquakes have extensively damaged such structures. Experimental and numerical studies on soft brick unreinforced masonry structures are scarce in literature. The 2001 Bhuj earthquake which struck the Kutch region in the western part of India, *was the strongest intraplate earthquake to have occurred in the past century*. The earthquake caused widespread damage to unreinforced brick masonry (URM) structures in the region. Assessing the vulnerability of the non-engineered masonry structures in this region is complicated by the lack of ground motions and realistic models for cyclic response of masonry. In this study, a suite of strong ground motions for the region is generated using the modified stochastic finite fault method. Numerical simulation of soft brick unreinforced masonry panels subjected to lateral loads is performed. At the panel level, the masonry structure is modelled using the micro modelling approach within a finite element framework. Cyclic load analyses are performed on the finite element model to understand the complex hysteretic behaviour of unreinforced soft-brick masonry walls. A hysteretic model was calibrated to experimental data of unreinforced masonry shear walls. Nonlinear time history analyses are performed on validated models of two unreinforced masonry shear walls. The analytical results correlate well with observed damage to URM structures. Seismic fragility curves indicate high vulnerability of URM structures under the expected range of seismic intensities for the region.

Numerical Analysis of Soft Brick Masonry Walls

Numerical models are used for a better understanding of the behaviour of masonry walls for scenarios different from the ones tested in experiments. In this paper, the simplified micro-modelling strategy is adopted, and numerical simulations are performed to assess the lateral load response of masonry walls made with soft bricks. In this paper, the in-plane behaviour of soft brick URM at the panel level is numerically investigated using the simplified micro modelling approach. Lourenco and Rots (1997) developed a multi-surface interface model by including three yield effects: cap model for compressive failure, tension cut-off for tensile failure and Mohr-Coulomb failure envelope for shear failure. All the basic types of failure mechanisms associated with masonry, namely diagonal shear failure, bed-joint sliding failure and flexural failure are evaluated. The crack interface reproduces the jump from one head joint into the other, implying that all inelastic phenomena occur in the interface elements resulting in a robust type of modelling. In micro-modelling, zero thickness interface is adopted, and the size of the unit is expanded by half mortar thickness in both directions. Numerical analysis was performed using FEM platform DIANA[®], to obtain the monotonic load-deformation response of the masonry under a constant applied compression. Brick and mortar properties of the wall were obtained from experiments carried out brick and mortar prisms by Ravula and Subramaniam (2017). The shear and tension parameters of the joint interface were taken the same for the three aspect ratios to observe the influence of brick and mortar strengths. For cracks, the tensile strength, f_t was taken as $1/10^{\text{th}}$ of brick strength, and high stiffnesses (k_n, k_t) were considered as suggested by Lourenco and Rots (1997). For joints, the normal stiffness, k_n and the tangential stiffness, k_t , were calculated using Equation (7) and (8). The values of cohesion, c , friction angle, μ and cap compressive strength were taken from Ravula and Subramaniam (2017). Diagonal cracking marks the ultimate or peak load carrying capacity of the wall (marked in Figure 1). The cyclic load response of wall obtained from the numerical analysis is shown in Figure 1. The non-linear analysis was carried out in two stages. In the first stage, axial stress was applied to its full value, and in the second stage, cyclic displacements of 6 cycles was applied.

* Corresponding Author: Professor, Department of Civil Engineering, I.I.T. Hyderabad, Kandi, Sangareddy, Hyderabad, Telangana 502285, INDIA. Email: KVLS@iith.ac.in

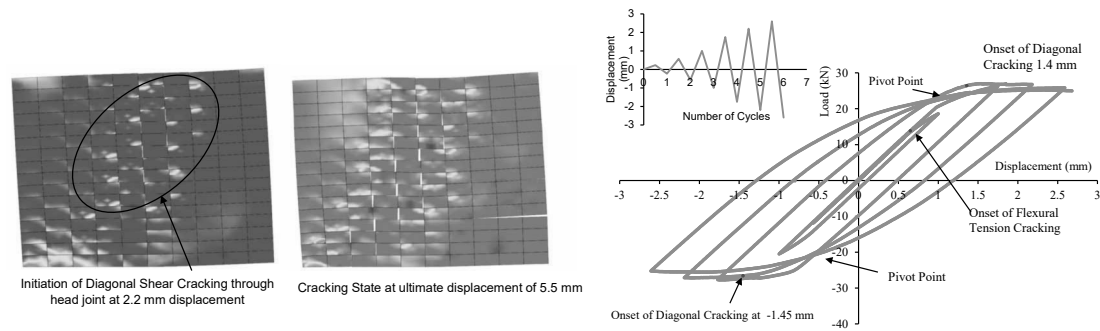


Figure 1: Stages of Shear Diagonal Stepped Cracking for Shear Load Response; Cyclic load response

Ground Motions and

Strong motion records from the 2001 Bhuj earthquake are not available. In such regions where a rich database of historical strong motions is unavailable, modified records may be obtained either by generating artificial records or by altering natural records. Both physical and numerical models are available to generate synthetic records, which have a natural appearance and strong motion duration similar to that of a real record. In this study, the modified stochastic finite fault method is used to generate synthetic ground motions. Beresenev and Atkinson (1997) extended the stochastic point source model to large faults by dividing entire fault into smaller sub-faults and considering each sub-fault as a point source. Table 1 shows the characteristics of the synthetic ground motions generated for various towns in Gujarat. These towns are situated across various seismic zones as per the seismic zonation map of India (IS1893:2016). The simulations were conducted at hard rock sites with shear wave velocity of 2900 m/s. The simulations were also carried out at generic rock using crustal amplification factors estimated for eastern North America at the NEHRP B/C boundary ($V_s = 760$ m/s). The values at Anjar, Naliya, Junagarh, Ahmedabad, and Anand are comparable at the NEHRP B/C conditions ($V_s 760$ m/s). The values at Khambaliya, Jamjodhpur, and Amreli compare well with PGAs estimated at these sites for hard rock conditions. These sites are hard rock sites situated on Deccan basalt. The epicentral distance of the station, the peak ground acceleration (PGA), are tabulated.

Table 1 Comparison of PGA values – Present Study and Recorded

S. No.	Site	Site Class (NEHRP)	Epicentral Distance (km)	Recorded PGA (g)	Recorded PGA (g) $V_s 760$ m/s (Corrected to B/C)	PGA (g) of Simulated GM $V_s 760$ m/s B/C (NEHRP)	PGA(g) of Simulated GM $V_s 2900$ m/s (Hard Rock)
1	Anjar	C	44	0.65	0.580	0.564	0.315
2	Kandla	C	53	0.35	0.326	0.446	0.241
3	Niruna	D	97	0.32	0.241	0.360	0.208
4	Naliya	C	147	0.29	0.215	0.222	0.123
5	Khambaliya	A	150	0.072	0.143	0.192	0.104
6	Jamjodhpur	A	166	0.088	0.088	0.128	0.073
7	Dwarka	D	188	0.085	0.061	0.199	0.107
8	Porbandar	D	206	0.076	0.054	0.143	0.076
9	Junagarh	A	216	0.075	0.075	0.084	0.049
10	Amreli	A	225	0.039	0.039	0.080	0.045
11	Ahmedabad	D	238	0.11	0.080	0.080	0.046
12	Cambay	D	266	0.20	0.143	0.062	0.038
13	Anand	D	288	0.058	0.041	0.053	0.032

In Figure 2 the PGA and the PGV are correlated with drift displacements of the walls. The limit states of cracking, ultimate and collapse are marked for reference. It is observed that ground motions with high PGA levels ($>0.1g$) excited the walls to the post peak regime causing collapse. This corresponds well with actual damage to masonry structures as observed in reconnaissance surveys (Jagadish et al., 2001).

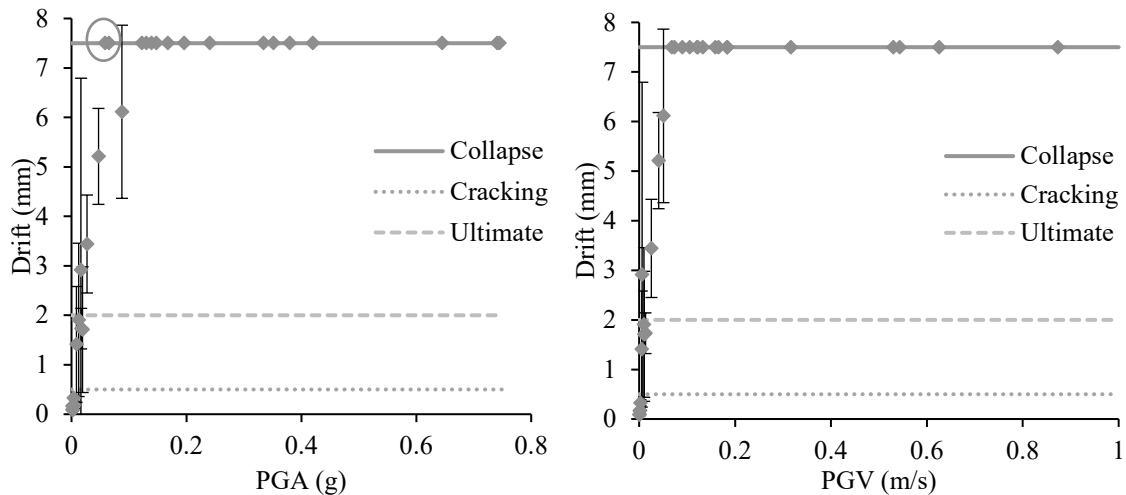


Figure 2. (a) Drift versus PGA (b) Drift versus PGV

References

- Vemuri, J., Ehteshamuddin, S., & Kolluru, S. V. (2018). Evaluation of seismic displacement demand for unreinforced masonry shear walls. *Cogent Engineering*, 1480189.
- Ravula, M.B. and Subramaniam, K. (2017) Experimental investigation of compressive failure in masonry brick assemblages made with soft brick. *Materials and Structures*, 50:19.
- Lourenco PB, Rots JG (1997) Multi-surface interface model for analysis of masonry structures. *Journal of Engineering Mechanics*, 123(7), 660–8.
- Shing P, Cao L (1997) Analysis of partially grouted masonry shear walls. US Department of Commerce, Gaithersburg, MD20899, NIST GCR, 97-710
- Oliveira D, Lourenco P. (2004) Implementation and validation of a constitutive model for the cyclic behaviour of interface elements. *Computers and Structures*, 82(17), 1451–61.
- TNO DIANA BV. (2011). *Diana user manual. Release 9.4.4*, Delft, Netherlands
- Boore D, (1983) Stochastic simulation of high-frequency ground motions based on seismological models of the radiated spectra, *Bulletin of Seismological Society of America*, 1983, 73(6): 1865–1894.
- Anderson J and Hough S, (1984) A model for the shape of the Fourier amplitude spectrum of acceleration at high frequencies, *Bulletin of Seismological Society of America*, 1984, 74(5): 1969–1993.
- Beresnev IA, and Atkinson, GM, (1997) Modeling finite fault radiation from the w_n spectrum, *Bulletin of Seismological Society of America*, 1997, 87(1): 67–84.
- Narayan JP and Sharma ML (2004) Effect of Local Geology on Damage Severity during Bhuj, India earthquake, *Proceedings of the Thirteenth World Conference on Earthquake Engineering*, 2004, Paper No.2042, August 1-4, Vancouver, Canada
- Jagadish, K., (2003). Behaviour of masonry structures during the Bhuj earthquake of January 2001, *Journal of Earth System Science*, **112** (3), 431-440

THE WAY OF LEADERSHIP AT CRISIS MANAGEMENT

TETSURO ITO

Visiting Professor, University of Tokyo, Tokyo, Japan t-g-ito@iis.u-tokyo.ac.jp

Keywords: *Way of Leadership, Crisis Management, Accountability*

1, IMPORTANCE OF CRISIS MANAGEMENT

It is important for a leader to know what he should perform based on the occasion of the crisis. The following crisis management actions are basic at the time of crisis.

- 1) Grasping of the situation by information collection
When a crisis occurs, it becomes important how you collect necessary information quickly and precisely.
- 2) Predicting the development of the situation with limited information.

While there is limited information it is necessary to guess what is taking place and to predict how the situation will develop.

3) Quick response

It is vital to build a system to take action quickly and decide a policy to cope with a crisis.

4) Decision making

It is important to decide what kind of policy and system is to be taken to cope with a crisis quickly.

5) Operation

It is needed to build up the system and handle the operation to cope with a crisis appropriately.

6) The crisis communication

Emergency outbreak increases the importance of communication among people compared to the normal time.

2. THE LEADERSHIP

The role of leader at the time when emergency situation occurs is important. Important thing for leader is to judge the situation and to decide what to do. In case of emergency, it sometimes happen that information about the situation is limited, it is required that leader makes quick judgement and decides the countermeasures to deal with the emergency.

It is dangerous for a leader to watch the situation and not to make any decision during the emergency. A delay of the first action due to leader's decision to wait until the situation is fully understood can produce irreparable situation. Quick judgment of the situation and determination of countermeasures for a crisis is ability which is needed for a leader.

2. ACCOUNTABILITY OF LEADER

It is important for a leader to explain by himself on the occasion of the outbreak of the crisis what kind of crisis is taking place, what the coping policy is and how he or she is going to deal with the situation. It is important that a leader shows readiness and posture that he will be responsible for the actions taken during the crisis management.

When a crisis takes place, the trust for a leader is important to people above all since there is no choice for them unless they trust the decision of the coping policy and method of their leader. It is also important that a leader shows the leadership, gains trust from the people, and to give people relief. And these attitude encourages the subordinate. The leader should speak his or her thought resolutely and must act to show strong determination to deal with a situation by his or her own responsibility, and gain trust from the people.

3, THE WAY OF LEADER

The judgement of the situation by the leader at the time of the crisis outbreak and the decision of the coping policy are naturally accompanied by the responsibility. It is the worst to put off the decision because he or she is afraid of making an error. Leader must have the readiness to take responsibility for the result and the courage to make decision quickly and to carry out the countermeasures which leader regards as the best measures.

The leader who watches the situation, does not dare to judge the situation, dodge one's responsibility, and not cope with the crisis should be said that he or she is the least desirable leader at the time of the emergency. And it may be said the true value of the leader appears in the case of a crisis. Therefore, it is necessary for the leader to develop mental attitude preparing for a crisis all the time.

DEVELOPMENT OF DISASTER PROCESS MANAGEMENT SYSTEM

MUNEYOSHI NUMADA¹ and KIMIRO MEGURO²

¹ Associate Professor, Institute of Industrial Science, The University of Tokyo, Tokyo, Japan, numa@iis.u-tokyo.ac.jp

² Professor, Institute of Industrial Science, The University of Tokyo, Tokyo, Japan, meguro@iis.u-tokyo.ac.jp

Keywords: PGA, BOSS, Disaster Process, Information Management

1. INTRODUCTION

This research is to define the response process and optimization of workload needed for disaster response in local government level. The focus of the research is to simulate the available and necessary responses based on the disaster occurrence situation based on the location of hazard attack, social conditions etc. A developed system called BOSS (Bosai or Business Operation Support System) is to support a disaster process management for a disaster situation. 48 kinds of works and about 500 processes are defined to analyze disaster responses in BOSS.

2. METHOD

To show how the response system works, after the location of a disaster has been identified, social data, the damage estimation and the necessary responses are described. The PGA (Peak Ground Acceleration) distribution according to the monitored data for an earthquake disaster and the floods distribution for a meteorological disaster are used to calculate the damage situation, and then the volume of response workload is evaluated based on the damage level. USGS (U.S. Geological Survey) feeds the API (Application Programming Interface) of earthquakes monitoring data as real-time Geo-JSON style (Figure 1). BOSS connects to the real time API of earthquake occurrences by USGS. Big process manages the detail process in BOSS (Figure 2). Detail explanation about the process is shown to understand the contents of the process. Some necessary documents are linked to the detail processes. BOSS is used in the Kumamoto prefecture in Japan where experienced for the 2016 Kumamoto earthquake disaster

for the verification and update PDCA cycle for the response processes.



Figure 1: Real-time PGA distribution and affected population map

3. CONCLUSIONS

The basic disaster response processes are defined based on the analysis of past disaster responses in local governments. Then developed system BOSS is implicated in the local government to support the initial responses.

The training system is needed to educate the stakeholders to understand effective disaster responses by BOSS. This research also developed the disaster management training program by Disaster Management Training Center in the University of Tokyo (DMTC) to provide the professional disaster related knowledge and skills.

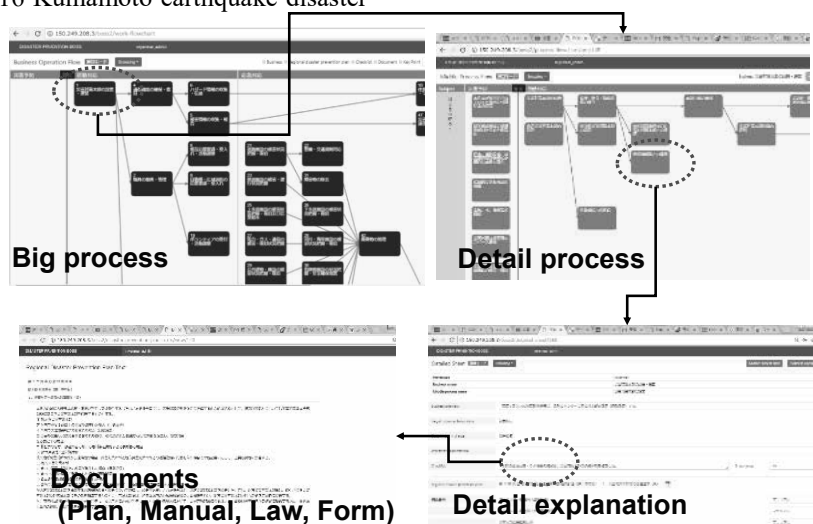


Figure 2: Organization of the data transfer in BOSS

TOWARDS A DISASTER RESILIENT SOCIETY USING REMOTE SENSING TECHNOLOGY

H. GOKON¹, Y. KATAIE², M. KUWA³, S. KONDO⁴ and K. MEGURO⁵

¹ Assistant Professor, ICUS, IIS, UTokyo, Tokyo, Japan, gokon@iis.u-tokyo.ac.jp (corresponding author)

² Visiting Associate Professor, Wakayama University, Wakayama, Japan, kataie_y0001@pref.wakayama.lg.jp

³ Visiting Associate Professor, Wakayama University, Wakayama, Japan, kuwa_m0001@pref.wakayama.lg.jp

⁴ Associate Professor The School of Regional Design, Utsunomiya University, Japan, kondos@cc.utsunomiya-u.ac.jp

⁵ Professor, ICUS, IIS, UTokyo, Tokyo, Japan, meguro@iis.u-tokyo.ac.jp

Keywords: Tsunami, Remote sensing, Disaster management

1. Introduction

Tsunami causes heavy and extensive damages along coastal regions. In case of the 2011 Tohoku earthquake and tsunami disaster, 561 km² was inundated with the maximum run up height of 40.5 meters. 127,829 buildings were collapsed by the tsunami. 15,894 people were killed and 2,562 were still missing as of 10 February 2016. Under this situation, we might face the difficulties to understand comprehensive impacts caused by a tsunami disaster due to break downs of communication network and interceptions of emergent routes. This will lead to delays of decision makings that are related to disaster response. Therefore, the decision maker need to comprehend the impacts as soon as possible. Remote sensing technology is an only solution for this problem. Satellite / airborne remote sensing technology enables us to identify the extensive impacts within a short time without visiting the affected areas. Especially, synthetic aperture radar (SAR) is very useful because of the wide availability that works under all weather conditions in day and night time.

Opportunities to use remote sensing technologies for a disaster response in Japan have been increased. However, recent advanced technologies are not fully utilized for the response activities done by local governments. One of the possible reason is that effects for mitigating the work loads and damage assessment time have not been evaluated quantitatively. Therefore, this study aims at evaluating the effects in case of a local government affected by the 2011 Tohoku earthquake and tsunami.

2. Method

This study is divided into two parts; (1) A development of damage estimation methods with remote sensing technology for discussing limitations and capabilities in disaster response, (2) Evaluating the effects of the method for reducing the work loads and saving time.

2.1 A review of damage estimation methods

Gokon et al.(2016, 2017) developed methods for estimating building damages in tsunami affected areas using X-band SAR satellite data and L-band SAR satellite data.

Based on a change detection technique using pre- and post-event SAR data, damage ratios of washed-away buildings were estimated using damage function developed by Gokon et al.(2016, 2017) (Figure 1,

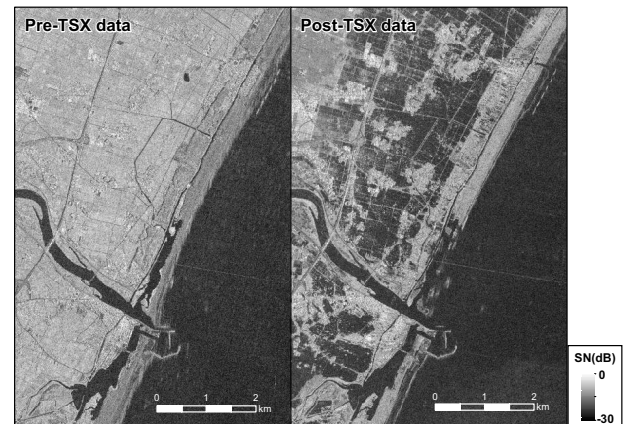


Figure 1: Pre- and post-event TerraSAR-X data

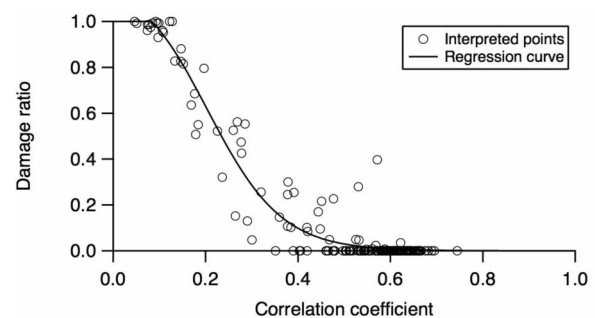


Figure 2: Damage function

Figure 2). The number of washed-away buildings were estimated by multiplying by the pre-event number of buildings in local scale (Figure 3). Finally, the results were assessed by comparing with truth data showing the pearson's correlation coefficients of 0.98 – 0.99 in case of using X-band SAR data, and 0.87 – 0.98 in case of using L-band SAR data (Figure 4).

2.2 Effects of reducing work loads and saving time

To evaluate the effects of remote sensing in reducing the work loads and shortening time of disaster response, Ishinomaki City, which was devastated by the 2011 Tohoku earthquake and tsunami, was selected as the study area. Building damages caused by the tsunami, schedules of building damage survey for victim's certificate and number of persons who assigned for the survey were investigated.

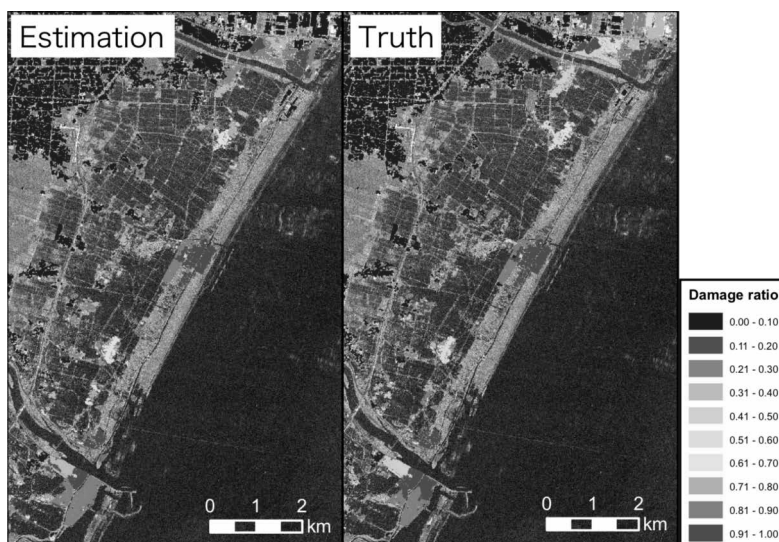


Figure 3: Damage ratios of washed-away buildings.

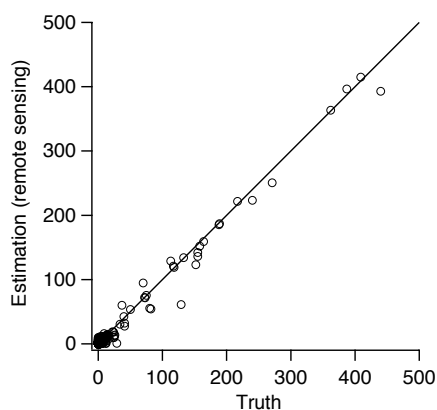


Figure 4: Accuracy assessment of damage estimation.

Next, reducing work loads and saving time are estimated by comparing the historical data in Ishinomaki City, time for damage estimation using remote sensing technology and performance of the damage estimation.

2. Results and discussion

The results of the investigation in Ishinomaki City is specified as follow.

Building damage in Ishinomaki City was 44,076 (Collapsed : 14,263, Major damage : 9,465, Partial damage : 2,356, Slight damage : 17,992). Building damage surveys were performed totally three times.

First survey was conducted from 25th to 27th in March 2011 to identify the collapsed areas by 2 groups including 2 persons for each, that is 4 persons / day. The second survey was performed from 4th April 2011 to 4th May 2011. This time, 10 groups with 3 persons for each, that is 30 persons / day, investigated building damage based on interpretations from outside and an inundation depth at the location of the building. The third survey was conducted from 20th May 2011 to 31st May 2011 by 10 groups with 3 persons for each. Not only from outside of the building, but also inside was investigated this time.

The proposed remote sensing method can identify the devastated areas with high performance. Therefore, there

is a possibility to contribute to the first survey. Image processing time for estimating the damage in coastal regions of Miyagi prefecture can be finished within one day by one person. The observation time of TerraSAR-X satellite imagery was 13 March 2011(JST). So, if we could finish the image processing within one day, we might have been able to finish the identification of collapsed areas by 14 March 2011. In that case, decision making for the second and third surveys might be shorten for 2 weeks. Furthermore, 4 persons * 3 days = 12 (persons*day) might be saved. As the result of this discussion, we found the possibility to reduce the time for decision making for building damage survey and victim’s certificate, and saving the limited resources soon after the tsunami disaster.

3. CONCLUSIONS

Effectiveness of remote sensing technologies for disaster response was evaluated in case of the 2011 Tohoku earthquake and tsunami. As a remote sensing technology using SAR data is utilized for building damage survey for victim’s certificate, 14 days might be shortened, and 12 persons*day might be saved in human resources.

REFERENCES

[1] H. Gokon, S. Koshimura and K. Meguro, Verification of a method for estimating building damage in extensive tsunami affected areas using L-band SAR data, Journal of Disaster Research (JDR), Vol.12, No.2, 2017
 [2] H. Gokon, S. Koshimura and M. Matsuoka, Object-based method for estimating tsunami-induced damage using TerraSAR-X data, Journal of Disaster Research, vol.11 (2016), No.2, pp.225 - pp.235

GENERATION OF GROUND MOTION PREDICTION EQUATION FOR IRAN

Chenna RAJARAM¹, Ramancharla PRADEEP KUMAR²

¹ Assistant Professor of Civil Engineering, Rajeev Gandhi Memorial College of Engineering & Technology, Nandyal, INDIA, drchenna78@gmail.com

² Professor of Civil Engineering, International Institute of Information Technology - Hyderabad, Gachibowli, Hyderabad, INDIA ramancharla@iiit.ac.in

Keywords: Ground Motion Prediction Equation, Ground Acceleration, Hazard, Earthquake

ABSTRACT

For the assessment of risk of any area three components are necessary viz., Hazard, Exposure and Vulnerability. While most of the times Exposure and Vulnerability are easy to obtain compared to Hazard. The selection of Ground Motion Prediction Equations (GMPE) is a fundamental component of any seismic hazard analysis. Current research is focused on catalogue of the earthquakes occurred in Iran from 1974 to 2017, which is taken from Building & Housing Research Center (BHRC), Iran. The catalogue consists of 13 strong to major earthquakes (6.0 > Mw > 7.8) and 660 seismic stations in Iran. The catalogue consists of 13 strong to major earthquakes (6.0 > Mw > 7.8) and 660 seismic stations in Iran. The GMPE at bedrock level is calculated

$$\log_{10}(Y) = 3.731 + 0.238M - 2.776 \log_{10} \sqrt{R^2 + h^2} + 0.289S + 0.48F + \epsilon$$

1. INTRODUCTION

Geophysical parameters play a vital role in generating synthetic accelerograms. Estimation of these parameters needs huge earthquake catalogue and ground motion data. Over estimation or under estimation of these parameters lead unrealistic ground motion records, which cause effect to the structure. In this study, Ground Motion Prediction Equation (GMPE) is derived for Iran. GMPE equations are frequently used for engineering purposes to estimate peak ground acceleration (PGA). This PGA helps to estimate amount of seismic force acting onto the structure. Numerous studies have been done worldwide on GMPE to estimate seismic hazard. Literature suggested few GMPE equations can be used for Iranian region [1]-[5]. The present study attempts to propose GMPE exclusively for Iranian region with Iranian seismic catalogue.

2. GROUND MOTION PREDICTION EQUATION

The GMPE relationships are commonly represented as ground motion parameters in a function form. They depend on the magnitude of the earthquake, distance from source to site, type of fault, soil conditions etc. So, these seismological parameters should be chosen carefully for a region. Peak ground motion values are approximately log-normally distributed. As a result, regression is usually used on the logarithm of predictive term than the term itself. Earthquake magnitude is typically defined as the logarithm of some peak motion parameters. Consequently, the magnitude is approximately proportional to the logarithm of peak

ground motion values. The energy of seismic waves gets attenuated as waves travel away from the source. The amplitudes of body waves decrease proportionally to the reciprocal of distance and surface wave amplitudes decrease proportionally to the reciprocal of square root of distance. And seismic energy is proportional to the square of wave amplitudes. The general functional form of GMPE is expressed as follows:

$$f(Y) = a + f_1(M) + f_2(R) + f_3(S) + f_4(F) + \sigma \quad (1)$$

Where Y is the ground motion parameter to be predicted, e.g. peak ground acceleration, peak ground velocity etc. $f_1(M)$ is a function of magnitude, $f_2(R)$ is a function of epicentral distance, $f_3(S)$ is a function of site categories like rock and soil sites, $f_4(F)$ is a function of type of fault, and σ is a value of relating uncertainties in the predicted $f(Y)$. It is necessary to consider the variable separation in the relationship. First, it is reasonable to assume that function f_1 depends only on M. In this model, the seismic variables are considered independently; no coupled terms of these variables are taken into account. The forms of $f(Y)$ and $f_1(M)$ are selected as:

$$f(Y) = \log_{10}(Y); \quad f_1(M) = bM \quad (2)$$

To investigate the attenuation resulting from geometric spreading and material anelasticity and scattering effect, $f_2(R)$ can be expressed as,

$$f_2(R) = c \underbrace{\log_{10}(R^2 + h^2)}_{\text{geometrical spreading}} + \underbrace{\frac{dR}{R}}_{\text{anelastic attenuation}} \quad (3)$$

It is in general inappropriate to assume that the function f_2 depends only on R. The parameter h is called fictitious depth and is determined by regression and incorporates all of the factors that tend to limit motions near the source. The parameter h is introduced to allow for the fact that the source of the peak motion values may not be the closest point on the rupture. If the source of the peak motion were directly below the nearest point on the surface projection of the rupture, the value of h would simply represent the depth of that source. Theoretical study showed that the seismic wave amplitudes decrease approximately as 1/R at far distances and converge to a finite value as distance goes to zero. This is due to one of the effects from the near field term of the seismic radiations, and it is noted that this holds true even when the distance is zero, that is when station is located on the fault plane. Thus, it is more appropriate and natural to introduce the form $f_2 \sim (R+h)^{-1}$ or $(R^2+h^2)^{-0.5}$ than to keep 1/R. One important point in this form is that the variable h depends on the magnitude M, since the near field territory depends on

the fault size of the earthquake, and on M . The variable h is a function of M , and therefore, the function f_2 depends on M as well as on R .

The function $f_3(S)$, is not free from the non-linear response of the ground when the ground surface at the station is covered with soft soil, which means that the function depends both on the site categories S and on the amplitude that comes into the surface layers, which intern depends on M and R . The function form for $f_3(S)$, relating to the site categories, can be taken as,

$$f_3(S) = eS \quad (4)$$

Where e is the coefficient for regression and S represent the site categories, 1 for soil site and 0 for rock site. The final functional form for modeling the ground motion attenuation can be represented as follows:

$$\log_{10}(Y) = a + bM + c \log_{10} \sqrt{R^2 + h^2} + dF + eS + \sigma \quad (5)$$

Where σ is the standard deviation of the logarithm of Y , M is the magnitude, R is the epicentral distance.

3. GMPE ANALYSIS

The dataset consists of 660 seismic station records in the Iran for studying the GMPE relationship. The Iranian earthquake information and ground motion records are taken from BHRC (<https://ismn.bhrc.ac.ir/en> dated: 20 August 2018). The seismic stations are located on both soft and rock sites, hence the term $f_3(S)$ is taken as zero. Current study considers shear wave velocities ranges 180 m/s to 1170 m/s. Based on Iranian code of practice for seismic resistant design of buildings (2005), shear wave velocities are considered for V_s more than 375 m/s as rock type and less than 375 m/s as soil type. The analysis also considers type of fault namely strike-slip fault and dip-slip fault. The term S represent the site categories, 1 for soil site and 0 for rock site. The term F represents, 1 for dip-slip fault and 0 for strike-slip fault. The distribution of dataset used in this analysis is from the earthquakes with a magnitude range of 6-7.8 and an epicentral distance range of 10-300 km. The distribution of seismic magnitude data with respect to hypocentral distance is shown in figure 1.

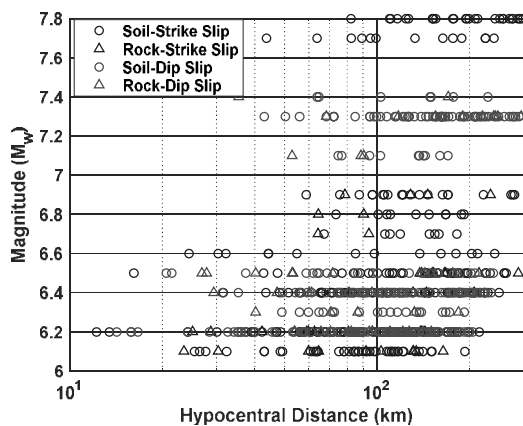


Figure 1. The distribution of data with magnitude to hypo-central distance

Figure 2-3 shows the distribution of PGA with respect to epicentral distance, magnitude and logarithm of

epicentral distance. In this analysis, the term h is taken as 16.38, 29.42, 40.84 and 49.0 for magnitudes $M6.0$, $M6.7$, $M7.4$ and $M7.8$ respectively. The dataset consists of two orthogonal horizontal components of PGA values, the maximum value has been chosen for the purpose of analysis.

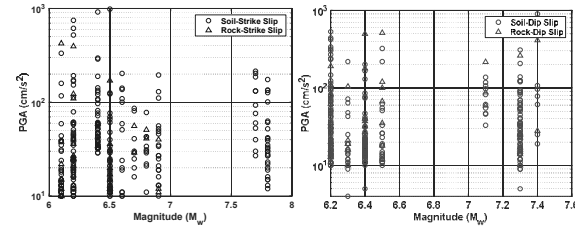


Figure 2. The distribution of PGA with magnitude

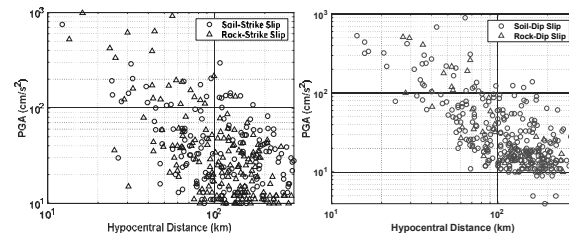


Figure 3. The distribution of PGA with hypo-central distance

The coefficient c in equation 5, which is a negative value, means the attenuation rate with respect to epicentral distance for a fixed M [6]-[9]. In other words, it is a weighted average of c 's, each of which is obtained from a data set of one earthquake at all epicentral distances. The slope c must not be calculated for the dataset of all earthquakes. The coefficient c must be greater than 1.0 for the short period amplitude attenuation relation, since this term includes the geometrical spreading of body wave and inelastic attenuation. Hence, the analysis considered the weighted average of c 's for a fixed at all epicentral distances. Similarly, the coefficient b means the amplitude increase rate with respect to magnitude at a fixed distance. In other words, it is a weighted average of b 's, each of which is obtained from a dataset at a particular distance range for all earthquakes. In this analysis, the weighted average of b and c are taken at all epicentral distances and at all earthquakes, respectively.

The residual values represent the deviations of the predicted values from the observed values. It can be defined as,

$$\text{Residual} = \log_{10} \left(\frac{Y_{\text{observed}}}{Y_{\text{predicted}}} \right) \quad (6)$$

Where Y_{observed} is the observed value from ground motion record (e.g. PGA), while $Y_{\text{predicted}}$ represents the value predicted by the GMPE. The residual can describe the extent to which the predicted values are consistent with the recorded values. The regression coefficients are calculated using regression analysis. The GMPE obtained for Iranian region from the analysis is shown below.

$$\log_{10}(Y) = 3.731 + 0.238M - 2.776 \log_{10} \sqrt{R^2 + h^2} + 0.289S + 0.48F + \varepsilon \quad (7)$$

faults, *Ph.D Dissertation, International Institute of Information Technology, Hyderabad, India, 2016.*

4. CONCLUSIONS

A study has been conducted to derive GMPE for Iran region. For this purpose, ground motion dataset is taken from BHRC from 1974 to 2017. The proposed GMPE for Iran region yields good results. Though, there is a difference between PGAs due to insufficient database in the region, the PGA value gives satisfactory result. The proposed GMPE equation for Iranian region is as follows

$$\log_{10}(Y) = 3.731 + 0.238M - 2.776 \log_{10} \sqrt{R^2 + h^2} + 0.289S + 0.48F + \varepsilon$$

REFERENCES

- [1] R. R. Youngs, S. M. Day, and J. L. Stevens, Near field ground motions on rock for large subduction earthquakes, *Proceedings of Earthquake Engineering & Soil Dynamics II. Geotechnical Division, ASCE*, 1988, pp. 445-462. USA.
- [2] C. B. Crouse, Ground-motion attenuation equations for earthquakes on the Cascadia subduction zones, *Earthquake Spectra*, vol. 7, No.2, 1991, pp. 201-236.
- [3] N. P. Theodulidis, and B. C. Papazachos, Dependence of strong ground motion on magnitude-distance, site geology and macroseismic intensity for shallow earthquakes in Greece: I, peak horizontal acceleration, velocity and displacement, *Soil Dynamics and Earthquake Engineering*, vol. 11, 1992, pp. 387-402.
- [4] G. M. Atkinson, and W. Silva, An empirical study of earthquake source spectra for California earthquakes, *Bulletin of the Seismological Society of America*, vol. 87, No. 1, 1997, pp. 97-113.
- [5] W. B. Joyner, and D. M. Boore, Peak horizontal acceleration and velocity from strong motion records including records from the 1979 Imperial Valley, California earthquake, *Bulletin of the Seismological Society of America*, vol. 71, No. 6, 1981, pp. 2011-2038.
- [6] Y. Fukushima, and T. Tanaka, A new attenuation relation for peak horizontal acceleration of strong earthquake ground motion in Japan, *Bulletin of the Seismological Society of America*, vol. 80, No. 4, 1990, pp. 757-783.
- [7] T. Masuda, and M. Ohtake, Comment on A new attenuation relation for peak horizontal acceleration of strong earthquake ground motion in Japan by Y. Fukushima and T. Tanaka, *Bulletin of the Seismological Society of America*, vol. 82, No. 1, 1992, pp. 521-522.
- [8] J. G. Anderson, and S. E. Hough, A model for the shape of the Fourier amplitude spectrum of acceleration at high frequencies, *Bulletin of the Seismological Society of America*, vol. 74, No. 5, 1984, pp. 1969-1993.
- [9] C. Rajaram, Numerical modeling of near-fault seismic ground motions for strike-slip and dip-slip

A STUDY OF SURFACE DEFORMATION IN PIPALKOTI, INDIA

V.MAURYA¹, D. MEGHANADH², A. TIWARI³, A. B. NARAYAN³, R. DWIVEDI⁴, T. R. MARTHA⁵

¹Junior Research Fellow, GIS Cell, MNNIT Allahabad, vipinmaurya2010@gmail.com

²Research Scholar, GIS Cell, MNNIT Allahabad rgi1703@mnnit.ac.in(corresponding author)

³Research Scholar, Department of Civil Engineering, IIT Kanpur atiwari@iitk.ac.in

³Research Scholar, Department of Civil Engineering, IIT Kanpur avadhbn@iitk.ac.in

⁴Assistant Professor, GIS Cell, MNNIT, Allahabad ramjid@mnnit.ac.in

⁵Scientist SF, NRSC, ISRO, Govt. Of India, tapas_martha@nrsc.gov.in

Keywords: Surface deformation analysis, InSAR, StaMPS, Landslide

ABSTRACT

Frequency of disasters such as landslides has increased in the last few decades in India. Loss of property and human lives due to disasters are irreparable. The well-known disaster, Kedarnath landslide (2013) in Uttarakhand, had alone swallowed more than 5000 lives and affected 4200 villages. Such events require the necessity of research in the field of surface deformation analysis of landslide in order to reduce risk and prepare early rescue methods. This study presents a surface deformation analysis of Pipalkoti, a landslide prone area in Uttarakhand, using multi-temporal Synthetic Aperture Radar Interferometry (MT-InSAR) technique.

The study uses temporal data of the European Environmental Satellite (ENVISAT) and 11 interferometric single look complex SAR images from ENVISAT covering a period of 12 months has been used for analyzing surface displacement. The computations of surface movement along with its rate (in mm/yr) were performed by using StaMPS (Stanford Method for Persistent Scatterers) algorithm, which detects phase stable pixels called Persistent scatterers (PS) pixels to calculate time-series displacement. The analysis results indicate the intensity of land mass movement, which would be helpful in mitigating the risk associated.

INTRODUCTION

Landslide, a geomorphic phenomenon, is a type of landmass movement under the influence of gravity. Movement landmass or debris flow triggered by unstable slopes, seismic or volcanic activity resulting into a landslide, are always serious concern regarding safety of people living in mountain regions.

Techniques being used for surface deformation study are global positioning system (GPS), total station (TS), terrestrial laser scanner (TLS), geotechnical investigation and satellite imaging. These above techniques except satellite imaging require minimum a personnel at the study area to collect data of interest i.e. limited regarding data collection only at accessible locations. On the other hand, advantage with satellite imaging is wider coverage and any time data availability.

In active satellite imaging, Synthetic Aperture Radar (SAR) is the most frequently used method for deformation analysis. SAR has the advantage of having sufficient number of satellites providing data in different frequency bands with high resolution, independency on weather conditions, data capturing in different modes of whole day and night with wide coverage. In SAR images product, acquired after signal processing of the received echoes of the transmitted electromagnetic chirp-pulses, we have used

Interferometric Wide (IW) Swath single look complex (SLC) images of Environmental satellite (Envisat). Pixels of SLC images hold magnitude and phase values where magnitude represents backscattering of signal scattering property of the target in pixel and proportionally brightness in the image, and phase helps in retrieval of change in location of the pixels on the ground [1]. Interferometric SAR (InSAR) is an effective technique used in deformation study which utilizes interferometric phase i.e. difference of phases of two SAR images. As an extension of InSAR, researchers proposed Differential-InSAR (D-InSAR) technique by subtracting DEM and interferometric phase which helps out in calculation of phase component due to displacement in the image. But in case of decorrelation of signals, this technique gives no measurement. To surmount this issue, [2-3] presented the concept of permanent scatterer on the basis of amplitude dispersion index. This technique finds itself bounded for urban areas only, as man-made structures have strong backscattering coefficient and this technique is not suitable for non-urban areas and requires knowledge of temporal variation in the deformation rate [4-5]. To overcome this problem, a new method was proposed of stable pixel (persistent scatterer (PS)) selection on the basis of phase stability

known as PS-InSAR and formulated as Stanford Method of PS (StaMPS) [5].

In recent years, multi-temporal Synthetic Aperture Radar Interferometry (MT-InSAR) has emerged as an important tool which uses temporal SAR data for estimating the time series displacement of radar targets. MT-InSAR processing can be performed in two ways: PS-InSAR and SBAS (Small baseline subset). This study presents a surface deformation analysis of Pipalkoti, Uttarakhand using MT-InSAR technique based on PS-InSAR and processed by StaMPS.

STUDY AREA

Uttarakhand state contains high elevated mountains and peaks and because of being hilly state and having unstable elevated slopes, there are a large number of landslide prone areas. The study area is located at 1.4 km upstream from Pipalkoti on Srinagar-Badrinath road. Further, there are multiple landslide locations within 50 km upstream Pipalkoti. The study area is shown in figure1. The dataset-details used for the analysis is given in Table1. The study uses 11 Envisat SLC images covering a period of 12 months to analyze surface displacement.

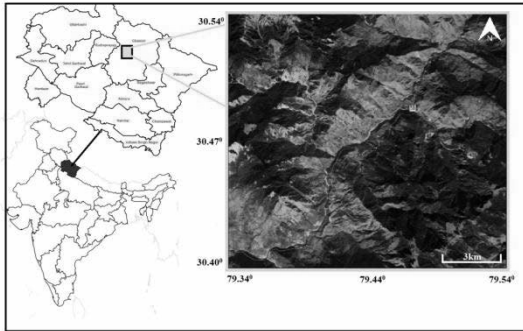


Figure1. Google earth view of the study area located on Rudraprayag-Badrinath route

METHODOLOGY: StaMPS-based PS-InSAR

StaMPS method was proposed by [5] which extracts coherent radar target based on phase stability of pixels and performs better than old method of permanent scatterer based on amplitude stability. StaMPS method works in four steps: Interferogram generation, phase stability estimation, PS selection and displacement estimation.

Firstly, Doris (Delft object oriented radar interferometric software) is used for interferogram generation and to remove phase component due to topography and orbital inaccuracies. In this process, first a master image is chosen on basis of minimizing sum-decorrelation or maximizing the sum-correlation,

and rest are taken as slave. Then for every master-slave pair, interferograms are generated. Correlation can be given as follows:

$$\rho_{total} = \rho_t * \rho_s * \rho_d * \rho_n \quad (1)$$

$$\approx \left(1 - f\left(\frac{T}{T_c}\right)\right) \cdot \left(1 - f\left(\frac{B_{perp}}{B_{perp}^c}\right)\right) \cdot \left(1 - f\left(\frac{F_{DC}}{F_{DC}^c}\right)\right) \cdot \rho_{thermal}$$

Where ρ_t is temporal correlation, ρ_s is the spatial correlation, ρ_d is correlation in Doppler frequency, and ρ_n is correlation related to noise and T represents temporal baseline, c used for critical, B_{perp} denotes spatial perpendicular baseline, F_{DC} for doppler centroid baseline and $\rho_{thermal}$ for thermal noise and $f(x)$ is expressed as:

$$f(x) = \begin{cases} x & x \leq 1 \\ 1 & x > 1 \end{cases}$$

Then in phase stability estimation step, initially PS pixels are selected on the basis of amplitude dispersion index D_A given as

$$D_A = \frac{\sigma_A}{\mu_A} \quad (2)$$

Where σ_A is standard deviation and μ_A as mean of the amplitude values for each pixel in the set of SLC images. Pixels of high amplitude dispersion index are selected as PS.

In next step, equation(3) is used to estimate phase stability of PS,

$$\varphi_{x,i} = W\{\phi_{d,x,i} + \phi_{a,x,i} + \Delta\phi_{S,x,i} + \Delta\phi_{\theta,x,i} + \phi_{N,x,i}\} \quad (3)$$

where $\varphi_{x,i}$ is the wrapped phase for x^{th} pixel in the interferogram, $\phi_{d,x,i}$ is the phase change due to the pixel motion in the direction of flight, $\phi_{a,x,i}$ is the phase due to atmospheric delay, $\Delta\phi_{S,x,i}$ is the residual phase due to satellite orbit inaccuracies, $\Delta\phi_{\theta,x,i}$ is the phase due to look angle error, $\phi_{N,x,i}$ is the noise term and W is the wrapping operator.

Then, as a measure of phase stability, γ_x given as

$$\gamma_x = \frac{1}{N} \left| \sum_{i=1}^N \exp(\sqrt{-1}(\varphi_{x,i} - \tilde{\varphi}_{x,i} - \Delta\hat{\phi}_{\theta,x,i}^u)) \right| \quad (4)$$

Where N denotes number of interferograms, $\phi_{x,i}$ is a wrapped estimate of the spatially correlated parts of the interferogram phase, namely the atmospheric error, the satellite orbital inaccuracy error, and the look angle error. The term $\Delta\hat{\phi}_{\theta,x,i}^u$ is the unwrapped estimate of the residual topographic phase error.

Based on the chosen threshold value of γ_x , PS pixels are selected for processing. In the next step to estimate displacement, spatially uncorrelated look angle (SULA) error and 3D unwrapping is done. Now, spatially correlated look angle (SCLA) error is estimated and subtracted to get phase component due to deformation $\Delta\phi_{d,x,i}$. Final outcomes of the StaMPS processing are time-series and velocity maps with annual rate. StaMPS processing is summarized in figure 2.

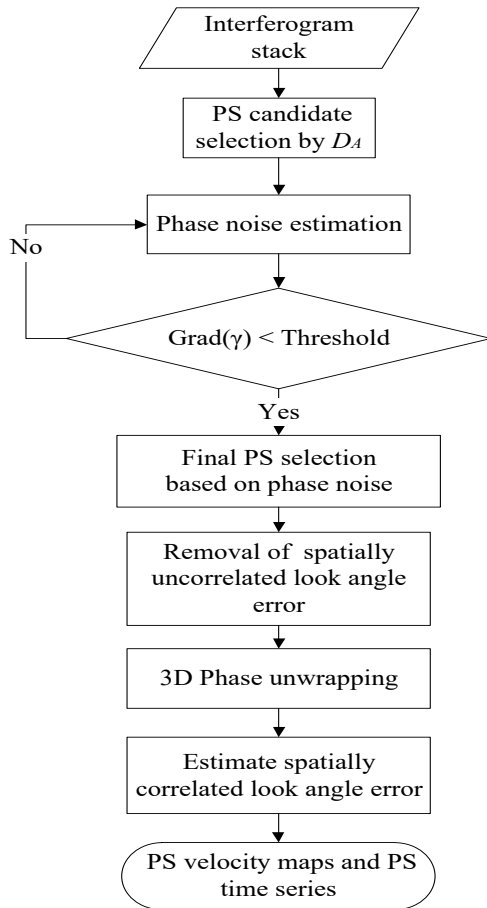


Figure2: Flowchart of PS-InSAR processing

RESULTS AND DISCUSSION

In this section, the results of StaMPS-based PS-InSAR of the 11 ENVISAT ASAR SLC images are discussed with their interpretations. With 12 SLC images, 11 geocoded single-master interferograms are generated for the PS-InSAR method. The values of 0.4 and 0.005

are adopted for D_A and γ , respectively, for the selection of PS candidates which resulted in ~ 8000 PS pixels, forming a dense network of PS pixels. The PS velocity plot (Figure3) shows displacement of -62 to 84 mm/yr. Analysing the displacement rate, we can identify subsidising and uplifting areas and their rate of change in mm/yr. In study area, subsidence and uplift rate in Pipalkoti varies from -24 to 8.2 mm/yr. Areas affected with high displacement rate are Hailang, Gulabkoti, Langsi, Dwing and Jalgwar. Figure4 shows GSI (Geological Survey of India) points along with StaMPS result confirms validity of results.

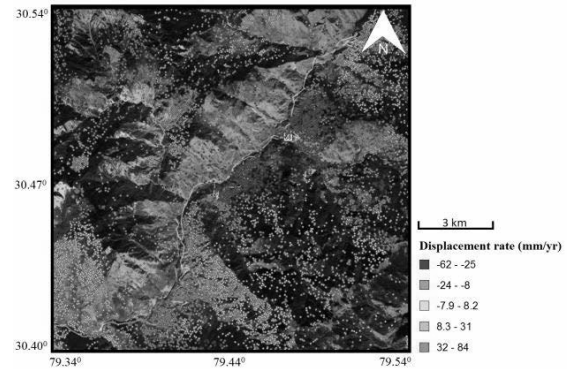


Figure 3: 1D LOS deformation map obtained from PSI processing of the Envisat dataset.

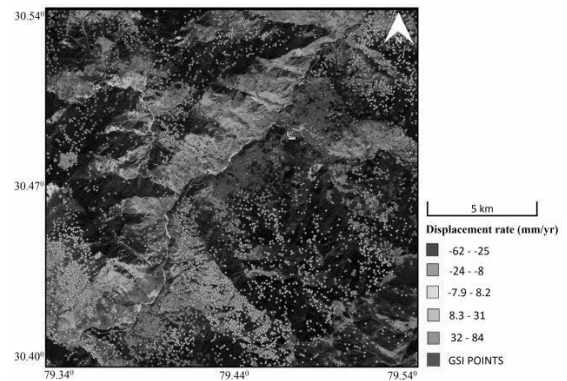


Figure 4: 1D LOS deformation map obtained from PSI processing of the Envisat dataset with GSI points.

CONCLUSION

11 ENVISAT images covering a time period of 12 months were used for deformation analysis of the study area. Result shows the 1D LOS deformation map obtained using the StaMPS approach for the Envisat dataset along with landslide prone locations identified by GSI. Obtained displacement values show high subsidence in the region between Pipalkoti and Hailang along the Rudraprayag-Badrinath route.

ACKNOWLEDGEMENT

Authors are thankful to European Space Agency (ESA) for providing ENVISAT ASAR images and to ISRO for providing technical support in data-processing.

REFERENCES

- [1] A. Tiwari., R. Dwivedi., O. Dikshit., and A. K. Singh., (2016). “A study on measuring surface deformation of the L’Aquila region using the StaMPS technique”. *International Journal of Remote Sensing*, 37(4), 819-830.
- [2] A. Ferreti., C. Prati, & F. Rocca., (2000). “Nonlinear subsidence rate estimation using permanent scatterers in differential SAR interferometry”. *IEEE Transactions on Geoscience and Remote Sensing*, 38(5), 2202-2212.
- [3] A. Ferreti., C. Prati, & F. Rocca., (2001). “Permanent scatterers in SAR interferometry” . *IEEE Transactions on geoscience and remote sensing*, 39(1), 8-20.
- [4] A. Hooper., H. Zebker., P. Segall., and B. Kampes., (2004). “A new method for measuring deformation on volcanoes and other natural terrains using InSAR persistent scatterers”. *Geophysical research letters*, 31(23).
- [5] A. Hooper., P. Segall., and H. Zebker., (2007). “Persistent scatterer InSAR for crustal deformation analysis, with application to Volcán Alcedo, Galápagos”. *Journal of Geophysical Research*, 112(B07407), 19
- [6] R. Dwivedi., P. Varshney., A. Tiwari., A. B. Narayan., A. K. Singh., O. Dikshit., and K. Pallav., (2015). “Monitoring of landslides in Nainital, Uttarakhand, India: Validation of PS-InSAR results”. In *Urban Remote Sensing Event (JURSE), 2015 Joint* (pp. 1-4). IEEE.

USMCA 2018

SESSION 3

BUILDING SAFETY I

ANTIINDUCE MEASUREES OF UNDERGROUND SUBWAY STATION

S. KONISHI¹, M. HORI², S. ITO³, and Y. AOKI⁴

¹ Director of Civil Engineering, Structure Maintenance Division, Tokyo Metro Co.,Ltd., Japan, s.konishi.r4r@tokyometro.jp (corresponding author)

² Staff, Structure Maintenance Division, Tokyo Metro Co.,Ltd., Japan, m.hori.x4g@tokyometro.jp

³ Vice Director, Structure Maintenance Division, Tokyo Metro Co.,Ltd., Japan, sato.itou@tokyometro.jp

⁴ Manager of Station, Structure Maintenance Division, Tokyo Metro Co.,Ltd., Japan, yo.aoki@tokyometro.jp

Keywords: Anti-induce Measures, Flood, Subway Underground Station, Hinged Door

1. INTRODUCTION

Because of recent extreme weather events, counter-measures for heavy rains are particularly important for safety of subway. Tokyo Metro Co., Ltd. (hereinafter, Tokyo Metro) is taking measures against urban flood disaster assumed by Central Disaster Prevention Council or each municipality and Large-scale Flood Disaster once a 1000 year probability for reducing damage from submerged and early recovery (Fig.1) [1], [2].

The report describes Tokyo Metro's improvement policy and descriptions of various types of underground waterproofing doors and the performance required of them.

2. OUTLINE OF WATER PROOFING FACILITIES

We are developing and installing various waterproofing facilities at all tunnel entrances (Fig.2), ventilation openings (Fig.3) and entrances of underground stations (Fig.4). Also substation and signaling machine rooms which are built on ground level is measures against flooding for early recovery at ground level.

3. WATER PROOFING FACILITIES FOR UNDERGROUND STATION ENTRANCE

Among these, underground station entrances are expected to suffer the most damage. Most Tokyo Metro station entrances are situated on sidewalks, there are many obvious spatial restrictions. In light of these,

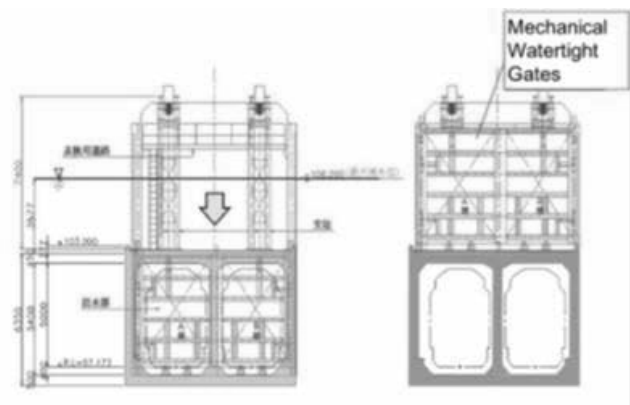


Figure 2: Mechanical watertight gates of tunnel entrance in which doors drop down from above

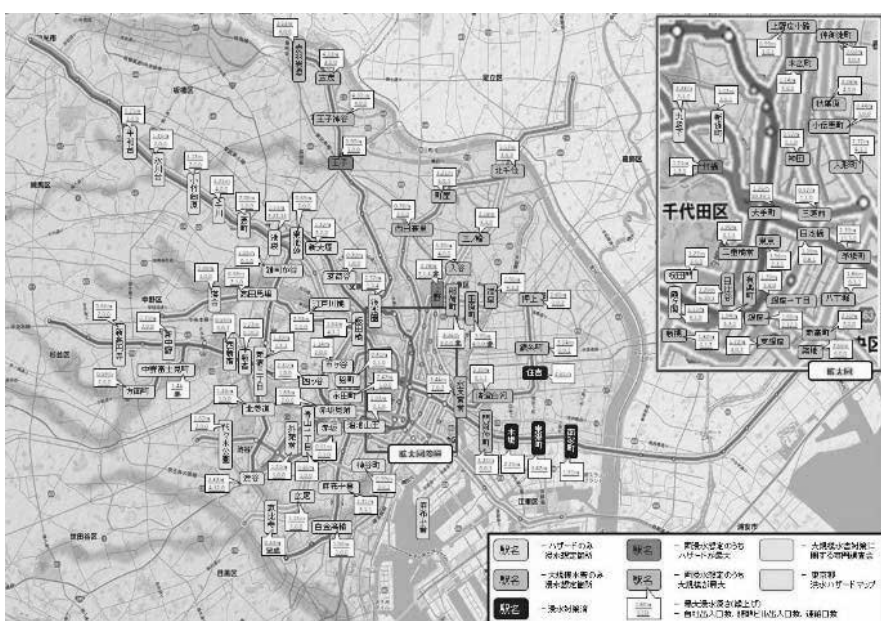


Figure 1: Conceptual diagram of expected damage in the Tokyo Metro Network

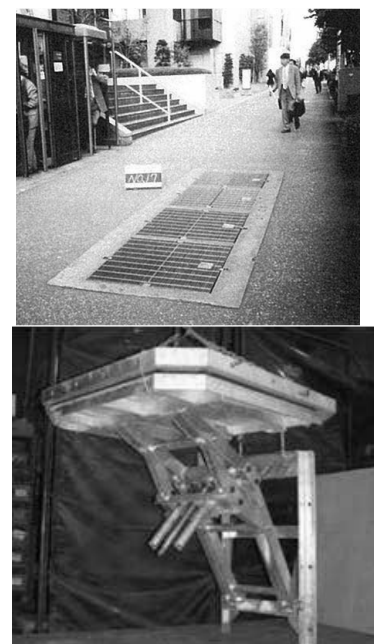


Figure 3: Flood preventing machine for ventilation

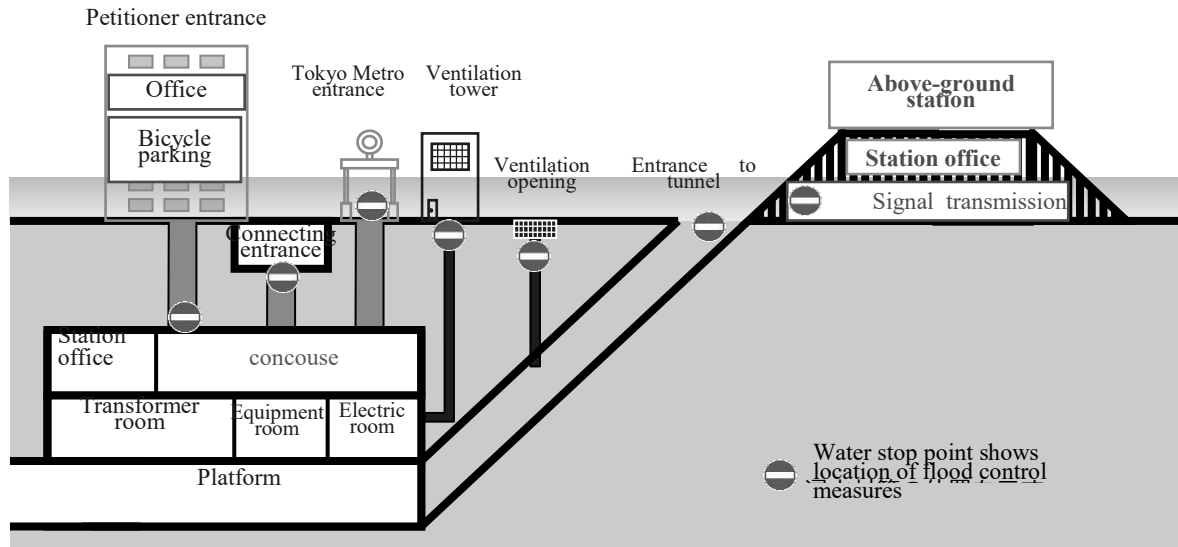


Figure 4: Tokyo Metro Flood Control Measures



Figure 5: Bi-fold water stop door



Figure 8: Vertical bi-fold door

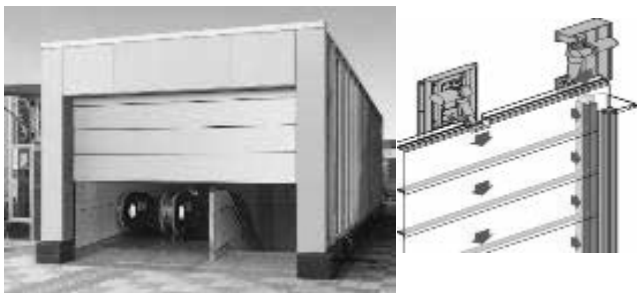


Figure 6: Waterproofing shutter



Figure 7: Horizontal bi-fold door

restrictions, conventional waterproofing doors, hinged doors, cannot be used to improve all entrances. Thus we have continued to develop counterpressure doors, hinged double doors, bi-fold watertight doors (Fig.5), shutters (Fig.6), horizontal bi-fold doors (Fig.7) vertical bi-fold doors (Fig.8) and other types of waterproofing doors that fit to the environments of individual entrances. In addition, many buildings, which Tokyo Metro tunnels connect underground, are not prepared for the disasters flood damage, meaning that Tokyo Metro must take action on its own property to prevent flood water inundation from such buildings. Thus, we have developed counterpressure sliding doors capable of withstanding water pressure from flooding up to 15 m depth.

REFERENCES

- [1] Cabinet Office website: Disaster risk reduction information website (Expected Flood Damage to Subways, etc., during an Arakawa River Levee Breach)
- [2] Tokyo Metropolitan Government website: Tokyo Disaster Prevention website (Map of expected inundation zone)

EVALUATION OF RESPONSE REDUCTION FACTOR 'R' FOR A 16 STOREY SLENDER REINFORCED CONCRETE BUILDING USING PERFORMANCE BASED SEISMIC ENGINEERING.

NIRANJAN GODAGE¹, R.PRADEEPKUMAR²,

¹ M.Tech (CASE), Earthquake Engineering Research Centre-IIIT-Hyderabad,India,niranjangodage@gmail.com

² Professor, Earthquake Engineering Research Centre IIIT-Hyderabad,India,,ramancharla@iiit.ac.in

Keywords: Static Non-Linear Pushover Analysis, Response Reduction factor R, reserve strength, ductility, redundancy

1. ABSTRACT

The current industry followed standards for seismic design in India is based on Linear Static and Dynamic analysis procedure recommended by IS1893. This procedure incorporates the non-linear response of a structure using a code prescribed value for R i.e. Response reduction factor, however in reality these values are difficult to justify for different structural configurations. Also it is difficult to predict the behavior of critical structural elements once the structure goes in to nonlinear zone. The present study focuses on estimating the actual value of 'R'. A linear force based analysis is performed using IS-1893 recommended value of R. The structure is designed using IS 13920 ductile detailing procedure and remodeled. A displacement controlled push over analysis is carried out to determine the performance of the structure in the nonlinear zone. The actual value of R is then estimated based on reserve strength, ductility and redundancy in the structure.

2. INTRODUCTION

In recent times there has been a significant advancement in computational capabilities of 3D structural analysis packages, unleashing its full potential will help us in having a better control over the anticipated behavior of the structure in the nonlinear zone. Also it has been observed in the past earthquakes that well designed and detailed structures were able to withstand more lateral loads than they were designed for. This inherent capacity of a structure to dissipate energy through inelastic behavior can be attributed to strength, ductility and redundancy in the structure, which is represented as

$$R = R_s * R_R * R_\mu$$

This value of **R** can be obtained from push over curve as shown in Fig.1 where

Strength factor ' R_s ' is the ratio of Design base shear to that of base shear at yielding.

Ductility factor ' R_μ ' is the ratio of roof displacement at yielding to some predefined limits.

Redundancy factor ' R_R ' depends on number of vertical framings participating in the seismic resistance.

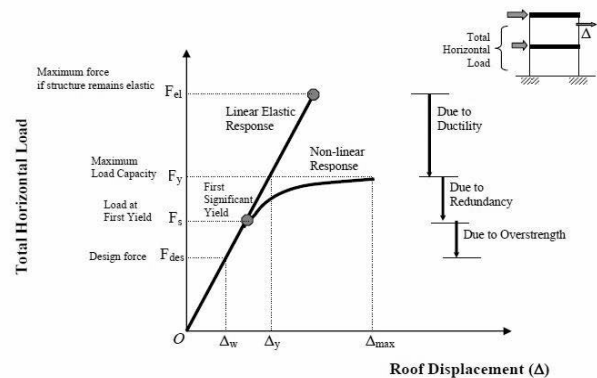


Fig.1. Definition of Response Reduction Factor

$$\text{Response Reduction factor} = \frac{\text{Maximum elastic force } F_{el}}{\text{Design force } F_{des}}$$

Table 1

R values as per IS 1893 for Dual Structural Systems

1	Ordinary RC Shear walls +RC OMRFs	3
2	Ordinary RC Shear walls +RC SMRFs	4
3	Ductile RC Shear walls + RC OMRFs	4
4	Ductile RC Shear walls +RC SMRFs	5

3. PUSH OVER ANALYSIS

Push over Analysis (POA) is considered as a recent advancement in earthquake resistant design of structures. The promise of POA is to produce structures with predictable seismic performance. The main concept of POA procedure is based on seismic demand and capacity.

3.1 Demand:

Ground motions during an earthquake produces complex horizontal displacement patterns in the structures. It is impractical to trace this lateral displacement at each time-step to determine the structural design parameters and hence the seismic demand is the static equivalent parameter accounting for the dynamic effect on the structure.

3.2 Capacity

The overall capacity of a structure depends on the strength and deformation capacity of the individual components of the structure. In order to determine capacities beyond the elastic limits, some form of Nonlinear Analysis, such as the pushover procedure is required. As the name implies, it is the process of pushing the structure horizontally with a prescribed loading pattern incrementally until the structure reaches a limit state (ATC-40 1996) i.e. target displacement.

4. CASE STUDY

In the present case study a G+13 storey signature structure with a slenderness ratio of around 7 to be constructed in Deonar, Mumbai (Zone 3) is analyzed. Linear Static and Dynamic Analysis, displacement controlled Push over analysis is carried out to determine the performance in the non linear zone, hinge sequencing mechanism, base shear, seismic demand and capacity is compared in both X,Y direction.

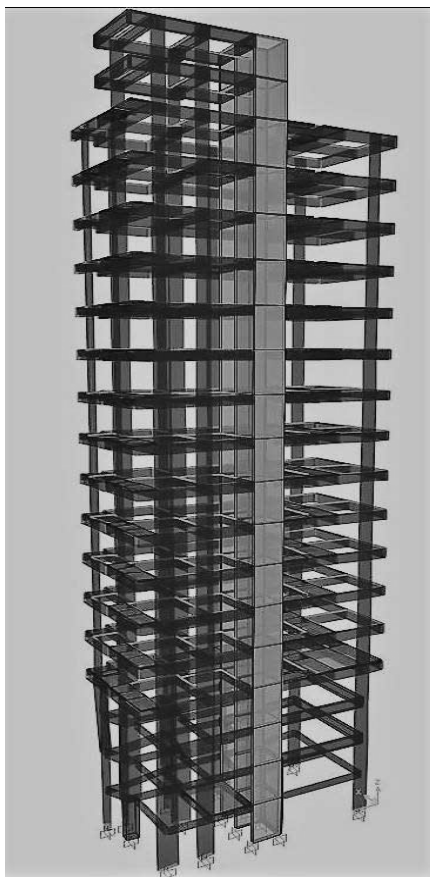


Fig.2. 3D View of RC building model in SAP2000

4.1 Modeling of the structure:

The linear numerical analysis was done using ETABS and the structure was remodeled in SAP 2000 using Guidelines of ATC-40 and FEMA 356 .The overall

Performance evaluation was done using capacity spectrum curves. Plastic hinge hypothesis was used to capture the nonlinear behavior according to which plastic deformations are lumped on plastic hinges and rest of the system shows linear elastic behavior.

4.2 Modeling Schema for Linear Analysis

- 1) Developing a 3D model for the Building in ETABS.
- 2) Defining all the material properties, frame sections, load cases and mass source.
- 3) Performing linear static and dynamic analysis using IS 1893 specifications.
- 4) Designing all structural elements using ductile detailing principles.

4.3 Modeling schema for Nonlinear Analysis.

- 1) Remodeling the structure in SAP 2000 with detailed reinforcement using section designer.
- 2) Assigning auto hinge properties available in SAP 2000 as per ATC-40 to the frame elements which are expected to yield. For beams assigning default hinge that yields based on flexure (M3), for the column assigning default hinge that yields based on the interaction of the axial force and bending moment (P M2 M3).
- 3) Application of gravity load followed by static push over load case (which will start from final state of the gravity pushover).
- 4) Gravity load case involves loading the structure with DL+0.25LL, where gravity load application is forced controlled while that of lateral load is displacement controlled.
- 5) Assigning first modal response of the structure as load pattern for the lateral Push-x and Push-y case.
- 6) Obtaining Push over curves i.e plot of base shear v/s roof displacement and Performance levels for building model in X and Y directions.

5. ANALYSIS & RESULTS:

5.1 Linear Analysis

Linear Static	Linear Dynamic	Bhuj		Koyna		
		Vx	Vy	Vx	Vy	
EQX	2364.6	THX	507.1	135	3898.7	1671.4
EQY	2225.8	THY	146.3	530.8	2481.4	3861.2

Table 2:Base shear values in kN

5.2 Nonlinear Analysis

Push over curves and Performance levels for building models are obtained in X and Y directions. The capacity of the building is determined by pushover curve while the performance levels of the structure is determined based on Hinge sequencing mechanism.

5.2.1 Hinging mechanism from Push-X and Y case

The overall performance level for G+13 story building models were found between B and IO levels in both

directions. It has been observed that very few (7-8 out of 1476) assigned hinges went beyond CP performance level at a displacement value of around 33 mm. However there is no indication of strength degradation at any displacement value within range of target displacement. The hinge location and performance level is carefully studied and the associated member is redesigned.

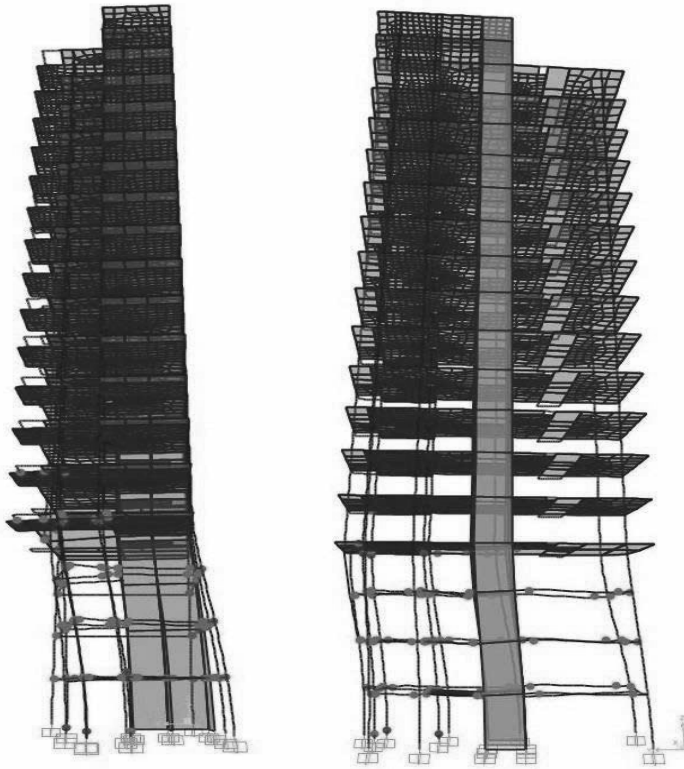


Fig 3. Hinge mechanism for PUSH-X, Y case

5.2.2 Capacity Curves

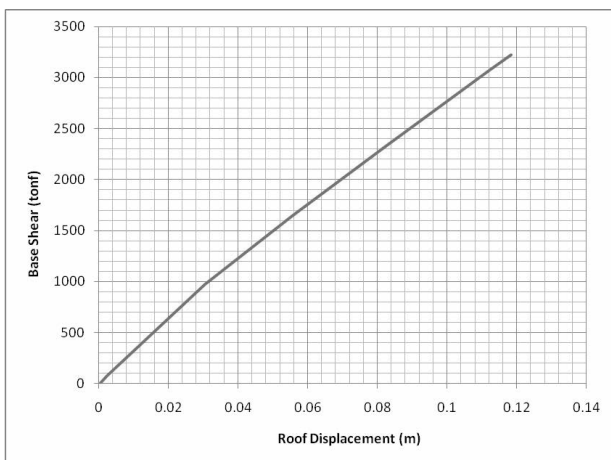


Fig 4 Plot of Resultant Base Shear v/s Monitored Displacement for PUSH-X case.

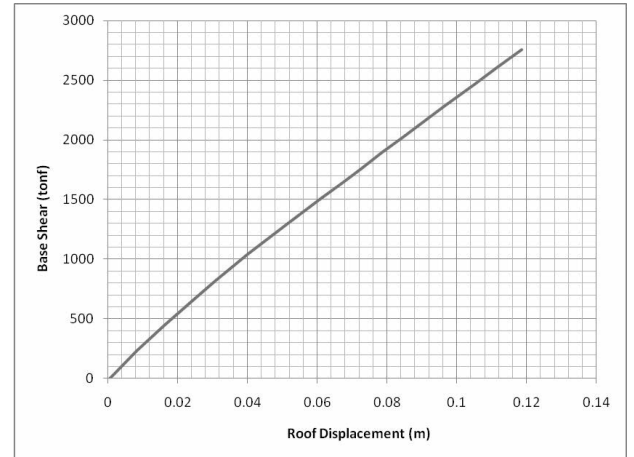


Fig 5 Plot of Resultant Base Shear v/s Monitored displacement for PUSH-Y case

5.2.3 Performance point.

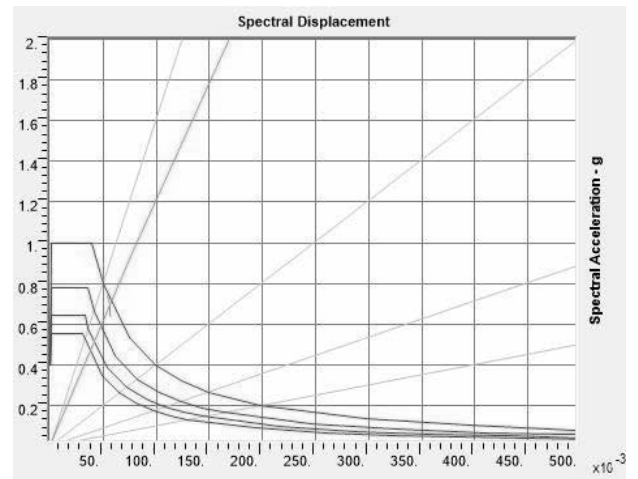


Fig 6 Plot of Spectral Displacement v/s Spectral acceleration for PUSH-X case

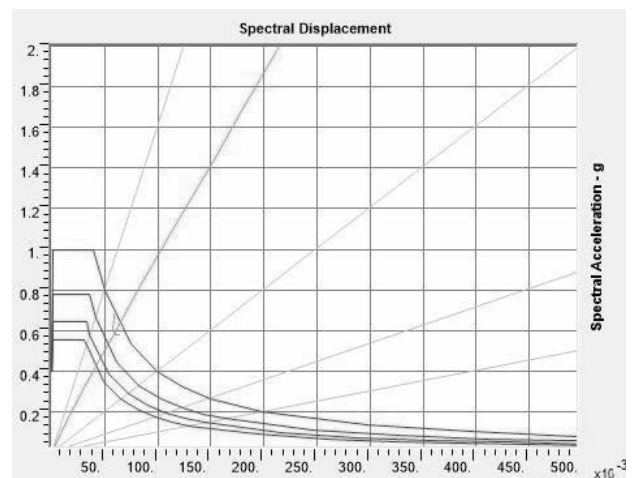


Fig 7 Plot of Spectral Displacement v/s Spectral acceleration for PUSH-Y case

The performance point for PUSH-X case was obtained at a resultant base shear of **6968.4 kN** corresponding to the monitored roof displacement of **22 mm** while for the PUSH-Y case it was obtained at a resultant base shear of **8448.6 kN** corresponding to displacement of **32 mm**.

5.3 Evaluation of Response Reduction Factor R

5.3.1 Estimation of strength factor:

Maximum Base Shear from Push over curve

$$V_x = 6968.4 \text{ kN}$$

$$V_y = 8448.6 \text{ kN}$$

Design base shear from Linear EQ Analysis

$$EQ_x = 2364.6 \text{ kN}$$

$$EQ_y = 2225.8 \text{ kN}$$

Using equation for strength factor using ATC-19

$$R_{si} = V_i / EQ_i$$

$$R_{sx} = 2.94 \quad R_{sy} = 3.79$$

5.3.2 Estimation of ductility factor

Maximum drift capacity = 5 x yield drift (assumed limit)
 $\mu = 5$.

Using equation for ductility derived by Miranda and Bertero

$$R_\mu = \{(\mu - 1 / \Phi) + 1\}$$

Where

$$\Phi \text{ for medium soil} = 1 + \{1 / (12T - \mu T)\} - \{(2 / 5T)^* e^{-2(\ln(T) - 0.2)^2}\}$$

For X direction

$$\Phi_x = 0.913 \text{ for } T_x = 1.64 \text{ sec}$$

$$R_{\mu x} = 5.38$$

For Y direction

$$\Phi_y = 0.828 \text{ for } T_y = 1.16 \text{ sec}$$

$$R_{\mu y} = 5.84$$

5.3.3 Estimation of redundancy factor As per ATC-19

Drift redundancy ratio is 1 if there are more than 4 lines of vertical seismic framing in a structure

$$R_r = 1$$

5.3.4 Estimation of Response reduction factor(R)

$$R = R_s * R_\mu * R_r$$

Hence

$$R_x = 2.94 * 5.38 * 1 = 15.81$$

$$R_y = 3.79 * 5.84 * 1 = 22.13$$

DISCUSSIONS:

1) Pushover analysis is numerically demanding and may cause numerical difficulties for the software used to run the analysis. Simplifying the model as much as possible is helpful in completing the run and reducing the computation time.

2) Hinges were not assigned to shear wall as it is expected to remain linear elastic till the performance point, development of any shear hinges was considered undesirable from the design objective which also

ensured that the expected moment rotation demands on frame elements to be on a conservative side.

3) Numerous trial runs were performed to create a striking balance between computation time for analysis and accuracy of the model.

4) In order to reduce the computation time the iterative convergence tolerance was set to the order of 0.01 without much compromising the accuracy of the model thereby making this analysis suitable for design office settings.

5) Upon performing initial pushover runs hinges were found to develop up to 4th Slab level in columns and hence additional tie beams were added without compromising the architectural constraints thereby increasing the redundancy in the lower stories.

6. CONCLUSIONS

1) There is not much mathematical basis for R values tabulated in IS Code and it has been observed that these values underestimate the inherent capacity of the structure to undergo inelastic deformation beyond yield

2) In the present study the building was initially designed and detailed considering R=5 however from push over analysis it was observed that the R value obtained went beyond 15. This considerable increase in capacity could be attributed to the combined lateral resistance offered by Ductile detailed RC Shear wall + SMRF.

3) The current code prescribed value for R is based on the principle of uniformly reducing the seismic demand at a global level without taking in to account the individual member capacity which can be considerably higher than its demand at member level.

4) A comprehensive study needs to be performed to detail hinges in RC members similar to shear fuses so that hinge formation is localized and latent capacity of the structural member is triggered to resist the demand at member level.

REFERENCES

- 1) ATC-40. "Seismic evaluation and retrofit of concrete buildings." Volume 1 and 2. Applied Technology Council, California, 1996.
- 2) SAP2000 nonlinear version 19. Computers and Structures, Inc, CA.
- 3) ETABS nonlinear version 16.2.1. Computers and Structures, Inc, CA.
- 4) Pushover Analysis of a 19 storey concrete shear wall building Rahul Rana¹, Limin Jin² and Atila Zekioglu³
- 5) Formulation of Response Reduction Factor for RCC Framed Staging of Elevated Water Tank using Static Pushover Analysis Mr. Bhavin Patel¹ and Mrs. Dhara Shah²
- 6) Proposed draft provisions and Commentary on Indian Seismic Code IS 1893(Part 1), Sudhir Jain, CVR Murthy.

A PROPOSAL FOR AN OPTIMIZED SOLUTION FOR OPEN STOREY PROBLEM IN NON-ENGINEERED INFILLED MASONRY REINFORCED CONCRETE FRAMED BUILDINGS IN NEPAL

Kishor TIMSINA¹, Chaitanya K GADAGAMMA², Hideomi GOKON³, Kimiro MEGURO⁴

¹ Graduate Student, Department of Civil Engineering, The University of Tokyo, ktimsina@iis.u-tokyo.ac.jp (Corresponding author)

² Project Assistant Professor, Institute of Industrial Science (IIS), The University of Tokyo, chaitugk@iis.u-tokyo.ac.jp

³ Assistant Professor, ICUS, Institute of Industrial Science (IIS), The University of Tokyo, gokon@iis.u-tokyo.ac.jp

⁴ Professor, ICUS, Institute of Industrial Science (IIS), The University of Tokyo, meguro@iis.u-tokyo.ac.jp

Keywords: Infilled RC-frame, soft-story, optimization, performance, Applied Element Method.

1. INTRODUCTION

Urban and semi-urban areas of Nepal are rapidly growing in the recent years. Reinforced concrete with masonry infill (RC) buildings has become very popular in these areas. The data obtained from the National Population and Housing Census (CBS 2012) shows that there are currently about 540,000 RC buildings of 3-5 stories. Most of them are non-engineered buildings and constructed with the involvement of masons and owners only [1]. Generally, in the urban areas, the ground floor of more than 90% of the RC buildings are open for commercial shutter or parking and close the upper floor with infill masonry for the residential purpose (figure 1)[2]. So, the construction of this kind of non-engineered buildings without considering the consequences of the open ground storey has resulted in many vulnerable buildings. Reduction of the infill in a story relative to the ones above increases the inelastic deformation demand on the columns of that story owing to concentration of the global lateral drift demands to that story and the near-fixity conditions of the columns of that story at floor levels, as the infill panels of neighboring stories restrain the drift there. Thus ultimately results in the soft storey collapse of the open floor [3][4]. In recent 2015 Gorkha Earthquake (7.9Mw), the significant loss in RC frame buildings was due to the soft storey collapse (figure 2) of the ground floor of these buildings due to a reduction in strength and stiffness [5].

A questionnaire survey has been conducted with 35 Engineers who are working in 20 different municipalities of Nepal, who are directly involved in building permit and construction supervision. It suggests that the soft storey problem in Nepal is a socio-technical problem. The social aspects influencing the construction and retrofitting of the buildings with the soft storey are i) livelihood of the people, i.e. their business/ parking and livings ii) economy of the people iii) promotional system for the implementation. The technical aspects are i) methodology of the construction ii) availability of the materials. There are many existing technical solutions to address the soft storey problem, but many of these solutions are not acceptable by the landlords due to their social and economic benefits, as most of these solutions

disturb the business of the landlords. Many other solutions provide better performance and enough space for the business purpose, but they are very costly. This issue has led to the construction of vulnerable buildings with inadequate performance during earthquakes. People need a cost-effective solution with locally available materials which provides enough business space and performance during an earthquake.



Figure 1: Typical RC frame building with infill masonry building with soft storey



Figure 2: Soft storey damage of RC frame Building with open ground floor

The survey suggests that a feasible cost people can afford is within 10% of total cost of the building with the locally available material, minimum space required for the business shutter is 3 meters in length and desired performance level is life safety during a large earthquake. Following different existing solutions for soft storey problems are analyzed in according to cost (C), material availability (A), usability (business space) (U) and performance (P) [3], [4], [6], [7], [8], [9], [10].

Applied Element Method [11] has been used for the study of performance. H=high, L=low

SN	Method of strengthening	C	A	U	P
1.	Building with soft storey				L
2.	Retrofitting with the addition of infill wall in the open storey			L	
3.	Strengthening all columns and beams	H			
4.	Strengthening columns and beams of the open floor only	H			L
5.	Strengthening columns of the open floor only				L
6.	Strengthening with steel bracing	H	L	L	

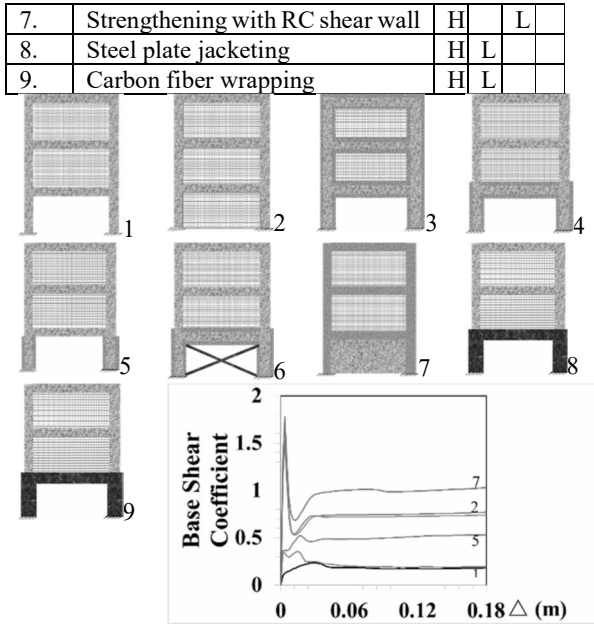


Figure 3: Different strengthening options

2. METHODOLOGY

Available methods of strengthening have either very costly, or very low availability of materials, or very low usability, or deficient performance. According to material availability, concrete is readily available material and performance wise strengthening with RC shear wall has high base shear coefficient than others (figure 3).

The RC infill shear wall is then proposed to optimize to get a practical and feasible solution according to performance, cost, and usability. The cost of the retrofitting which includes the cost of materials, construction and business disturbance is minimized as an objective function subjected to performance constraints for collapse prevention, and social constraints of business space, and material properties.

The optimization problem is an iterative and dynamic non-linear constrained problem with implicit performance constraint. The analysis is done by incorporating non-linear sequential quadratic programming (NLSQP) in Applied Element Method[12]. Figure 4 shows the flowchart of this optimization scheme.

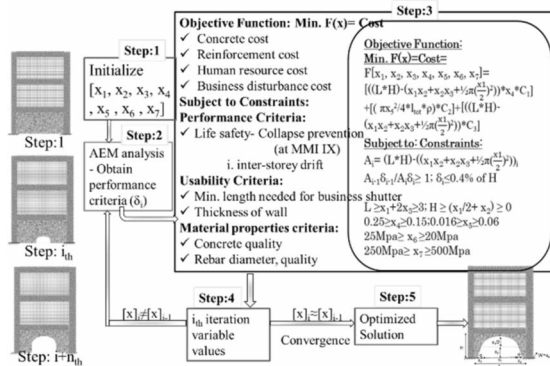


Figure 4: Flowchart of optimization scheme in AEM

4. CONCLUSION

A tool for developing an optimized solution using RC infill wall for soft storey problem incorporating socio-technical constraints is developed. The figure 5 shows the sample of the solution developed.

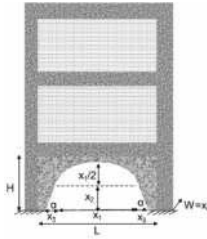


Figure 5: Sample of optimized solution

REFERENCES

- [1] A. M. DIXIT, "PROMOTING SAFER BUILDING CONSTRUCTION IN NEPAL," p. 9.
- [2] D. Gautam, H. Rodrigues, K. K. Bhetwal, P. Neupane, and Y. Sanada, "Common structural and construction deficiencies of Nepalese buildings," *Innov. Infrastruct. Solut.*, vol. 1, no. 1, Dec. 2016.
- [3] S. Makran, "Preliminary observations on the origin and effects of the January 26, 2001 Bhuj (Gujarat, India) earthquake," 2001.
- [4] D. R. Sahoo and D. C. Rai, "Design and evaluation of seismic strengthening techniques for reinforced concrete frames with soft ground story," *Eng. Struct.*, vol. 56, pp. 1933–1944, Nov. 2013.
- [5] T. Pokharel and H. M. Goldsworthy, "Lessons learned from the Nepal earthquake 2015," *Aust. J. Struct. Eng.*, vol. 18, no. 1, pp. 11–23, Jan. 2017.
- [6] H. B. Kaushik, D. C. Rai, and S. K. Jain, "Effectiveness of Some Strengthening Options for Masonry-Infilled RC Frames with Open First Story," *J. Struct. Eng.*, vol. 135, no. 8, pp. 925–937, Aug. 2009.
- [7] R. Davis, P. Krishnan, D. Menon, and A. M. Prasad, "Effect of Infill Stiffness on Seismic Performance of Multistorey RC Framed Buildings in India," p. 9.
- [8] M. N. Fardis and T. B. Panagiotakos, "SEISMIC DESIGN AND RESPONSE OF BARE AND MASONRY-INFILLED REINFORCED CONCRETE BUILDINGS. PART II: INFILLED STRUCTURES," *J. Earthq. Eng.*, vol. 1, no. 3, pp. 475–503, Jul. 1997.
- [9] I. Erdem, U. Akyuz, U. Ersoy, and G. Ozcebe, "An experimental study on two different strengthening techniques for RC frames," *Eng. Struct.*, vol. 28, no. 13, pp. 1843–1851, Nov. 2006.
- [10] S. Altin, Ö. Anil, and M. E. Kara, "Strengthening of RC nonductile frames with RC infills: An experimental study," *Cem. Concr. Compos.*, vol. 30, no. 7, pp. 612–621, Aug. 2008.
- [11] K. Meguro and H. Tagel-Din, "APPLIED ELEMENT METHOD FOR STRUCTURAL ANALYSIS," *Doboku Gakkai Ronbunshu*, vol. 2000, no. 647, pp. 31–45, 2000.
- [12] K. Schittkowski, "NLPQL: A FORTRAN subroutine solving constrained nonlinear programming problems," *Ann. Oper. Res.*, vol. 5, no. 2, pp. 485–500, 1986.

Comparison of Base joint column reactions of Buildings on various slopes and Non linear static analysis

SANA SULTANA¹, PRADEEP KUMAR RAMANCHARLA²

¹ M tech, Civil, IIT HYDERABAD, India, ssanasultana15@gmail.com

² Professor, Civil, IIT HYDERABAD, India, ramancharla@iit.ac.in

Keywords: Hill slopes, equivalent static analysis, pushover analysis, base column joint reaction

1. ABSTRACT

In the world most of the population lives on hills, mountains, because of scarcity of flat land available. As the hilly regions are more susceptible to earthquakes and landslides. Buildings on hilly regions are prone damage at time of earthquake. So there was a huge loss due to Nepal earthquake, Nepal is situated near to Himalayas. Common building typology on hilly regions is G+3, so G+3 with 3 Bays in X-direction and Y-direction building is considered on hilly regions of slopes. Slopes considered for the study of damage pattern are 0°, 15°, 30°, 45°. When building is constructed on zero slope or flat surface region after the application of horizontal loads there is no short column effect as the shear is equally distributed to all the columns. When the building is on the sloped region shear is dominated in short column and there is unequal distribution of shear in columns, so short columns fails first. Equivalent static analysis is carried out and Base column joint reaction is calculated on sloped regions and compared with varying slopes of 0°, 15°, 30°, 45°. Base column joint reaction is more in short column and less at long columns. To reduce the base column joint reaction at short column and to transfer base column joint reaction force from one column to next columns, infill wall is modeled. After equivalent static analysis, pushover analysis is carried out to find the energy in the buildings of varying slopes of 0°, 15°, 30°, 45° with and without infill modeling and energy curves and compared.

When the building is on the sloped region shear is dominated in short column and there is unequal distribution of shear in columns, so short columns fails first. Equivalent static analysis is carried out and Base column joint reaction is calculated on sloped regions and compared with varying slopes of 0°, 15°, 30°, 45°. Base column joint reaction is more in short column and less at long columns. To reduce the base column joint reaction at short column and to transfer base column joint reaction force from one column to next columns, infill wall is modeled. After equivalent static analysis, pushover analysis is carried out to find the energy in the buildings of varying slopes of 0°, 15°, 30°, 45° with and without infill modeling and energy curves and compared.

2. INTRODUCTION

There is a huge population increase in the past years and most of the population in the world lives on the hilly regions either because of land scarcity or beautiful sceneries. So there is a haphazard construction of buildings. Construction at hilly regions is different

compared to flat surface, so typical houses built on hilly regions specially in India, Nepal, Bangladesh etc are of G+3 to G+5. These buildings are unsymmetrical in geometry and irregular in stiffness As hilly regions are more vulnerable to earthquake, so providing safety measures to buildings on various slopes is more important. Recent earthquakes like Nepal earthquake showed worst effects particularly buildings on slopes as the buildings on hilly slopes lacks simple and regular configuration, adequate lateral strength, stiffness and ductility.

LATERAL BEHAVIOUR OF BUILDINGS ON SLOPES

Nepal earthquake known as GORKHA earthquake (M8.1) of April 2015 and Kangara earthquake (M7.8) of 1905 shillong were the most devastating earthquakes. Most of the earthquakes triggers due to Himalayan plates. Earthquake shows worst effects, when a building is situated on hilly regions. As the buildings on slopes do have unsymmetrical in both horizontal and vertical directions. Buildings on slopes posses variation of stiffness and mass.

Dynamic characteristics of building on hills are very differently from the buildings on the topography, because buildings are irregular and unsymmetrical in vertical and horizontal directions. Centre of stiffness and centre of mass are not coinciding with each other, these type of buildings are subjected to torsional behaviour. The short, stiff columns on uphill side attracts much higher lateral forces and prone to damage.

3. CASE STUDY AND ANALYSIS:

A different cases of G+3 buildings on slope angles of 0°, 15°, 30°, 45° are analyzed as per IS 456 and IS1893 in SAP2000 as shown in figures

Structural element sizes

Beams : 300X300 mm

Columns : 300X300 mm

Slab : 120mm thick

Material Properties

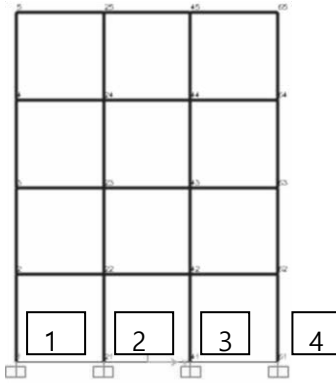
Grade of concrete : M25

Grade of steel reinforcement bars : Fe415

Loading

Live Load : 3kN/m²

Floor Finish load : 1kN/m²



G+3 Frame

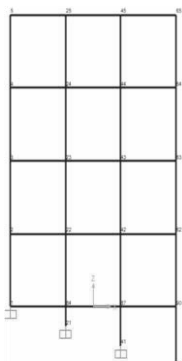
The above building is subjected to Earthquake analysis of Nepal earthquake

Two types of analyses were conducted equivalent static analysis and pushover analysis

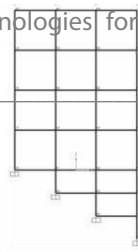
Equivalent static analysis:

This method is a simplified technique to substitute the effect of dynamic loading of an earthquake by a static lateral force on a structure. Total seismic force or base shear is calculated in horizontal directions of two axes. This method is the best suited for low rise and symmetrical buildings.

Frames are modeled for equivalent static analysis



On 15 degree slope without infill

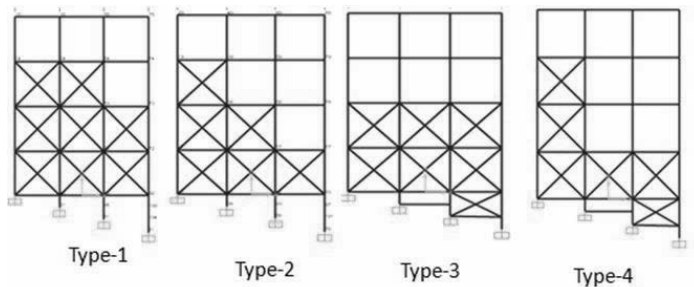


On 30 degree slope without infill



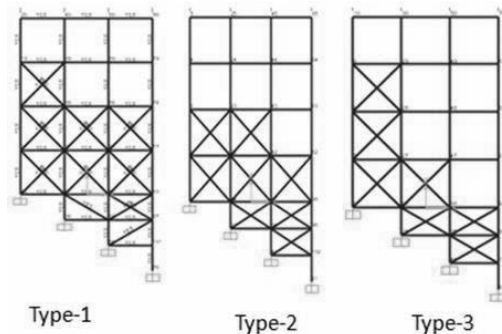
On 45 degree slope

Frames with masonry infill and different inertias of columns are modeled for equivalent static analysis on 15 degree slope



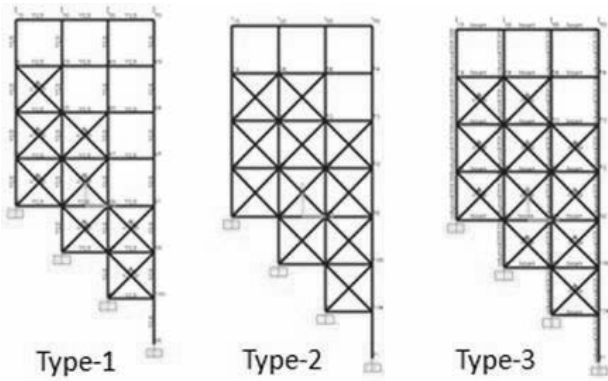
Type-1 and Type-2 column sizes are 400X300 mm
 Type-3 and Type-4 column sizes are 400X500 mm and column 2, 3, 4 are 400X300 mm

Frames with masonry infill and different inertias of columns are modeled for equivalent static analysis on 30 degree slope



Type-1 sizes of Column 1- 300X300, Column 2,3,4 - 300X300
 Type-2 sizes of Column 1- 300X300, Column 2,3 - 400X300, Column 4- 300X300
 Type-3 sizes of Column 1- 300X300, Column 2,3 - 400X300, Column 4- 300X300

Frames with masonry infill and different inertias of columns are modeled for equivalent static analysis on 45 degree slope



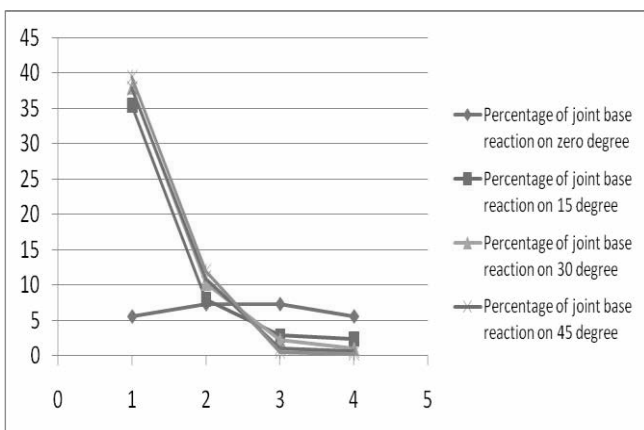
Type-1 column 1 – 400X500, column 2&3 – 400X300, column 4 – 400X500
 Type-2 column 1 – 500X600, column 2 & 3 – 400X300, column 4 – 400X500
 Type-3 all columns 400X300

4. RESULTS AND DISCUSSIONS:

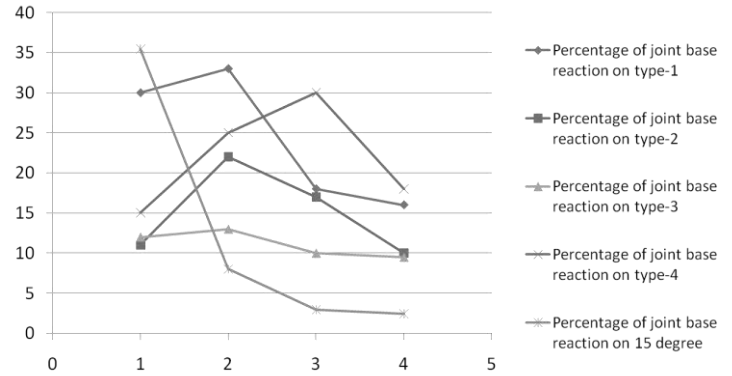
Comparison of percentage of joint base column reactions with out infill at column -1, column -2, column -3, column -4

Columns	Percentage of column joints on zero degree	On 15 deg	On 30 deg	On 45 deg
1	5.6	35.4	38.02	37.8
2	7.3	8	10.21	11
3	7.3	2.92	2.24	1.064
4	5.6	2.4	1	0.7

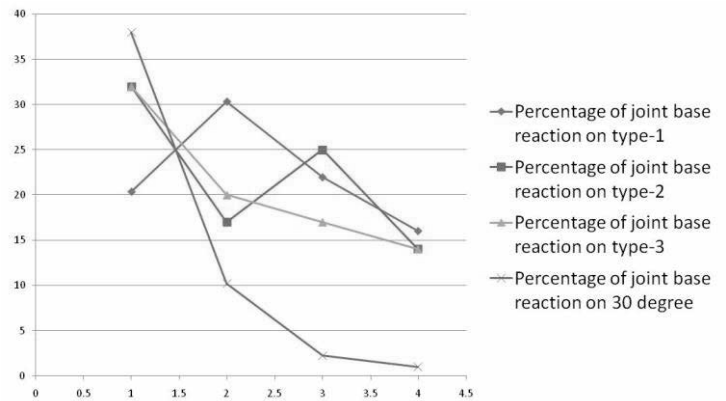
X-axis represents columns and Y-axis represents percentage of base column reaction



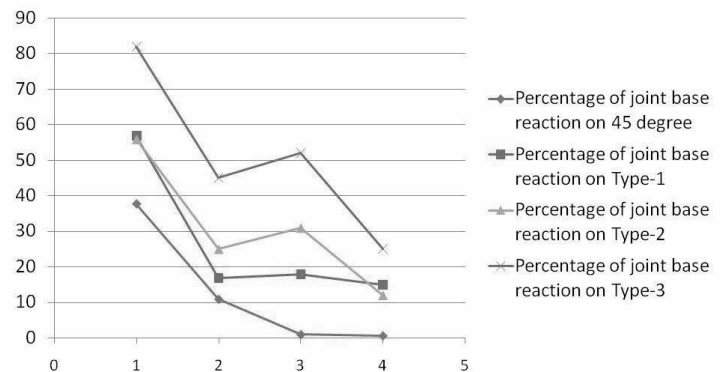
Equivalent static analysis on 15 degree frame with infill and comparison of percentage of column joint shear



Equivalent static analysis on 30 degree frame with infill and comparison of percentage of column joint shear



Equivalent static analysis on 45 degree frame with infill and comparison of percentage of column joint shear



Pushover analysis:

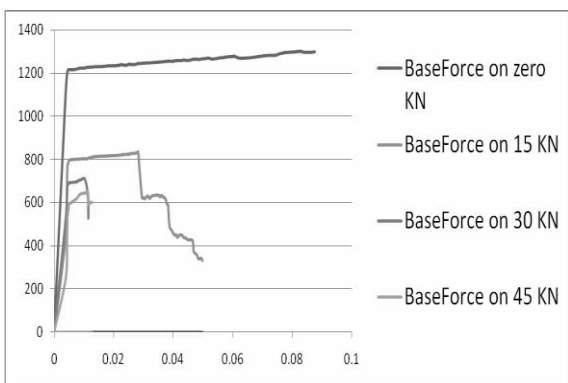
After designing and detailing the RC frame structure, a linear static pushover analysis is carried out for evaluating structural response.

Rc frame with infill masonry and with out infill is carried out on 0°, 15°, 30°, 45°

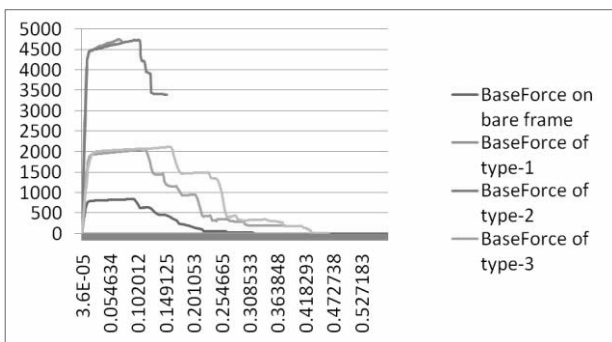
Pushover curves without infill on Zero degree

X axis represents displacement in mm

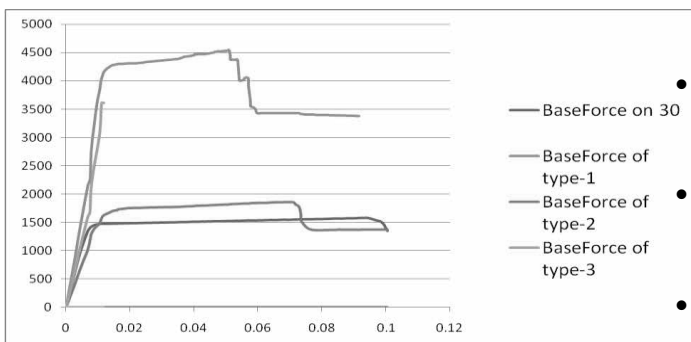
Y axis represents Base force in KN



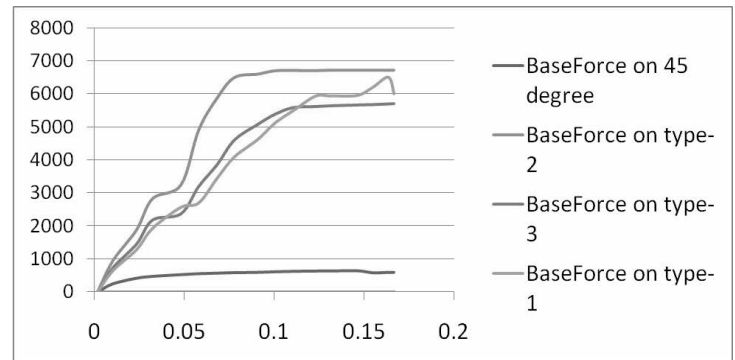
Pushover curves on 15 degree slope.



Pushover curves on 30 degree slope.



Pushover curves on 45 degree slope



Conclusions:

- When equivalent static analysis is done to building on zero slope every column takes equal shear and column joint base reaction higher at inner columns than outer columns.
- When building is on slope and analyzed with earthquake loads shorter columns tends to take more shear force.
- That's why percentage participation of base column shear is more in short columns in equivalent static analysis graphs
- With infill masonry base column shear is distributed to columns where long columns participate lesser in shear.
- In case of 15 degrees at least there is a participation of shear of long columns is 2% or 1% whereas in 30 degrees and 45 degrees it's going till 0%
- In case of 15 degrees slope, type-2 and type-4 are better configurations in taking column base shear.
- In case of 30 degrees slope, type-1 and type-3 are better configurations
- Pushover curves of zero degrees has more energy compared to slope
- As said on 15 degrees in pushover analysis type-2 and type-4 have more area under curve.

REFERENCES:

1. Agarwal, P. K. and Shrikhande, M. “*Earthquake Resistant Design of Structure*” Fourth Edition, Prentice Hall 2006.
2. Ashwani, K., Pushplata, “*Building Regulations for Hill Towns of India*”, HBRC Journal, 2014
- 3 .Babu, N. J. and Balaji, K.Y.G.D, “*Pushover analysis of unsymmetrical framed structures on sloping ground*” International Journal of Civil, Structural, Environmental and Infrastructure Engineering Research and Development (IJCSEIERD) ISSN 2249-6866 Vol. 2 Issue 4 Dec - 2012 45-54.
- 4.Birajdar, B. G. and Nalawade, S. S., “*Seismic analysis of buildings resting on sloping ground*”, 13th World Conference on Earthquake Engineering, Vancouver, B.C., Canada, Paper No. 1472, 2004.
- 5.Chopra, A. K., “*Dynamic of Structures: Theory and Application to Earthquake Engineering*” [M]. 2nd ed. Upper Saddle River, N.J: Pearson/Prentice Hall, 2007.
6. Fajfar, P., “*A nonlinear analysis method for performance based seismic design*”, Earthquake Spectra, vol. 16, No. 3, pp. 573-592, 2000.
7. IS 1893-2002(Part-1), “*Criteria for Earthquake resistant design of structures Part, General provisions and buildings*”, Bureau of Indian Standards, New Delhi 110002.
- 8.Sreerama, A. K. and Ramancharla, P. K., “*Earthquake behaviour of reinforced concrete framed buildings on hill slopes*”, International Symposium on New Technologies for Urban Safety of Mega Cities in Asia (USMCA 2013), Report No: IIIT/TR/2013/-1.
- 9.Yang, P. and Wang, Y., “*A study on improvement of pushover analysis*”, Proceedings of 12th World Conference on Earthquake Engineering, 2000, Auckland, New Zealand
- 10 Y. Singh & Phani Gade, D.H. Lang & E. Erduran “*Seismic Behavior of Buildings Located on Slopes - An*

Analytical Study and Some Observations From Sikkim Earthquake of September 18, 2011”

NUMERICAL STUDY OF A NEW RETROFITTING METHOD FOR WEAK RC FRAME BUILDINGS WITH MASONRY INFILL WALLS USING PP-BAND MESH TECHNIQUE

S.C.SADINENI¹, H.GOKON² AND K.MEGURO³

¹PhD student, Department of Civil Engineering, the University of Tokyo, Japan

silpa@iis.u-tokyo.ac.jp (corresponding author)

²Assistant Professor, ICUS, IIS, the University of Tokyo, Japan

³Director/Professor, ICUS, IIS, the University of Tokyo, Japan

Keywords: 3D-Applied element method, PP-band mesh, Seismic retrofitting, In-plane isolation

1. INTRODUCTION

Reinforced concrete with masonry infill (RCMI) buildings are a major part of the building inventory in the urban sprawl. Many of them are either designed only for gravity loads or non-engineered (“weak frames”) in seismically active regions. Non-ductile beam-column joints, improper rebar splicing, insufficient shear reinforcement, and low-quality materials are typical features of the weak RC frames with masonry infills (WRCFMI). The collapse of WRCFMI buildings during earthquakes has shown that their response is vastly influenced by the interaction between the bounding frame and its walls. Not only in-plane interaction of masonry infills is a problem but also the out-of-plane collapse. The effect of masonry infill walls in the weak frame can be defined by the type of non-engineering defect present in the structure and the material properties. Masonry infill walls increase shear demand on the column which may result in premature collapse. Also, the diagonal strut formation of the masonry infill walls shows a detrimental effect on the beam-column joint. To mitigate the wall induced damage, many retrofitting methods have been proposed to strengthen the frames and isolate the walls. Many of the wall isolation techniques are not popular as they make infill wall more vulnerable in the out of plane direction and also giving the connection between the wall and frame is very complex and expensive process.

In this paper, we propose a PP-band mesh detailed wall isolation retrofitting technique which considers the load-bearing capacity of the wall, benefits of wall isolation, out-of-plane vulnerability, cost, and construction complexity.

2. METHODOLOGY

The primary objective of this paper is to propose and investigate PP-band mesh detailing wall isolation method for WRCFMI buildings. This proposed strategy isolates the infill wall from columns and beam (Figure 1). The flexible soft material is provided in the vertical gaps between wall and column for fire insulation, namely polystyrene foam. Due to this isolation, premature failure of the columns can be avoided and keeps the wall intact before the inelastic state. At higher drifts, when the RC frame exceeds the width of the gap, higher strength and stiffness can be provided by the infill wall. A thin weak

mortar layer is used between beam and wall as a top interface. At lower drifts, weak mortar layer cracks and lateral shear transfer from the bounding frame can be avoided. In this case, transfer of vertical loads from beam to the wall should not be a problem. Overall these interfaces play the key role in effectively mitigating the undesirable interaction between frame and wall at moderate story drifts. And also, they act as a good energy dissipation zones.

Finally, to minimize the out-of-plane collapse of the wall due to in-plane isolation, PP-band mesh is provided. Cracks in the masonry infill due to in-plane forces drastically reduce the out-of-plane strength, but with PP-band mesh wall will regain its strength. PP-band encourages progressive collapse while keeping the integrity of the wall [3]. Due to this, during inelastic stages, an alternative load path will form.

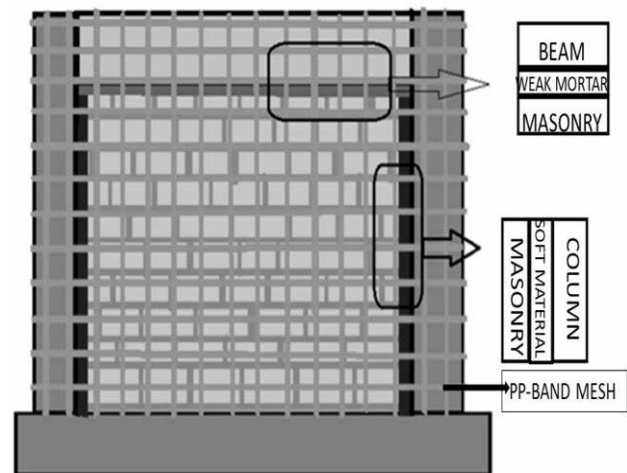


Figure 1: Layout of PP-band mesh detailed wall isolation method

3. NUMERICAL STUDY

A three dimensional Applied Element Method (3D-AEM) is used to test the effectiveness of the proposed technique. Using the AEM a structure can be analyzed from an initial stage of loading until collapse [2].

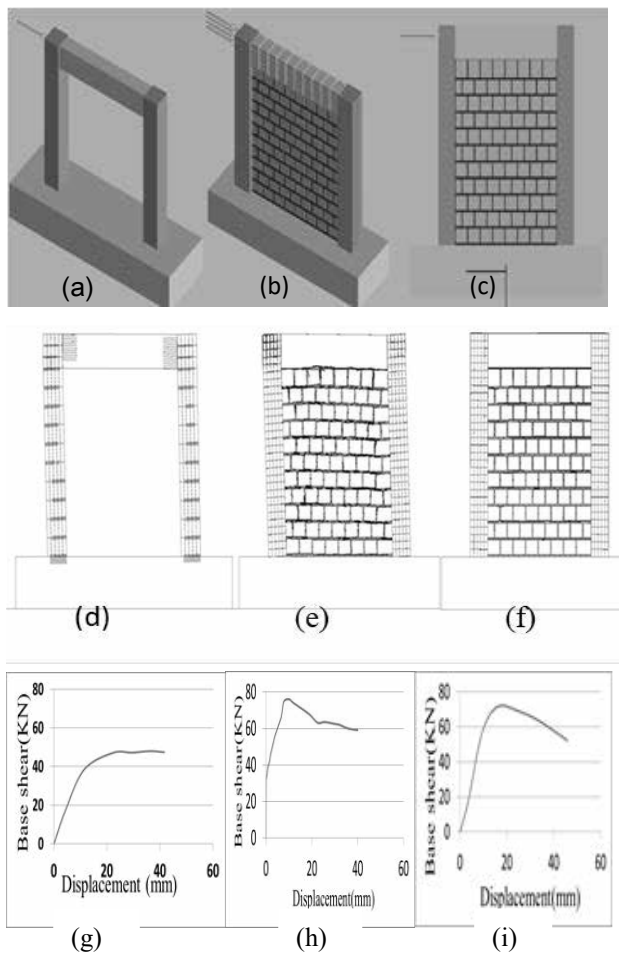


Figure 2: Simulation results for bare frame, infilled frame, wall isolation using cellular material: (a), (b), (c) Initial stage; (d), (e), (f) Final stages of cracking; (g), (h), (i) Base shear force-Displacement curves

To validate the effectiveness of the tool to capture the frame-infill interaction and its failure modes, the calibration of the numerical model in 3D-AEM user interface was made based on the experimental results obtained by Tsantilis et al. [1] on the in-plane cyclic loading of isolation of masonry infills in RC frames using cellular material. The numerical model of the infill panel is defined using micro modelling approach. According to the obtained results, isolated specimen initially behaves like a bare frame, as the drift levels increases it quickly comes in contact with the wall and behaves like tight fit infill frame (Figure 2). Tight fit infill specimen experienced more severe cracks comparatively with the isolated specimen. Numerical results show good agreement with the experiment.

Next, to study the effectiveness of the newly proposed technique to improve the performance of WRCFMI structures, a two-story two-bay RC infilled box type buildings (Buildings with bare frame, infilled and proposed retrofitting technique) was selected with non-ductile beam-column joints and improper spacing of the stirrups. The response and failure mechanism of above-mentioned cases are compared under earthquake loading. In this paper, the collapse pattern of bare frame building (Figure 3) and infilled frame building (Figure 4) are

presented. In the bare frame building, initially, cracks started at the end of columns and beam-column joints and finally building failed due to the brittle failure of columns. With the infilled frame, it is observed that due to the collapse of the infills in the ground story produced a soft story effect which eventually leads to collapse.

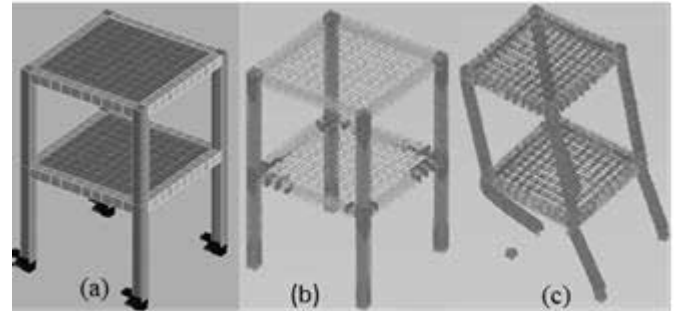


Figure 3: Bare frame: (a) Initial stage; (b) Cracking; (c) Collapse

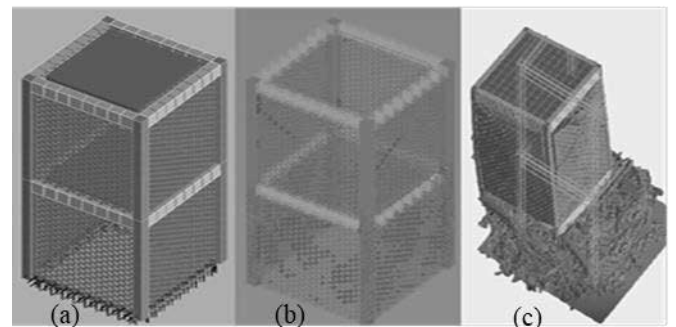


Figure 4: Infilled frame: (a) Initial stage; (b) Cracking; (c) Collapse

4. CONCLUSIONS

In the paper, we proposed a novel retrofitting technique for the WRCFMI frames using PP-band mesh detailed wall isolation approach. By the calibration of numerical simulation using the AEM with experimental results, we can say that the AEM was able to capture the behavior of masonry infilled frames and the effects of wall isolation. A 3D numerical analysis of RC bare frame and Infilled frame with non-engineering defects were also presented. Remaining results will be presented at the USMCA2018 in Hyderabad, India.

REFERENCES

- [1] A. V. Tsantilis and T. C. Triantafyllou, 2018 "Innovative seismic isolation of masonry infills using cellular materials at the interface with the surrounding RC frames," *Eng. Struct.*, vol. 155, pp. 279–297.
- [2] Meguro, K. & Tagel-Din, H. S. (2002). Applied Element Method Used for Large Displacement Structural Analysis. *J. Nat. Disaster Sci.* 24, 25–34.
- [3] Sathiparan, N. & Meguro, K (2013) Shear and flexural bending strength of masonry wall retrofitted using PP-band mesh. *Construction* 14, 3–12.

USMCA 2018

SESSION 4

URBAN SAFETY

TERRITORY CLUSTERING ON VISUAL ATTRACTIONS OF MULTI-OBJECTS

Miyuki WAKASUGI¹, Yudai HONMA²

¹ Graduate Student, Graduate School of Engineering, the University of Tokyo, Tokyo, Japan, miyuki-w@iis.u-tokyo.ac.jp

² Associate Professor, Institute of Industrial Science, the University of Tokyo, Tokyo, Japan, yudai@iis.u-tokyo.ac.jp

Keywords: visual attraction, multi-objects, territory clustering

1. INTRODUCTION

In this research, we propose a new territory clustering method which focuses on the visual attractions of multiple objects. There are plenty of situations to analyze visual perceptions in urban safety fields. One typical example is evacuation from damaged buildings. It is required to allocate the sign of an emergency exit, but there are also several obstacles which shield our visibility. It means that there are both “attractive” objects and “unattractive” objects in disaster-stricken regions. It is important to organize such spaces regarding visual perceptions. For this purpose, we first calculate a visual balance of attractive vs. unattractive objects. Then we categorize spaces based on total visual balance and clarify spatial cluster pattern which characterizes disaster regions.

2. FORMULATION

Let us calculate visual effects by multiple objects. Space is a two-dimensional plane, and we suppose a polar coordinate system (r, θ) . We also assume that the position of an evaluator is the origin of space O, and we call it “evaluation point” from now on. In this paper, we assume that all objects can be represented by polygons, and the vertex coordinates of each object k are given as $[p_k^1, p_k^2, \dots, p_k^{M_k}]$. Further, each object has visual attractiveness (or visual unattractiveness) S_k .

Let us define a visual vector v_k to represent viewing the object k from the evaluation point O. For this purpose, we have to calculate both direction and length of v_k (see Figure 1). First, we state how to determine the direction. Since we deal with several types of shape objects including thin objects or large objects, we give the direction to visual vector in the direction to the nearest part of the object. Precisely to say, the direction of v_k is defined as follows:

$$\arg(v_k) \stackrel{\text{def}}{=} \arg(p_k^{\min}) \quad (1)$$

where p_k^{\min} is the coordinates of the nearest part of object k . In the case, p_k^{\min} should be either the nearest vertex of the polygon or the intersection of the perpendicular line to the polygon edge:

$$p_k^{\min} = \min(x \in C_k | \forall x' \in C_k, |x| \geq |x'|) \quad (2)$$

$$C_k = \{p_k^m\} \cup \{q(p_k^m, p_k^{m+1})\} \quad (3)$$

Here, $q(\cdot)$ is the intersection of the perpendicular line from the viewpoint O to the line segment pp' which satisfies (4):

$$Oq(p, p') \perp pp' \quad (4)$$

Next, the length of the visual vector will be described. Each object has an attractiveness (or unattractiveness) value. It means that attention is attractive if the value is positive, and unattractive if negative. When negative, the direction would be the opposite.

It is natural to express the length of the visual vector as a function of both attractiveness degree of the object and the distance to the object. In other words, it is nothing other than assuming that there is a spatial interaction relation between the viewpoint and the object. Thus, the length of the visual vector v_k is defined as (5):

$$|v_k| \stackrel{\text{def}}{=} S_k \exp[-\gamma |p_k^{\min}|] \quad (5)$$

Note that $|p_k^{\min}|$ expresses the distance from the viewpoint to the object k , because the origin of the coordinate system is in the evaluation point.

In addition, we suppose that each object has a transparent degree and $|v_k|$ will be decreased based on that value if it passes through other objects. Examples of opaque objects are walls and glasses, meanwhile ponds and furniture would be transparent. As a result, the visual vector which also incorporates the transparency is expressed as (6):

$$|v_k| \stackrel{\text{def}}{=} \prod_{k' \in C_k} t_{k'} \times \exp[-\gamma |p_k^{\min}|] \quad (6)$$

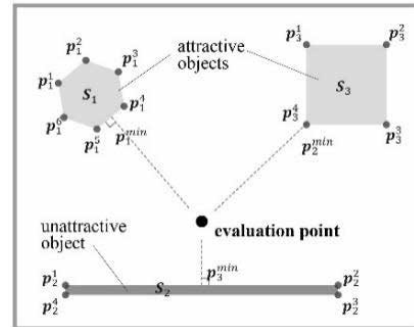


Figure 1: set objects as coordinates

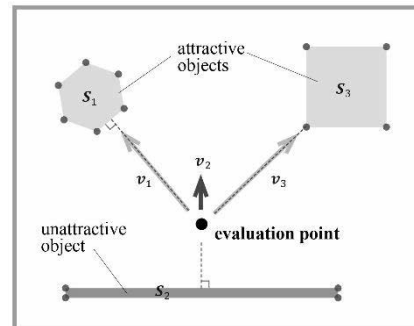


Figure 2: generate vectors from the evaluation point

where t_k is a transparent degree of object k (the range is $[0,1]$) and C_k is a set of objects which get crossed with the segment Op_k^{\min} .

As described above, the visual vector for the object k is described by from (1) to (5). Since there are $|K|$ objects in the target space, a set of viewing vector (6) is given as follows:

$$V = [v_1, v_2, \dots, v_k, \dots, v_{|K|}] \quad (7)$$

Figure 3, 4 is an example which is applied the model to Barcelona Pavilion. This building is regarded as one of the most sophisticated Architectures in the world. In the plan view of Barcelona Pavilion, we can confirm several objects affect results, such as ponds and statue (attractive), walls and glass walls (unattractive). As in Figure 1 and 2, evaluation points are arranged in the plan view (Figure 3), and the influence of attractive and unattractive objects is calculated and shown in Figure 4.

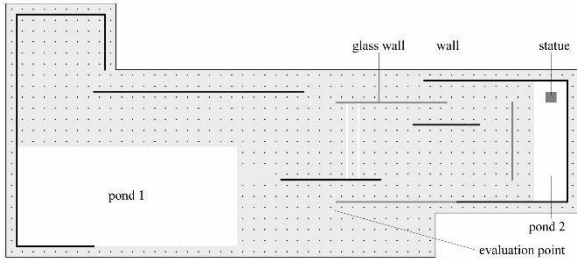


Figure 3: evaluation points on the plan of Barcelona Pavilion

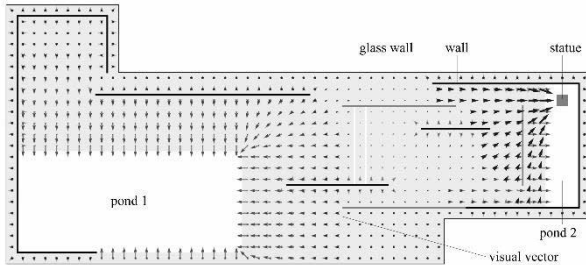


Figure4: generate visual vectors from each evaluation points

3. VISUAL VECTOR SIMILARITY

(7) is a "distribution" of vectors, so we can discuss a variety of things by simply observing a result (Figure 2). However, to focus on the characteristics more specifically, we first focus on the maximum vector. The maximum vector is defined as

$$v_{\max} = [v_k | \forall k', |v_k| \geq |v'_k|] \quad (8)$$

Since v_{\max} can be interpreted as a representing visual vector, the absolute value of $|v_{\max}|$ and the argument $\arg(v_{\max})$ express the features of viewpoint.

To extract the largest visual vector, that means, it is also possible to determine which object has the largest influence at each evaluation point. The visual attractive power relationship is shown in Figure 6.

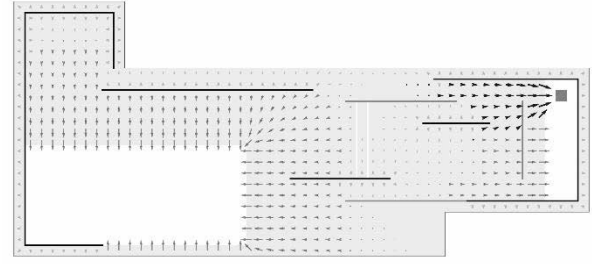


Figure5: maximum visual vectors

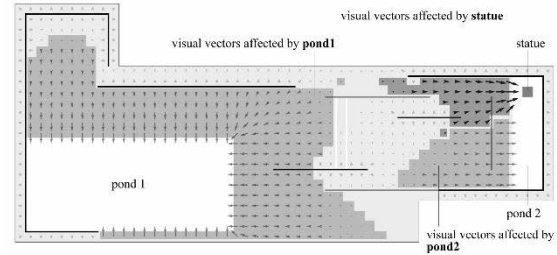


Figure 6: visual attractive power relationship

Furthermore, it is also possible to simplify the visual vectors by synthesizing vectors. The synthetic vector is defined as

$$v_{\text{total}} = \sum_{k \in K} v_k \quad (9)$$

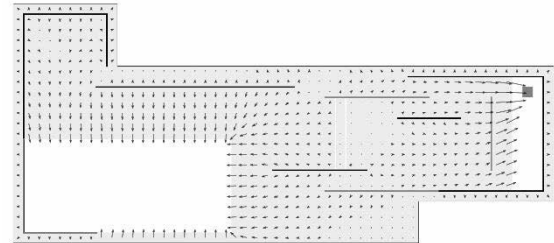


Figure 7: synthetic visual vectors

In any cases, by focusing on the "length" and "angle" of the vector, the characteristics of the space can be clarified. Moreover, if it needs to compare the evaluation point O and the evaluation point O' , it is easy to compare, that is simply focused on V and V' . The dissimilarity of V and V' can be calculated in several ways, such as comparing the length of vectors(9), comparing the angle of vectors(10), and calculating the inner product of vectors(11). Here we assume that the characteristic of V is expressed as v_{\max} :

$$d(V, V') = \frac{||v_{\max}| - |v'_{\max}||}{\max(|v_{\max}|, |v'_{\max}|)} \quad (10)$$

$$d(V, V') = \frac{|\arg(|v_{\max}|) - \arg(|v'_{\max}|)|}{\pi} \quad (11)$$

$$d(V, V') = -1 \times \langle v_{\max}, v'_{\max} \rangle \quad (12)$$

For (9) and (10), they are standardized, and the ranges are $[0, 1]$.

4. CLUSTERING

Now, let us explain how to analyze clustering of the space from the visual vector. The procedure is as follows. First, we set a plurality of viewpoints O_1, O_2, \dots, O_N in the target space. Then, calculate $N \times N$ dissimilarity matrix between arbitral viewpoints:

$$D = [d(\mathbf{V}_i, \mathbf{V}_j)] \quad (13)$$

It is well known that D is the essential information for various clustering methods. For example, if we solve the p -median problem by interpreting the N viewpoints into both the demand point and the facility candidate point, we can obtain a representative viewpoint and clustering.

We calculated this dissimilarity matrix for two types of representative visual vectors (maximum vector or synthetic vector). For each type, we clustered vectors by a degree of three types, dissimilarity of length only, dissimilarity of angle only, dissimilarity of angle and length. Results are shown from Figure 8 to Figure 13. All of them are clustering into four parts. Figure 8 to Figure 10 are clustering figures about max visual vectors. Figure 11 to Figure 13 are clustering figures about total visual vectors.

In each of clustering using maximum visual vector or synthetic visual vector, it can be seen there are areas made by effects of the visual attraction of ponds or the statue.

In this paper, we made clustering for 2 types, maximum visual vector and synthetic visual vector, but in both cases, the one cluster areas are classified in the similar place. It can be said that the figures clustered based on the length of the visual vectors (Figure 8 and 11) show how much the influence on the direction of the visual strength depending on the distance from the attractive or unattractive object. Next, the figures clustered by the angle of the visual vectors (Figure 9 and 12) can be thought of as the orientation of the face of people who evaluate the space when viewing the object. Finally, the figures are clustered by the indexes of these two indicators, the angle and length of visual vectors (Figure 10 and 13) are considered to be more realistic space. In each cluster it is assumed to be similar visual recognition.

We think this clustering method can be applied to an evacuation planning. Setting the evacuation guidance lights as a visual attractive object allows you to plan the optimum evacuation route so that visually attracted areas are continuous.

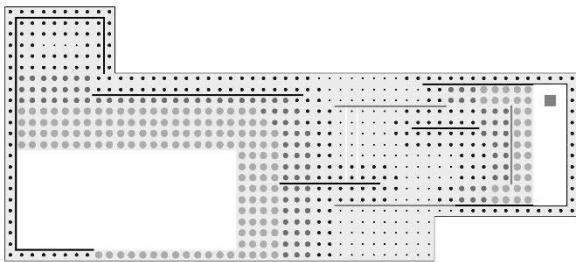


Figure 8: clustering by length of the maximum visual vector

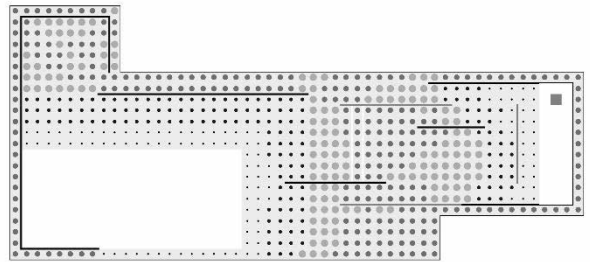


Figure 11: clustering by length of the synthetic visual vector

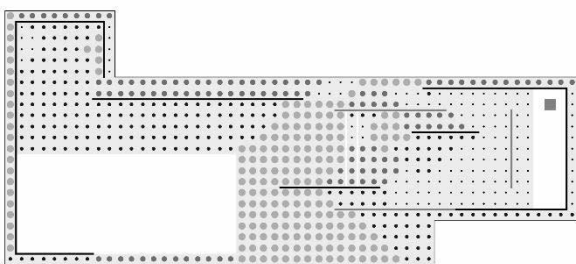


Figure 9: clustering by angle of the maximum visual vector

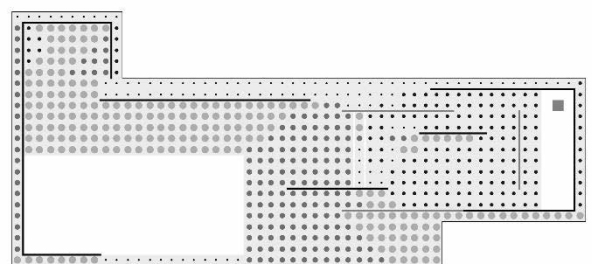


Figure 12: clustering by angle of the synthetic visual vector

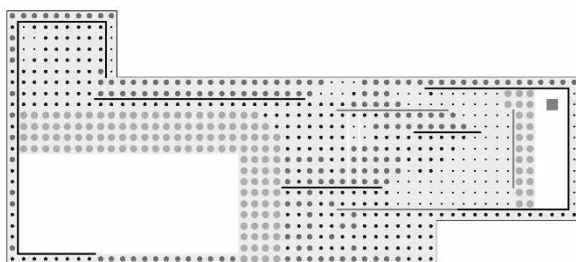


Figure 10: clustering by angle and length of the maximum visual vector

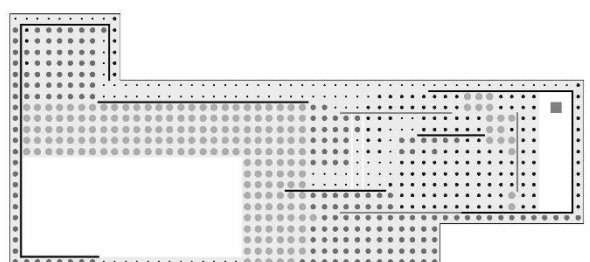


Figure 13: clustering by angle and length of the synthetic visual vector

A NOVEL TECHNIQUE FOR ESTIMATING EXPANSION OF RESIDENTIAL, COMMERCIAL AND INDUSTRIAL REGIONS IN INDIAN MEGACITIES

PRAKHAR MISRA¹ and WATARU TAKEUCHI²

¹ Post-doctoral Fellow, Department of Civil Engineering, The University of Tokyo, Tokyo, Japan, mprakhar@iis.u-tokyo.ac.jp (corresponding author)

² Professor, Department of Civil Engineering, The University of Tokyo, Tokyo, Japan, wataru@iis.u-tokyo.ac.jp

Keywords: Digital building height, digital surface model, nighttime light, urban morphology, GDP, population

1 INTRODUCTION

Urban land-use maps are important in several applications such as disaster response simulation, transport planning, emission inventory, etc. However they are not publicly available in several developing countries across the world as they have data restrictions, are outdated or do not exist as GIS data. Identifying residential, commercial and industrial regions is particularly interesting due to their different contribution in emissions inventories. High spatial resolution emission inventories have been recommended by IPCC AR5 report [1] under Tier III approach for emission estimation to overcome the current uncertainties in Tier I approaches that rely mostly on statistical data. Currently none of the developing countries have used Tier III approach which is critical to manage their grown urban air quality issues [2]. Further it is also important to monitor expansion of these land-use classes along with socio-economic growth parameters.

1.1 Objective

The objective of this paper is a) identification of land-use urban morphology in terms of residential, commercial and industrial regions, and b) estimating their expansion function with socio-economic growth.

2 METHODOLOGY

The flowchart of dataset and methodology employed for estimating expansion of residential, commercial and industrial regions is shown in Figure 1.

2.1 Data location

Data location consist of 6 Indian megacities (referred as Tier -1): New Delhi, Mumbai, Chennai, Bengaluru, Hyderabad and Kolkata, and 10 medium sized cities (referred as Tier -2): Agra, Ahmedabad, Allahabad, Amritsar, Kanpur, Lucknow, Ludhiana, Patna, Raipur and Jaipur. These cities were chosen due to high presence of fine particulate matter (PM_{2.5}) [6].

2.2 Data used

Digital Building height: An original digital building height model derived from freely available digital surface datasets for the year 2001 ('ASTER Global Digital Elevation Model v2') and 2011 ('ALOS World 3D') was used as height of buildings [3]. Figure 2 shows differences in building height for residential, commercial and industrial areas. Its spatial resolution is approximately 30 m.

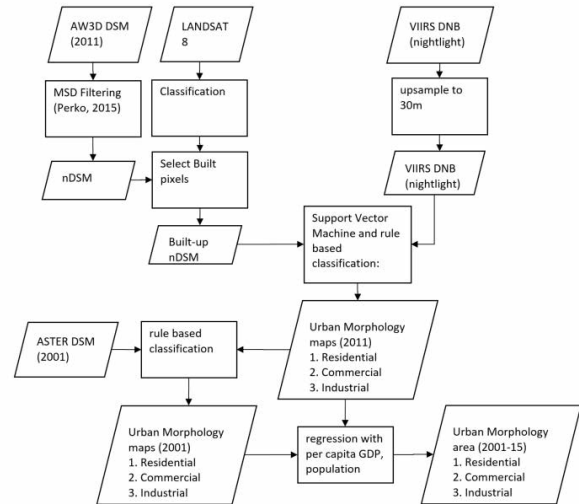


Figure 1: Overall flowchart to estimate emission parameters and generate annual emission trend

Nighttime light: Nighttime light was derived from annual median composite for the 2014 VIIRS DNB band. Its spatial resolution is approximately 15 seconds (750 m).

Socio-economic data: Yearly population projections from United Nations population projections [5]. District level gross domestic product (GDP) data was downloaded from Government of India's Open Government Data (OGD) Platform (<https://data.gov.in/>).

Training data and classification: Training areas was selected in the form of polygons by identifying residential (R), commercial (C) and industrial (I) areas using field visits and visual interpretation in Google Earth Pro. Thereafter building heights and nighttime lights over the training areas were used as describing features into support vector machine for classification.

2.3 Urban expansion model

Following Seto et al. [4] that urban population growth and GDP per capita drive urban expansion, we used the following simple model to estimate area (A) :

$$A_{UM} = f(GDP_{pc}, Population) \forall UM \in R, C, I \quad (1)$$

3 RESULTS AND DISCUSSION

Classified land-use map is shown for a sample region in Figure 4. Tall residential buildings could not be identified ow-

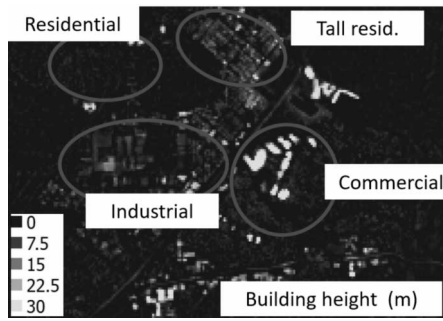


Figure 2: Digital building height model extracted from AW3D DSM shows height difference in residential, commercial and industrial areas. Example location shown is South of New Delhi ($28^{\circ}29.744'N$, $77^{\circ}5.138'S$).

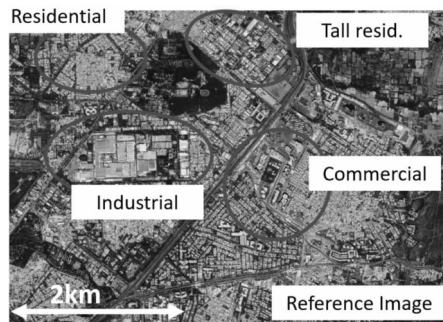


Figure 3: Polygons were drawn with help of Google Earth Pro to select residential, commercial and industrial areas as training data. This location is same as Figure 2.

ing to similarity with industrial regions. Accuracy of classification differed for each city. Abundance of heterogeneous classes in close proximity led to errors, e.g. school building, bridges, overbridges, etc. Generally high accuracy was seen for residential areas (87% to 100%) and commercial areas (64% to 95%). Accuracy over industrial areas varied greatly from 49% to 97%.

As seen in Table (1), land-use area of residential, commercial and industrial regions in Tier-1 cities was correlated with per capita GDP (ranging from 0.65 to 0.89). In Tier-2 cities, land-use area was correlated with both per capita GDP and population size (ranging from 0.69 to 0.77). This implies that more industrial areas are found in regions

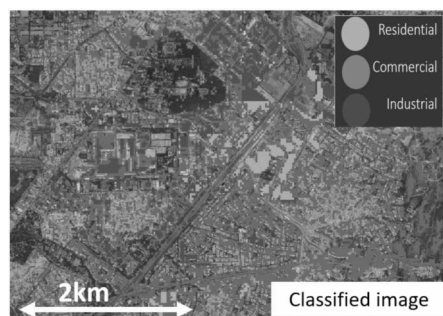


Figure 4: Land-use urban morphology map for residential, commercial and industrial areas obtained after SVM classification. This location is same as Figure 2.

Table 1: Summary of urban expansion equations for area of residential (R), commercial (C) and industrial (I) regions for Tier 1 and Tier 2 cities.)

Tier	Equation	R^2
1	$R = 0.0008GDP_{pc} + 0.0021pop - 8.44$	0.75
1	$C = 9.32\log(GDP_{pc}) + 0.0008pop - 97.73$	0.61
1	$I = 4.004\log(GDP_{pc}) + 0.0005pop - 42.80$	0.83
2	$R = 8.17\log(GDP_{pc}) + 20.43\log(pop) - 216.93$	0.72
2	$C = 1.20 \times 10^6 GDP_{pc} + 0.0005pop - 4.88$	0.76
2	$I = 4.67 \times 10^6 GDP_{pc} + 0.0012pop - 1.40$	0.81

with higher population although underlying drivers of urban growth in the two types of cities could be different. The latter may also be true for a reverse relationship of high population converging towards industrial areas since migration from economically backward regions to industrial hubs is common in Indian cities. A logarithmic relationship of industrial areas with per capita GDP in Tier-1 cities could also point to gradual stagnation in new industrial settlements.

4 CONCLUSION

Land-use maps of urban morphology for residential, commercial and industrial regions can be classified using building height and nighttime light with accuracies higher than 49% with industrial areas requiring improvement in accuracy. Further expansion patterns suggests that commercial and industrial areas expand differently compared to residential areas in Tier-1 and Tier-2 cities. To ensure accurate land-use area expansion representation, building height products from other years are required to be developed.

References

- [1] IPCC. "Summary for Policymakers". In: *Climate Change 2014: Mitigation of Climate Change. Contribution of Working Group III to the Fifth Assessment Report of the Intergovernmental Panel on Climate Change* (2014), pp. 1–33. arXiv: arXiv:1011.1669v3.
- [2] Prakhar Misra, Aya Fujikawa, and Wataru Takeuchi. "Novel decomposition scheme for characterizing urban air quality with MODIS". In: *Remote Sensing* 9.8 (2017), p. 812.
- [3] Prakhar Misra and Wataru Takeuchi. "Digital Surface Model (DSM) Datasets for Built Structure Height Estimation over Indian Cities". In: *International Remote Sensing Symposium (ISRS)*. Nagoya, Japan, 2017, pp. 1–4.
- [4] Karen C. Seto et al. "A Meta-Analysis of Global Urban Land Expansion". In: *PLoS ONE* 6.8 (2011). Ed. by Juan A. Añel, e23777. arXiv: 1203.2655.
- [5] United Nations. *UN Population Division*. (Visited on 12/24/2017).
- [6] World Health Organization. *Ambient (outdoor) air pollution in cities database 2014*. 2014. (Visited on 08/30/2015).

water level. As for height, it tends to increase with the increase in initial ground water level. Focusing on the circle plots and $y=x$ line, it seems that the ceiling of an initial cavity tends to be the same or a little higher than initial ground water level. On the other hand, width of an initial cavity tends to increase much less steeply than height.

3.2 GROUND ARCHING

Ground arching is a phenomenon that force acting between soil particles transfer in arched shape above subsidence part to stabilize the structure. It is assumed that if the thickness of covering soil above a cavity is short compared to the width of the cavity ground arching cannot develop and the cavity will collapse^[1].

Figure 5 shows the relationship between the thickness of covering soil above a cavity and the width of a cavity immediately before collapse. As shown in figure 3, y_1 and y_2 in figure 5 stand for the minimum and maximum thickness of covering soil respectively. According to figure 5, there seems to be correlation between the mean thickness of covering soil $((y_1+y_2)/2)$ and the width of a cavity.

This relationship enables us to roughly estimate whether a cavity is stable or not. If the plot of a cavity is under the line, it means that the covering soil is not thick enough to stabilize. In other words, ground arching cannot develop and the cavity is likely to collapse. Since this linear relationship can be useful to estimate the stability of a cavity, further investigation should be conducted.

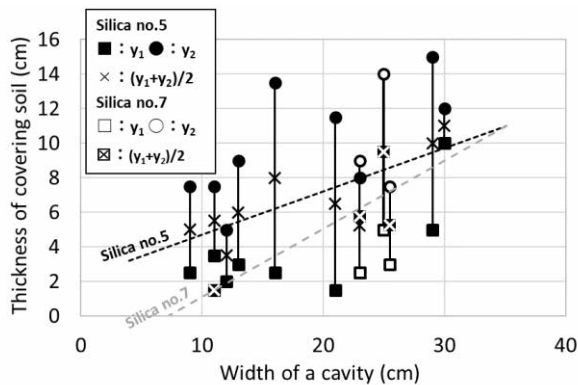


Figure 5: Thickness of covering soil vs. width

3.3 HISTORY OF CAVITY EXPANSION

Based on the field survey conducted at national roads in Japan, Nakata reported that a cavity tends to expand horizontally rather than vertically^[2]. Figure 6 shows the history of cavity expansion in the model tests. Each group of plots connected by line stands for how the thickness of covering soil and width of a cavity changed in each test. In general, width of a cavity tends to increase more than mean thickness of covering soil decreases. It means that a cavity tends to expand horizontally and this corresponds to the report by Nakata^[2]. It can be said that first a cavity expands horizontally and then expands vertically.

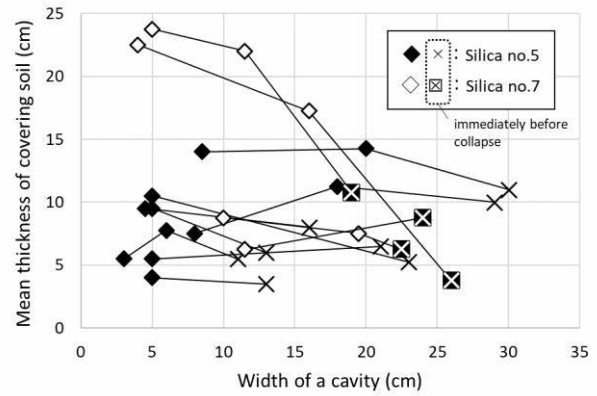


Figure 6: History of cavity expansion.

Line 1 and 2 in figure 5 are steeper than others and that can be ascribe to their different way of cavity expansion. As shown in figure 7, vertical shear band was formed at the moment of cavity expansion in line 1 and 2 and this could lead to the relatively steep decrease in the thickness of covering soil.

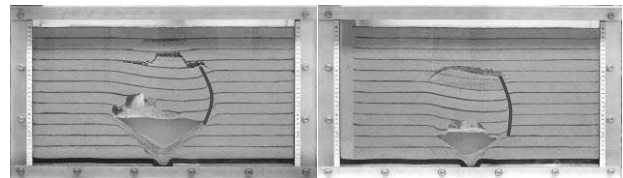


Figure 7: Cavity expansion in line 1 (left) and 2 (right)

4. CONCLUSION

In the model tests simulating cavity formation/expansion, followings were observed.

1. The ceiling of an initial cavity tends to be the same or a little higher than initial ground water level.
2. The width of an initial cavity tends to increase much less steeply than height.
3. Immediately before collapse, there seems to be correlation between the thickness of covering soil and the width of a cavity. The thickness of covering soil tends to be larger with the increase in the width of a cavity.
4. This relationship enables us to roughly estimate whether a cavity is likely to collapse or not.
5. A cavity tends to expand horizontally rather than vertically.

REFERENCES

- [1] R. Kuwano, Y. Ohara, and R. Sera (2018), An investigation of mechanism of cavity expansion and cave-in formation in sand observed in model tests, 53rd conference by Japanese geotechnical society, Takamatsu, July 2018
- [2] Y. Nakata, R. Kuwano, R. Sera (2018), A study on progress of subsurface cavities under national roads in Japan, Japan Society of Civil Engineers 2018 Annual Meeting, Sapporo, August 2018 (in Japanese)

DISCOM: A ROBUST POST-DISASTER COMMUNICATION INFRASTRUCTURE

A.PADITYA VARMA¹, ABHINAV KOLLA², RISHAAD³, DILIP KUMAR⁴, PRAFULLA KALAPUTAPU⁵, BHARGHAVA RAJARAM⁶

¹ Second Year Student, Civil Engineering, Mahindra Ècole Centrale, Hyderabad, India, adityavarma170124@mechyd.ac.in

² Second Year Student, Civil Engineering, Mahindra Ècole Centrale, Hyderabad, India, abhinav170113@mechyd.ac.in

³ Second Year Student, Civil Engineering, Mahindra Ècole Centrale, Hyderabad, India, rishaad170130@mechyd.ac.in

⁴ Faculty, Civil Engineering, Mahindra Ècole Centrale, Hyderabad, India, venkata.pasupuleti@mechyd.ac.in

⁵ Faculty, Computer Science Engineering, Mahindra Ècole Centrale, Hyderabad, India, prafulla.kalaputapu@mechyd.ac.in

⁶ Faculty, Electrical & Electronics Engineering, Mahindra Ècole Centrale, Hyderabad, India, bharghava.rajaram@mechyd.ac.in

Keywords: Disaster Management, Communication System, Ad-hoc, Bluetooth network, Emergency, Broadcast, Mobile Application.

1. INTRODUCTION

One of the most immediate and significant impacts of flooding and natural disasters is the sudden and wide-scale breakdown of communications infrastructure. When public communication networks fail, the impact can be widely felt and has the ability to interrupt access to standard mobile or landline telecommunications, and as an extension, access to the Internet. Locating those who maybe trapped or injured becomes nearly impossible for emergency responders, and rescue efforts are further complicated by the inability to coordinate via standard methods of communication. Whether these systems are completely or just partially knocked offline, communications systems during a natural disaster can be the difference between life and death for those affected.

2. COMMUNICATION INFRASTRUCTURE FAILURES

Physical Damage to Network Devices: Perhaps the most common cause of communications failures during disasters is the physical damage to devices or components that make up the network infrastructure. Hurricane-force winds, floodwaters, and seismic activity can all create physical disturbances that have power to do significant damage to cities and the vulnerable communications equipment that's responsible for supporting these areas.

Network Congestion: When disaster strikes, the "pipes" that make up our communications networks often become congested with exceptionally high levels of data traffic, as those impacted seek to contact family and friends, emergency personnel work to coordinate relief efforts, and hundreds more upload pictures and videos of the damage.

3. SMARTPHONE AND EMERGENCY RESPONSE

Based on smartphone shipment 2015 release research suggests that for 60% of all handheld gadgets are smartphones and the numbers are still growing and it is getting more popular among common people. In smartphones, number of emergency applications are growing that are beneficial in emergency response. Due to the innovations in GPS technology, this can be very helpful in the tracking of assets and also helpful to send information to emergency management headquarters for the analysis of destruction caused by the disaster [1]. In a critical circumstances, number of users use their smart phones are represented in percentage. 50% users use their smart phones in emergency situations including local accidents, 14% users use their smart phones to notify the emergency management authorities to get help in case of any disaster, 8% users use their smart phones for medical emergency, 5% use their phones for emergency helpline [2]

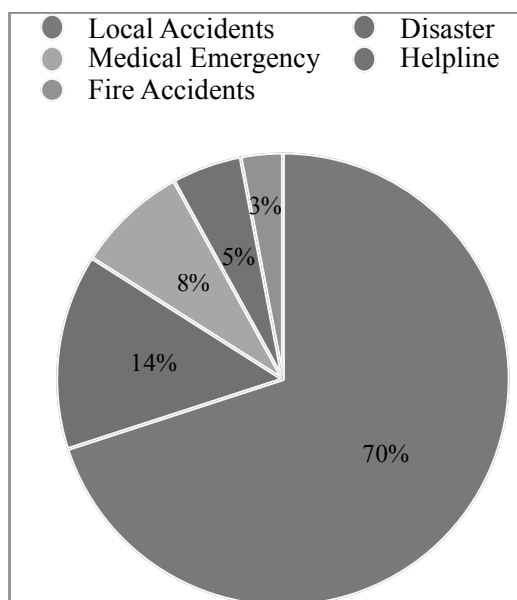


Chart -1: Usage of Emergency Applications [2]

4. IDEA OF AD-HOC NETWORKS

Ad hoc networks have been proposed as an appealing communication technology to deal with the unexpected conditions emerging during and/or after the occurrence of a disaster because network connections cannot always be preserved in a disaster scenario. Ad-hoc networks allow for the rapid deployment of fiber-like connectivity in situations where capacity is needed on an expedited basis, and they allow both victims and emergency workers to communicate when it is most important.

These network connections can be established quickly, even in areas where regular infrastructure has been devastated, by using a wireless transport device atop a mobile platform such as a COW (cellular on wheels) or a COLT (cellular on light trucks). The vehicle simply manoeuvres into the area and can begin transmitting within a matter of hours, much faster than the time it takes to repair or replace existing network infrastructure equipment. In fact, a number of COWs were deployed in the aftermath of Hurricane Katrina to provide critical phone service to rescue and recovery workers when the area’s cellular networks had otherwise been completely cut off, and allowed the responders to organise their efforts and focus on the areas most devastated by the storm. [3]

5. OUR CONCEPT

The failure of communications networks is a common occurrence during many disaster scenarios, and yet we have continued to see this preventable sequence of events play out time after time with deadly, expensive, and potentially preventable consequences with constructing temporary communication infrastructure such as COW and COLTs.

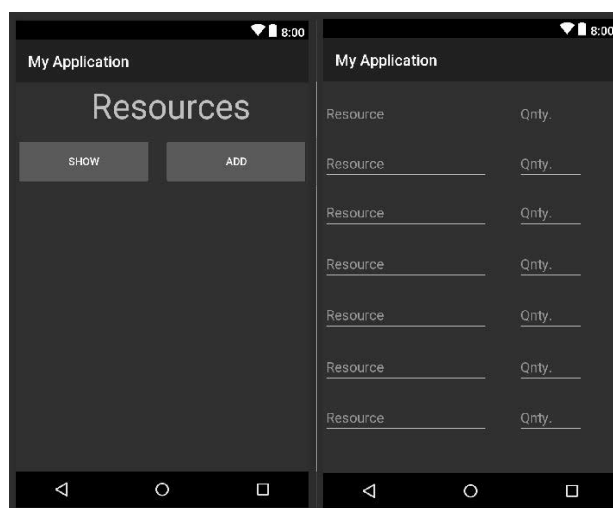


So in this work, we present *DisCom*, a simple post-disaster smartphone-based application of lite version running low on memory which establishes an ad-hoc bluetooth network for the purpose of communicating the supply and demand of basic essentials and resources near users within a well-defined range with no internet access

and cellular network to communicate. DisCom implements a broadcast-based network wherein each user broadcasts the availability or demand for certain essential resources.



The data received is then mapped with the help of the Google Maps API, which now shows a map of all available resources in the vicinity. This broadcast packet is cumulative wherein each user not only broadcasts their data, but also the data received from other users in order to establish a network. The broadcast is repeated at a predetermined interval or on user prompt. If the status of resources changes with respect to any user, the updated data is broadcast and the necessary changes are enacted across all users on this network. DisCom also broadcasts in a chatbot medium their GPS location, and status.



6. CONCLUSION

The applicability of ad hoc networks in disaster scenarios is still in an initial phase. Most works done on this idea are only based on simulations rather than real experimentation. While DisCom does not focus on

security or efficiency, it provides a simple relief communication infrastructure in the wake of a disaster, without the need for any additional resources.

REFERENCES

- [1] Hafsa Maryam, Qaisar Javaid, Munam Ali Shah, Muhammad Kamran, "A Survey on Smartphones Systems for Emergency Management (SPSEM)", (IJACSA) International Journal of Advanced Computer Science and Applications, Vol. 7, No. 6, 2016, Page 302.
- [2] S.Mythili and E.Shalini, "A comparative study of Smart Phone Emergency Applications for Disaster Management", International Research Journal of Engineering and Technology (IRJET), Volume: 03 Issue: 12 | Dec -2016, Page 394.
- [3] When Communications Infrastructure Fails During a Disaster - Written by Christina Richards
<https://www.drj.com/articles/online-exclusive/when-communications-infrastructure-fails-during-a-disaster.html>

USMCA 2018

SESSION 5

BUILDING SAFETY II

EFFECT OF INFILL WALL STIFFNESS ON SEISMIC ANALYSIS OF HIGH RISE BUILDING HAVING MASS IRREGULARITY

SUSMITHA YELLA¹ and MAGANTI JANARDHANA²

¹Formerly P.G. Student, JNTUH College of Engineering Hyderabad, Hyderabad, India,

²Professor, JNTU Hyderabad, Hyderabad, India.

Irregular buildings constitute a large portion of the modern urban infrastructure. In multi storeyed framed buildings, damage due to earthquake ground motion generally initiates at locations of structural weaknesses present in the lateral load resisting frames. In some cases, these weaknesses may be created by irregularities in stiffness, strength or mass between adjacent storeys. Such irregularities between storeys are often associated with twisting of buildings. There are many examples of failure of buildings in past earthquakes due to irregularities in mass. Irregularities in mass arise in buildings due to many reasons like using one floor for both residential and commercial activities, construction of swimming pool in a floor or use of one floor for storing heavy materials etc. When such buildings are located in a high seismic zone, the structural engineer's role becomes more challenging. Therefore, the structural engineer needs to have a thorough understanding of the seismic response of irregular structures. Infill panels are widely used as partition walls as well as external walls of the building to fill the gap between RC frames. The infill walls (non-structural members) may provide considerable stiffness to the building and hence may improve the performance of the RC building during ground motions. The effects of non-structural infill walls are not included generally during analysis and design of reinforced concrete structures. However, these infill walls have considerable effect on the structural response as studied by many researchers all over the globe. In this paper, a 21-storyed RC frame having mass irregularities in the elevation is considered. The effect of ground motion on RC framed building has been carried out by considering infill wall stiffness and without the stiffness of infill wall. Equivalent Lateral Force method and Response Spectrum method are adopted for the seismic analyses. The analysis is carried out using commercially available software package SAP 2000 and comparison of different parameters like storey shear, storey drift, time periods is carried out.

Keywords: *Infill wall, Mass irregularity, Base Shear, Storey Drift*

1.Introduction :

In recent years, some floors of buildings are used for different purposes like car parking, storing heavy mechanical appliances, for observatory towers at top etc. This results in variation of mass, and stiffness at different storeys. When such buildings are located in a high seismic zone, the structural engineer's role becomes more challenging. Therefore, the structural engineer needs to have a thorough understanding of the seismic response of irregular structures. In recent past, several studies have been carried out to evaluate the response of irregular buildings.

2.Description of Building :

A commercial cum residential building of G+20 irregular building having the base dimension of plan 23.62 m × 25.15 m with stilt floor of 3m height and typical floor height of 4.0 m is considered for the analysis.

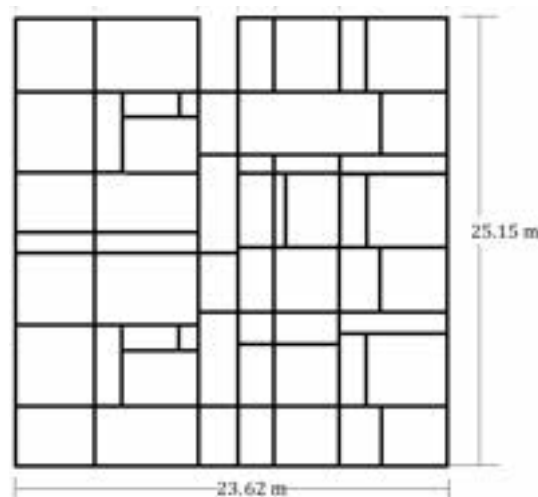


Figure.1. Typical floor plan of the building

¹Email: susmitha.thesmilinggirl@gmail.com

²Email: prof.jmaganti@gmail.com

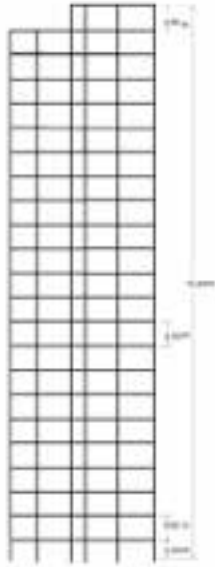


Figure.2.Elevation of the building

The building has 21 storyes symmetrical in plan with 5 bays in X direction and 8 bays in Y directions, and its plan and elevation are shown in Figs 1 and 2 respectively. The superstructure is modelled using the commercially available software SAP2000 (v14.0.0) [3] as a space frame.

1. Input Data

The parameters and loads considered for the analysis are as per IS 1893 (Part1)-2002 [1] and are mentioned below.

A. Seismic Parameters:

Seismic Zone:	III
Type of soil:	Medium
Importance factor:	1
Response reduction factor:	3
Damping ratio:	5%
Type of structure:	OMRF

B. Loads

Unit Weight of Concrete:	25.0 kN/m ³
Live Load (Residential):	2.0 kN/m ²
Live Load (Commercial):	15.0 kN/m ²
Live Load (Cellar):	5.0 kN/m ²

Live Load (Roof):	1.5 kN/m ²
Stair Case Load –Live:	7.734 kN
Stair Case Load –Dead:	30.937 kN
Wall load (230 mm thick):	16.0 kN/m
Wall load (115 mm thick):	8.0 kN/m
Dead Load (Commercial) :	12.75 kN/m ²

C. Section properties :

Plinth Beam Size:	400 × 500 mm
Roof Beam Size:	400 × 650 mm
	400 × 750 mm
Column Size:	450 × 1500 mm
	1500 × 450 mm
	500 × 1500 mm
	1500 × 500 mm
Slab Thickness:	100 mm ,150 mm & 250mm
Thickness of Wall:	230 mm & 115 mm

D. Material Properties:

Grade of Concrete:	M35
Grade of Steel:	Fe500

E. Infill Walls :

The infill walls are modelled as equivalent struts and shown in the Figure 3 and the strut parameters are calculated using Eq. (1) and shown in Table 1

The equivalent width (w) of the infill wall proposed by Hendry [2] is given by

$$w = \frac{1}{2} \sqrt{\alpha_h^2 + \alpha_L^2}$$

Where

$$\alpha_h = \frac{\pi}{2} \left[\frac{E_f I_c h}{2 E_m t \sin 2\theta} \right]^{1/4}$$

$$\alpha_L = \frac{\pi}{2} \left[\frac{E_f I_b L}{2 E_m t \sin 2\theta} \right]^{1/4}$$

$$\theta = \tan^{-1} \left(\frac{h}{L} \right)$$

θ = slope of infill wall diagonal to the horizontal,

E_m = Elastic Modulus of masonry wall= 2720.0 N/mm²,
 E_f = Elastic Modulus of masonry of frame material,
 t = Thickness of the infill wall,
 h = Height of the infill wall,

¹Email: susmitha.thesmilinggirl@gmail.com

²Email: prof.jmaganti@gmail.com

L = Length of the infill wall,
 I_c = Moment of Inertia of the column of the frame,
 I_b = Moment of Inertia of the beam of the frame, and
 w = Width of the Equivalent Strut.



Figure . 3. Building with infill walls

Table 1: Equivalent strut parameters in X and Y-Directions

Strut	Equivalent Width (m)	Thickness (m)	Strut	Equivalent Width (m)	Thickness (m)
X-Direction			Y-Direction		
01	2.00	0.23	06	2.50	0.23
02	2.25	0.23	07	2.00	0.23
03	2.00	0.115	08	1.75	0.23
04	2.50	0.115	09	2.35	0.115
05	2.25	0.115	10	2.00	0.115

3. Results and Discussion

The regular building and a building with mass irregularity were analyzed by adopting linear static and dynamic analyses procedures, using commercially available software SAP 2000 (v14.0.0). Also effect of infill wall stiffness is also studied.

3.1. Results of Linear Static Analysis : The lateral loads in a regular building are relatively lesser when compared with that of building having mass irregularity except for the top floor where it is almost equal. This may be due to increase of overall weight of the structure as shown in the Figure 4. With the introduction of mass irregularity in the structure at 3rd floor (as per table 5 of IS 1893 (part 1):2002 mass is increased by 200% compared to the floor at the top), there is an increase in seismic weight of the floor at the level 15 compared to increase in the mass. Lateral load is not getting changed with the introduction of infill wall stiffness. This is because mass effect of diagonal strut is not taken into account.

¹Email: susmitha.thesmilingirl@gmail.com

²Email: prof.jmaganti@gmail.com

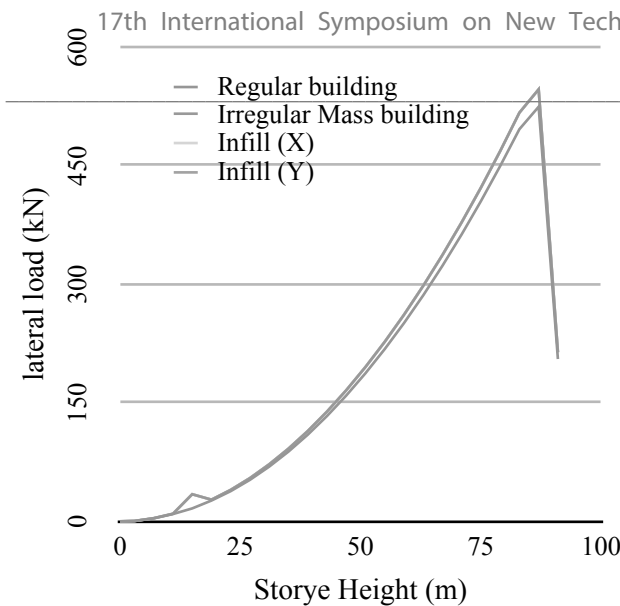


Figure.4. Lateral Loads on Storeys of Regular building and Building having mass irregularity along with infill wall stiffness

Storey shears of regular building are slightly less when compared with that of building having mass irregularity as mass of the structure is increased as shown in Figure.5

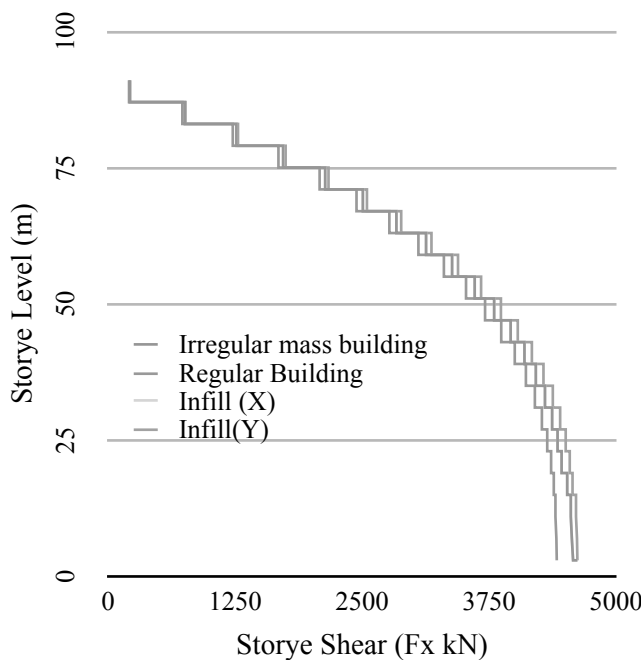


Figure.5. Storey shears of Regular building and Building having mass irregularity along with infill wall stiffness.

It is observed that that the storey drifts of a regular building is almost equal with building having mass irregularity till 3rd floor (level 15) where there is no change in mass as shown in the Fig.6. With the introduction of mass irregularity in building at storey

level 15 there is slight increase in the drift. As per the IS 1893:2002(part 1), the drift of any floor should not be more than 0.004 times the storey height. i.e., 0.016m in this case for a storey height of 4m. The storey drifts of all the storeys of regular building and building having mass irregularity with and without the effect of infill wall stiffness are satisfying the drift limits prescribed by the IS 1893 (Part1):2002.

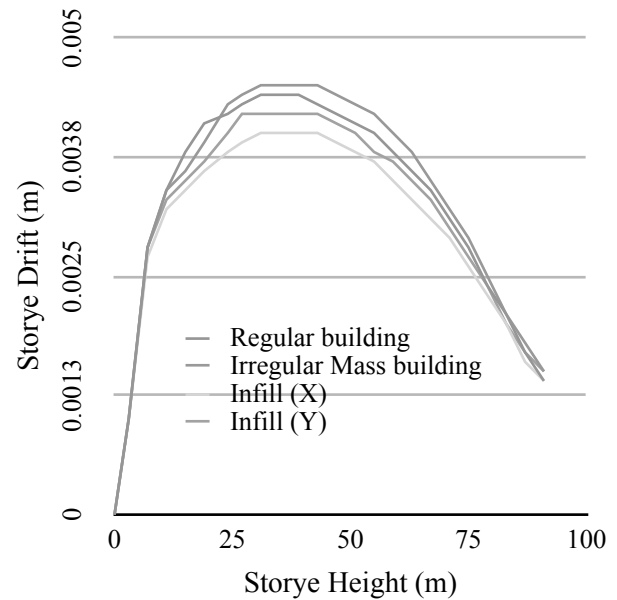


Figure.6. Inter storey drifts of Regular building and Building having mass irregularity along with effect of infill wall stiffness.

The storey displacements of regular building is less compared to that of building having mass irregularity due to difference in mass of the storey as shown in the Figure 7. Storey displacements of building having mass irregularity by considering effect of infill wall stiffness are relatively lesser compared to that of building having mass irregularity in both X and Y direction. Further, storey displacements are the least for the building having infill wall in the X direction.

¹Email: susmitha.thesmilingirl@gmail.com

²Email: prof.jmaganti@gmail.com



Figure.7. Storey displacements (max) of Regular building and Building having mass irregularity including the effect of infill wall stiffness.

From Figure 8 it can be observed that the storey overturning moments of regular building are more than that of the building having mass irregularity.

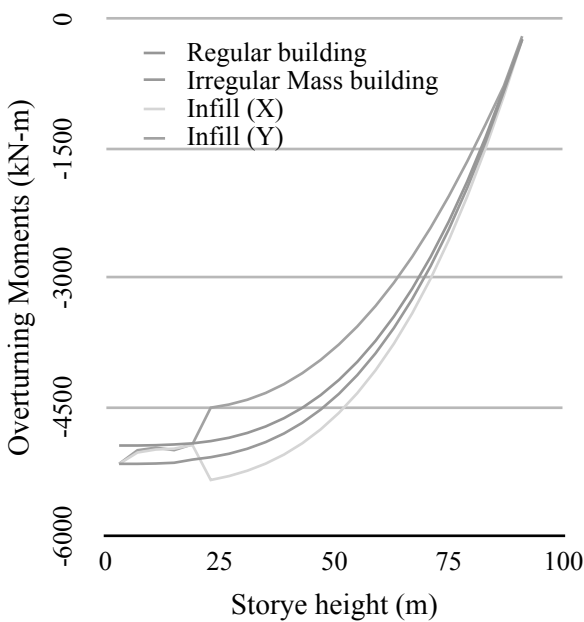


Figure.8. Storey overturning moments of Regular building and Building having mass irregularity along with effect of infill wall stiffness.

3.2. Response Spectrum Analysis :

The time period of regular building is relatively higher when compared to that of building having mass irregularity as shown in the Figure 9. It can also be observed that with the increase in the stiffness of the building, the modal period is getting reduced.

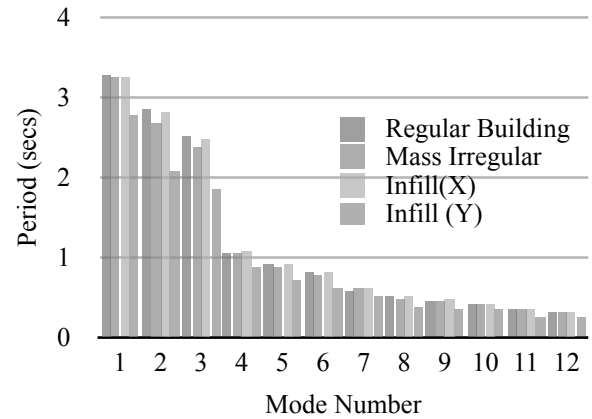


Figure.9. Variation of time periods with number of modes of regular and mass irregular building along with effect infill wall stiffness.

From the Figure 10, it can be observed that storey shears of regular building is slightly lesser when compared with building having mass irregularity as mass of the structure is increased.

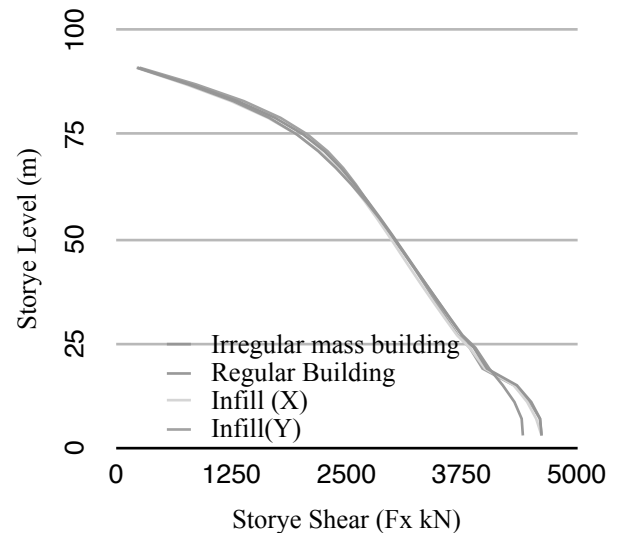


Figure.10. Storey shears of Regular building and Building having mass irregularity along with infill wall stiffness. (Response Spectrum Method).

¹Email: susmitha.thesmilinggirl@gmail.com

²Email: prof.jmaganti@gmail.com

It can be observed from Fig 11 the variation of storey drifts in response spectrum method.

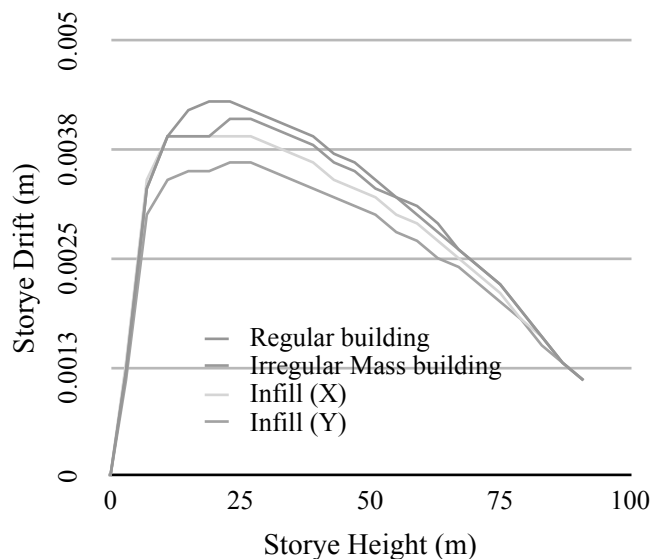


Figure.10 Storey drifts of Regular building and Building having mass irregularity including effect of infill wall stiffness. . (Response Spectrum Method)

By observing the trend in Figure 11 it is clear that the storey displacements of regular building is less compared to that of building having mass irregularity due to difference in mass of the storeys.

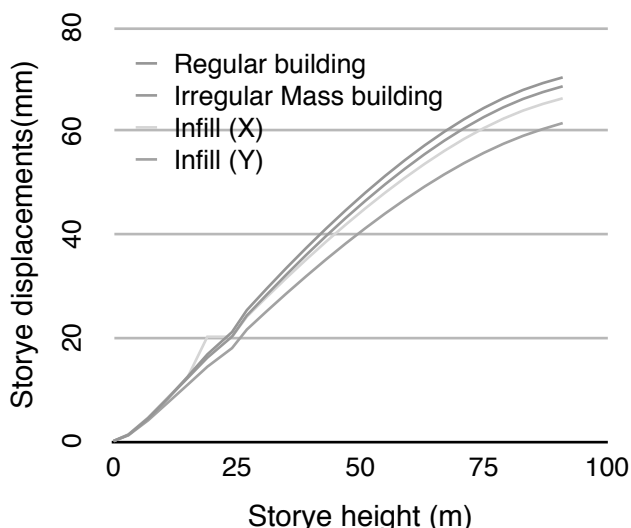


Figure.11 Storey displacements (max) of Regular building and Building having mass irregularity including the effect of infill wall stiffness. . (Response Spectrum Method).

4. Results and Conclusions :

Based on the analysis of G + 20 storeyed building having mass irregularity, following conclusions are drawn.

- i. Storey drift is a not only a function of storey height but also depends on the weight of that storey. Also introduction of infill wall stiffness can reduce the storey drifts.
- ii. Storey shears of buildings having mass irregularity are relatively higher than that of regular buildings. Storey shear of the structure, if infill wall stiffness are considered, are quite larger than the structure without infill wall stiffness. Hence, stiffness of infill walls should be considered for design since it represents a true picture of the behavior of structure.
- iii. Displacements of the different storeys for building having mass irregularity are relatively higher than that of the regular building. For the same building with introduction of infill stiffness, the displacements are considerably getting reduced.
- iv. Time period is getting reduced with the increase in number of modes. The time period of building with mass irregularity is comparatively lesser than that of regular building as stiffness of the building considered is higher than that of a regular building.
- v. Time periods of the model with infill walls are lower than the model without infill walls, because the infill walls further increase the overall stiffness of the structure and hence lower the time periods.

5. References :

- [1] IS 1893(Part 1): 2002 “Criteria for earthquake resistant design of structures”, Part1 General Provisions and building, Bureau of Indian Standards
- [2] Paulay, T. and Priestley, M. (1992) “Seismic Design of Reinforced Concrete and Masonry Buildings”, John Wiley & Sons, Inc., New York
- [3] SAP 2000. Integrated Software for structural analysis and Design, Computers and Structures Inc., Berkeley, CA, USA
- [4] Koalasani.Rajshekar and Maganti.Janardhana (2016) “Effect of infill wall stiffness on seismic analysis of high rise buildings resting on sloping ground”, Structural Engineering Convention (SEC-2016).

¹Email: susmitha.thesmilinggirl@gmail.com

²Email: prof.jmaganti@gmail.com

SEISMIC BEHAVIOR OF FLAT SLAB BUILDINGS IN SEISMIC ZONES BY LINEAR DYNAMIC ANALYSIS: A COMPARISON BETWEEN THE CONVENTIONAL BUILDINGS TO FLAT SLAB BUILDINGS

DR NARENDER BODIGE¹ and A. NARESH²

¹Associate Professor, Anurag Group of Institutions, Venkatapur, Ghatkesar, Hyderabad, India, Email: drnbodigece@cvsr.ac.in

²PG Student, Anurag Group of Institutions, Venkatapur, Ghatkesar, Hyderabad, India, Email: atheninaresh@gmail.com

ABSTRACT

In the present situation, a fast growing economy and rapid urbanization of the country in India leads the requirement of more infrastructure development. The more employment opportunity is in urban cities which lead to the fast rate of the construction and more demand for space requirement of commercial buildings. Flat slab building is more popular in the multistoried building because of the absence of deep beams, and story height can be reduced, use of space, easier formwork and shorter construction time. However, past earthquake studies show that many buildings with flats have performed poorly. The flat-slab structural system is significantly more flexible for lateral loads than traditional RC frame system and that make the system more vulnerable under seismic events. This is mainly due to inadequate resistance for punching shear under the earthquake loading. Unfortunately, many of upcoming cities are in high seismic zones and need to understand the seismic behaviour of the flat slab buildings. To understand the seismic behaviour of flat slab building, three model of three dimensional i.e G+3, G+7, and G+11 multistoried building having a flat slab without drop, flat slab with drop, flat slab with perimeter beam, flat slab with drop and perimeter beam and the conventional slab is considered and analyzed using ETABS software. The performance and behaviour of all the models in IS code seismic zone-II, zone III and zone-IV have been studied. The main objective of the present work is to compare the behaviour of multi-storey buildings having conventional RC frame and flat slab with different cases and also study the effect of the height of building. Linear dynamic analysis for different earthquake ground motion is carried out and compare with response spectrum analysis.

Keywords: Flat Slab, Conventional frame, ETABS, Seismic zones, Linear dynamic analysis, Earthquake ground motions

INTRODUCTION

The flat slab is a reinforced concrete slab supported by columns with, or without drops. The columns may be with, or without, column heads. These buildings are more popular in the multistoried building because of the absence of deep beams, and story height can be reduced, use of

space, easier formwork, shorter construction, flexibility in room layout, Ease of Installation of building services, reduced cladding costs and prefabricated services. This building is more attractive in recent time in India due to the fast-growing country in the economy and this brings demands in increasing of infrastructure facilities along with the growth of population and face a shortage of land. The Major cities in India like Delhi, Mumbai, Hyderabad, Bangalore, Chennai has started to construct the mid-rise to high rise flat slab building for commercial use and this construction of activities increase day by day as exponential form due to more job opportunity and increasing industrial hubs in an urban centre. These buildings are efficient in resisting gravity load but have excessive lateral drift when subjected to seismic loading. However, past earthquake studies show that many buildings with flat slab have performed poorly. In Christchurch earthquake (2011) flat slab building causes punching shear failure of the slab-column connections. The columns of structure punched through the concrete slab floor systems, dropping the floors and roof and completely collapsing the interior of the building in Northridge Earthquake (1994). In the Loma Prieta earthquake (1989) excessive lateral drift observed due to excessive interior damage, increase P-delta effect and failure of the slab-column connection. It is mainly due to inadequate resistance for punching shear under the earthquake loading. The seismic analysis of flat building is studied least touched area and past literature shows that study the basic parameter i.e various aspects and behaviour of flat slab building under the earthquake forces. G. Patwari and G. Kalurkar (2016), studied the effect of RC flat slab with the shear wall at a different location for various heights of the building. A comparison of the seismic behaviour of flat slab structure with conventional RCC Structures is done by D.N. Shinde et.al (2016) and N.mircic et.al (2008), studied the bearing capacity of flat slab with comparison of other models i.e frame, flat slab with shear wall, flat slab strengthened by perimeter beam and flat slab strengthened by shear wall and perimeter beam. Flat slab buildings are studies very limited and not understand Flat slab with different slab-column joints with over conventional building and including effects due to seismic zone and ground motion

of low, medium and high rise buildings. Unfortunately, many of upcoming cities are in high seismic zones and need to understand the seismic behaviour of the flat slab buildings. This paper study the comparison of the seismic performance of low, mid and high rise flat slab with and without a drop, and perimeter beam over the conventional RC storey building for different seismic zones i.e Zone-II, III and IV. The analysis and design are carried out in numerical software. Dynamic responses of different models of buildings are carried out for different earthquakes ground motion.

BUILDING MODELING

In this paper, five building models with varying height i.e low (G+3), Medium (G+7) and High rise (G+11) buildings are considered to understand the seismic behaviour of flat slab building over conventional RC Frame Building; the model-1 consist of conventional frame (CF), Model-2 is flat slab without drop (FS), Model-3 is flat slab with drop (FSD), Model-4 is flat slab with perimeter beam (FSB) and Model-5 is flat slab with drop and perimeter beam (FSDB). The symmetrical plan of building with plan size of 12m x 15 m and three bays in both x and y-direction chosen as shown in figure1(a) and. In total fifteen model were considered for this study and geometry, material property and loads are listed in the table.1 The analysis and design are carried out for gravity loads by using ETABS commercial Software and support are assumed as a fixed base. Drop panel size and drop thickness decide based on IS 456 -2000. For Linear dynamic analysis five different earthquake ground motion data chosen based on tectonic region i.e Bhuj (Gujarat), ElCentro (Imperial Valley), Chamoli (Uttarakhand), Uttarkashi (Garhwal), Chamba (Himachal Pradesh) and details are shown in table.2.

Table.1: Building details

Geometry Properties	
Plan dimensions	12m x 15m
No. of storey	G+3, G+7 and G+11
Storey Height	3.6m
Thickness of slab	200mm
Drop size	1.5m x 1.5m
Drop thickness	250mm
Material properties	
Grade of concrete	M 25
Grade of steel	Fe 415
The density of reinforced concrete	25 kN/m ³
Size of column	450mm x 450mm
Size of beam	300mm x 300mm
Loads	
Live load	3 KN/m ²
Seismic Loads	
	As per IS 1893-2002

Zone	II, III & IV
Zone factor (Z)	0.1, 0.16 and 0.24
Response reduction factor (R)	3
Importance factor (the I)	1
Soil type	2
Damping ratio	0.05

Table.2 Earthquake Details

Name of earthquake	Year	Magnitude (M _w)	Time Interval (Sec)
Bthuj	26 January 2001	7.7	0.005
ELcentro	18 May 1940	6.9	0.02
Uttarkashi	19 October 1991	6.8	0.02
Chamba	24 March 1995	5.1	0.02
Chamoli	29 an March, 1999.	6.8	0.02

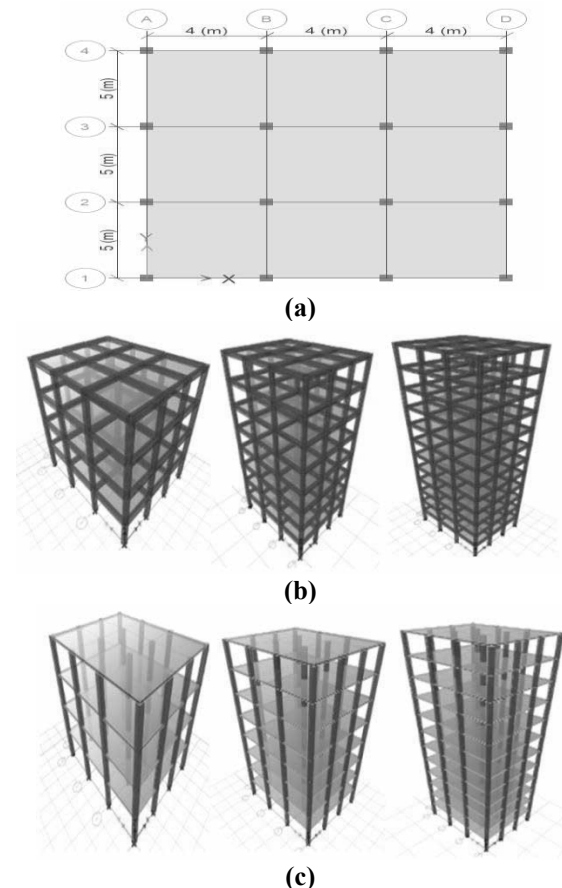


Figure 1: Building details (a) Plan of Building, Three-dimensional view of (b) conventional RC frame with G+3, G+7, and G+11 buildings and (c) Flat slab frame with G+3, G+7, and G+11 buildings.

RESULTS AND DISCUSSIONS

The main objective of the study is to understand the seismic performance of flat slab building and its

performance compared with RC conventional building. The analyses and design are carried out using ETABS software version 2016. Firstly model analysis is carried out for total twelve building model i.e G+3, G+7 and G+11. The time period and frequency of G+3, G+7 & G+11 building as shown in the table.3, table.4 and table.5 respectively and mode shapes of the G+3 conventional building shown in Figure.2 . The first mode indicates the natural frequency of building and all models of modes time period shown in table.2. In all models, as mode number increases frequency is also increasing till the 12 modes. After three mode shapes, there is a sudden decrement in the time period up to 40 % and sudden increment in frequency as similar to the time period. Similar results were observed in G+7 and G+11 Buildings. From the model analysis, it shows that more time period in the flat slab and less in conventional building and order of natural period will increase model-1, model-5, model-4,model-3 and model-2 but model-1 time period very close model-5 time period. It is observed that time period of the flat slab with drop and perimeter beam is very close to conventional RC building and which gives stiffer than a flat slab with and without a drop. In similar observation found in G+7 and G+11. For G+3 RC Building, the maximum time period is in flat slab i.e 0.925 sec and minimum is in conventional building 0.719 sec and flat slab with drop and perimeter beam is 0.739 sec. In case of G+7 RC Building, the maximum time period is in flat slab i.e 2.0 sec and minimum is in conventional building 1.497 sec and flat slab with drop and perimeter beam is 1.55sec. Similarly G+11 building, maximum time period is in flat slab i.e 3.15 sec and minimum is in conventional building 2.29 sec and flat slab with drop and perimeter beam is 2.38sec respectively. Time period obtained from IS 1893-2016 for a moment resisting frame building without brick infill panels is 0.55 sec, 0.932sec and 1.26 sec for G+3, G+7 and G+11 storey building respectively. These values are lesser than the time period obtained from a numerical method for all models. It concludes that time period of the flat slab with drop and perimeter beam very close to the conventional building and also similar observation found as low, mid and high rise building. After model analysis, response spectrum analysis is carried out for twelve models and obtained base shear, storey shear, storey displacement and storey drift for different seismic zones i.e Zone-II, III & IV using the numerical software and zone factors values are taken from IS 1893-2016. Results of Base shear, storey shear, storey displacement, storey drift is shown in Figure.3 to 6. Results shows that as storey increase the base shear increase and zone increase base shear also increases as shown in Figure.3. The maximum base shear is observed in the conventional frame (CF) and the minimum is in flat slab without a drop (FS) of G+3, G+7 and G+11 building model. Base shear of flat slab without drop building is reducing by fifteen percentage of conventional frame building and flat slab with drop and perimeter beam (FSDB) is reduced by seven

percentage of conventional frame building for G+3, G+7 and G+11 building model and varying seismic zones. For G+3 Building, base shear of zone-III and IV are 1.6 and 2.4 times of base shear of zone-II. Similar observation found in G+7 and G+11 storey building. All Building models i.e G+3, G+7 and G+11 flat slab with drop and perimeter beam of base shear very close to the conventional building and followed by a flat slab with the drop.

Table.3: Mode Number with respective time period and frequency of G+3Building.

Model	CF		FS		FSD		FSB		FSDB	
	T	ω_n								
1	0.719	1.392	0.925	1.081	0.788	1.269	0.781	1.281	0.739	1.353
2	0.681	1.468	0.848	1.179	0.764	1.31	0.73	1.37	0.712	1.405
3	0.598	1.672	0.756	1.323	0.68	1.47	0.604	1.656	0.598	1.672
4	0.218	4.597	0.255	3.92	0.229	4.374	0.229	4.369	0.22	4.544
5	0.209	4.788	0.241	4.158	0.223	4.475	0.218	4.594	0.214	4.676
6	0.182	5.485	0.211	4.742	0.196	5.102	0.182	5.490	0.181	5.528
7	0.115	8.724	0.118	8.445	0.113	8.84	0.115	8.685	0.113	8.84
8	0.112	8.909	0.115	8.66	0.112	8.936	0.112	8.903	0.111	8.97
9	0.097	10.348	0.098	10.18	0.095	10.49	0.095	10.51	0.095	10.545
10	0.078	12.858	0.074	13.58	0.073	13.68	0.075	13.26	0.075	13.293
11	0.077	12.912	0.073	13.65	0.073	13.71	0.075	13.33	0.075	13.339
12	0.066	15.238	0.061	16.4	0.061	16.47	0.064	15.66	0.064	15.679

Note : T-Period in sec and ω_n -Frequency in Hz

Table.4: Mode Number with respective time period and frequency of G+7 Building.

Model	CF		FS		FSD		FSB		FSDB	
	T	ω_n								
1	1.497	0.668	2.001	0.5	1.682	0.595	1.656	0.604	1.555	0.643
2	1.416	0.706	1.808	0.553	1.627	0.614	1.539	0.65	1.495	0.669
3	1.244	0.804	1.637	0.611	1.467	0.682	1.263	0.792	1.25	0.8
4	0.478	2.091	0.612	1.633	0.526	1.899	0.521	1.919	0.493	2.029
5	0.454	2.202	0.561	1.783	0.511	1.957	0.488	2.05	0.475	2.104
6	0.399	2.507	0.504	1.985	0.457	2.187	0.403	2.481	0.399	2.505
7	0.266	3.755	0.32	3.126	0.284	3.517	0.284	3.525	0.271	3.685
8	0.254	3.934	0.299	3.349	0.277	3.608	0.268	3.729	0.263	3.806
9	0.224	4.472	0.265	3.774	0.245	4.077	0.224	4.456	0.223	4.492
10	0.175	5.705	0.196	5.092	0.181	5.537	0.182	5.498	0.176	5.678
11	0.169	5.912	0.187	5.34	0.177	5.641	0.174	5.734	0.172	5.818
12	0.148	6.775	0.163	6.12	0.154	6.483	0.147	6.806	0.146	6.847

Note : T-Period in sec and ω_n -Frequency in Hz

Table .5: Mode Number with respective time period and frequency of G+11 Building.

Model	CF		FS		FSD		FSB		FSDB	
	T	ω_n								
1	2.297	0.435	3.153	0.317	2.596	0.385	2.552	0.392	2.389	0.419
2	2.184	0.458	2.854	0.35	2.52	0.397	2.378	0.421	2.307	0.434
3	1.895	0.528	2.574	0.388	2.263	0.442	1.927	0.519	1.905	0.525
4	0.746	1.34	0.998	1.002	0.835	1.198	0.823	1.215	0.774	1.293
5	0.709	1.41	0.91	1.099	0.81	1.234	0.768	1.302	0.746	1.34
6	0.618	1.617	0.818	1.223	0.727	1.376	0.627	1.594	0.621	1.611
7	0.425	2.351	0.547	1.827	0.468	2.136	0.463	2.158	0.439	2.28
8	0.403	2.482	0.504	1.986	0.454	2.203	0.433	2.309	0.422	2.369
9	0.356	2.807	0.451	2.216	0.408	2.454	0.36	2.777	0.357	2.803
10	0.289	3.466	0.352	2.84	0.31	3.226	0.309	3.237	0.295	3.392
11	0.275	3.638	0.329	3.039	0.302	3.312	0.291	3.433	0.285	3.508
12	0.242	4.128	0.291	3.434	0.268	3.731	0.244	4.106	0.242	4.14

Note : T-Period in sec and ω_n -Frequency in Hz

Storey shear, storey displacement and storey drift as shown in figure.4, 5 and 6. Sudden increasing storey shear at below the top floor level for G+3 and as well other models, and rest floors increases gradually. Maximum storey shear in Conventional frame building and minimum

in flat slab buildings and FSDB storey shear close to CF building for G+3, G+7 and G+11. Storey displacement results shows that as storey increasing, storey displacement increasing and maximum storey displacement increasing and maximum storey

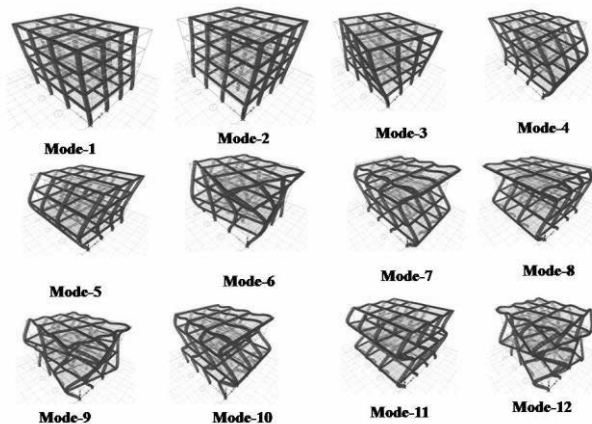


Figure.2: Mode shapes of G+3 conventional building

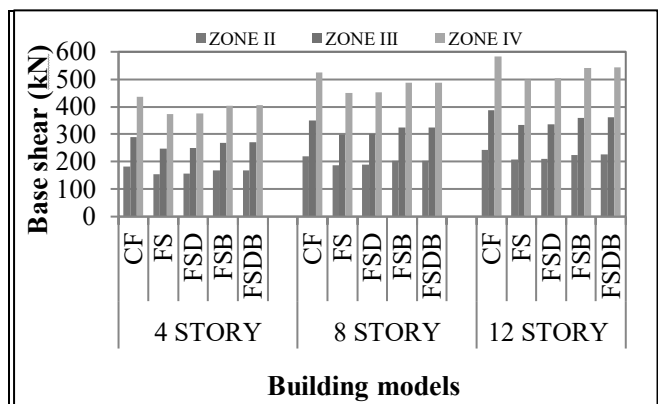


Figure.3 : Base shear of buildings models with different seismic zones.

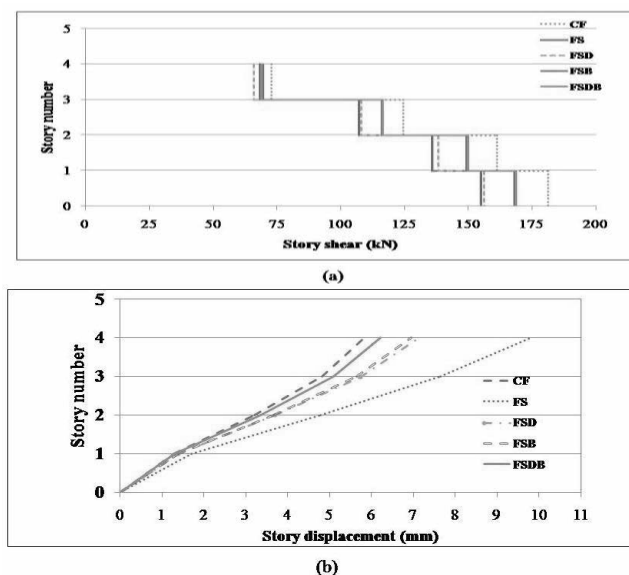


Figure.4 : (a) Storey shear and (b) Storey displacement of G+3 Building of zone-II.

displacement in flat slab and minimum in Conventional frame building observed and similar observation in G+7 and G+11 buildings. However in all three zones, zone II shows less and zone IV showing more results in terms of base shear, story displacement, story drift, story shear

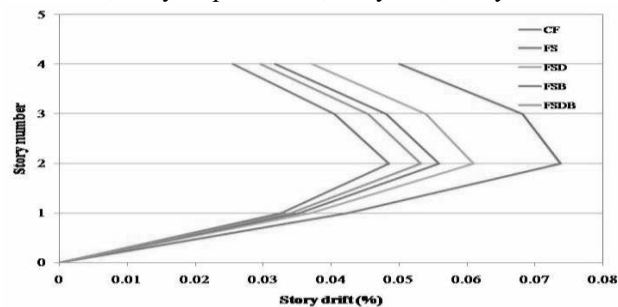
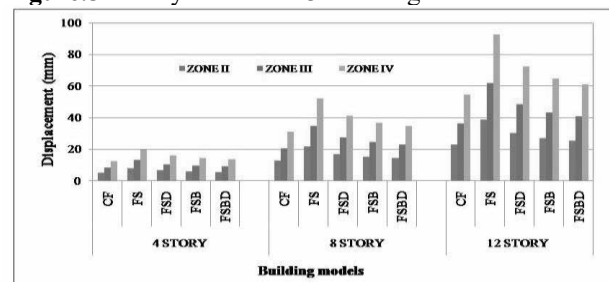
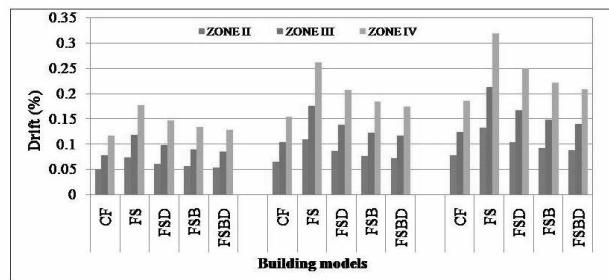


Figure.5: Storey drift of G+3 Building with zone-II.



(a)



(b)

Figure.6: (a) Maximum displacement of building models with different seismic zones (b) Maximum drift of building models with different seismic zones

Linear dynamic analysis

To understand the dynamic behaviour of the buildings, five major earthquake ground motions of Elcentro, Uttarakashi, Chamba, Bhuj and Chamoli have been considered, which are different in their nature of predominant frequencies. Dynamic linear Analysis is given basic idea of the understanding the behaviour of fat slab building under the action of earthquake ground motion. In this displacement time history measure at roof level for all models and results are presented in table 6 and Figure.7(a) is Elcentro ground motion and Figure.7(b) is linear dynamic response at roof level of conventional and flat slab building. When observe the results obtained from time history analysis for all 5 models in all three cases (i.e. G+3, G+7 and G+11 story. Model 1 (4 story conventional frame) shows less displacement than model 2 (4 story flat

slab). By providing of drop, perimeter beam to the flat slab (i.e. model 3, model 4, model 5), the displacements are reduced and this three models model 5 (flat slab with drop and perimeter beam) showing less displacement for all five earthquake data consideration. The flat slab showing more displacement than all other models. When compare the flat slab with conventional frame, conventional frame showing less displacement and when providing drop, perimeter beam to the flat slab, flat slab with drop and perimeter beam combination showing less displacement than flat slab. Linear response of individual building varying ground motion to ground motion.

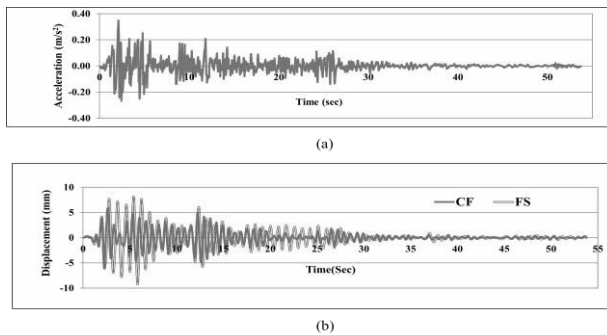


Figure.7:(a) Elcentro ground motion and (b) Roof displacement response of G+3 CF and FS building.

Table 6: Linear displacement response of top storey (mm) for different earthquakes.

S	M	EC	UK	CM	BJ	CL
4	CF	5.81	6.35	5.39	5.47	6.36
	FS	9.28	7.92	7.88	8.08	9.39
	FSD	8.06	7.00	6.32	7.37	8.24
	FSB	7.15	7.10	6.17	6.72	7.25
	FSBD	6.87	6.91	5.92	5.98	6.45
8	CF	12.08	11.1	10.80	18.26	13.82
	FS	23.26	17.45	11.15	34.61	21.70
	FSD	18.68	14.79	8.77	17.15	19.47
	FSB	16.95	14.06	9.42	16.88	18.77
	FSBD	15.14	13.15	9.082	16.29	16.85
12	CF	21.33	24.82	17.12	24.60	22.98
	FS	43.16	19.45	16.84	47.76	40.68
	FSD	39.05	19.05	13.25	28.28	37.67
	FSB	31.94	20.37	14.76	22.23	35.19
	FSBD	27.70	21.95	16.07	20.99	28.94

Note :S-storey, EC-Elcentro, UK-Uttarakashi, CM-Chamba, BJ-Bhuj, CL-Chamoli

CONCLUSIONS

Flat slab building more attract very recent time in urban centres due to industrial and infrastructure development. But recent earthquake, flat slab building shows poor performance. These building need to understand indepth analysis and design aspect in seismic forces. In this paper, we compare the seismic performance of conventional

building to flat slab building and also major earthquake occurred in india. A compare the response spectrum results with the linear time history results, Only Chamba earthquake data shows similar behavior in terms of response in all five models in all cases. And when compare the all five earthquake data's response for all models Chamba earthquake data is only giving less response to the structure. In seismic point of view, for construction of flat slab structure, flat slab with drop and perimeter beam combination is gives better results. From results it can concluded that flat slab with drop and perimeter beam showing better results in terms of story displacement and story drift. So, to avoid seismic failures, flat slab with drop and perimeter beam are best. When compare to flat slab without drop and flat slab with drop, flat slab with drop and perimeter beam is more resisting lateral forces

REFERENCES

- [1] D.N.Shinde et.al (2016), "Comparative study of seismic response of flat slab structure and conventional RC framed structure", (International Journal of innovative and emerging research in engineering) volume 3, issue 6, June, 2016.
- [2] G. Patwari and G. Kalurkar (2016), "Comparative study of RC flat slab & shear wall with conventional framed structure in high rise building", International Journal of engineering and research (IJER), volume no.5 issue: special 3, pp. 612-616, 28 Feb. 2016.
- [3] N.mircic, R. P. Apostolska (2008), "Seismic performance of flat-slab building structural systems". (14th world conference on earthquake engineering, Beijing, China) October 12, 2008.
- [4] Francisco Galvis, Eduardo Miranda, Pablo Heresi, Héctor Dávalos and José Ramón Silos, Preliminary Statistics of Collapsed Buildings in Mexico City in the September 19, 2017 Puebla-Morelos Earthquake
- [5] Bolton, P.A., ed., 1993, The Loma Prieta, California, Earthquake of October 17, 1989—Public response: U.S. Geological Survey Professional Paper 1553-B, 69 p.1994.
- [6] Preliminary Reconnaissance Report (Earthquake Engineering Research Institute, Oakland, CA, 1994)
- [7]. Northridge Earthquake Archived 2004-09-04 at the Wayback Machine. Southern California Earthquake Data Center. Retrieved October 6, 2006.
- [8] IS 1893 (Part 1) 2002, "Criteria for Earthquake Resistant Design of Structure," BIS 2002.
- [9] IS 456:2000, "Code of practice for plain and reinforced concrete", code practice fourth revision, Bureau of Indian Standards, New Delhi, July 2000.
- [10] IS 875 (part 2) – 1987, "Code of practice for Design loads (other than earthquake)for buildings and structures", second revision, June 1998.

SEISMIC PERFORMANCE ASSESSMENT OF BUILDINGS LOCATED ON A SLOPING GROUND

PRADEEP KUMAR PANDRE¹, SHREYASVI C², and KATTA VENKATARAMANA³

¹Former M. Tech Student, Department of Civil Engineering, National Institute of Technology Karnataka, Surathkal, Mangalore, India, pradeep.pandre@gmail.com

²Research Scholar, Department. of Civil Engineering, National Institute of Technology Karnataka, Surathkal, Mangalore, India, shreyasvic@gmail.com (corresponding author)

³Professor of Civil Engineering, Department. of Civil Engineering, National Institute of Technology Karnataka, Surathkal, Mangalore, India, ven.nitk@gmail.com

Keywords: Set back building, Step back – Set back building,

1. GENERAL INTRODUCTION

The present work comprises of two sets of buildings namely step back (SB) and step back set back (SB-SB) buildings resting on the sloping ground. The different sloping angles considered here are 20°, 25° and 30°. The elevation of different sets of models with a standard storey height of 3m and bay width of 4m is shown in Fig. 1-3.

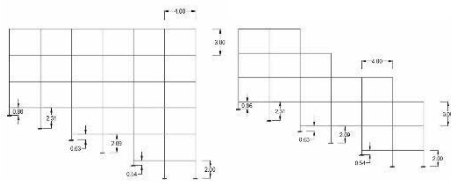


Fig.1 20° Step Back and Step Back-Set Back Building

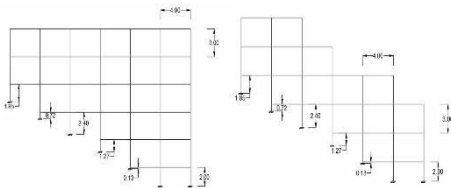


Fig.2 25° Step Back and Step Back-Set Back Building

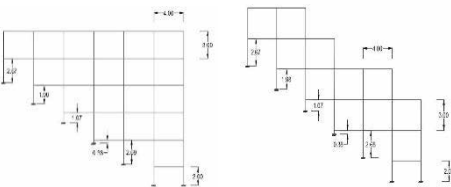


Fig.3 30° Step Back and Step Back-Set Back Building

2. RESPONSE SPECTRUM RESULTS

The response of the structure is considered in the form of the natural period, mode shapes, storey displacement,

and base shear. Site-specific response spectrum obtained from the seismic hazard analysis of the Mangalore region [2] is considered for the analysis and the same has been shown in Fig.4

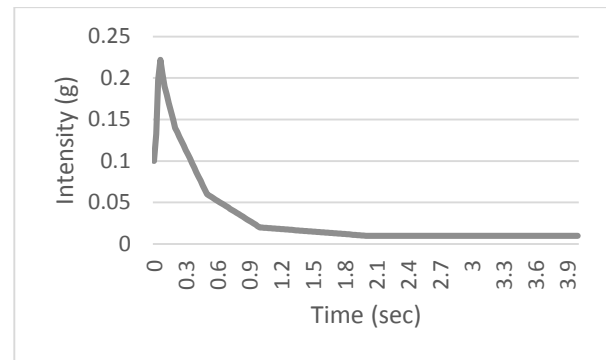


Fig.4 Site-specific response spectrum of Mangalore

2.1 Natural Period and Base Shear

The natural period of the building decreases with the increase in the slope of the building for both the cases. When compared between step back and step back-set back buildings resting on the same sloping ground, step back-set back buildings turns out to have a smaller natural period.

Table 1 Natural period and base shear

Slope ↓	Natural Period (sec)		Base Shear (kN)	
	SB	SB-SB	SB	SB-SB
20°	0.59	0.464	3052	2575
25°	0.52	0.38	3013	2351
30°	0.5	0.322	2798	2019

2.2 Storey Displacement

The top storey displacement decreases with the increase in the sloping angle for both the building types

considered in the study. Similarly, between step back and step back-set back buildings, the latter performs well with comparatively lesser top storey displacement.

Table 2 Storey Displacement

Storey	Step back buildings			Step back-set back buildings		
	20°	25°	30°	20°	25°	30°
Base	0.00	0.00	0.00	0.00	0.00	0.00
1 st	0.07	0.02	0.46	0.07	0.01	0.32
2 nd	0.52	0.48	0.17	0.42	0.57	0.11
3 rd	2.74	1.64	1.71	1.64	0.90	0.93
4 th	6.70	4.99	4.63	3.81	2.32	2.31
5 th	9.96	8.37	7.52	7.00	4.39	3.68
6 th	11.85	10.43	9.48	8.89	6.27	4.90

2.3 Mode Shapes

The first and second mode is significant in translational motion in X and Y direction [1]. However, significant torsion was observed in higher modes and the same has been presented in Fig. 5.

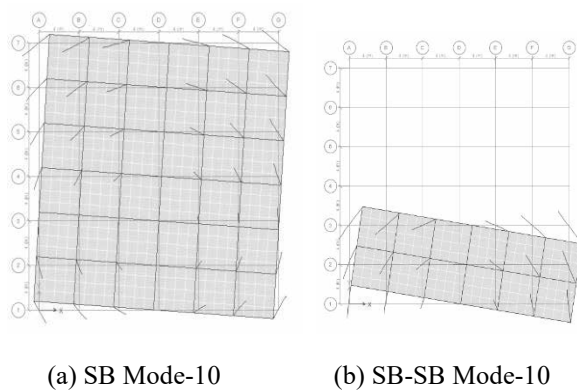


Fig.5 Mode shape of a step back and a step back-set back building on 20° sloping ground

3. PUSHOVER ANALYSIS

3.1 Hinges Formation

Hinges assigned to various structural members serve as an indicator for assessing the performance level of a chosen element. Since the size of the column at the ground level varies with the sloping angle, short column effect comes into play. These short columns attract more earthquake forces, as a result, the sequence of hinge formation begins from the columns in the lower storey.

3.2 Base Shear v/s Displacement

The behavior of both the building configurations in terms of base shear indicated that the step back buildings

can withstand lesser deformation when compared to the step back – set back buildings. In addition, the latter can accommodate higher base shear when compared to the former.

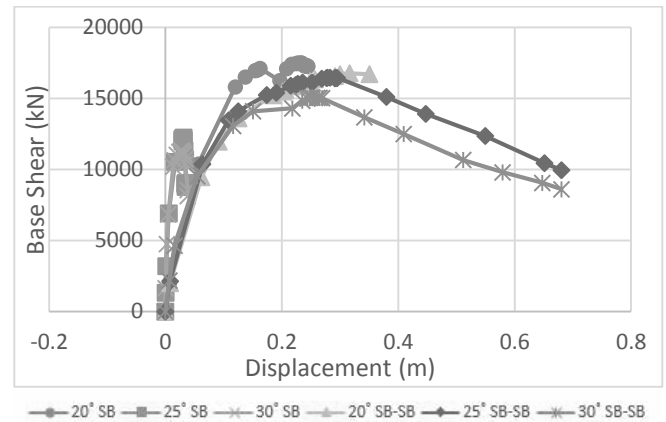


Fig.6 Base shear v/s roof displacement

4. CONCLUSION

The assessment of 2 building configurations i.e. step back(SB) and step back set back building (SB-SB) resting on 3 different sloping angles (20°, 25°, and 30°) were analyzed. The following observations were made from the study.

- The storey displacements in both the building models are almost same in the lower storeys. However, with the increase in the storey height the difference seems to double and SB-SB shows lesser displacement.
- The SB-SB can accommodate large inelastic deformation when compared to SB.

Based on these observations it can be inferred that SB-SB building configuration performs better (ductile behaviour) on a sloping ground than SB.

REFERENCES

- [1] Ghosh, R., & Debbarma, R. (2017). "Performance evaluation of setback buildings with open ground storey on plain and sloping ground under earthquake loadings and mitigation of failure," *International Journal of Advanced Structural Engineering*, 9(2), 97-110
- [2] Shreyasvi C. & Katta Venkataramana (2017). "Quantification of seismic hazard for Mangalore region", Indian Geotechnical Conference – 2017, IIT Guwahatti. (TH-12, no. 502)

DEVELOPMENT OF CRACK DETECTION SYSTEM FOR IMAGE VISUAL INSPECTION WITH AI USING SUPER HIGH RESOLUTION CAMERA

Takahiro MINAMI¹, Makoto FUJII², Junichi TAKAYAMA³, Tomotaka FUKUOKA⁴
Shinya SUDA⁵, Shuya OKUMURA⁶ and Kazuo WATANABE⁷

¹ Master (Eng), Kanazawa university, Dept. of Environmental Design, taketaka0503@stu.kanazawa-u.ac.jp

² Ph.D., Assistant Professor, Kanazawa university, Geosciences and civil Engineering, fujii@se.kanazawa-u.ac.jp

³ Dr., Eng., Professor, Kanazawa university, Geosciences and civil Engineering, takayama@staff.kanazawa-u.ac.jp

⁴ Dr., Informatics, Kanazawa university, Geosciences and civil Engineering, fukuoka@se.kanazawa-u.ac.jp

⁵ WorldLink&Company Co., Ltd SkyLink Japan, s.suda@skylinkjapan.com

⁶ WorldLink&Company Co., Ltd SkyLink Japan, s.okumura@skylinkjapan.com

⁷ Dr., Agri, Affiliated Assistant Professor, Kyoto university, Environmental Coexistence, isseiw@cseas.kyoto-u.ac.jp

Keywords: bridge inspection, diagnostic imaging technology, automatic crack detection

1. INTRODUCTION

In Japan, there are about 730,000 bridges with a length of 2 m or longer, and many of these were built during a period of high economic growth. Parts that were repaired during emergencies and bridges placed in harsh environments age notably. Under these circumstances, there is a shift from breakdown maintenance that attempts countermeasures after major damage occurs, to preventive maintenance that extends the healthy lifespan of bridges by taking countermeasures while the damage is mild. To take preventive countermeasures, bridges must be inspected and diagnosed routinely, and the health condition of bridges must be well understood. In 2014, with a comprehensive standard stipulated by the federal government, the close visual inspection of all bridges by road maintenance staff was required every five years.

As issues with the continuing close visual inspection of bridges are surfacing, the remote imaging system is expected to become a new inspection method that replaces close visual inspection. This has led to a large number of studies [1] [2] [3] [4]. In this study, we propose a new inspection method to replace the current close visual inspection. Using images of an entire pier with 100 million pixels taken with a super-high-resolution camera (SHRC), and an inspection environment similar to that of on-site close visual inspections by human inspectors was created.

2. DIAGNOSTIC EXPERIMENT USING IMAGE WITH 100 MILLION PIXELS

The target bridge was a double-span steel-welded bridge with I-beams having a length of 41.30 m and total width of 4.70 m in Hakui City, Ishikawa Prefecture.

Fig.1 shows cracked and corroded steel reinforcement of the pier photographed from 12.5 m away with the SHRC. Areas marked with red dotted lines indicate cracks and corrosion of steel reinforcement. Although cracks cannot be confirmed in the entire image of the pier, by zooming in, cracks and corrosion of steel reinforcement can be clearly confirmed. About 0.1mm cracks could be visually confirmed. Images taken with the SHRC do not have poor pixel quality when zoomed

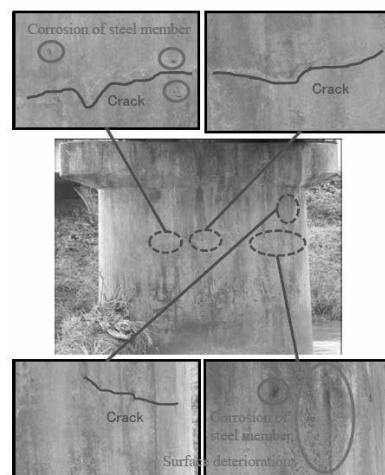


Figure. 1: Cracks photographed with SHRC

in; thus, cracks and corrosion of steel reinforcement can be confirmed.

Using a 52-inch 4K-resolution monitor and designated software, we created a setting where the entire image of the pier, captured with the SHRC, can be observed. Brightness, saturation, and contrast can be adjusted, and one can smoothly zoom in and out of the image. In this study, we used A0 paper with the entire pier printed as the media to record the diagnostic results of cracks.

In the diagnostic experimental environment, two staff with civil engineering degrees but without inspection experience visually detected cracks in the image of the entire pier.

We performed a diagnostic experiment to determine if experienced inspectors can identify cracks in the image. The experienced bridge inspectors were Mr. A (Hakui City staff) and Mr. B (Ph.D. in engineering, technician in construction department/steel structures and concrete, concrete diagnostician); the inspectors zoomed in and out of the photograph of the pier on a display monitor.

We interviewed the diagnosticians about the diagnostic potential of the images. Their opinions were that they were able to detect cracks in a similar manner as a close visual inspection. If we can incorporate this method in an actual inspection, there is further utility in that the inspection cost can be reduced, and diagnostic results can

become more objective. However, there are some results that are difficult to identify regarding whether they are marks from construction formwork or cracks, and there is damage that is difficult to diagnose with images alone.

Each detection result detected the lateral crack at the center of the pier. The detected positions of the cracks were mostly the same. However, depending on the diagnostician, the detection results had slight differences. The reason for this was the participants' experience with bridge inspection.

3. EXAMINATION OF PRECISION FOR CRACK IDENTIFYING AI

In this chapter, we aim to formulate AI that automatically detects locations of cracks from 100-million-pixel images. To formulate AI that is able to identify cracks by understanding the feature values of images that contain cracks, we used the image recognition service [5]. This allows for the creation of an image recognition engine without an image recognition logic by tagging uploaded images and formulating AI. Using a 100-million-pixel image in which cracks were identified by experienced bridge inspectors, areas with cracks and without cracks were cut out separately (about 80.9 KB per image) and were used as teaching data. Images that included the areas of cracks were tagged as "with cracks" and "concrete," and images without cracks were tagged "concrete" for learning. In some cases, images contained grass; therefore, we added the tag "grass." There were 48 images tagged with "cracks," 82 images tagged with "concrete," and 14 images tagged with "grass," which were used as teaching data. In this manner, a crack-diagnosing AI was created.

A post-learning evaluation was performed with two indexes: precision that how well images were classified, and recall that expressed the number of images that were accurately identified among all images that should have been accurately identified. Table 1 shows a post-learning evaluation of the AI.

Using the AI to identify cracks, we diagnosed if each image divided by the mesh contained cracks. The diagnostic results were evaluated with probability which is calculated by AI. The probability of cracks contained in the image input in AI, probability of containing concrete, and probability of containing grass were output. In this study, we only considered cracks and set a threshold for convenience. If the probability of cracks was less than 30%, it was labeled a "low probability of crack formation," 30 to 60% was "moderate probability of crack formation," and 60% or higher was "high probability of crack formation." The crack diagnostic results by AI are shown in Fig.2. For locations that were identified to have cracks by humans using the image, the AI often identified these locations as "high probability of crack formation." The AI often identified locations where cracks could not be visually confirmed as "low probability of crack formation." This indicated that the automatic detection of locations with cracks by AI may be possible.

Table 1: Precision of AI crack identification

	Precision	Recall
The whole	95.1%	88.2%
Crack	92.3%	70.8%
Concrete	95.5%	98.8%
Grass	100.0%	85.0%

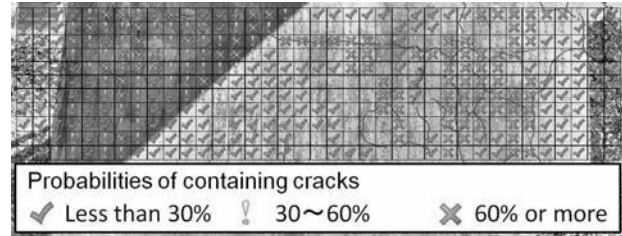


Figure 2: Diagnostic results of cracks by AI

However, areas without visual confirmation of cracks were misdiagnosed as "moderate to high probability of crack formation" if there were boundaries of shadows and marks of formwork. This was likely owing to a problem with the teaching data that were used when the AI was being prepared. An increase or improvement of the teaching data is necessary.

4. CONCLUSIONS

Using the images taken with a SHRC, we performed a diagnostic experiment on the cracks and verified the diagnostic potential of the images. As a result, although there were some crack detection errors between diagnosticians, the detection results of cracks were mostly similar.

We prepared an AI that identifies cracks in images based on the diagnostic results of the cracks. An examination of the AI's precision showed that cracks were identified to a certain degree, indicating that locations of cracks may be automatically delineated from an image with 100 million pixels.

REFERENCES

- [1] Nishimura S, Kimoto K, Matsuoka N, Otani H, Ogata T, Matsuda H (2013) "The development and evaluation of telemetry in bridge maintenance" J Appl Surv Technol Vol.24, pp52-61
- [2] Koch C, Paal S, Rashidi A, Zhu A, König M. Brilakis I (2014) "Achievements and challenges in machine vision-based inspection of large concrete structures" Adv Struct Eng Vol.17, pp303-318
- [3] Yeum CM, Dyke SJ (2015) Vision-based automated crack detection for bridge inspection. Computer-Aided Civil Infrastruct Eng Vol.30, pp759-70
- [4] Sinha K, Fieguth PW, Polak, MA (2003) Computer vision techniques for automatic structural assessment of underground pipes. Computer-Aided Civil Infrastruct Eng Vol.18 pp95-112
- [5] Custom Vision Service - Microsoft Azure, <https://docs.microsoft.com/ja-jp/azure/cognitive-services/custom-vision-service/> Accessed 2017.12.17

USE OF EXISTING COMPONENTS OF STRUCTURE AS TUNED MASS DAMPER

O R JAISWAL¹ and VIKAS M THAKUR²

¹Professor, Dept. of Applied Mechanics, VNIT, Nagpur, India, orjaiswal@apm.vnit.ac.in

²Asst. Professor, Civil Engg. Dept, JDCOEM, Nagpur, India, vikasmsthakur@gmail.com (corresponding author)

Keywords: Tuned Mass Damper, optimum parameters of TMD, Existing component as TMD

1. INTRODUCTION

Mega cities face variety of challenges like, urban industrial safety, urban traffic safety, waste treatment and disposal problems, safety against natural calamities like hurricanes, floods, earthquakes, tsunamis etc. This article deals with safety of civil engineering structures against earthquake and wind loads. An extreme wind event or an earthquake can severely damage civil engineering structures like buildings, bridges, towers, chimneys, water tanks etc. Safety of structures against these loads is essential.

Structural designers have since long used vibration control techniques to control vibrations of civil engineering structures under wind and earthquake loads. Vibration control techniques are broadly classified in four types namely: Passive control, Active control, Semi-active control and Hybrid control. Passive control devices in the form of an additional fixture like viscous dampers, elasto-plastic dampers, and friction dampers have been used in many applications. Tuned mass dampers (TMDs) have been proposed and discussed since last 120 years. In last so many years, the theory of TMD has been well-developed and experimented and it is brought to technological level. Since 1970s, it is being used in buildings and other civil engineering structures for controlling the wind and seismic response. Use of TMD requires deployment of additional mass, stiffness and damper. In recent past, researchers and engineers have attempted to use existing components of structures as TMD. This avoids deployment of additional devices. This approach is quite attractive, since it eliminates the requirement of any additional mass and also, since the existing part is used, there are no additional maintenance requirements. While using the existing components, one has to suitably provide the required stiffness and explore the possibility of providing additional damping. Further, depending on the damping available for this existing component, one can suitably tune the TMD frequency. Six such applications, wherein existing components are deployed as TMD are reviewed in this paper. Further, based on research performed at VNIT Nagpur India, use of existing component as TMD is proposed for elevated water tanks and for RC chimneys.

2. REVIEW ON EXISTING STRUCTURES WHERE COMPONENTS ARE USED AS TMD

Matta and De-Stefano [1] have reported use of roof garden mass as TMD for a 6 story Portasiena Linear building at Siena, Italy. The plan dimension of building is 26m x 42m. The roof garden is created on a RC slab

supported on 28 rolling pendulum bearings which provide the required stiffness (Figure 1). These bearings rest on low load bearing RC floor which is also used for maintenance of bearings. This roof garden has mass which is 5.8% of building mass and with respect to 1st modal mass, TMD has almost 17% mass. The optimum frequency ratio is 0.39. Optimum damping ratio is 0.465 which is achieved with the help of viscous dampers which are located with each bearing (Figure 1). Through a numerical simulation it is shown that such a TMD leads to 45% reduction in peak displacement and around 23% reduction in peak acceleration of main building. Rolling pendulum bearing deployed in this application is robust since there will be no permanent displacement, and TMD (roof garden) regains its original position after vibrations.

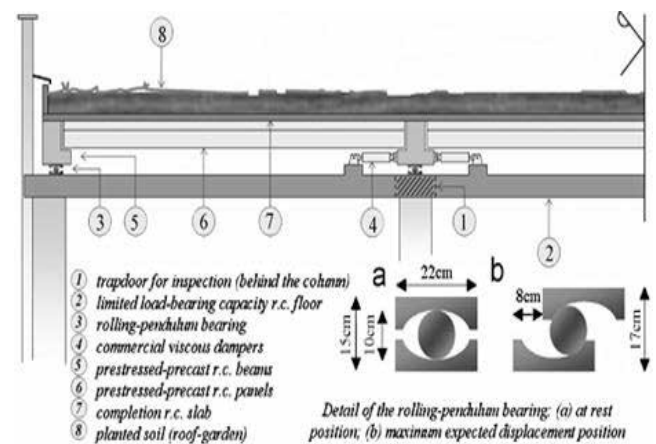


Figure 1. Roof-garden TMD in Portasiena Linear Building, Siena, Italy [1]

Next application is described by Kidokoro [2] regarding Swatch group's building, Nicolas G. Hayek Center. This is a 14 story building constructed on 2007 in Tokyo, Japan installed with TMD derived from floor slabs at various levels of building. The floor slabs are mounted on slider and rubber bearings on the corbel extending from columns of main structure (Figure 2 and 3). The plan dimension of building is 12.6m x 31.2m. The TMD system is implemented by disconnecting slabs of four upper floors (9th, 10th, 12th and 13th floor) from the main structure (Figure 4). All four floors together have mass 10% of building mass. Through non-linear time history analysis it is shown that this TMD leads to 37% reduction in seismic forces.

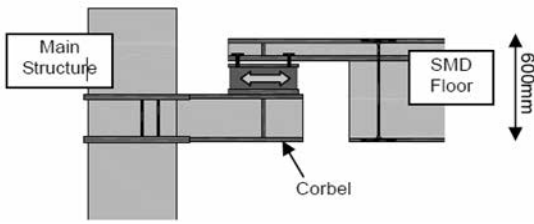


Figure (2a) Section view of Rubber bearings [2]

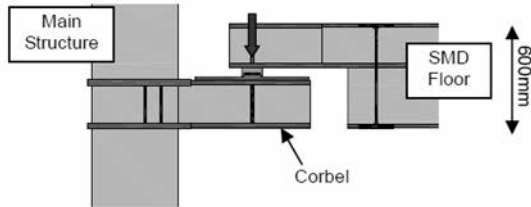


Figure (2b) Section view of Slider bearings [2]

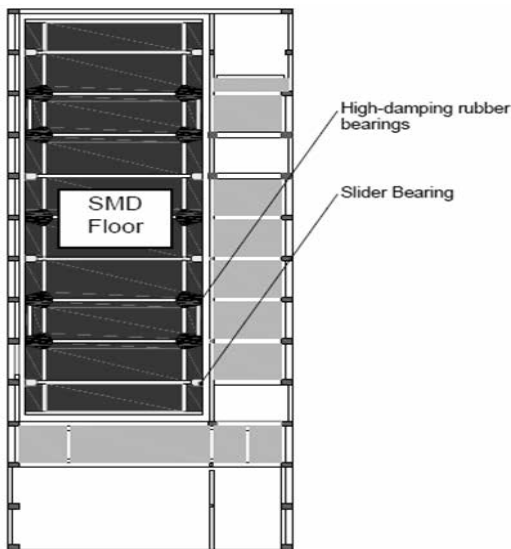


Figure 3. Plan view of TMD floor [2]

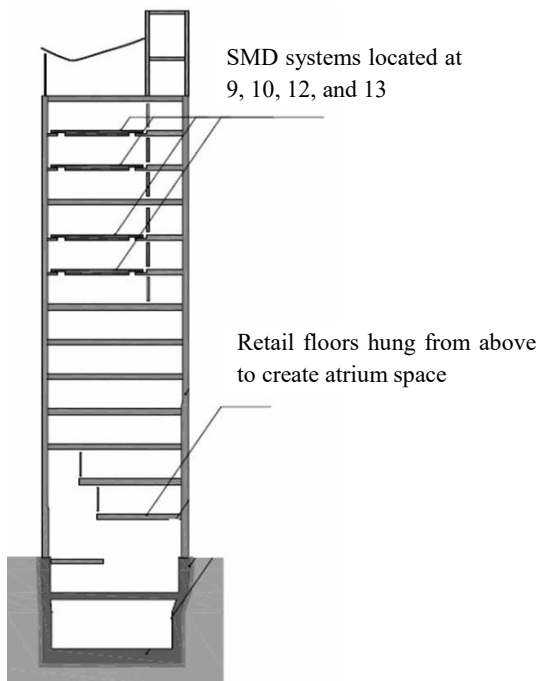


Figure 4. TMD at Nicolas G. Hayek Center, Tokyo, Japan [2].

Nagase and Hisatoku [3] have shared details of ice thermal storage tanks used as TMD in 37 story Crystal Tower office building, completed in 1990 at Osaka, Japan. The tanks are suspended with cables from frame girder at the roof (Figure 5). The weight of each tank is 90 tonnes and four such tanks are placed in larger dimension of building and two tanks are placed in shorter plan dimension. The mass ratio of damper to effective mass of building in longer direction is 2.5% and in shorter direction it is 1.3%. The length of cable is kept variable between 3.5m and 4.5m in longer plan direction and between 3m and 4m in shorter plan direction. Oil dampers are provided to absorb tank swinging motion and to damp the building sway motions. The damping ratios are chosen more than the optimum values. The damping ratio in longer direction is 0.12 and it is 0.09 in shorter direction. The wind tunnel test and modal analysis have shown that this damper can reduce wind-induced motions by 50%. After deployment of TMD this building has witnessed two extreme loading events. One is Typhoon 9019 on 19th September 1990. During this event, dynamic response is recorded. Then, through numerical simulation, it is shown that recorded response is 50% less than the response without this TMD. The Second event witnessed by this building is earthquake of 24th September 1990. Again through numerical simulation it is shown that due to presence of TMD, seismic response has decayed rapidly.

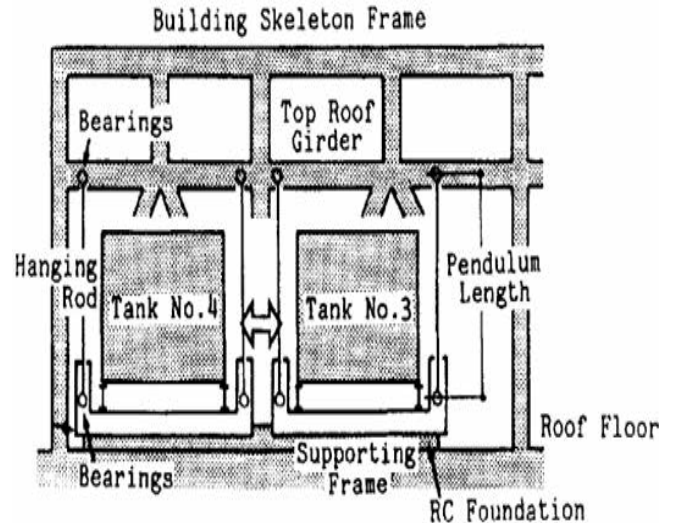


Figure 5. Ice storage tanks as pendulum type TMD [3]

Tadashi [4] has shown details of ice thermal storage tank TMD in 31-story Proctor & Gamble Japan headquarters, constructed near Kobe in 1993. Here also like in crystal tower, ice thermal storage tanks hanging from rooftop was used as TMD mass (Figure 6). Mass ratio was 1% and each tanks weighs 90 tonnes. Dampers were principally designed to protect structure from strong wind motions.

The 36-story Sea Hawk Hotel completed in 1995 and located in Fukuoka, Japan was fitted in with the pendulum type TMD. Here water tank of weight 132

tonnes is used as mass damper. Dampers are designed to reduce the torsional vibrations of building due to the maximum wind speed of 86 Kmph [4].

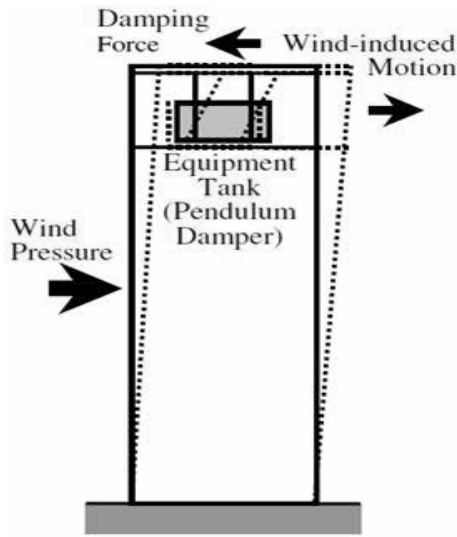


Figure 6. Conceptual model of Building with pendulum type TMD [4]

Hoang et al. [5] proposed retrofit scheme in the form of TMD for Minato bridge in Osaka, Japan. Span of bridge is 510m. Old existing bearings of the bridge were replaced by a new floor deck-isolation system (Figure 7). Floor deck-isolation system comprise of sliding bearings and rubber bearings. Damping is achieved with the help of sliding bearings which act as linear viscous damper and rubber springs increases period of bridge and act as elastic spring. Floor decks and isolation system together form a large mass TMD, making mass ratio 77%. In the process of design of TMD, a 3-D Finite element model was made and Kanai-Tazimi spectrum was used to model earthquake. The optimally designed TMD based on Kanai-Tazimi spectrum were shown effective for ground motion time histories of similar frequency content.

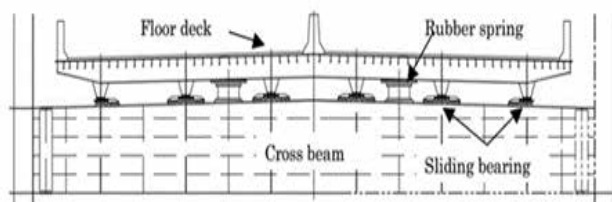


Figure 7a. Floor deck-isolation system of Minato Bridge in Osaka, Japan [5].

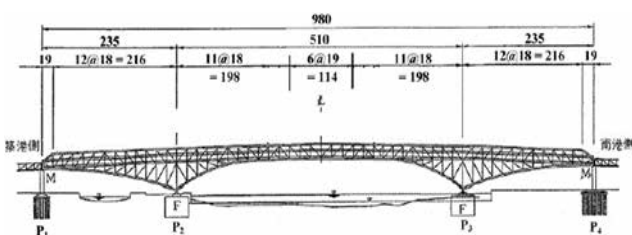


Figure 7b. Longitudinal view of Minato Bridge in Osaka, Japan [5].

3. RESEARCH WORK AT VNIT ON USE OF EXISTING COMPONENT AS TMD

In recent past, under two sponsored R & D projects at VNIT, Nagpur attempts have been made to use existing components of structure as TMD. This has been attempted for two structures, i.e. elevated water tank with frame staging and tall RC chimney. In the case of elevated water tank on frame staging, the TMD is derived from roof slab and columns inside the container [6]. Here, roof slab is laterally detached from wall (Figure 8). Thus roof slab with column inside the container acts as TMD. For an elevated water tank of 350 m³ and staging height of 12m, it is shown that such TMD leads to about 20% reduction in base shear. This TMD is not yet implemented nor has any experimental verification been done.

In the case of tall RC chimney, the maintenance platform is used as TMD. In the tall RC chimney, maintenance platforms are provided at regular intervals along the height. One such platform at the top level was used as TMD (Figure 9a and 9b). For this purpose it was proposed that bearing will be inserted at the support of the platform. This mass of platform acts as TMD mass, and the stiffness and damping is provided by bearings. The effect of such a TMD was studied for along-wind and across-wind response. A 273 m tall RC chimney was considered and the top most platform was converted into TMD with mass ratio of about 1% and TMD damping is taken as 5%. It is shown that such TMD leads to about 25% reduction in base shear. Thus, for tall RC chimneys, use of maintenance platform as TMD offers a good option to suppress along-wind and across-wind response [7].

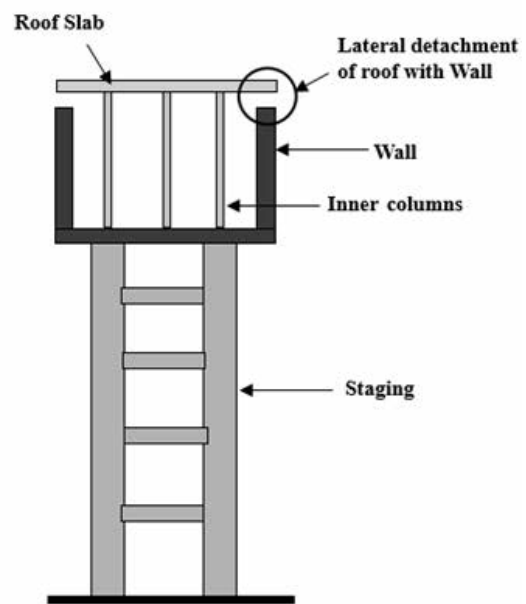


Figure 8. Proposed TMD for elevated water tank [6]

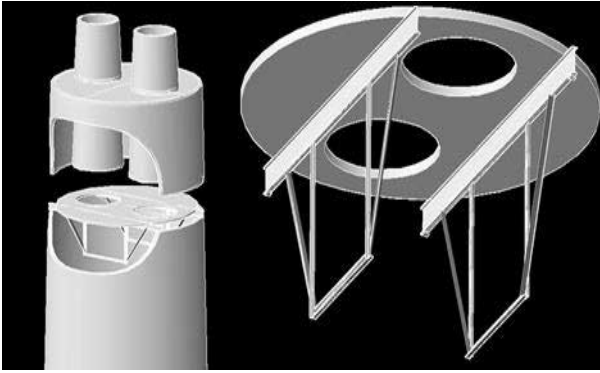


Figure 9a. Geometric details of maintenance platform [7]

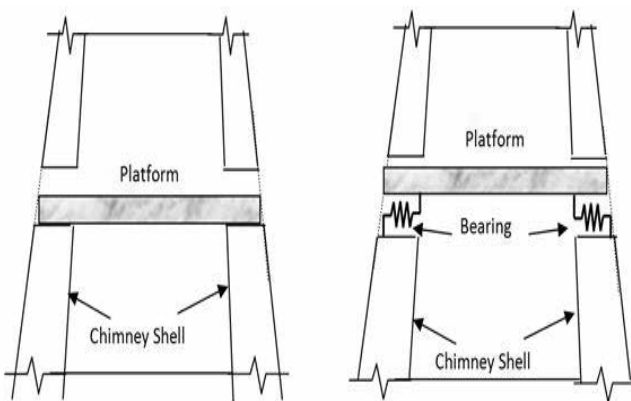


Figure. 9b. Details of maintenance platform and elastomeric bearing as TMD [7]

4. DISCUSSION

Use of TMD is now quite common and has been implemented in many buildings, bridges and other structures. Of late, efforts are made to use existing components of structure as tuned mass damper. In this approach, the damping of TMD is either kept same or greater than that of the main structure. This approach of using existing part of structure as TMD has certain advantages such as there is no need of deployment of heavy extra mass and space in structures. This TMD certainly helps in energy dissipation. Six such applications are reviewed in this paper. These applications are for buildings and bridge. In case of building [1], roof garden is mounted on bearings to act as TMD. In other type of application, utility equipments such as ice thermal storage tanks or water tank are suspended with cables to act as pendulum type TMD. In bridge floor deck-isolation system is converted to TMD.

Use of existing part as TMD is not yet outlined for structures other than buildings and bridges. Under sponsored R & D projects at VNIT such approach of use of existing components of structure as TMD been carried out for two structures, i.e. elevated water tank on frame staging and tall RC chimney. It is shown that such TMD is effective in reducing dynamic forces. There is a need

for experimental verification of such TMDs for elevated water tank and RC chimney.

REFERENCES

- [1] E. Matta and A. De Stefano, (2009) "Seismic performance of pendulum and translational roof- garden TMDs," *Mechanical Systems and Signal Processing*, 23(3), 908-921.
- [2] R. Kidokoro. "Self Mass Damper (SMD): Seismic control system inspired by the pendulum movement of an antique clock," *14th World Conference on Earthquake Engineering*. Beijing, China, 2008.
- [3] T. Nagase and T. Hisatoku, (1992) "Tuned-pendulum mass damper installed in crystal tower," *The structural design of tall buildings*, Vol. 1, 35-56.
- [4] Nagashe T. "Earthquake records observed in tall buildings with tuned pendulum mass damper," *12th World Conference on Earthquake Engineering*., Auckland, New Zealand, 2000.
- [5] Hoang N, Fujino Y, Warnitchai P, (2008) "Optimal Tuned Mass Damper for seismic application and practical design formulas," *Engineering Structures*, 30, 707 -715.
- [6] Jaiswal OR. "Simple tuned mass damper to control seismic response of Elevated Tank," *13th World Conference on Earthquake Engineering*. Vancouver, B.C., Canada, 2004.
- [7] K R C Reddy, O R Jaiswal, P N Godbole, (2011) "Wind Response Control of Tall RC Chimneys", *Journal of Wind & Structures*, Vol. 8(1), 1-9.

USMCA 2018

SESSION 6

TOOLS AND TECHNIQUES IN DISASTER MANAGEMENT

SHEAR CHARACTERISTICS OF VERY LOOSE VOLCANIC SOIL CAUSING SLOPE DISASTER

Itsuki Sato¹ and Reiko Kuwano²

¹ Master Student, The University of Tokyo, Institute of Industrial Science, Tokyo, Japan, i-sato@iis.u-tokyo.ac.jp

² Professor, The University of Tokyo, Institute of Industrial Science, Tokyo, Japan, kuwano@iis.u-tokyo.ac.jp

Keywords: Volcanic soil, Cementation, Particle crushing, Landslide, Slope disaster

1. INTRODUCTION

Soil having a high void structure derived from volcanoes is distributed widely in various places in Japan, and it caused some slope disasters in the past (**Table 1**). The past large-scale slope disasters include Ontake land slide with a slack surface of loose pumice stone layer caused by the 1984 Western Nagano Prefecture earthquake, gentle slope disaster caused by the pumice layer of Minamiaso village due to the 2016 Kumamoto earthquake (**Figure 1**), slope disaster of Izu Oshima where the slope that had been evaluated as safe in the hazard map collapsed due to the torrential rain caused by typhoon, the case of the 2008 Iwate-Miyagi Nairiku earthquake where sediment flowed over a long distance on a gentle slope with a gradient of 1° to 2° due to deposition of loose non-plastic volcanic ash soil with cementation. In this research, focusing on the fact that slope disasters such as muddy flow and long-distance flow are triggered by volcanic pumice layers with high void, extremely loose soil with volcanic cementation was reproduced by adding cement in the laboratory, and its strength characteristics was investigated by performing CD tests and CU tests at several confining pressures.

Table 1: Typical Japanese volcanic soils^{1),2),3),4),5)}

	Kanto Loam	Shirasu	Masado	Scoria
Cementation	Yes	Yes	No	Yes
Crushable Particles	No	Yes	Yes	Yes
ρ	Small	Small	Small	Small
Maximum	3.38	1.68	1.11	1.23
Viscosity	Large	Small	Small	Non-plastic



Figure 1: Landslide at Takanodai of Aso in Kumamoto earthquake (2016)

2. SPECIMEN PREPARATION

In general, the micro-structure and fabric of naturally deposited volcanic soils are neither homogeneous nor isotropic, and it is hard to collect a sufficient number of undisturbed samples repeatedly with equivalent quality. Thus, artificial samples of extremely loose soil were produced in the laboratory to understand fundamental behaviors of such specific soils systematically.

In this study three types of samples having cementation were prepared as follows:

- (1) mix DL clay, which is non-plastic fine, and ordinary portland cement at specific mixture ratios (**Table 2**).
- (2) add specific amount of water (**Table 2**) and mix it with the material enough for 2 minutes.
- (3) using suction, pour the mixture loosely into a mold whose diameter is 5cm and height is 10cm to achieve the weight calculated to be the designed void ratio (**Table 2**).
- (4) keep molds in a moist curing box for 7 days.
- (5) put them in a drying oven for 24 hours.
- (6) start experiments immediately after taking samples from the drying oven.

By following this procedure, a lot of specimens having almost same cementation and density were prepared to conduct experiments systematically.

Table 3 shows averaged values of the saturated density (ρ_s), the dry density (ρ_d) and the void ratio (e) of each specimen type prepared in the laboratory. The loose DL clay specimen was also prepared for a better comparison with the three specimen types (namely, A, B, and C), that exhibit higher void ratio values than the loose DL clay. Specimen A is standard (reference) sample, B has less cementation than A due to smaller amount of cement, and C has higher void ratio than A.

Table 2: Contents of artificial specimens

Specimen	Mass ratio	Designed void ratio
	DL clay:Cement:Water	
A	85:15:25	2.1
B	90:10:25	2.1
C	85:15:25	2.7

Table 3: Material properties of prepared specimens

Specimen	ρ_s (g/cm ³)	ρ_d (g/cm ³)	e
A	2.69	0.89	2.02
B	2.66	0.89	1.99
C	2.69	0.75	2.61
Loose DL clay	2.65	1.03	1.58

3. RESULTS AND DISCUSSIONS

The volume change during the initial consolidation stage is illustrated in **Figure 2**. Specimen A shows low volumetric strain at low confining pressure levels similar to loose DL clay, but its compressibility changes suddenly at around 150kPa and increases after the sudden jump. It is hypothesized that cementation between particles was lost at the pressure level. The larger compressibility observed after the loss of cementation compared with loose DL clay implies that extremely loose structure was ascribed to this high compressibility. Specimen B also exhibits a sudden jump due to loss of cementation at around 70kPa followed by a similar compressibility with specimen A, which had similar void ratio. As for specimen C, loss of cementation was not observed, probably because specimen C had a high void ratio and cementation was too weak to retain against the initial back pressure.

CD test results of specimen A are shown in **Figure 3**. At confining pressures of 50 and 100kPa, prior to the loss of cementation, a peak strength was observed at a small strain. After cementation was lost, specimen A showed greatly loose behavior. At all confining pressures, significant negative dilatancy was observed.

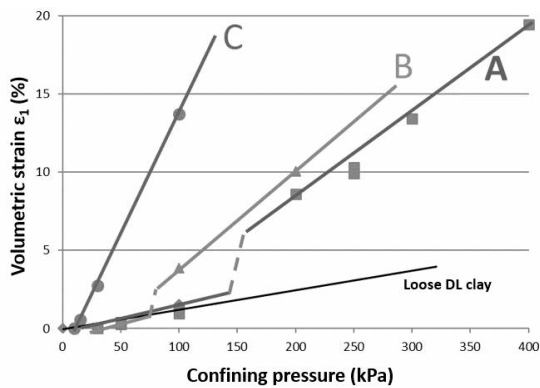


Figure 2: Volumetric strain during consolidation stage

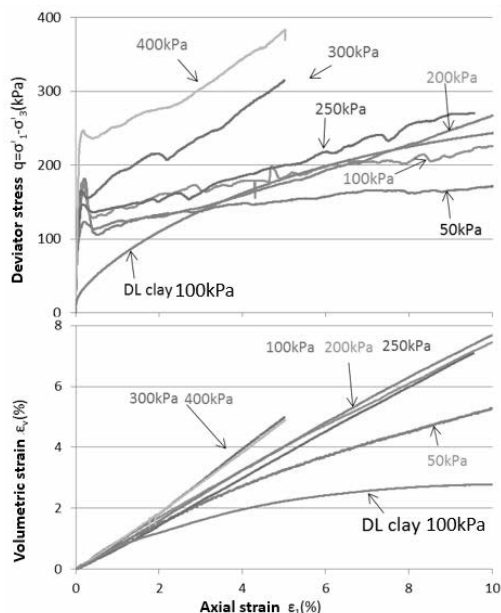


Figure 3: CD test results of specimen A at several

confining pressure levels

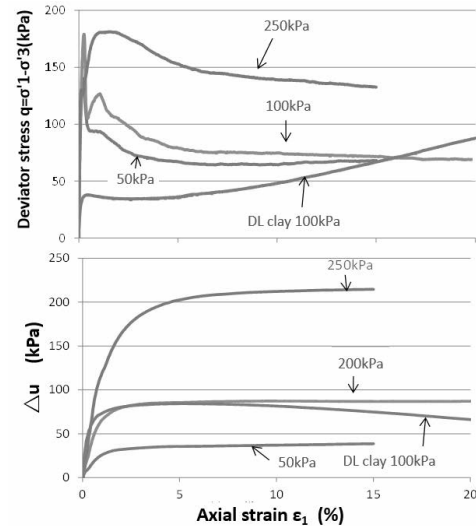


Figure 4: CU test results of specimen A at several

confining pressure levels

Referring to **Figure 4** for CU test results of specimen A, in the case of low confining pressures, 50kPa and 100kPa, the specimen type shows a peak strength at a low axial strain as observed in CD tests. In all cases, the deviator stress reaches a residual (steady) state when the axial strain reaches 20%. It is hypothesized that once extremely loose soil's cementation is lost, the strain can develop dramatically in a short time in the field.

4. CONCLUSIONS

Extremely loose soil kept by cementation exhibits greatly high shear strength and low compressibility when cementation is kept. However, once cementation is lost, high compressibility and significant negative dilatancy can be observed. In undrained compression tests, after the shear strength reaches its peak and the cementation is lost, a brittle behavior can be observed in which the shear strength converges to a residual state.

REFERENCES

- [1] H. Murata, M. Hyodo, N. Yasufuku: *Compressive and shear characteristics of undisturbed decomposed granite soils paying attention to the degrees of weathering*, Journal of JSCE, 382 / III-7, pp. 131-140, 1987.
- [2] O. Kusakabe, Y. Maeda, M. Ohuchi, T. Hagiwara: *Strength - deformation characteristics of an undisturbed scoria and effects of sample disturbance*: Journal of JSCE, No. 439 / III - 17, pp. 69 - 78, 1991.
- [3] J. Yang, N. Moroto: *Shear strength of undisturbed volcanic cohesive soils undergoing cementation*: Journal of JSCE, No. 617 / III-46, 175-189, 1999.
- [4] T. Nishioka, S. Shibuya: *Engineering Properties of Three Local Soils and their Engineering Applications*: the Japanese Geotechnical Society, 65-1 (708), 2017.
- [5] S. Miura, K. Yagi: *Mechanical behavior and particle crushing of volcanic coarse-grained soils in Japan*, Characterization and Engineering Properties of Natural Soils p 1169 - 1204, 2003.

A STUDY OF PENETRATION RESISTANCE VALUE AT LOOSE AREA UNDER THE CAVITY: EXPANSION PROCESS OF SUB-SURFACE CAVITY

M.OKAMURA¹, M.ABE², K.KITAMURA³, H.NISHIYAMA⁴, R.HATAKEYAMA⁵ and R.KUWANO⁶

¹Engineer, Disaster Reduction Department, GEO SEARCH Co., LTD., Tokyo, Japan, m-okamura@geosearch.co.jp (corresponding author)

²Section Chief, Disaster Reduction Department, GEO SEARCH Co., LTD., Tokyo, Japan, m-abe@geosearch.co.jp

³Associate director, Road and River Department, Fujisawa City, Kanagawa, Japan, fj0-dorokasen-s@city.fujisawa.lg.jp

⁴Section Chief, Road and River Department, Fujisawa City, Kanagawa, Japan, fj0-doji@city.fujisawa.lg.jp

⁵Senior Unit Chief, Road and River Department, Fujisawa City, Kanagawa, Japan, fj-doji@city.fujisawa.lg.jp

⁶Professor, ICUS, IIS, the University of Tokyo, Tokyo, Japan, kuwano@iis.u-tokyo.ac.jp

Keywords: road cave-in, sub-surface cavity, expansion, penetration resistance

1. INTRODUCTION

A collaboration among Fujisawa city, IIS Univ. of Tokyo and GEO SEARCH address the countermeasure against road cave-in through various approaches in Fujisawa city since April 2017. Road cave-in causes traffic accidents / disturbances, especially in emergency situations. The purpose of this collaborative study is to investigate the mechanism of cavity formation and expansion. Thus, the study is important in maintaining road function safety. The study includes the monitoring surveys of sub-surface cavity using GPR (Ground Penetrating Radar) every 6 months, the detailed investigation of subsurface cavity, and regional evaluation based on the result of the surveys. As a part of the study, some of surveyed cavities were observed in detail by open-cut method. This paper describes the expansion process of sub-surface cavities.

2. PURPOSE AND METHODS OF PENETRATION RESISTANCE TEST OF GROUND BELOW THE CAVITY

Because there are various mechanisms of cave-in formation, an identification of the cause of the sub-surface cavity is essential for reliable repair. In this study, the factors of cavity formation and the ground conditions were investigated in detail at ten cavity-locations.



Figure1: Portable cone penetration test

After removing the pavement, digging up to the top of the cavity and measuring the size of cavity, the value of penetration resistance of the ground below the cavity was measured by a portable cone penetrometer (Fig. 1). The ground condition below the cavity is one of valuable information that shows the expansion process of the cavity. And the reason for using a portable cone penetrometer is that it is easy to understand the ground conditions accurately. Next, based on the result of the penetration test, the ground was further dug down to the point where the cavity originally generated. During the digging, the condition of the ground was carefully observed. After the causes of cavity were identified, repair works were carried out. In this study, all of ten cavities that investigated in detail were located in a sand layer by washing out due to damaged sewage pipes - cracked or broken (Fig.2). However there were differences in ground conditions such as the presence of groundwater.

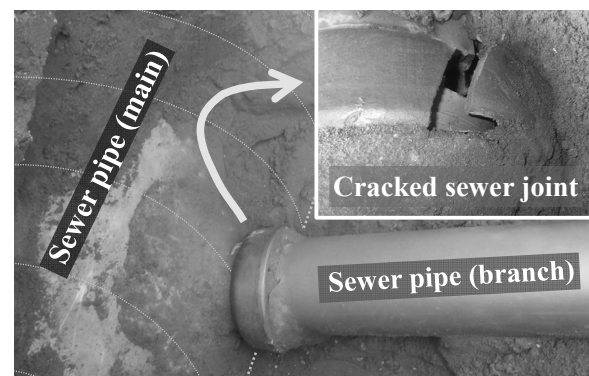


Figure 2: Damaged sewer joint

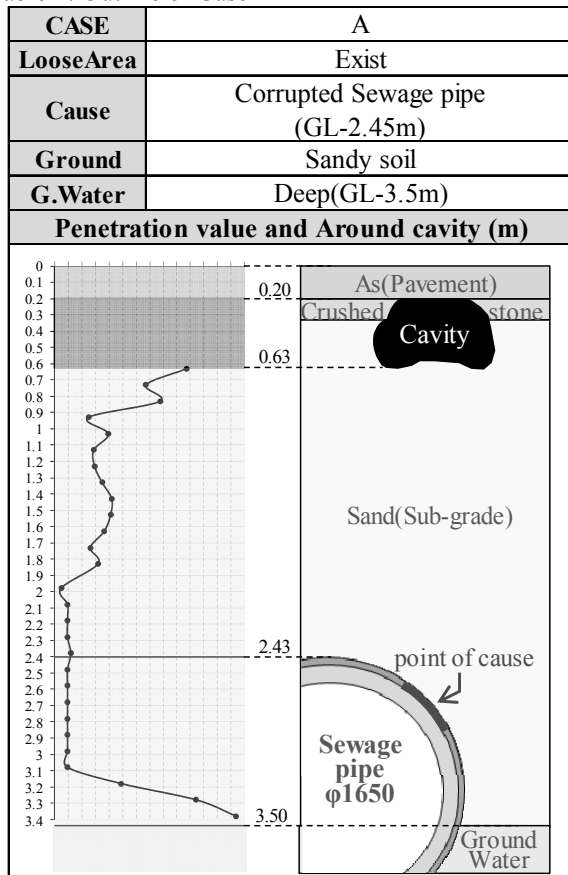
3. RESULTS AND DISCUSSION

The relevance between the value of looseness below the cavity and the occurrence of cavity is considered according to the ground condition.

Case-A is a typical cavity that caused by washing out and expanded in a short period in a sand layer. The washing out of the sand occurred from small damaged joint of sewage pipe. As shown in Table 1, the result of penetration test, the soil below the cavity was uniform and very loose between the bottom of cavity (GL-0.63m)

and the ground water level (GL-3.5m). The similar conditions were observed at other three sites in this study.

Table 1: Outline of Case-A



Case-B is another typical cavity that expanded slowly in sand and gravel layer with high groundwater level (Fig. 3). As shown in Table 2, the ground water level was GL-1.45m. It appeared between the bottom of cavity (GL-0.30m) and the damaged point of sewage as the factor of the cavity (GL-1.64m). The penetration resistance value of below the cavity was not uniform. Although it went up and down, the overall trend becomes larger with the depth. The similar type of cavities and loosening were observed at other two sites in this study.

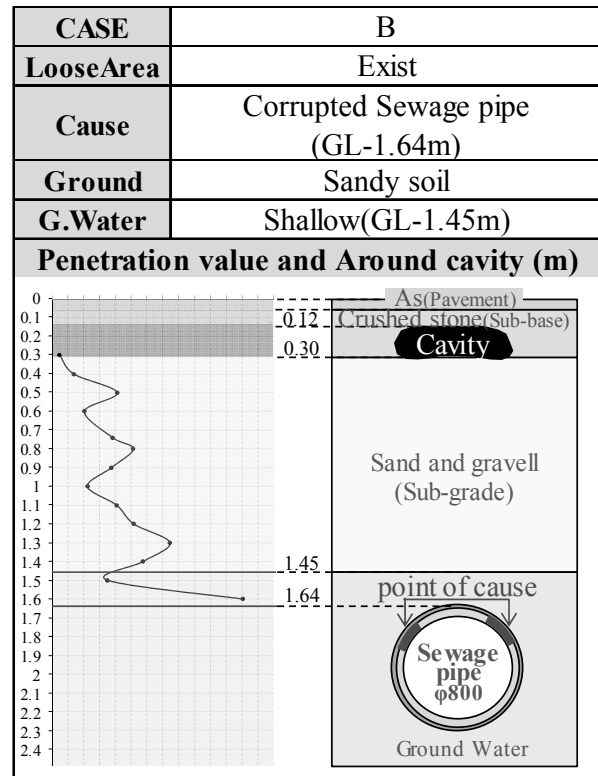


Figure 3: Sewer pipe and ground water (CASE-B)

Previous researches by laboratory model tests^[1] reported two key factors for the expansion of cavity,

which are the fluctuation of water level and type of ground. A cavity in highly permeable model ground expands with the fluctuation of water level. In actual ground, it corresponds to the fluctuation of groundwater in a sand layer. The process is that a cavity expands upward while repeating the collapse of upper sand with the fluctuation of water level. It may be suggested that the non-uniform penetration resistance is the sign of repeated sand collapse, although it should be noted that the non-uniform cone penetration resistance can be caused by the presence of gravels.

Table 2: Outline of Case-B



4. CONCLUSION

The finding of this study based on the detailed investigation in actual ground is that the penetration resistance value may reveal a process of cavity expansion.

It is difficult to investigate the cause of cavity under road maintenance work in short time in usual way. Consequently, this consideration based on actual cases seems to be a lead to great breakthroughs in research into the causes and mechanisms of cavity.

If the process of expansion of cavity is estimated by simple method, it helps to solve the issue to maintain roads in optimum approaches.

REFERENCE

- [1] R. Kuwano, R. Sera, Y. Ohara. 2018. Model tests to simulate formation and expansion of subsurface cavities. Proc. of 9th international conference on physical modelling in geotechnics, ICPMG2018, pp.1087-1092.

AN INVESTIGATION OF URBAN SAFETY IN YANGON'S BACK DRAINAGE SPACE: IDENTIFICATION OF EXISTING CHALLENGES AND ROLES OF STAKEHOLDERS CONSIDERING THE POTENTIAL AS URBAN COMMONS

T. MATSUSHITA¹, E. ROELL², A. KUBOTA³, and K. MEGURO⁴

¹ Project Researcher, International Center for Urban Safety Engineering, Institute of Industrial Science, the University of Tokyo, Japan, matsu-t@iis-u-tokyo.ac.jp (corresponding author)

² Founder & Director, Doh Eain, emilie@doheain.com

³ Project Professor, Department of Urban Planning, the University of Tokyo, Japan, ak@td.t.u-tokyo.ac.jp

⁴ Professor & Director, International Center for Urban safety Engineering, Institute of Industrial Science, the University of Tokyo, Japan, meguro@iis.u-tokyo.ac.jp

Keywords: Back Drainage Space, Yangon, urban safety, urban commons, stakeholders

1. BACKGROUND & OBJECTIVE

Yangon's cityscape is transforming at an unprecedented speed in rapid urban development which started since the democratization of the country in 2012. The city is facing typical problems caused by increasing urban population, such as traffic congestion and lack of housing, as an increasing number of new development projects with large scale commercial buildings and high-rise condominiums are springing up in the city. Despite the rapid transformation, the Central Business District (CBD) of Yangon still holds the appearance of the original grid plan built during the colonial period giving a sense of nostalgia to visitors today.

After the British colonized the city in 1852, a new city plan of wide roads in a grid pattern was implemented with an emphasis on the importance of proper drainage systems as Yangon was suffering from frequent floods. Back Drainage Space (BDS), a 15-foot wide back alley with open gutters and underground sewage facilities, was built behind buildings as a part of the scheme to provide sufficient space for air ventilation and light to keep the city sanitary and protect the city from disasters such as flood and fire. In the early days, the space not only served its purpose but residents used it for unintended purposes such as a social space or passage. However due to a lack of proper maintenance, the space became dirty and the local authority closed access to BDS in the 1980s. Over nearly three decades that passed while BDS became unused, some residents kept throwing trash into the alley, causing most residents to keep their doors and windows closed.

Recent democratization has brought various changes to Myanmar. Urban areas especially had to accommodate growing needs in response to rapid social and economic development. BDS became a place of social experimentation, initiated by a social enterprise / NPO called *Doh Eain* which promotes the utilization of BDS as a space for the community. The local government has begun to take action by cleaning and repairing BDS around the city at the same time. This movement of place-making has inspired many and brought great encouragement, increased the level of public interest and shown promising positive support by the government. There are approximately 180 BDSs in Yangon today. Comprising a large part of the urban infrastructure and cityscape of central Yangon, there is a serious need to

reexamine the function and spatial quality of BDS in the face of Yangon's urban renewal. Considering the potential of BDS and searching to find ways in which BDS can be utilized as urban commons in the future, the authors conducted a series of field surveys with residents and the authorities to grasp the history, understand the current condition of BDS and to examine effects of on-going place-making activities.

2. METHODOLOGY

This research is based on a series of field surveys conducted between 2016 and 2018. Due to a lack of official records or documentation to comprehend the historical background of BDS, the authors started by conducting semi-structured interviews with residents in the CBD. Based on the findings, some issues were selected as themes for Focus Group Discussions (FGDs), such as intended use and management of the space, in order to get a deeper understanding of the subject as well as people's perception and desires regarding BDS. In addition to the qualitative research, household surveys were conducted in areas where projects were implemented by *Doh Eain* to measure the project impacts, along with ocular surveys to get quantitative data of target communities. While the interviews and FGDs were conducted with residents and ward officers who were actively engaged with the activities, as they were selected by the ward officer or members of the community, household surveys were conducted to randomly selected residents including those residents who were not actively engaged or had no interest in the project. This allowed for diverse views and perspectives on BDS and the project. Ocular surveys of two BDSs with all buildings facing the BDS were conducted to grasp the actual condition of the built environment such as the number of stories and units, building period and condition of the means to access the BDS, such as staircases and doors at the back of the buildings connecting to BDS. The survey questions are categorized into five themes: history, current conditions, community profile, project participation and preference and management. This paper focuses on some key findings related to urban safety and identifies existing challenges and the roles of stakeholders are discussed as a critical factor in considering the potential of the space as urban commons.

3. PROCESS OF A PLACE-MAKING PROJECT

Doh Eain implemented the *Alley Garden Project*, together with community members and authorities in six locations in the CBD, during 2017 and 2018. Multiple stakeholders include residents, the ward and township officers, parliamentary members, five departments from the city government called Yangon City Development Committee (YCDC) and *Doh Eain*. BDS is under the jurisdiction of YCDC and each one of those five departments within YCDC has responsibility for specific management tasks regarding BDS. The project's implementation process was created based on a principle of people's participation which encouraged the formation of a resident committee for project administration and management as well as the participation of the residents in the activities such as meetings and design workshops. The funding structure of the project is a unique model developed by *Doh Eain* with 20% of the total cost of the project implementation provided by residents themselves while the remaining 80% is provided by *Doh Eain*.

4. FINDINGS

In summary, the surveys revealed that the project brought positive impact overall by increasing the usage of BDS from nearly zero to 50%, improving the residents' perception about BDS and encouraging communication among different stakeholders. However, despite its success in increasing the usage of BDS, the survey revealed that the participation level in the project by the residents was low, mainly limited to the committee members and the ground floor residents directly affected by the changes.

The key findings related to urban safety are categorized into five sub-themes of current conditions: accessibility, safety, security, density and ownership. In terms of accessibility, even though many residents thought that BDS became useful after the project, it revealed that most residents do not have direct access to BDS from their units due to a lack of emergency staircases. Most old buildings have no rear staircase while most high-rise buildings have rear staircase but unused and most ground floor units have back doors but often closed or unused. Regarding the security, most people feel safer after the project but some security measures need to be considered if the usage of BDS increases and if it becomes open to public. The survey also revealed that most buildings are owned by multiple owners and neighborhood with new high-rise buildings are 1.5 times more populated than neighborhood with old buildings.

5. ANALYSIS: EXISTING CHALLENGES AND ROLES OF STAKEHOLDERS

A lack of accessibility to BDS is caused by a number of reasons. As this can be a serious safety threat in case of disaster, it is important to investigate the causes for such situations. For buildings which have a staircase but it is unused, it is due to deterioration caused by a lack of maintenance or misuse of the space as personal storage by the residents and also by a lack of law enforcement by the

city government to regulate the residents to maintain and use the staircase properly. It can be said that the unsanitary condition of BDS did not encourage the residents to gain accessibility. For the rest of buildings which have no staircase, they are considered to be non-conforming buildings and in the majority of cases, they were built before the government mandated buildings to be built with emergency staircases.

Ocular surveys revealed that most non-conforming buildings without staircases were under four stories high, and likely to have been built during the colonial period or under the Burma Socialist Programme Party, the military regime led by Ne Win, while modern buildings that are usually over seven stories high had some means of egress installed. The latter are likely to have been built either after the regulation was in place or just out of common practice or necessity before or after the regulation. There were two types of egress observed, one that is built into the building with space for the staircase and the other that is only attached on the surface of the building like a ladder, obviously not as safe as the former. There is a big challenge to fix this situation because of 1) a lack of finance to pay for the repair or to install new staircases by the owners and 2) a difficulty in getting consensus among many owners of different units of a single building.

Therefore, the old, deteriorated structures and complicated ownership patterns of buildings may hinder the changes necessary for BDS to be used safely as urban commons. The survey revealed that in spite of living in deteriorated old structures, 51% of the residents are not concerned about natural disaster such as earthquake or fire and this low level of awareness suggests that it may be difficult for residents to invest in necessary renovations. On the other hand, although the owners are responsible for upgrading their own property, as this issue concerns the living safety of many citizens especially in the CBD, the city government may be required to take a more active role in encouraging some sort of resolution. The alleyway project may be a good opportunity to facilitate this since recognizing the usefulness and well-being of BDS may convince stakeholders such as residents and city government to take action towards securing the accessibility of BDS.

6. CONCLUSION

The study revealed that the project to utilize BDS for the community brought positive impact to the community while also bringing attention to the existing safety issues of lack of emergency accessibility. Further study is needed to investigate alternative solutions involving multi-stakeholders to improve the condition to bring various public benefit.

ACKNOWLEDGEMENT

We would like to thank the residents, local authorities, volunteers and *Doh Eain* for their support and cooperation in this study. The field study was made possible by the opportunity provided by the SATREPS program supported by JST and JICA.

A SIMPLIFIED NUMERICAL MODEL TO EVALUATE POST-EARTHQUAKE INITIAL SITUATION ASSESSMENT TOOLS AND TECHNIQUES

M.S. HOSSAIN¹, K. CHAITANYA², M. NUMADA³, N. MORIMURA⁴ and K. MEGURO⁵

¹ Graduate Student, Department of Civil Engineering, UTokyo, Tokyo, Japan

² Assistant Professor, IIS, UTokyo, Tokyo, Japan

³ Associate Professor, ICUS, IIS, UTokyo, Tokyo, Japan

⁴ Professor, Department of Emergency and Critical Care Medicine, UTokyo, Tokyo, Japan

⁵ Professor, ICUS, IIS, UTokyo, Tokyo, Japan

Correspond to M.S. HOSSAIN (shak-h@iis.u-tokyo.ac.jp)

Keywords: Emergency response, post-earthquake initial situation assessment, simplified numerical model

1. INTRODUCTION

The estimates of UNISDR reveal that around 1.35 million people were killed by natural disasters from 1996 to 2015, while more than half of them have died due to earthquakes [1]. Large-scale catastrophic events like earthquakes represent one of the greatest challenges to emergency response system [2]. It is also well known that earthquake emergency response is nothing but fight against time as the time passes the possibility of finding alive trapped victims goes down [3]. However, the most fundamental activities to save lives include initial situation assessment, forming teams for emergency response, securing emergency routes and IC networks, search and rescue, evacuation, damage assessment and maintain public relations [4]. As the first task of emergency response is the initial situation assessment, in this research a simplified numerical model has been developed to evaluate post-earthquake initial situation assessment tools and techniques. Further, the model was verified by the 1995 Great Hanshin Awaji (Kobe) earthquake disaster on firefighting activities.

2. SIMPLIFIED NUMERICAL MODEL

The model consists of three main parts, which are input, system/process, and output. Figure 1 shows the flowchart of the simplified numerical model.

Input: The input components are further divided into scenario input and system input. Scenario input includes affected areas, number of trapped victims at each affected area, the total number of the fire station and firefighters (i.e., first responders) for this particular area and travel time from the fire station to affected area.

The system input refers to all the possible tools and techniques, which are smartwatch (proposed), remote sensing, uncrewed aerial vehicles, emergency call, social media, fast reconnaissance survey, and mass media to gather information, i.e. damage and trapped victims of the affected area. Based on observations and expert concerns, it is assumed that smartwatch will follow a straight line pattern. The remote sensing and UAVs will follow stair-step type pattern, emergency call and social media will follow exponential type pattern, fast reconnaissance survey and mass media will also follow 'S' type pattern to transmit trapped victims location and damage level of the affected area to the emergency manager (Incident Command Center).

System / Process: The first step of the system / process is to estimate maximum information at each time.

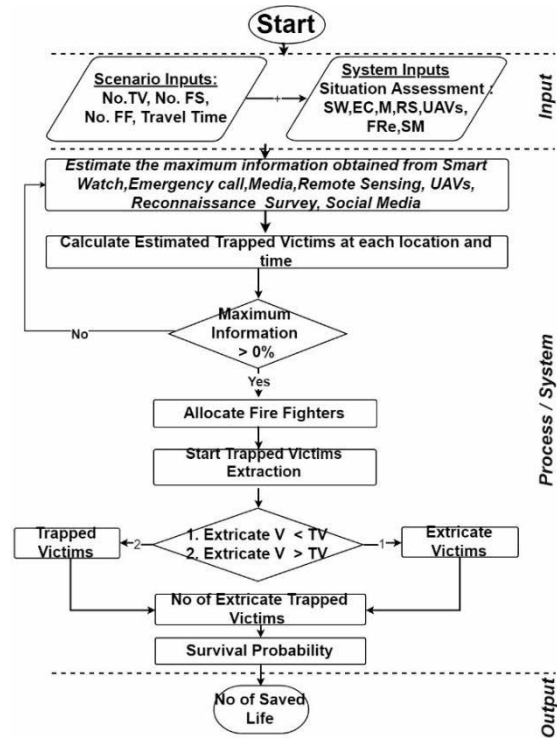


Figure 1: Flowchart of a simplified numerical model

The second step of the system or process is to calculate the estimated trapped victims at each location and time. The following equation has been used to calculate estimated trapped victims.

$$\text{Estimated Trapped Victims} = \text{Trapped Victims} \times \text{MaxInfo}$$

When information about the trapped victims becomes available then, the third step is to allocate resources. In this study total fire station represents total resources unit. An equation has been proposed in this study to allocate the resources unit, which is given below:

$$\text{Allocate Resources Unit} = \frac{((\text{EsTV}[1] - \text{ExTV}[1]) \times \sum \text{nFSt} \times \text{MaxInfo})}{(\sum (\text{EsTV}[i] - \text{ExTV}[i]))}$$

EsTV = Estimated Trapped Victims

ExTV = Extricate Trapped Victims

nFSt = No of Fire Station (No of Resources Unit)

MaxInfo = Maximum Information

The fourth step of system/process is to extricate trapped victims. The following equation is used to extricate trapped victims:

$$\text{Trapped Victims Extraction} = \frac{nFSt \times mFSt \times dt}{Emh}$$

$nFSt$ = No of Fire Station (No of Resources Unit)

$mFSt$ = No of Fire Fighters involved to extraction TV at each Fire Station

dt = $time[i + 1] - time[i]$

Emh = Extricate Man Hours

The final step of system/process is to use survival probability. The following survival probability has been developed based on the 1995 Great Hanshin Awaji earthquake disaster firefighters data (Figure 2) [5].

$$\text{Survival Probability}(\%) = 0.0105 \times time^2 - 1.976 \times time + 97.058$$

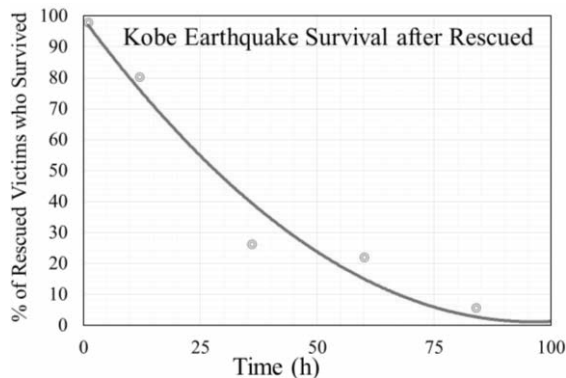


Figure 2: Survival Probability

Output: The final output of the proposed model is the number of saved life at each location and each time. The following equation has been used to know the number of saved lives:

$$\text{No of Saved Lives} = \text{No of Extricate TV} \times \text{Survival Probability}$$

3. MODEL VERIFICATION

To verify the simplified numerical model, data of firefighter activities during 1995 Great Hanshin Awaji earthquake disaster have been used. In total Kobe firefighters extricated 1886 trapped victims from ten affected area of Kobe city [5]. There were 29 fire stations in Kobe city and total 1298 full time firefighters. Based on trapped extracted by Kobe firefighters. The extricate man hours (man hours need to extricate one trapped victims) have been assumed to 8 man hours up to victims, from 12 to 24 hours 12 man hours, from 24 to 48 hours 30 man hours, from 48 to 72 hours 35 man hours, from 72 to 96 hours 61 man hours and from 96 to 120 hours 119 man hours [5]. Travel time from fire station to affected area have been considered from one to four hours with the assumption that less severely affected area took less time and high severely affected area took higher time. The information index (which is the availability of

post-earthquake damage and / or trapped victim information's to incident commanders) from the affected area to the incident command center (ICC) have been considered only from emergency call and fast reconnaissance survey.

Figure 3 shows the number of saved lives at actual case and model case. In the real case, Kobe firefighters rescued 735 alive victims, while the model gives 744 alive victims [5]. However, in the case of day basis save lives, the difference between actual and model result is less than 10 persons expected day two.

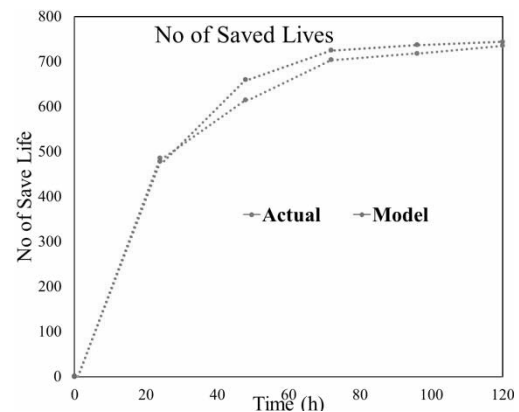


Figure 3: No of save lives

4. CONCLUSION AND FUTURE WORK

A numerical model has been developed in this research that has a potential to help the earthquake emergency response system. Investigating the previous earthquakes and emergency response, learning to know that rapid initial situation assessment after an earthquake is the one of most essential task to increase number of save life of the trapped victims by allocating the resources efficiently and appropriately over time. This proposed model can be used by emergency stakeholders to know the robustness of their post-earthquake initial situation assessment tools and techniques, which will help them to take timely initiatives for awareness and preparedness for proper response. However, further study is necessary to include the randomness in the information dissemination of various post-earthquake initial situation assessment as well as the resource constraints along with information availability in simplified numerical model.

5. REFERENCES

- [1] CRED & UNISDR. (2016) Poverty and Death: Disaster Mortality 1996-2015. Report
- [2] Chan, T. C., Killeen, J., Griswold, W. and Lenert, L. (2004), Information Technology and Emergency Medical Care during Disasters. Academic Emergency Medicine, 11: 1229-1236. doi:10.1197/j.aem.2004.
- [3] M. Statheropoulos, A. Agapiou, G. Pallis, K. Mikedi, S. Karma, J. Vamvakari, M. Dandoulaki, F. Andritsos, and C. P. Thomas, "Factors that affect rescue time in urban search and rescue (USAR) operations," Natural Hazards, vol. 75, no. 1, pp. 57-69, 2015.
- [4] "Total Process of Disaster Management" [Online]. Available: <http://www.numa.iis.u.tokyo.ac.jp/1.svg>
- [5] Fire Fighter Activities in 1995 Great Hanshin Awaji Earthquake. Kobe city Fire department, 1995.

DEVELOPMENT OF FLOOD INUNDATION MAPPING TECHNIQUE IN ASIA WITH AHI-8, MODIS AND AMSR2 MEASUREMENTS

Wataru Takeuchi¹, Kwak Youngjoo² and Jonggeol Park³

¹ Professor, Institute of Industrial Science, The University of Tokyo, Japan
wataru@iis.u-tokyo.ac.jp (corresponding author)

²Principal researcher, ICHARM-UNESCO, Japan

³Associate Professor, Tokyo University of Information Science, Japan

ABSTRACT

In cloudy area of the Earth, MODIS limits the sensor's ability to quantify biophysical processes in heterogeneous landscape. A passive microwave sensor AMSR2 is not subject to cloud contamination although its spatial resolution is relatively coarse. In this paper, a new spatial and temporal adaptive data fusion model algorithm is presented and demonstrated to blend MODIS and AMSR2 to predict daily land surface water coverage. The MODIS 8 day composite 1km normalized difference water index (NDWI) and AMSR2 daily 16km normalized difference frequency index (NDFI) are used to map land surface water coverage (LSWC) which is effective to monitor agriculture and flood monitoring issues. It was found that the algorithm accurately predicts daily LSWC of AMSR2 at an effective fractional coverage close to that of MODIS.

Index Terms— Data fusion, image enhancement, agriculture and flood monitoring

1. INTRODUCTION

1.1. Needs for better information

Land surface water coverage is one of the critical parameters for agriculture and flood monitoring. The dynamic nature of this parameter ideally requires observations with high temporal and spatial resolutions. In cloudy area of the Earth, optical sensor limits the sensor's ability to quantify biophysical processes in heterogeneous landscape. A passive microwave sensor is not subject to cloud contamination although its spatial resolution is relatively coarse.

Advanced Microwave Scanning Radiometer for Earth Observation System (AMSR2) presents a potential for flood and waterlogging monitoring and soil moisture estimation because of the ability of the microwave signal to penetrate through cloud and provide an all-day data and its sensitivity to surface water [Li *et al.*, 2016]. It can fast reveal large-scale flood patterns.

The Normalized Difference Water Index (NDWI) is a satellite-derived index from the visible (VIS) and Short Wave Infrared (SWIR) channels derived from Moderate resolution imaging spectro-radiometer (MODIS) [Takeuchi *et al.*, 2004]. The SWIR reflectance reflects changes in both the vegetation water content and the spongy mesophyll structure in vegetation canopies, while the VIR reflectance is affected by leaf internal structure and leaf dry matter content but not by water content. NDWI can monitor flood patterns at finer spatial resolution than AMSR2 at the expense of cloud contamination.

The complementary nature of the measurements in the optical and microwave domain implies a need for integrating them for improved coverage in space and time. The potential for synergistic analysis of microwave and optical data to monitor land surface water coverage observations has been identified earlier [Mori, *et al.*, 2009]. The more precise calibration between AMSR2 and MODIS was conducted to find the relationship between AMSR2 and MODIS for land surface water coverage (LSWC).

1.2. Objective of this project

In this paper, a new spatial and temporal adaptive data fusion model algorithm is presented and demonstrated to blend MODIS and AMSR2 to predict daily land surface water coverage.

2. METHODOLOGY

2.1. A flowchart and data used in this study

Cloud free MODIS 8-day composite of VNIR and SWIR channels are used to compute the normalized difference water index (NDWI). NDWI are carefully interpreted to choose water or inundated area and it was found that 0 was the threshold to distinguish land and water with NDWI image. NDWI images in 1km resolution were aggregated into 16km by spatial average and they were defined as land surface water coverage (LSWC). AMSR2 daily mosaics including 18.7 and

23.8GHz are used to compute normalized difference polarization index (NDFI). Then NDFI derived from AMSR2 were calibrated with MODIS derived LSWC. Finally daily LSWC were derived from the calibration model solely from AMSR2 NDFI.

2.2. Land surface water coverage mapping

MODIS is used to monitor flood patterns at finer spatial resolution than AMSR2. The SWIR reflectance reflects changes in both the vegetation water content and the spongy mesophyll structure in vegetation canopies, while the VIR reflectance is affected by leaf internal structure and leaf dry matter content but not by water content. We used normalized difference water index (NDWI);

$$NDWI = \frac{VIS - SWIR}{VIS + SWIR} \quad (1)$$

where VIS represents the reflectance value of visible channel and SWIR short wave infrared, respectively. MODIS channel 1 is used as VIS and channel 7 as SWIR. NDWI is defined by extending the idea of NDVI with the combination of VIS, NIR and SWIR channels and each index has the symmetric expression as a function of VIS, NIR and SWIR.

AMSR2 is used to monitor flood patterns at more frequent time resolution than MODIS. When atmospheric transmission is near to 1, we can obtain Normalized Frequency Index (NDFI) as follows [Takeuchi *et al.*, 2006];

$$NDFI = \frac{TB_{18.7V} - TB_{23.8V}}{TB_{18.7V} + TB_{23.8V}} \quad (2)$$

where $TB_{18.7V}$ and $TB_{23.8V}$ are the brightness temperature of vertical (V) polarization at 18.7GHz and 23.8GHz. NDFI is less affected by atmospheric conditions and is not dependent on the soil temperature. The rise of water level in rivers, lakes and reservoirs caused a severe flood and water-logging disaster. NDFI provides a sensitive indicator of the presence of surface water and it has a good capability to distinguish the water surface and land surface.

In order to access the reliability of the AMSR2 derived NDFI, we have selected MODIS data with 1km spatial resolution 8-days composite acquired almost at the same satellite pass time with AMSR2 data to compare with NDFI.

3. RESULTS AND DISCUSSIONS

3.1. Comparison of MODIS NDWI and AMSR2 NDFI images

In order to access the reliability of the AMSR2 NDFI maps, we selected MODIS NDWI as a comparison. Figure 1 shows a comparison of AMSR2 NDFI and MODIS NDWI maps in Amazon river flooded area observed at September 30, 2006. A flood area is located in the middle reaches of the Amazon river and it is one of the most biggest flood plain in the world.

A fairly good agreement could be found between AMSR2 NDFI and MODIS NDWI. From AMSR2 NDFI and MODIS NDWI maps, we knew that the area was absolutely covered by waterlogging.

3.2. Calibration of MODIS LSWC as a function of AMSR2 NDFI

Because the emitted microwave signal is sensitive to both the water and the soil moisture at or near the soil surface, the fractional water coverage estimated by using passive microwave data AMSR2 is a combination of water area and wet soil area. However it is impossible to distinguish the wetness and flooding effects solely by AMSR2 coarse resolution. MODIS NDWI images are used to map water area and they were aggregated into AMSR2 resolution by spatial averaging defined as MODIS LSWC.

Figure 2 shows a comparison between AMSR2 NDFI and MODIS LSWC. NDFI indicates both water and wet soil area whereas LSWC represents water area only. In this sense we defined that the envelope curve at the outer edge represents the water area only. As indicated by a linear line in Figure 2, AMSR2 LSWC was calibrated as a function of NDFI.

3.3. Flood and water logging monitoring AMSR2 LSWC

According to the principle that the higher AMSR2 LSWC values will be associated to a relative increase of both water area and soil moisture, we have chosen the other two flood prone areas in Asia including Ganges delta and Mekong delta.

Figure 3 shows daily changes of LSWC at flood prone areas in Asia including Ganges delta (24.8N, 91.0E) and Mekong delta (11.0N, 105.3E). According to those data, we found that land surface water coverage dropped down to zero from 60 to 120 days of year in dry season and flooding season starts at 150 days of year and continued until 360 days of year in Ganges delta. Mekong delta has more clear discrepancy between dry and season at 220 days of year.

Figure 4 shows seasonal changes of LSWC at flood prone areas in Asia including Ganges delta (24.8N, 91.0E) and Mekong delta (11.0N, 105.3E). Brighter area indicates high abundance of water coverage at that pixel.

4. CONCLUDING REMARKS

This study demonstrated a new spatial and temporal adaptive data fusion model algorithm to blend MODIS and AMSR2 to predict daily land surface water coverage. The MODIS 8 day composite 1km normalized difference water index (NDWI) and AMSR2 daily 16km normalized difference frequency index (NDFI) are used to map land surface water coverage (LSWC) which is effective to monitor agriculture and flood monitoring issues. A fairly good agreement could be found between AMSR2 NDFI and MODIS NDWI. From AMSR2

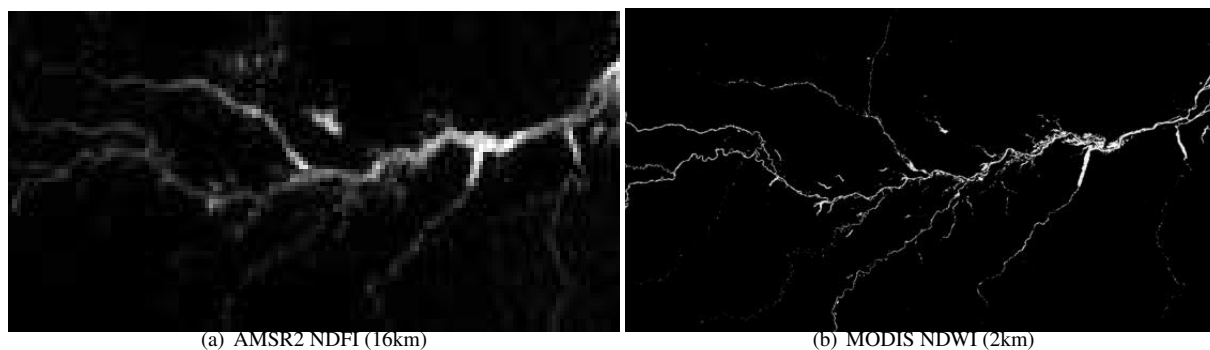


Fig. 1. Comparison of AMSR2 NDFI and MODIS NDWI maps in Amazon river flooded area observed at September 30, 2016.

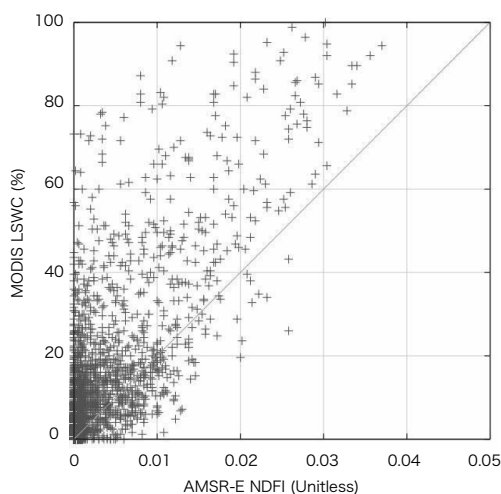


Fig. 2. Comparison between AMSR2 NDFI and MODIS LSWC. NDFI indicates both water and wet soil area whereas LSWC represents water area only.

NDFI and MODIS NDWI maps, we knew that the area was absolutely covered by waterlogging. A comparison between AMSR2 NDFI and MODIS LSWC shown that NDFI indicates both water and wet soil area whereas LSWC represents water area only. We defined that the envelope curve at the outer edge represents the water area only and AMSR2 LSWC was calibrated as a linear function of NDFI. Finally AMSR2 LSWC daily values were used to map flood prone areas and it was found that the algorithm accurately predicts daily LSWC of AMSR2 at an effective fractional coverage close to that of MODIS.

5. REFERENCES

- [Dasgupta *et al.*, 2006] Dasgupta, S. and J. J. Qu, 2006. Combining MODIS and AMSR-E-based vegetation moisture retrievals for improved fire risk monitoring. *Proceedings of the SPIE*, 6298, 62981B.
- [Li *et al.*, 2016] Li Xi and Wataru Takeuchi, 2016. Land surface water coverage estimation with PALSAR and AMSR-E for large scale flooding detection. *Terrestrial, Atmospheric and Oceanic Sciences*, 27(4), 473-480.
- [Mori, *et al.*, 2009] Mori, S., W. Takeuchi and H. Sawada, 2009. Estimation of land surface water coverage (LSWC) with AMSR-E and MODIS. *Proceedings of 2nd joint student seminar at AIT: Bangkok, Thailand*.
- [Sippel, *et al.*, 1994] Sippel, S. S. K. Hamilton and J. M. Melack, 1994. Determination of inundation area in the Amazon river flood plain using the SMMR 37 GHz Polarization difference, *Remote Sens. Environ*, 70-76, 48.
- [Takeuchi *et al.*, 2004] Takeuchi, W. and Y. Yasuoka, 2004. Development of normalized vegetation, soil and water indices derived from satellite remote sensing data. *Proceedings of 25th Asian Conference of Remote Sensing (ACRS): Changmai, Thailand*.
- [Takeuchi *et al.*, 2006] Takeuchi, W., D. Komori, T. Oki and Y. Yasuoka, 2006. An integrated approach on rice paddy irrigation pattern monitoring over Asia with MODIS and AMSR-E. *Proceedings of the AGU: San francisco, USA*.
- [Temimi, *et al.*, 2007] Temimi M, R. Leconte R and F. Brissette, 2007. Flood and soil wetness monitoring over the Mackenzie River Basin using AMSR-E 37 GHz brightness temperature. *J. of Hydrology*, 333(24): 317-328.
- [Zheng, *et al.*, 2008] Zheng Wei, C. Liu, Z. Xin and Z. Wang, 2008. Flood and Waterlogging Monitoring over Huaihe River Basin by AMSR-E Data Analysis. *Chin. Geogra. Sci.*, 18(3) 262-267.

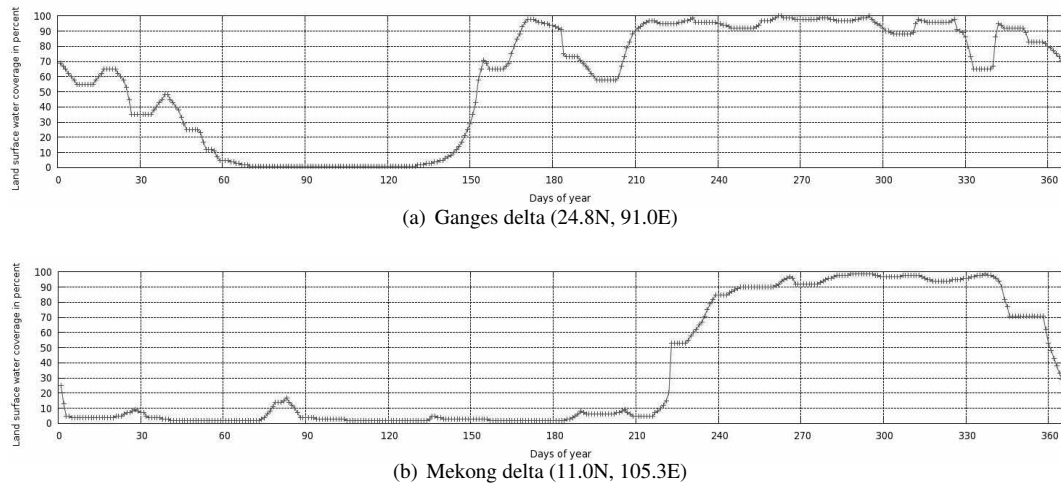


Fig. 3. Daily changes of LSWC at flood prone areas in Asia.

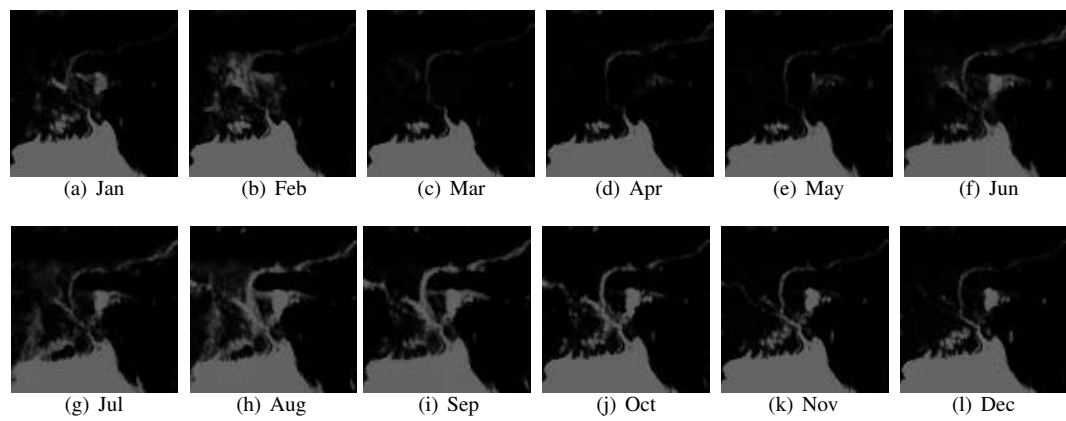


Fig. 4. Monthly changes of LSWC in Ganges delta centered at (24.8N, 91.0E). Brighter area indicates high abundance of water coverage at that pixel.

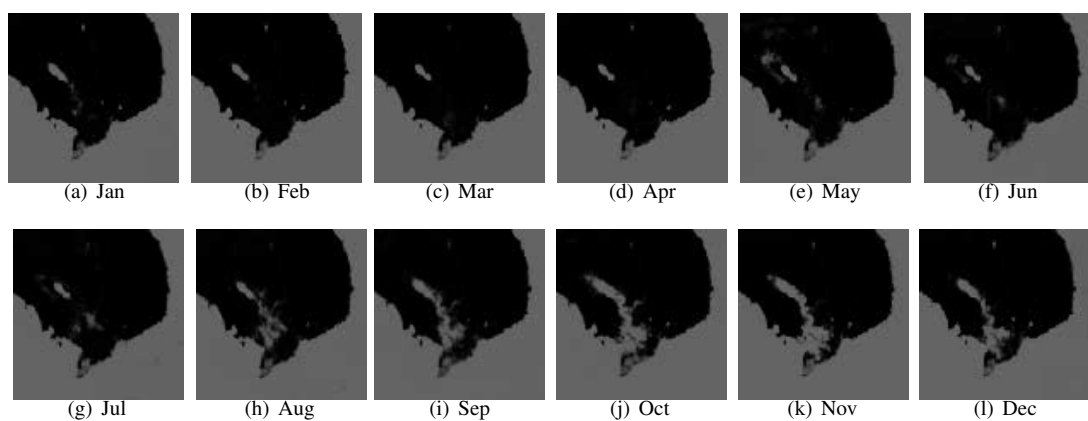


Fig. 5. Monthly changes of LSWC in Mekong delta centered at (11.0N, 105.3E). Brighter area indicates high abundance of water coverage at that pixel.

USMCA 2018

**POSTER PRESENTATIONS
SEISMIC SAFETY OF STRUCTURES**

EFFECT OF ASPECT RATIO AND ELEVATION PROFILE ON MODE SHAPES OF TALL BUILDING

P. D. VELANI¹ and P. K. RAMANCHARLA²

¹ PhD Student, Earthquake Engineering Research Center, City, International Institute of Information Technology-Hyderabad, Hyderabad, India, pulkit.velani@research.iiit.ac.in (corresponding author)

² Professor of Civil engineering and Head of Earthquake Engineering Research Center, International Institute of Information Technology-Hyderabad, Hyderabad, India, ramancharla@iiit.ac.in

Keywords: Tall buildings, aspect ratio, time period, torsion

1. INTRODUCTION

Due to rapid urbanization, many tall buildings are coming up not only in metros (tier 1) but also in tier 2 and 3 cities. On the other hand, it's clearly known that large part of the country i.e. around 56% are of India's land mass is prone to moderate to severe earthquake events. Also it's clearly evident from past earthquakes such as Bhuj 2001, many multistory buildings over 200 km away from the epicenter i.e. in Ahmedabad suffered severely. Design of high-rise buildings is not same as the design of low-rise and mid-rise buildings Bureau of Indian standards has come up with special code IS 16700[1] which gives provisions for designs of Tall buildings. To understand and implement the provision of this code sufficient experience and expertise is required.

In this paper one such provision, about torsion irregularity stipulates that the first two modes of vibration should be translation modes and the torsion mode cannot be earlier than the third mode of vibration, is discussed. Observation on how buildings with different aspect ratios result in giving radically different first natural periods is outlined.

2. METHODOLOGY

The phase 1 of parametric study consists of design of rectangular tower (type 1 as per Figure 1), to be constructed in seismic zone IV, serving as a commercial building in India. The total height of building is considered in such a way that it will qualify as a tall building as per IS 16700. This tower has been analyzed and designed as per applicable Indian codes for reinforced concrete building. The response spectrum method of dynamic analysis is carried out and relevant safety checks for fundamental period, inter storey drift etc. were verified.

In phase 2, two alternate towers of type 2 and type 3 were analyzed and designed. The elevation of overall tower type was maintained as shown in Figure 1. And the size of towers was selected by ensuring approximately equal usable carpet area of all three types. Further, all these towers were analyzed and design in ETABS and observation is made based on the time period values and base shear arrived.

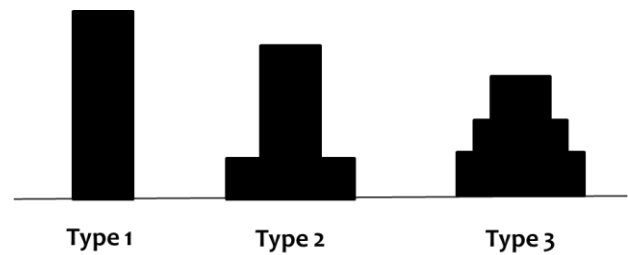


Figure 1: Type of building elevation adopted in parametric study

Table 1: Common data used in parametric study

Parameters	Values/Details
Functional Use	Commercial building
Structural system	Structural Wall System
Location	Seismic Zone IV
Soil Type	Type II (Medium Soil)
Concrete Grade	M30 to M60
Steel Grade	Main steel: HYSD 500 Ties/Stirrup: HYSD 415
Floor Finish	1 kN/m ²
Imposed Load	Typical Floor: 4 kN/m ² Roof: 1.5 kN/m ²
Cladding	2 kN/m ²
Parapet wall	4.6 kN/m

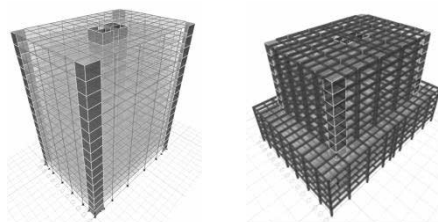


Figure 2: 3D FEM Model of Type of building elevation adopted in parametric study

3. RESULTS AND DISCUSSION

Starting with some initial plan dimensions and initial structural member's size iterative analysis and design procedure was adopted. The building were analyzed and design as per IS 1893:2016 and IS 16700:2017. The final

fundamental natural period values arrived are tabulated in Table 2. The gradual decrease in period was found in for type 1 to type2 and from type 2 to type 3 tower. This is very natural as selection of elevation profile of type 2 and type 3 will lead in increase in base dimension there by reduction of natural period of first mode. This period will decide the factor by which design base shear arrived from response spectrum will be scaled up. This scaling up of fore will lead to design of stiffer elements in a building which will further tend to reduce the period and this iteration goes on for couple of times till all the members are having capacity more than the demand.

Table 2: First three natural modes of building in two translations and one rotational direction

Direction	Mode	Time Period (sec)		
		Type 1	Type 2	Type 3
X - Direction	X1	1.72	1.139	0.911
	X2	0.452	0.318	0.254
	X3	0.203	0.144	0.115
Y - Direction	Y1	1.593	1.054	0.896
	Y2	0.419	0.307	0.261
	Y3	0.196	0.146	0.124
Rotation	Z1	1.422	0.928	0.631
	Z2	0.373	0.299	0.203
	Z3	0.169	-	0.092

4. CONCLUSION

It was observed that as for the same built up area:

1. Type 2 and type 3 tower gives more freedom to structural engineer for placement of lateral load resisting members. And there by overcoming the torsional mode as a predominant mode of vibration.
2. Going for type 2 and type 3 elevations profile will also tend to reduction in overall height of building. Such structural gives more stability as it gives wider base width.
3. Type 2 and type 3 towers is resulting in stiffer and stable structure, helping to achieve the life safety goal of infrastructure.
4. Structural engineer have freedom to take help of initial wider floors for resisting lateral load of the tower. This component of overturning resistance, referred as backstay effect, is critical in high-rise buildings.

The future work can be done by verifying the stated conclusion for more number of buildings with varying height and for different seismic zone of India.

REFERENCES

- [1] IS 16700 (2017) *Criteria for Structural Safety of Tall Concrete Buildings*, Bureau of Indian Standards, New Delhi, India
- [2] IS 1893(Part 1) (2016) *Criteria for Earthquake Resistant Design of Structures*, Sixth revision, Bureau of Indian Standards, New Delhi, India

ANALYSIS OF HILL SLOPE BUILDING FOR TWIST VARIATION WITH CHANGE IN ASPECT RATIO

RAHUL SURESH VISHWAKARMA¹, PRADEEP KUMAR RAMANCHARLA²

¹ Student, Earthquake Engineering Research center, IIIT Hyderabad, Hyderabad, India, rahul.vishwakarma@research.iiit.ac.in (corresponding author)

² Professor, Earthquake Engineering Research center, IIIT Hyderabad, Hyderabad, India, ramancharla@iiit.ac.in

Keywords: Hill slope building, twist, Aspect ratio, Axial load

1. INTRODUCTION

Buildings on hilly region are asymmetrical due to its increase in size of columns in valley direction. Because of this asymmetry there is eccentricity in the structure This leads to torsion and twist in the structure. This twist is smaller but gives a large axial forces on the beams of the floor which are near to ground level. In this paper we will see twist variation of each floor in the building. Which can be further used for the best aspect ratio of the building.

2.DETAILS

We will be dealing with three storey building above ground, slope of the ground as 30°, 40°, 45° As show in the figure 1. And will be changing length of the building in ridge direction and will see the changes in the twist

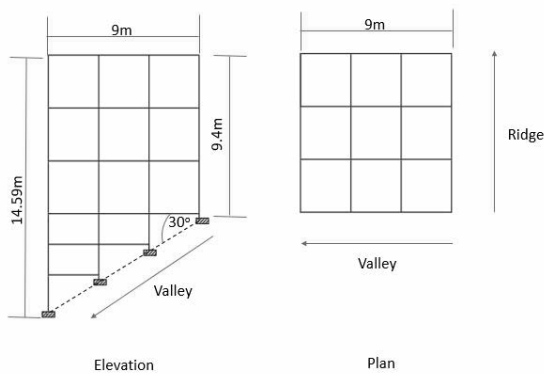


FIGURE 1: Plan and elevation of the building

When earthquake attacks such hilly buildings there are two type of the motion one is translation and one is rotation. This rotation and twist can be calculated by using diagonal vectors. For finding the rotation two vectors are taken, First vector is the opposite corner points of the building in its initial state and second is same two opposite corner points of the floor after the deformation(maximum displacement because of earthquake) .

Stiffness plays the important role in twist. As each frame along the valley has different stiffness so center of rigidity is near to shorter column as it will be more stiff. So center of mass will be in the middle of the floor. Difference in

the center of the stiffness and center of rigidity cause eccentricity in the structure. The lateral load is taken by center of mass so the floor will rotate about center of Stiffness.

Changing the length of the building along the ridge direction will increase the stiffness of the frames along valley direction and also decreases the twist.

3.ANALYSIS

An earthquake Chamoli of frequency 50Hz was taken and is normalized to 1g was applied across the valley direction to see the behavior of the building .

The length of the building was changed from 9m to 60m with the interval of 3m for first 10 values and then doubled the length for the last aspect ratio.

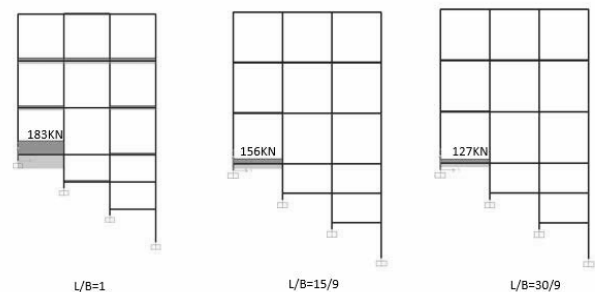


FIGURE2: Maximum axial forces in beams due to twist

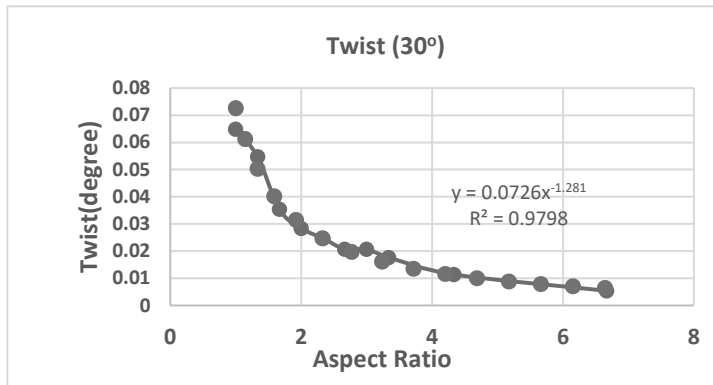
As shown in the figure 2 these are the maximum axial load on the ground floor beam(0 level) with three l/b ratio 1,15/9,30/9 the twist value decreases with the increase in aspect ratio.

Table 1: How the twist in the structure effected the axial load in 0th level beam for 30° slope

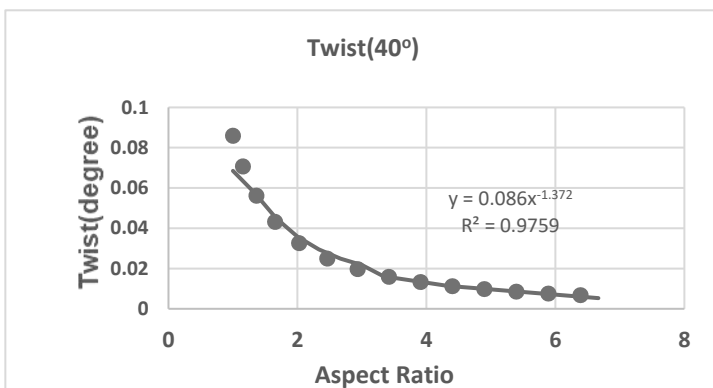
Aspect ratio	Effect of Aspect ratio on twist and Axial forces on beam	
	Twist (°)	Axial forces(maximum)(kN)
9/9	0.0649	183
15/9	0.0345	156
21/9	0.0247	139
30/9	0.0177	123
60/9	0.0054	118

From Table 1 and figure 4 we can see that how twist effect the axial forces of the 0th level beams. The decrease in twist decreases the Axial forces These axial forces can pull out the beam in the 0th level which can lead to key element failure. So we need to decrease the twist value. So there is need to know the configuration of the building for less twist.

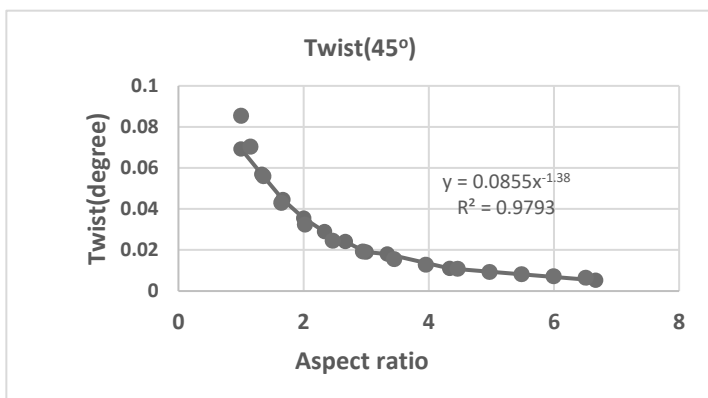
Twist variation of the figure with three slope angles are shown in figure 3



(a)



(b)



(c)

FIGURE 3: Twist Variation

The above graphs shows the variation with power function by the relations

$$y = ax^{-b}$$

where a and b are positive integer This is valid for $x(\text{aspect ratio}) > 1$ for hilly buildings.

The parameter a,b depends on the position of center of rigidity or eccentricity and the height of the floor.

The twist variation for 30° slope for all three floors with the aspect ratio is shown in the figure 4

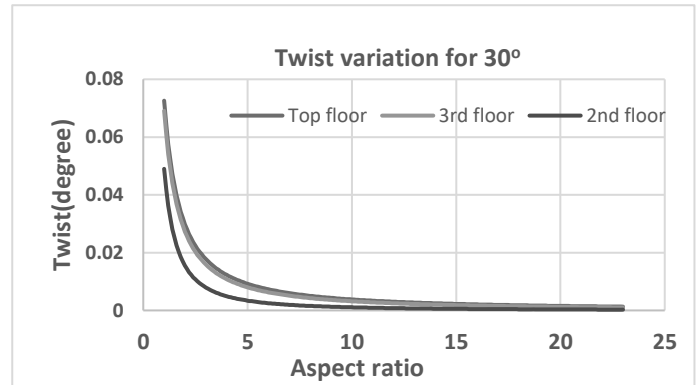


FIGURE 4: Twist variation for the floors in the building

The above graph is for the twist variation of the floors as we can see in the graphs the bottom floor has less twist values as compare to floors above it. This difference in the twist for every floor will be constant after an aspect ratio . The idea was that it will be the best aspect ratio for the building but as we see in the graph this happens for aspect ratio more than 15. which is much larger value. So more conclusion will be made in the upcoming months.

4. CONCLUSIONS

- Small twist can cause large axial forces in the ground floor beams.
- Decrease in twist decreases the axial load in the ground floor beams. As shown in the Table 1
- Twist decreases by a power function with increase in aspect ratio as shown in figure 3.

REFERENCES

- [1] Y.Singh ,Phani Gade, 15WCEE ,Seismic Behaviour of Building Located on Slopes-An Analytical Study and Some Observations From Sikkim Earthquake of September 18,2011
- [2] A.R Vijaya Narayanan,Rupen Goswami and C.V.R. Murty, 15WCEE 2012 Performance of RC Buildings along Hill Slopes of Himalayas during 2011 Sikkim Earthquake.
- [3] Aditya B. Deshmukh and Rupen Goswami, ICJ 2018 Use of Walls in controlling detrimental effects of stiffness irregularity in RC building on Hill slopes.

ANALYSIS OF REINFORCED CONCRETE BUILDING FOR STRONG COLUMN AND WEAK BEAM BEHAVIOUR

SWAPNIL NAYAN¹, PRADEEP KUMAR RAMANCHARLA²

¹ Student, Earthquake Engineering Research center, IIIT Hyderabad, Hyderabad, India, swapnil.nayan@research.iiit.ac.in (corresponding author)

² Professor, Earthquake Engineering Research center, IIIT Hyderabad, Hyderabad, India, ramancharla@iiit.ac.in

Keywords: Strong column weak beam, hinges, Area moment of Inertia, moments

1. INTRODUCTION

The complete failure and collapse of reinforced concrete building during an earthquake occurs due to the failure of the column elements. This is due to the fact that column elements are responsible for the load transfer of the structure to the footing hence making it the most important structural element to minimise life loss. To avoid the failure of column elements, IS 13920 : 2016 recommends that buildings should follow ‘Strong Column and Weak Beam’ (SCWB) design. It states that the total flexural capacity of beam (M_b) should be less than that of the column (M_c) at a joint. It is a way to design the building such that ‘Plastic Hinges’ form in beam elements of the structure rather than the column elements. The formation of plastic hinge dissipates the energy of the earthquake. Moreover it is desirable that these hinges form in the top storeys of the structure rather than the bottom stories. Hence by the formation of these plastic hinges in the beam, the structure can take larger deformations without collapse.

2. DETAILS OF THE STRUCTURE

A 6 storey 2 dimensional bare frame structure in earthquake zone IV, with soil type I (Rock or hard soils) and fixed base is considered. Initially a 6 storey (3 Dimensional) structure with 4 bays each in x and y direction is designed according to IS 456 : 2000, IS 1893 : 2016, IS 13920 : 2016 is designed and checked for the load combination given in IS 1893 : 2016, given below:

- i) $1.2[DL + IL \pm ELx]$
- ii) $1.2[DL + IL \pm ELy]$
- iii) $1.5[DL \pm ELx]$
- iv) $1.5[DL \pm ELy]$
- v) $0.9DL \pm 1.5ELx$
- vi) $0.9DL \pm 1.5ELy$

A single frame in the XZ direction is then selected for the analysis.

As moment distribution at a joint is directly proportional to the area moment of inertia (I) and modulus of elasticity (E) of the element, section sizes of the beams and columns are varied such that the ratio of area moment of inertia of column (I_c) to that of the beam (I_b) changes from 0.25 to 2 with an increment of 0.25. An

additional value of 1.4 is considered for the analysis as it is prescribed in IS 13920 : 2016. The structures consist of same beam and column dimensions carried throughout the structure.

Table 1: Details of structure

Sno.	I_c/I_b	Column Dimensions (mm)	Beam Dimension (b x d)(mm)
1	0.25	425 x 425	600 x 600
2	0.50	425 x 425	505 x 505
3	0.75	425 x 425	475 x 450
4	1.00	425 x 425	425 x 425
5	1.25	450 x 450	425 x 425
6	1.40	440 x 440	405 x 405
7	1.50	450 x 450	405 x 405
8	1.75	425 x 425	370 x 370
9	2.00	450 x 450	380 x 380

3. ANALYSIS

Pushover analysis is carried out on each structure to obtain the maximum base shear and roof displacement before collapse. The values from the pushover analysis is then used to construct fragility curve for the structures to obtain the maximum value of spectral acceleration (S_a) for the structure. This is done by changing I_c/I_b ratio as M_c and M_b are directly proportional to I_c and I_b respectively.

4. FRAGILITY CURVE

The area under the pushover curve gives the total energy dissipated in the structure. A damage parameter (D) is defined as the ratio of inelastic energy to the total energy of the structure.[1] The damage parameter is then plotted

against S_a at different steps. The value of D ranges from 0 (no damage) to 1 (complete collapse). The value of S_a at $D = 1$ shows the Spectral acceleration at which complete collapse occurs.

5. RESULTS

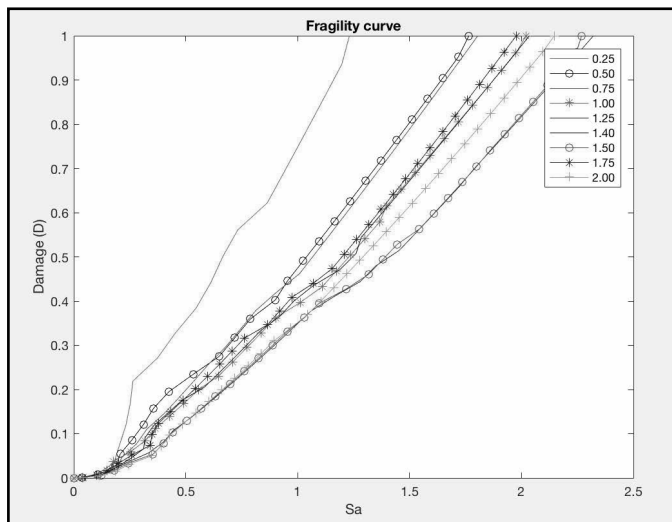


Fig 1: Fragility curve for different values of I_c/I_b for un-cracked section properties.

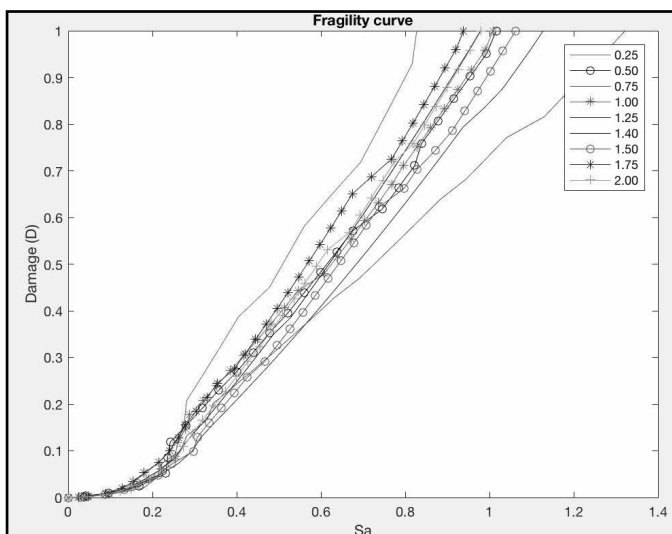


Fig 2: Fragility curve for different values of I_c/I_b for cracked section properties.

The maximum value of S_a for different values of the ratio I_c/I_b is given in the table below for both cracked and un-cracked section properties:

Table 2: Maximum S_a for different I_c/I_b

Sno.	I_c/I_b	$S_{a,max}$ (g) un-cracked	$S_{a,max}$ (g) cracked
1	0.25	1.231	0.828
2	0.50	1.765	1.016

Sno.	I_c/I_b	$S_{a,max}$ (g) un-cracked	$S_{a,max}$ (g) cracked
3	0.75	1.805	1.322
4	1.00	2.021	1.008
5	1.25	2.321	1.128
6	1.40	2.036	0.979
7	1.50	2.269	1.062
8	1.75	1.977	0.939
9	2.00	2.146	0.980

6. CONCLUSION

- Comparison of values of $S_{a,max}$ for cracked and un-cracked section shows that the value of $S_{a,max}$ for cracked section is significantly lower than it un-cracked counter part.
- When cracked section properties are considered, maximum S_a value occurs for $I_c/I_b = 0.75$. This is in contradiction with SCWB philosophy.
- When un-cracked section properties are considered, maximum S_a value occurs for $I_c/I_b = 1.25$, followed by 1.50.
- Results show that although code prescribes $M_c/M_b \geq 1.4$ but the actual value of M_c/M_b at which the structure dissipates the most energy may be different.

7. REFERENCES

[1] Pradeep Kumar Ramancharla, Rajaram Chenna, Swajit Singh Goud, Ajay Kumar Sreerama, Gagan Vignesh, Bhargavi Sattar (2014), Report No: IIIT/TR/2014/-1 “Hazard, Vulnerability, Risk Assessment of Himachal Pradesh”

[2] Mitesh Surana, Yogendra Singh, Dominik H. Lang (2018) “Effect of strong-column weak-beam design provision on the seismic fragility of RC frame buildings”

[3] ATC 40, “Seismic evaluation and retrofit of Concrete buildings” Volume 1

[4] IS 456 (2000) “Plain and reinforced concrete - code of practice” Fourth revision

[5] IS 1893 (2016) “Indian standard criteria for earthquake resistant design of structures, part 1” General provisions and buildings (sixth revision)

[6] Is 13920 (2016) “Ductile design and detailing of reinforced concrete structures subjected to seismic forces - code of practice” (First revision)

DAMS AND EARTHQUAKES

HARITHA BENDAPUDI¹, PRADEEP KUMAR RAMANCHARLA²

¹ Student, Earthquake Engineering Research center, IIIT Hyderabad, Hyderabad, India, haritha.bendapudi@research.iiit.ac.in (corresponding author)

² Professor, Earthquake Engineering Research center, IIIT Hyderabad, Hyderabad, India, ramancharla@iiit.ac.in

Keywords: dam, earthquake, strengthening, peak ground acceleration.

1. INTRODUCTION

The Koyna dam has been a topic of much query and analysis in the past few decades. The Koyna earthquake which occurred on December 11th, 1967 near Koyna dam, which was stable and nonseismic, left everyone baffled. Through the coming years many researchers have examined the reaction of Koyna ground motion on the dam via many techniques. In 1973, Anil K. Chopra and P. Chakrabarti examined the response of the dam to strong ground motion recorded during Koyna earthquake by FEM analysis and anticipated the cracking on the monoliths based on stress results. They concluded that the present design criteria of Koyna should be improved to prevent the damage which occurs due to tensile stresses which develop during earthquakes. [1]

Later, D. K Paul and A. R. Chandrasekaran found through a study that the apparent modulus of elasticity of concrete increase in the event of dynamic shaking. [2] It has also been found that system's dynamic stiffness is 40% more than static stiffness. Response of the dam has been analyzed under Static Pushover method and Incremental dynamic method by Nik Zainab et al [3] which proved D.K Paul et al's results. The response of concrete gravity dams to dynamic loading have been studied all over the world taking Koyna dam as reference. Its unconventional cross section has caused the maximum tensile stresses developing at the neck of the dam, which thus incurred maximum cracking. [4] O. Omidi and V. Lotfi have found that water compressibility and damping mechanism affect the seismic safety evaluation of the dam [5]. Sushu Gupta and I.D. Gupta have calibrated the attenuation relation for earthquake peak ground acceleration of Koyna region. [6]

The aim of the present study is to study the response of Koyna dam to static loading (inertia forces and hydrostatic loading) and the response of Koyna dam to dynamic loading (horizontal and vertical earthquake loads). The forces developed and the displacement at the neck of the dam are studied and compared. Then the PGA of the ground motion is increased to see the effect of difference in the response of the dam.

2. ANALYSIS OF KOYNA DAM UNDER STATIC AND DYNAMIC LOADING

The static analysis of the dam has been done by Finite Element Method in ABAQUS. 2D stability analysis of the dam has been done on monolith 17 of Koyna dam.

Monolith 17 is the tallest and most cracked. Through the frequency analysis in ABAQUS, the frequency of the first 4 modes has been found as 18.86 rad/sec, 49.97 rad/sec, 68.16 rad/sec and 98.269 rad/sec (3 Hz, 7.9 Hz, 10.8 Hz and 15.6 Hz) [7].

Under the action of static forces, the dam uniformly deforms to the right thus the dam face bends at an angle to the reservoir.

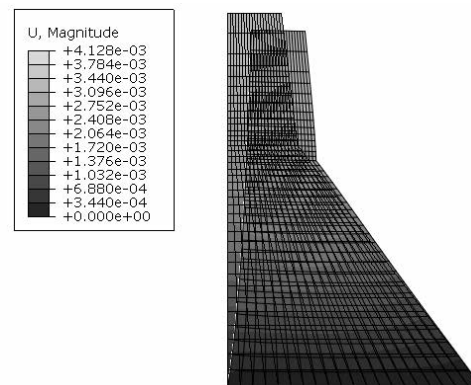


FIGURE 1: displacement of dam due to static loads (deformation factor 2E+3).

Compared to typical gravity dams, Koyna dam faces more deformation due to its cross-section [4].

Under the action of Koyna earthquake acceleration, the dam further deforms. Hydrodynamic forces act on the dam due to the water in the reservoir. Westergaard's equation has been considered to compute the hydrodynamic forces.

$$P = \frac{7}{8} \rho_w \sqrt{h_w} (h_w - y)$$

Where P is the hydrodynamic pressure, h_w is the height of water in reservoir and y is the length of ordinate.

The earthquake acceleration and the results of the dynamic analysis are as shown in Figure 2 and Figure 3.

The peak ground motion of horizontal earthquake acceleration is almost 0.5g. The peak ground acceleration for vertical acceleration is 0.3g.

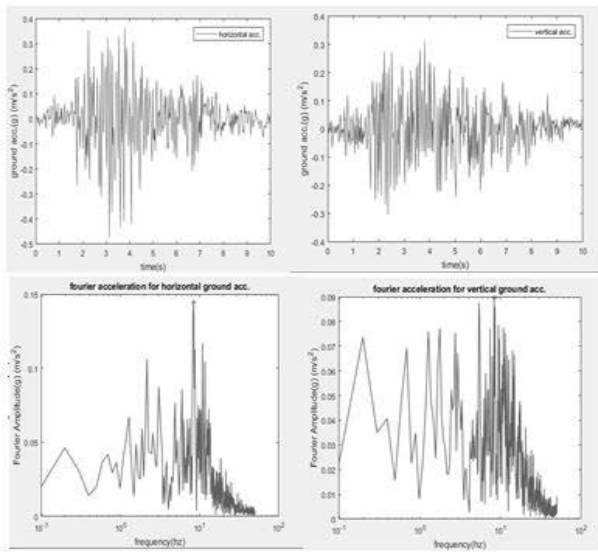


Figure 2: (Anti-clockwise from left top) Horizontal ground acc, Horizontal Fourier amplitude, Vertical Fourier amplitude, Vertical ground acceleration

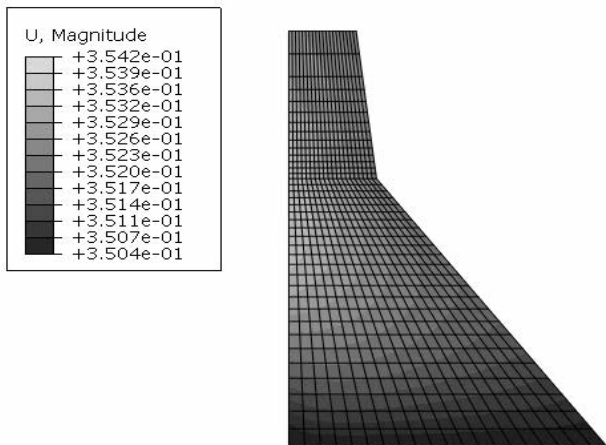


Figure 3: Displacement of Koyna dam under dynamic loading.

TABLE 1: Max displacement of node corresponding to increase in peak ground acceleration

S _{no.}	PGA (both vertical and horizontal direction)	Max. displacement	Max. stresses at toe ($\times 10^6$ N/m ²)
1	0.3g	0.309m	1.909
3	0.5g	0.352 m	2.2268
4	0.6g	0.504m	2.83
5	0.8g	0.815 m	3.63
6	1g	1.023m	3.766

By increasing the peak ground motion, it has been found that the maximum displacement occurs between time $t = 3.4$ sec to $t = 4$ sec in all cases

Based on that, the values of the peak deformation at the neck node are taken for each peak ground acceleration and the results are tabulated below.

3. CONCLUSIONS

The 2D finite element analysis of the dam is pertainable since the monolith has constant cross-sectional dimensions and material properties. Fourier acceleration of ground acceleration, it can be seen that the frequency of the dam coincides with prominent frequency of the earthquake. The stresses developed in the dam are highest near the neck portion while the displacements are highest near the crest. The dam has been nominally built to resist gravity loads. The earthquake loading has caused damage due to development of high tensile stresses near the neck of the dam. From the above results it can be concluded that with an increase in peak ground acceleration, the displacement of the dam increases and the stresses produced at the base of the dam are very high. Taking into account the fact that seismicity of Koynanagar increased after the dam was built, we may say that it may further increase in the future. Hence it is important for us to strengthen Koyna dam by considering higher PGA values too.

REFERENCES

- [1] Bulletin Of The Seismological Society Of America. Vol. 63, No. 2, Pp 381-397. April 1973 THE KOYNA EARTHQUAKE AND THE DAMAGE TO KOYNA DAM BY A. K. CHOPRA AND P. CHAKRABARTI.
- [2] Identification Of System Parameters Of The Koyna Dam From Accelograms Recorded On The Dam. D.K Paul And A.R Chandrashekarand S.L Bhingre Paper No. 1710 Eleventh World Conference On Earthquake Engineering.
- [3] Incremental Dynamic Analysis of Koyna Dam under Repeated Ground Motions by Nik Zainab Nik Azizan et al, published in IOP Conf. Series: Materials Science and Engineering 318
- [4] The earthquake experience at Koyna Dam and stresses in concrete gravity dams BY A. K. chopra and P. Chakrabarthi, Article in Earthquake Engineering & Structural Dynamics · January 1972
- [5] Plastic damage analysis of Koyna dam with different damping mechanisms with dam water interactions By O. Omid and V. Lotfi, published in WCEE 2012
- [6] The Prediction of Earthquake Peak Ground Acceleration in Koyna Region, India By Sushil Gupta and I.D. Gupta, Published in 13th World Conference on Earthquake Engineering Vancouver, B.C., Canada August 1-6, 2004 Paper No. 1437.
- [7] ABAQUS. (2012). Analysis User's Manual Volume 3: Materials (Abaqus 6.12). SIMULIA, Dassault Systèmes Simulia Corp., Providence, RI, USA.

RECOMMENDED FIELD INVESTIGATIONS FOR EARTHQUAKE SAFETY OF LOW, MEDIUM AND HIGH-RISE BUILDINGS IN DIFFERENT SOIL CONDITIONS

E. KEERTHANA¹, R. PRADEEP KUMAR²

¹ MS Student, Civil Engineering, International Institute of Information Technology, Hyderabad, India, e.keerthana@research.iiit.ac.in (corresponding author)

² Professor, Civil Engineering, International Institute of Information Technology, Hyderabad, India, ramancharla@iiit.ac.in

Keywords: Geotechnical Investigations, Structure, Soil

1. INTRODUCTION

Structures are supported by soil or rock at its base, and before construction of any proposed project it is necessary to understand the behavior of its base medium. Stability and strength provided by the soil or rock depends on the load applied by the type of structure at its base. Engineering properties and index properties of the soil are obtained from different soil tests and similarly properties of rocks obtained from rock tests. Depending on the site suitability respective field tests need to be adopted. Overall organization of activities to find the site conditions based on the physical properties of soil or rock together called as geotechnical investigations.

Soil plays one of the important roles during seismic events because of cyclic loading experienced by soil with different frequencies. From some of the past seismic events it is observed that failure of super structure was also due to failure of sub-structure, for not considering the soil at the foundation level as shown in figures 1, 2 & 3. For example, Niigata 1964 earthquake, in which one of the major causes of damage was failure of foundation caused by loss of bearing capacity due to liquefaction of sand or by ground movement where structures were supported by different soil strata [1]. The study of geophysical aspects of the soil at the site are not only useful for the safety of super structure against gravity, but also against the dynamic loading conditions at its base.



Figure 1: Niigata Earthquake 1964

Geotechnical investigations are economical when compared to the additional expenditure required for any unfavorable ground conditions previously undiscovered and found during or after the construction. The cost of site investigation is relatively small, usually less than



Figure 2: Mexico City Earthquake 1985



Figure 3: Kocaeli Earthquake 1999

0.5% of the total cost of the project [2]. Geotechnical investigations are necessary to provide information for structural engineers in design and construction to make a project most cost effective. These site investigations are not economical but also provide safety which is more important aspect of any project.

2. SOIL EXPLORATION TESTS BASED ON STANDARD CODES

IS1892:1979 is the Indian standard code of practice for subsurface investigations for foundations. This code mainly deals with subsurface investigations for foundations of multistoried buildings to determine sequence, extent, nature and engineering properties of each soil stratum for site affected by proposed project [3]. In this code, current methods of subsoil exploration methods are classified based on type of soil formation.

Table 1

S.No	Method	Type of formation
Reconnaissance Methods		
<i>i) Geophysical</i>		
1	Electrical resistivity method	Alluvial deposits weathered and fissured rock, buried channels and ground water
2	Seismic refraction method	Do
<i>ii) Sounding</i>		
3	Standard penetration test	Non – cohesive soils without boulders
	Static cone penetrometer test	Primarily used in cohesive soils
	Dynamic cone penetrometer test	Primarily used in cohesive soils
Exploratory Methods		
4	Shell and Auger	All types of soils specially soil of mixed type
5	Hand Auger	All soils except sands and gravels above water table
6	Simplified mud boring	Silts and sands or mixed soils especially below water table
7	Wash Boring	Soft to stiff cohesive soils and fine sand except gravel and boulders
8	Percussion drilling	Rocks and soils with boulders, except clay or loose sand
9	Rotary drilling	Rocks, fissured rock and all soils except cobbles and boulders
<i>i) Explanatory sampling</i>		
10	Open tube sampler and split tube sampler	Cohesive soils and silts
11	Double tube core barrel	Coarse sand and gravels; most suitable for soft rocks like shale and any weathered rock formation.
Detailed Investigations		
<i>i) Undisturbed sampling</i>		
12	Thin walled tubes 50 to 125 mm	Soils of medium strength
13	Piston type sampler	Clays and silts
14	Samplers with special core retainers	Do

15	Sand sampler	Sand without boulders
16	Solidification methods	Do
17	Open cuts and trenches	All types of formations
<i>ii) Bearing capacity tests</i>		
18	Plate load test	Clay and sandy formations
19	Load tests	Rocks
20	Vane shear test	Soft and sensitive clays

Engineering properties of soils are obtained from the field tests mentioned by the code. The capacity of the soil not only depends on type of formation but also depends on proposed project and type of structure. Eurocode 7 [4] also suggests these field tests based on the site requirements.

3. CONCLUSIONS

From past literature study on geotechnical investigations states mainly, the field tests based on type of soils. The ability of the soil to resist loads depends on the type of soil and also on type of structure. Under dynamic loading conditions soil shows the complex behavior [5] so it is very important to consider type of soil while designing structures in seismic zones. Structural design has to consider possible real site conditions, even under dynamic loading conditions. Soil behavior under different loading conditions are given by the field tests proposed by standard codes. All the field tests given in standard codes may not be required for the given site conditions, only specified field tests need to be performed based on proposed project and soil conditions. This paper is mainly on the field tests required for the different height of buildings founded on different type of soils. In this paper, type of soils is considered according to IS 1893 (Part 1):2016. In this code soil has been divided into three types as hard, medium and soft soil mainly based on standard penetration number (N) [6].

Table 2

S. No	Soil Type	Remarks
1	Rock or Hard Soils	N >30
2	Medium or Stiff Soils	10 <N<30
3	Soft Soils	N<10

Mainly three types of buildings are considered in this paper, they are low (5-storey), medium (10-storey) and high-rise (20-storey) buildings. This paper suggests the structural and geotechnical engineers with field tests necessary for low, medium and high-rise buildings founded on hard, medium and soft soils respectively.

REFERENCES

- [1] Japan National Committee on Earthquake Engineering, *Niigata Earthquake of 1964*
- [2] H. N. Wazoh., S. J. Mallo., (2014) “Standard Penetration Test in Engineering Geological Site Investigations – A Review,” *The International Journal of Engineering and Science*. (IJES) Vol 3 pp 40-48

- [3] IS: 1892-1979, *Indian Standard Code of Practice for Subsurface Investigation for Foundations.*
- [4] Eurocode 7: Geotechnical Design – Part 1
- [5] Miguel P Romo, Manuel J Mandoza and Silvia R Garcia., (2000) “Geotechnical Factors in Seismic Design of Foundations State-of-the-Art Report.” *12th World Conference of Earthquake Engineering.* (12WCEE)
- [6] IS: 1893(Part 1)-2016, *Indian Standard Criteria for Earthquake Resistant Design of Structures.*

FINITE ELEMENT ANALYSIS OF PUNCHING SHEAR OF REINFORCED CONCRETE FLAT SLAB

S. AGRAHARI¹, P.K. RAMANCHARLA²

¹ Student, EERC, IIT Hyderabad, Hyderabad, India, saurabh.agrahari@research.iiit.ac.in

² Professor and Head, EERC, IIT Hyderabad, Hyderabad, India, ramancharla@iiit.ac.in

Keywords: Flat Slab, Lateral loading, Finite Element Method, Concrete Damage Plasticity model, Punching shear.

1. ABSTRACT

Flat-slab building structures has significant advantages over slab-beam-column structures because of the free design of space, shorter construction time and cost-effective aspects. In the present situation of building construction around the world, Flat slab is becoming widely popular in the multi-storied buildings. However, many buildings with flat slab have performed poorly under the earthquake loading and therefore it is considered vulnerable under punching shear. The design code which is followed is not adequate for the punching shear of flat slab buildings under lateral loading.

To understand the behavior of building with flat slab subjected lateral loads, a numerical study is performed. A three-dimensional finite element analysis of reinforced concrete flat slab with software ABAQUS using the concrete damage plasticity model is presented. A reinforced concrete flat slab with and without column head and drop panel along with the columns is modelled. A study is performed for understanding the linear and nonlinear behavior of flat slab subjected to lateral static and dynamic loads.

2. RESULTS

Three flat slab systems are modelled, which are flat plate, flat slab with drop panel and flat slab with column head according to the IS 456 code. Analysis is carried on by taking load as the Elcentro earthquake ground motion and finally their punching shear stress values are compared.

Table 1: Maximum Punching shear value of flat plate, flat slab with drop panel, flat slab with column head.

<i>Flat slab Systems</i>	<i>Maximum Punching shear stress value (absolute value)</i>	
	<i>Along load direction</i>	<i>Across load direction</i>
Flat plate	0.79	0.34
Flat slab with drop	0.6	0.23
Flat slab with head	0.44	0.16

3. CONCLUSIONS

Flat slab with the column head performs much better in the dynamic earthquake loading than flat slab with drop panel.

Punching shear capacity of flat plate increase by considering the column head and it reduces its vulnerability to lateral load to a great extent.

There is no much improvement in the punching shear capacity by using the flat slab with drop panel.

REFERENCES

- [1] S. Agrahari and P.K. Ramancharla., (2017). Understanding The Behavior of Flat Slab by Linear and Nonlinear Finite Element Analysis., USMCA, Sendai
- [2] D.C. Dechka., (2001). Response of shear-stud-reinforced continuous slab-column frames to seismic loads., Calgary, Alberta
- [3] A.S. Genikomsou , M.A. Polak., (2015). Finite element analysis of punching shear of concrete slabs using damaged plasticity model in ABAQUS., Engineering Structures., Canada
- [4] A. Kabir and C.D.S. Islam., (2012) Nonlinear finite element analysis of Reinforced Concrete Plates in Punching shear.

Effect of Soil Structure Interaction on progressive Collapse analysis of transmission Tower

Anshu Singh RAJPOOT
Earthquake Engineering Research Centre, IIIT-Hyderabad, India
anshusingh.rajpoot@research.iiit.ac.in
and
Pradeep Kumar RAMANCHARLA
Professor & Head
Earthquake Engineering Research Centre, IIIT Hyderabad
ramancharla@iiit.ac.in

ABSTRACT

Transmission towers play an important role in the operation of a reliable electrical power system that is considered as a lifeline system. Many studies and recent earthquakes investigations have revealed that, many structures mostly transmission towers performed poorly during wind and earthquake load. Besides many contributing factors for damage, Size, depth of footing and different type's soil mainly structures on soft soil has also massive effect on structures. In case of transmission towers it should be in a straight line at some fixed distance irrespective of soil at that particular place. It is common practice in many earthquake prone areas around the world to analyse the structure using fixed base analysis. This is mainly due to lack of awareness regarding importance of SSI. In order to understand this phenomenon, a study has been performed to show the difference in response when the structure is on soft soil compare to fixed base.

Two case studies have been performed to understand the above phenomenon. A 400 KV transmission tower has been design with proper section. In first case base of transmission tower assumed as fixed base. In second case a proper soil domain with infinite elements has been model using acoustic element which is good for wave propagation. Finally progressive collapse analysis (birth to death analysis) has been performed on both the case studies. Both the case studies reveal that there is great difference in response due to SSI. In second case, it was observed more number of elements is getting failed as compare to first case.

Keywords: Soil structure interaction, Finite element method, infinite soil elements, performance of transmission tower.

Results

In case of Fix base Earthquake has been applied at base of footing as shown in figure-3. But while in second case (where soil domain has been modeled) Earthquake can be apply at two places. Either it can be at top of the surfaces as shown in figure-4, or it can be at base of the soil after modifying time history at particular depth of the soil as shown in figure-5. In all three cases maximum stress value has calculated at three different heights i.e $H=5m$, $H=25m$ and $H=55m$.

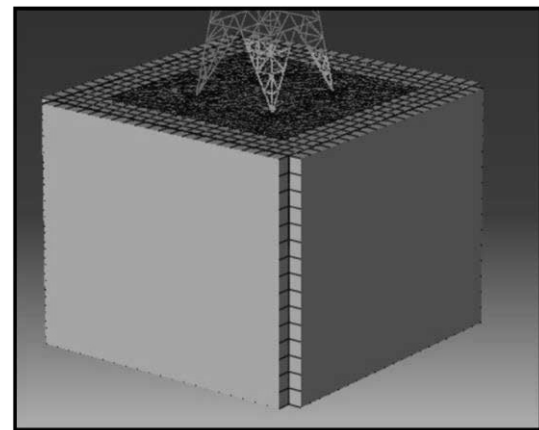
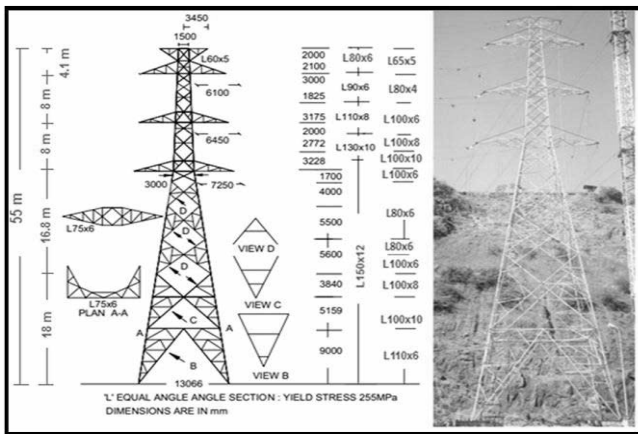


Figure-1 : 400 Kv transmission tower

Figure-2: Infinite soil model

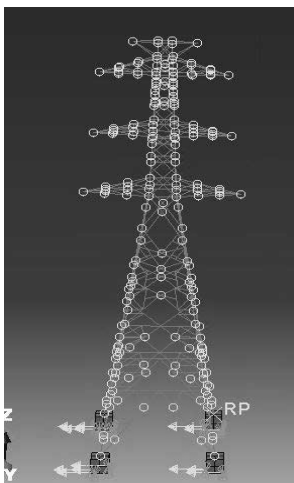


Figure-3

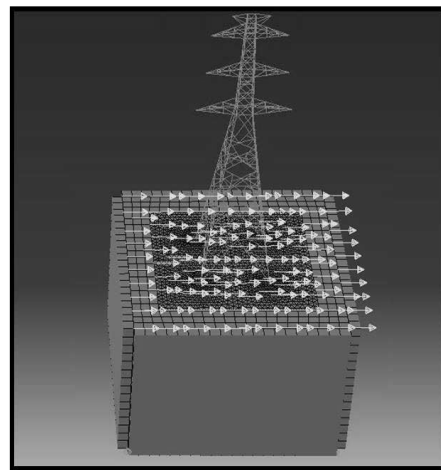


Figure-4

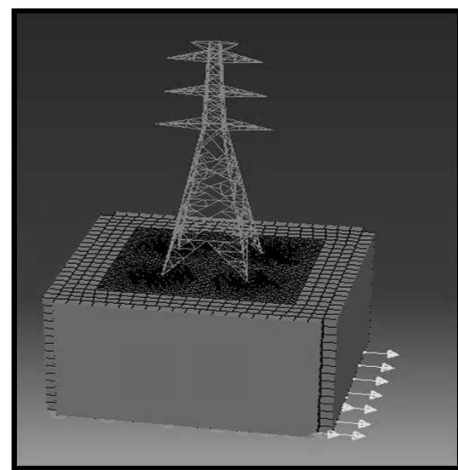


Figure-5

Table-1 : Stress values at different height in above cases.

Type	Stress at 5m(Mpa)	Stress at 25m(Mpa)	Stress at 55m(Mpa)
EQ applied at footing	340	180	22
EQ applied at top surfaces	220	80	15
EQ applied at top surfaces	320	260	25

In First case (earthquake is applied at footing) full force is transferred to footing and footing to tower. In third case (EQ applied at bottom surfaces) here also force is transferred from bottom to top and soil, effect the stress value mostly at mid height of transmission tower as shown in table-1. But in second case (EQ applied at top surfaces) here force is distributed in tower as well in soil that's why stress value is less compare to other cases.

USMCA 2018

SESSION 7

MAINTENANCE AND REHABILITATION

IMPORTANCE OF MAINTENANCE TO EVALUATE AND MAINTAIN SAFETY OF CIVIL STRUCTURES

TAKETO UOMOTO¹

¹ *Position, Professor Emeritus, University of Tokyo*

Keywords: *Importance of Maintenance, Safety Evaluation, Maintain Safety, Civil Structures, Durability Design*

1. Introduction

On March 11, 14:46, 2011, the massive “Great East Japan Earthquake” hit the country of Japan just off the Pacific coast. The magnitude of the earthquake was reported as 9.0, and shook Japan from Hokkaido to Nagoya City. The disaster was tremendous compared to Hanshin-Awaji Great Earthquake which took place in January 17, 1995. A large difference can be seen in not only the vibration of the ground caused by the earthquake, but the tsunami and nuclear power plant accident. Such earthquake disasters are occurring quite frequently compared to other countries. The data shows that the earthquake energy occurring in Japan is more than 10% of the whole earth.

On the other hand, population of Japan is estimated to reduce rapidly from now on because of fewer babies in a family (approximately 1.2 children per family) than needed to sustain the present population. Although high technologies have been developed in recent years, it is sure that fewer engineers will have to take care of this huge amount of structures from now on, which has never experienced in the past. Due to reduction in the economic growth, the budget for both construction and maintenance will be reduced in the future.

Considering these situations, the maintenance of existing structures in Japan must be done with the following conditions:

- 1) Rapid increase of existing structures reaching the age of 50 years after construction,
- 2) Less amount of engineers to maintain the structures,
- 3) Less amount of budget to maintain existing structures.

Although there are many hazards in every country, concrete structures are expected to be safe for long period of time. These structures may deteriorate by many causes including chemical reactions, physical loads, freezing and thawing, etc., as time passes by.

If the structure is deteriorated before the hazards, the structure may easily collapse and it would be difficult to maintain the safety of the people. In order to keep the safety of urban area, it is important to study and investigate not only on hazards but also on durability aspects of existing structures. Even a small amount of concrete spalling may cause large scale traffic accidents

as we experienced in tunnels for both railways and highways. Considering these situations, this paper explains what is happening now in Japan and how we are dealing with the problems through research and engineering.

2. General Maintenance Methods used till Now

The maintenance of concrete structures has been done mostly by the owners of the structures. In case of public structures, such as roads, bridges, ports, tunnels, railways, etc., the ministries or public organizations maintain the structure after the structures are completed. For the time being, the methods for the maintenance differ according to the owners of the structures. Although there are some differences, the main concept of the maintenance can be summarized as follows:

- 1) Periodic inspection and evaluation of deterioration degree
- 2) Detailed inspection and decision making
- 3) Repairing and strengthening of deteriorated structures

For periodic inspections, the inspectors inspect the structures visually, sometimes with the help of binoculars and hammers, once a year or once in several years according to the importance and time after the structure is completed. The inspectors are mostly trained engineers with experiences. The detailed inspection is done when the estimated degree of deterioration exceeds certain limit, or when some new phenomenon is found during the periodic inspection. The detailed inspection is done by visual inspections with the aid of non-destructive tests or taking core samples out from the inspected structure. The purpose of the inspection is to decide the cause of the deterioration and also to evaluate whether repair and/or strengthening is needed or not.

To repair or strengthen the existing structures, it is important to design and select sufficient methods and materials. The most popular repair method for corrosion of steel bars due to carbonation is to eliminate the carbonated concrete and replace it by new concrete and apply coatings with and without FRP sheets. But in case of steel corrosion due to chlorides from the surrounding environment, the high chloride concentrated portions of concrete are taken out, anti-corrosive treatment is applied to the surface of the bar, and

polymer cement mortar is generally used to repair the concrete before coating the concrete surface.

3. Standard Specification of Concrete by JSCE

The main proposals of the “Standard Specifications 2007” are the following two items:

- 1) Propose a new method to design and construct new concrete structures that can be used for specified lifetime without large amount of maintenance cost.
- 2) Propose an effective and economical system to maintain existing concrete structures with small number of engineers and workers.

The concepts of the new Standard Specifications are briefly explained in the following chapters.

3.1 Durability design of concrete structures for new structures

Performance-based durability design was introduced to “Standard Specification of Concrete Structures” by the Concrete Committee of JSCE in the year 2000 and be translated to English version in 2005 (JSCE, 2005c). Although durability of concrete structures was considered important in the previous specifications, performance-based design method was not used. The previous specifications described the importance of durability by proposing that the concrete structures are durable for a long time when specified materials, mixes, covers, etc. are used. But these specifications did not mention about the duration of service time, etc.

The proposed performance-based new durability design can be summarized as follows:

- 1) The concrete structure must be quantitatively checked whether the structure possesses required performance within the designed period.
- 2) The degree of deterioration of the structure in service for a specified cause must be specified.
- 3) To maintain the structure above the specified degree of deterioration, the required performance must be specified.

To examine the performance on durability, a kind of limit state design scheme was introduced for the durability of concrete structures. (For the details, please take a look at the specification.)

Generally, performance of concrete has to be verified to satisfy the required performances. Not only resistances against deterioration but also mechanism properties of concrete have to be verified.

According to the specification, minimum concrete cover thickness to prevent corrosion of reinforcing steel differs according to the type of cement to be used, water-cement ratio of concrete, years of service and exposed condition (wet or dry) of the structure to be constructed. When the structure is designed for long period of time, the cover thickness may become too large, and it is

recommended to use other countermeasures such as Epoxy-coated bars (See Figure 1), etc...



Figure 1: Epoxy-coated steel bars used for the reinforcement of concrete slab

3.2 Methods of maintenance proposed by JSCE

The methods used in the Standard Specification are basically the same as the conventional method. The differences are that the new method requires maintaining the structure within their required performances throughout their service life. Firstly, the listed below issues have to be clearly specified.

- 1) To maintain a structure, performances required for the structure must be clearly defined.
- 2) The performances required for general structures are “safety”, “serviceability”, “hazards to the public”, “aesthetics and landscape” and “durability”.

And the basic principles of maintenance works are as follows:

- (1) Structures must be maintained according to a designated maintenance category by formulating a maintenance program to retain the performance within the specified tolerances throughout their service life. And maintenance system includes adequate “initial inspection”, “deterioration prediction”, “inspection”, “assessment/judgment”, “remedial action”, and “record”.
- (2) To maintain a structure, in addition to the assessment and evaluation at the time of inspection, assessment and evaluation must be made throughout the service life of the structure based on prediction of deterioration.
- (3) To predict the deterioration, required performances of the structure must be clearly defined, and also the design service life must be made clear.
- (4) The records on design, construction, initial inspection, deterioration prediction, periodical inspection, assessment and/or evaluation, and remedial actions must be kept throughout the service life.

One of the difficulties is how to predict the degree of deterioration at the end of their service lives. There are several researches being done to predict the deterioration in numerical manner. In the published Standard,

several numerical prediction methods are introduced as references for structures suffering cyclic fatigue loads, carbonation induced corrosion and chloride induced corrosion. In case of cyclic fatigue, S-N curves are used to predict the service life. In case of carbonation induced and chloride induced corrosion of steel bars, diffusion equations for carbon dioxide and chloride are used to predict the degree of corrosion. Using these prediction methods, deterioration degree can be estimated to certain degree. But for other deterioration problems, which has not been studied numerically, a quantitative model has not been proposed yet. To deal with the problem, a qualitative method, namely "Grading method", is introduced in the Standard.

4. Problems in the Actual Existing Structures

One example of the problem is as follows: When a civil engineer is asked by the owner to check the safety of an old existing structure, one of the largest problems is that there are neither drawings nor construction records of the structure available. No problem may occur in case of important facilities, which is maintained with great care. But in case of normal structures, the owners do not know the importance of these documents.

To deal with the problem, NDI is not enough. Fortunately, our structures are not too old, and they are mostly designed and constructed by the method specified by JSCE, AIJ or other associations. Considering these, the only way is to re-design the structure again using the methodologies used at the time of construction. Figure 2 shows an example of re-designed bridge pier constructed about 35 years ago. From the figure, it is much easier for a civil engineer to check the safety of the structure under several hazards. It will become more important for the owners and engineers to keep these documents throughout the service life of a structure.

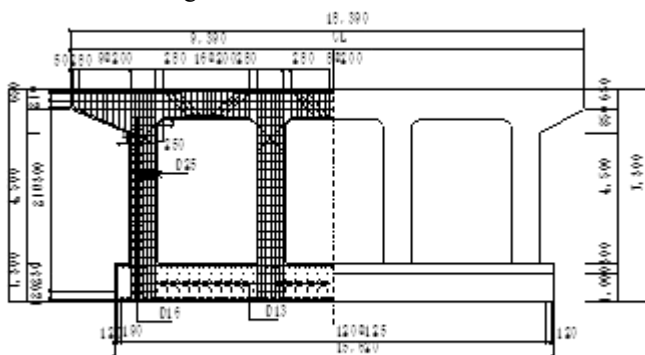


Figure 2: Re-designed reinforced concrete pier of a bridge (Okazaki, 2005)[4]

Another problem is that the inspectors may make mistakes in deciding the main cause of the deterioration. One example is shown below.

Large amount of cracks were observed inside the tunnel constructed more than 30years ago running under a river. The inspector insisted that the cracks are formed by the ground force acted on the tunnel linings due to false concrete work during the construction. But the inspected results show that cracks are concentrated in some specific areas. Comparing the distribution of the cracks and the settlement of tunnel, a good relation occurred between total amount of settlement after 30 years and the height of the ground surface (See figure 3). From these results, the main cause of the cracks formed in the tunnel were uneven settlement of the tunnel due to construction of new dikes and water pools in the river after the construction of the tunnel.

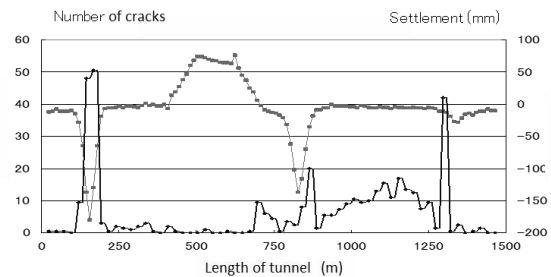


Figure 3: Distribution of cracks and total amount of settlement of a tunnel

5. Concluding Remarks

To sustain existing structures, durability of the structure is important. One good method is to construct durable structures, but for the existing structures, maintenance is the only way to deal with the problem. Although concrete committee of JSCE has set up a good system for maintenance of existing concrete structures, there are still many things to be done: not only researches but also education to the students and engineers about durability and maintenance.

REFERENCES

- [1] Concrete Committee of JSCE, Standard Specifications for Concrete Structures-2007 "Design". JSCE, Tokyo.
- [2] Concrete Committee of JSCE, Standard Specifications for Concrete Structures-2007, "Materials and Construction". JSCE, Tokyo.
- [3] Concrete Committee of JSCE, Standard Specifications for Concrete Structures-2007 "Maintenance". JSCE, Tokyo.
- [4] Okazaki, S., 2005. Development of monitoring system for RC bridge based on restoration design method. Thesis submitted to the University of Tokyo for Master of Engineering degree.
- [5] Uomoto, T., Katsuki, F., Takeuchi, M., Suzuki, S.; Effect of Surface Structures on Underground Concrete Tunnels, 2009

NATURE OF THE CORROSION PRODUCTS IN TENSIONED REINFORCING BARS

P.K. BEHERA¹, P.K. KATIYAR², S. MISRA³ and K. MONDAL⁴

¹PhD student, Department of Civil Engineering, IIT Kanpur, Kanpur, India, bprasannakumar99@gmail.com

²PhD student, Department of Materials Science & Engineering, IIT Kanpur, Kanpur, India, prvan@iitk.ac.in

³Professor, Department of Civil Engineering, IIT Kanpur, Kanpur, India, sud@iitk.ac.in

⁴Professor, Department of Materials Science & Engineering, IIT Kanpur, Kanpur, India, kallol@iitk.ac.in

Keywords: Reinforcing bars, reinforced concrete, corrosion, tensile stress, accelerated tests, test method

INTRODUCTION

Corrosion of reinforcing bars in reinforced concrete (RC) has attracted the attention of both – structural engineers and corrosion scientists. It is now known that corrosion results in the formation of different corrosion products on the surface of rebar, depending on several factors such as the state of the steel surface, availability of oxygen and water, nature of the surrounding concrete, etc. Study on the evolution of different corrosion products and how the composition of these rusts affect the critical corrosion for the onset of longitudinal cracks were carried out by Behera et al. [1]. Further, several studies have been carried out to establish the mechanism of corrosion and the transformation of corrosion products over a period of time. It has been established that the ratio of α/γ^* (i.e. $\alpha\text{-FeOOH} / (\gamma\text{-FeOOH} + \beta\text{-FeOOH} + \text{Fe}_3\text{O}_4)$) influences the further degradation of steel [2]. One other factor that has been explored to some extent, especially in the context of high strength steel wires and strands in pre-stressed concrete construction, is the effect of stress levels and composition and properties of the steel on its susceptibility to corrosion [3]. It is interesting to note that though reinforcing bars in normal reinforced concrete construction are also subjected to reasonably high levels of tensile strains inside concrete, virtually no published material is available on the effect of stresses on corrosion susceptibility. It should be noted that apart from the action of structural loads, tensile stresses in bars may arise due to bending and cranking, even before the bar is embedded in concrete.

EXPERIMENTAL DETAILS

The mild steel bars were stressed to different levels and subjected to accelerated corrosion using standard salt-fog chambers with an appropriately designed wetting and drying cycle. The corrosion and corrosion

products were monitored over a period of time using various techniques, such as polarization resistance, FTIR spectroscopy, etc.

RESULTS AND CONCLUSIONS

The results indicate that the behavior of stressed and unstressed samples is quite different, and the level of tensioning also affects various aspects of corrosion.

The results highlight the importance to carry out more extensive work in the area to better understand the corrosion in different segments of steel within any RC structure, and validate the results from sampling and data collection from the field.

ACKNOWLEDGEMENT

The support of staff in different laboratories at IIT Kanpur is gratefully acknowledged.

REFERENCES

- [1] Behera, P.K., Moon, A.P.K., Mondal, K., and Misra, S., (2016), *J. of Materials in Civil Engineering*, ASCE, V.28, No.12, p. 04016158-1-12.
- [2] Choudhary, S., Garg, A. and Mondal, K., (2016), *J. of Materials Engineering and Performance*, Springer, Vol. 25(7), pp.2969-2976.
- [3] Lee B.Y., Koh K.T., Ismail M.A., Ryu H.S. and Kwon S.J., (2017), *Advances in Materials Science and Engineering*, Article ID 8575816.

EXPERIMENTAL INVESTIGATION ON HEALING OF MICROWAVE-HEATED BITUMINOUS CONCRETE MIXTURES

N. S. L. APARNA¹, K. SUDHAKAR REDDY²

¹ Doctoral research scholar, Department of Civil Engineering, Indian Institute of Technology Kharagpur, Kharagpur, India, lakshmiaparna93@gmail.com

² Professor, Department of Civil Engineering, Indian Institute of Technology Kharagpur, India, ksreddy@civil.ernet.in

Keywords: Fatigue cracking, self-healing, Microwave heating, Indirect tensile strength

1. INTRODUCTION

India, with a wide road network of 56.03 lakh kilometer [1], has majority of its roads constructed as flexible pavements with bituminous mixtures. Major distresses in these pavements include permanent deformation (rutting) along wheel path and fatigue cracking originating both from top and bottom of the bituminous layers. Fatigue cracking occurs mainly due to the repeated application of loads. It not only reduces the load carrying capacity of the pavement but also aggravates the damage due to ingress of moisture into the pavement through the cracks. Thus, these cracks need to be sealed / repaired periodically for better performance of pavement. Bituminous mixes have the intrinsic property of healing the damage with time and temperature and thus are expected to heal by themselves during hot summers and long rest periods resulting in the extension of service life. Self - healing of bituminous mixtures depends on several factors which mainly include the climatic condition of the pavement which is practically difficult to control.

Thus, improving the self - healing capability of bituminous mixtures is an area that caught the attention of several researchers. As self - healing increases with increase in the temperature of mix, inducing heat into the mixture is proven to be a feasible way of improving healing [2, 3]. Heating by means of induction heating and microwave heating have been explored by researchers to enhance the healing characteristics of bituminous mixtures. The present study aims at using microwave heating, a faster heating method and which produces smaller thermal gradients [4], for healing of bituminous mixtures with different rest periods.

2. EXPERIMENTAL METHODS

2.1 Materials and Equipment

The binder used in this study was graded as VG40 as per IS 73 2013 and was supplied by Jalnidhi bitumen Ltd. Table 1 gives some properties of the binder used. BC 2 aggregate gradation was used to prepare the mixes according to [1] and the aggregates used were of basaltic nature. To improve the microwave absorbing capability of mix, steel wool of grade 000 (diameter of 0.035 mm) was selected as an additive after some preliminary investigations as it has higher microwave absorption compared to other coarser grades and is easier to mix. A microwave oven (Bajaj 1701MT DLX), capable of producing microwaves with 2.45 GHz frequency, rated

1200 W at full power was used as the source for microwaves (Figure 1).

Table 1: Properties of binder used in present study

Property	Value
Penetration	38 pen
Softening point	55 °C
Ductility	>100 cm
Mixing temperature at viscosity of 170 cP	170 °C
Compaction temperature at viscosity of 280 cP	157 °C

A split mould fabricated with 1.5 mm thick aluminum sheet with a suitable base plate was used to hold the specimens for keeping them in the microwave oven so that only the upper surface is exposed to the penetration of microwaves and thus simulating the practical condition of heating in the field.



Figure 1: Microwave oven with single split mould

2.2 Sample Preparation

Marshall method of compaction with 75 blows on each face of the specimen (recommended for high volume roads by Asphalt Institute MS-2) was used to compact the mixture containing aggregates, binder and additive. Steel wool was chopped into smaller pieces (3 mm – 5 mm) and added to the mixture of aggregates and bitumen. Mixtures were prepared to have a design air void content of 4% and steel wool (5% by weight of binder was added to the mix. Cylindrical samples of 100 mm diameter were cast for healing study.

3. EXPERIMENTAL METHOD

3.1 Healing cycle

Experiments in this study were conducted in three phases. They are; testing of samples to measure Indirect Tensile

Strength (ITS) followed by heating and further healing of the broken samples and testing the healed samples to measure ITS as described below.

The characterization of bituminous mixtures in terms of indirect tensile strength was done by the Marshall specimen along a diametric plane at a constant rate of 51 mm / min. acting parallel to and along the vertical diametrical plane of the specimen through two loading strips as per ASTM D 6931. The broken samples were kept inside the split mould and placed inside the microwave oven maintained at full power. Temperature of the exposed top surface was measured at regular intervals till it reached a range of 95 °C to 100 °C. The samples were taken out of the oven and were removed from the mould and allowed to heal for different durations; 3, 18 and 24 hours. The recovered indirect tensile strength at the end of the healing period strength at the end of rest period was measured. Immediately after heating, images were also taken with an Infrared camera on the top surface of the samples and along the depth to observe the heating uniformity.

3.2 Parameters evaluated from the experiments

i. **Indirect tensile strength:** Indirect Tensile Strength of bituminous mixtures is calculated as follows. (ASTM D 6931)

$$S_t = 2000P / (\pi \times T \times D) \quad [1]$$

St = IDT strength, kPa

P = Maximum load, N

T = Specimen height immediately before test, mm

D = specimen diameter, mm

ii. **Healing index:** The healing index of each sample at the end of each healing cycle, HI was defined as the percentage of ITS recovered at the end of healing cycle.

$$HI = (ITS_f / ITS_o) \times 100 \quad [2]$$

ITS_f = ITS of the sample after healing

ITS_o = ITS of normal sample

4. ANALYSIS AND DISCUSSION

4.2 Heating properties

The average time required for bringing the surface temperature of the mix to 95 °C to 100 °C with the microwave oven used in the study is 4.5 minutes. Uniformity of heating along the depth was measured in

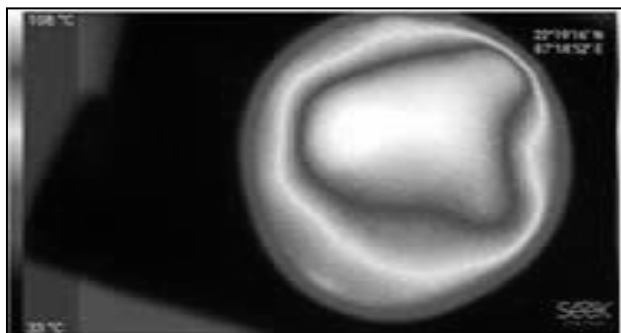


Figure 2: Infrared image of a heated sample

terms of the temperature gradient from top surface to bottom surface. There exists an average gradient of 30 °C over a depth of 60 mm. Figure 2 shows the temperature profile on the top surface of the heated sample inferring the basic heating phenomenon of microwave i.e., generation of heat from within.

4.3 Healing properties

Effect of healing periods on healing efficiency of mixtures was studied and table 3 shows that with increase in rest period, healing index was increased.

Table 3: Healing indices after different rest periods

ITS _o (kPa)	Healing period (hr)	ITS _f (kPa)	Healing index = (ITS _f / ITS _o) X100
1168	3	605	52
1211	18	833	69
1190	24	866	73

CONCLUSIONS

- The feasibility of heating bituminous mixes by microwave method has been demonstrated in this study. An average temperature gradient of 0.5 °C /mm was also observed along the depth of the specimen.
- The duration of healing period has been found to have an effect on the healing characteristics of the mixes.
- The information generated from the present study will be useful for identifying the conditions to be adopted for microwave heating and healing of the cracks in field bituminous layers. For this, it is however required that a more detailed laboratory investigation is to be done followed by field validation of this recommended conditions.
- Enhancement of healing by Microwave heating would not only increases the serviceable life of the pavement and reduces the life cycle cost but also aids in sustainable construction and maintenance practices by reducing the waste generated due to the milling of cracked pavement.

REFERENCES

- [1] Ministry of Road Transport Highways “Specifications on Road and Bridge works” (2013), fifth revision.
- [2] Liu, Q., Schlangen, E., van de Ven, M., van Bochove, G., van Montfort, J., (2012) “Evaluation of the induction healing effect of porous asphalt concrete through four point bending fatigue test” *Constr. Build. Mater.* 29, 403e409.
- [3] Menozzi, A., Garcia, A., Partl, M.N., Tebaldi, G., Schuetz, P., (2015) “Induction healing of fatigue damage in asphalt test samples”. *Constr. Build. Mater.* 74, 162e168
- [4] Gallego J., Val M. A., Contreras V. and Paez A. “Heating asphalt mixtures with microwaves to promote self-healing.” *Constr. Build. Mater.*, 42, 1-4, 2013.

STUDY OF FRESH AND HARDENED PROPERTIES OF CONCRETE IN PARTIAL REPLACEMENT USING FLY ASH AND LIMESTONE POWDER

M.C. YUVANKARTHICK¹, M. ANANTHKUMAR², and S. BARATHI KUMAR³

¹ Student, Civil Engineering, Amrita Vishwa Vidyapeetham, Coimbatore, Tamil Nadu, yuvankarthickmc@gmail.com

² Assistant Professor, Civil Engineering, Amrita Vishwa Vidyapeetham, Coimbatore, Tamil Nadu, m_ananthkumar@cb.amrita.edu (corresponding author)

³ Student, Civil Engineering, Amrita Vishwa Vidyapeetham, Coimbatore, Tamil Nadu, barathifdr@gmail.com

Keywords: Fly ash, limestone powder, flexural strength, compressive strength, workability,

1. INTRODUCTION

In the modern world the demand for cement has increased dramatically since being the important constituent of widely used concrete. The production of cement causes CO₂ emission and degradation of natural resources. To reduce this effect partial replacement of cement with various supplementary cementitious materials are carried out. One of them is fly ash. It was noted that fly ash usage reduces early strength, workability and increases high heat of hydration. Thus, to counteract these effects we introduced super plasticizers. In our study we tried to make the concrete more sustainable by using fly ash and limestone powder along with other usual materials of conventional concrete. A total of 9 concrete mixes were taken by varying the percentage of limestone powder, fly ash, cement and fine aggregates. Tests were conducted to assess workability, compressive strength, density and flexural strength.

2. MATERIALS

Ordinary Portland cement, fine aggregate, coarse aggregate, fly ash, limestone powder.

3. METHODOLOGY

Concrete mix design:

The concrete mix design was done for M30 grade concrete. And the resultant ratio was found out to be 1: 1.34: 2.87 by weight. To study the influence of Limestone and fly ash in concrete, ten different mixes including one control mix were used. S- controlled mix 0% L (limestone powder) and 0% F (fly ash), M1-15%L 0%F, M2-30%L 0%F, M3-0%L 25%F, M4-0%L 50%F, M5-15%L 25%F, M6-15%L 50%F, M7-30%L 25%F and M8-30%L 50%F.

Casting and curing of concrete specimen:

Nine concrete cubes of size 150x150x150mm were casted for each of the above mix, to check for compressive strength and density of concrete. Three flexural beams of dimension 750x100x100mm were casted for each mix. The concrete specimens were casted using steel moulds and compacted using needle vibrator. The cast specimen was kept in an ambient temperature

for 24 hours and after 24 hours it was demoulded and was placed for curing. The concrete specimens were cured for 1day, 7days and 28days, in order to determine 1day, 7 days and 28 days compressive strength. The test on fresh concrete i.e. the slump cone test was done immediately after mixing of concrete in the concrete mixer.

Testing of samples:

Workability- To find the workability of the sample slump cone test was conducted. Freshly prepared concrete was filled in the cone shaped container with three-layer tamping. Slump was measured by noting the difference in height to that of mould.

Density- It was calculated as the ratio of weight by volume of the hardened concrete specimen.

Compressive strength- the concrete cubes was tested with the help of Compressive Testing Machine. Once the concrete block fails and the load at which the failure occurs is displayed on the dial, the machine functioning is stopped. Compressive strength was calculated as the ratio of failure load by area under compression.

Flexural strength- the specially cast flexural beams were used. It was tested with the help of Flexural Testing Machine. Once the concrete block fails and the load at which the failure occurs is displayed on the dial, the machine functioning is stopped.

4. RESULTS

Workability:

The concrete mixes with fly ash alone showed reduced workability and limestone powder replacement alone showed slight improvement in the workability compared to that of control mix. The mixes with both limestone powder and fly ash replacement (M5, M6, M7 and M8) showed changes based on the percentage of replacement. The workability was maximum at M6 (15%L & 50%F) among the mixes with both cement and fine aggregates partially replaced.

Table 1: Workability variation in milli meters (mm).

Mix design	S	M	M	M	M	M	M	M	M
		1	2	3	4	5	6	7	8
Workability	76	77	82	30	5	58	62	41	45

Density:

The density of the hardened concrete can explain the mechanical properties of the concrete to some extent. M5 is found to be higher for both limestone powder and fly ash replacement.

Table 2: Density variation.

Mix design	S	M1	M2	M3	M4
Density (kg/m ³)	2530	2539	2524	2527	2515

M5	M6	M7	M8
2532	2515	2521	2513

Compressive strength:

Compressive strength of the hardened concretes was tested using compression testing machine at stages of 1 day, 7 day and 28 day to understand the strength gain of the concrete. M6 was found suitable with the highest strength after 7 days, 28 days and comparatively equal strength after 1 day. It was also greater than the conventional mix after 28 days.

Table 3: Compressive strength variation for 1, 7 and 28 days in (Mpa).

Mix Design	S	M 1	M 2	M 3	M 4	M 5	M 6	M 7	M 8
1 day	23	25	24	22	21	24	23	22	22
7 days	31	31	31	38	43	37	42	38	37
28 days	40	40	37	52	59	49	54	45	57

Flexural strength:

Flexural strength of the concrete with limestone powder replacing cement is low at 28days compared to the convention control mix. On the other hand, fly ash replacement improved the flexural strength linear to its content. In the mixes with limestone and fly ash replacement, the strength improved for fixed limestone and varying fly ash content. The flexural strength is maximum for M6 with 15% L and 50% F (4.96 MPa).

Table 4: Flexural strength variation in (Mpa).

Mix Design	S	M1	M2	M3	M4
Flexural strength	4	3.36	2.88	5.12	5.6

M5	M6	M7	M8
4.48	4.8	3.68	3.84

5. CONCLUSION

The workability of concrete mix containing fly ash alone was very low. But on the addition of super plasticizer like limestone powder improved the

workability to a usable range. The usage of limestone powder to improve workability is viable and economical option as limestone is a raw material already available in the cement industries. Density did not vary much as compared to that of conventional concrete. The compressive strength of the mixes with fly ash replacement alone showed good improvement. All the mixes with both limestone powder and fly ash showed better strength almost at all stages compared to the control mix. M6 showed the highest strengths among the mixes with both fly ash and limestone. The 7 days strength and 28 days strength showed an improvement of 38% and 34% in compressive strength respectively. The flexural strength among the concrete with both the replacement materials (LS & FA) reached its maximum in M6 concrete. The flexural strength was 4.96 MPa at 28 days of curing which is 24% increase compared to the conventional concrete.

Hence M6 concrete can be used in structural construction without any loss in strengths. This also improves the energy efficiency of the concrete, reduces the CO₂ emission and improves fly ash usage.

REFERENCES

[1] Parvati V. K and Prakash K.B, (2013) "Feasibility Study of Fly Ash as a Replacement for Fine Aggregate in Concrete and its Behaviour under Sustained Elevated Temperature," *International Journal Of Scientific & Engineering Research*, Vol.4, Issue 5, pp 87-90.
 [2] Rafat Siddique, (2002) "Effect of fine aggregate replacement with Class F fly ash on the mechanical properties of concrete," *Cement and Concrete Research*, Vol 33, pp 519-547.
 [3] Shirish V. Deol and Arun D. Pofale, (2015) "Parametric Study for Replacement of Sand by Fly Ash for Better Packing and Internal Curing," *Open Journal of Civil Engineering*, Vol 5, pp 118-130.
 [4] Dale P. Bentz, Taijiro Sato, Igor de la Varga and W. Jason Weiss, (2012) "Fine limestone additions to regulate setting in high volume fly ash mixtures," *Cement & Concrete Composites*, Vol 34, pp 11-17.
 [5] A Jayaraman, (2014) "Experimental Study on Partial Replacement of Natural Sand with M- Sand and Cement with Lime Stone Powder," *International Journal of ChemTech Research CODEN (USA): IJCRGG ISSN: 0974-4290*, Vol.6, No.2, pp 948-954.
 [6] Dale P. Bentz, Ahmad Ardani, Tim Barrett, Scott Z. Jones, Didier Lootens, Max A. Peltz, Taijiro Sato, Paul E. Stutzman, Jussara Tanesi and W. Jason Weiss, (2014) "Multi-scale investigation of the performance of limestone in concrete," *Construction and Building Materials*, Vol.75, pp 1-10.
 [7] Rafat Siddique, (2014) Utilization of industrial by-products in concrete, *Procedia Engineering*, Vol 95, pp 335-347.

A CASE STUDY OF EXTRADOSSED CREEK BRIDGES IN WESTERN COAST OF INDIA

Mohammed Younus Ahmed¹

¹ Manager, Transportation Roads and Bridges (TRB), Voyants Solutions Pvt. Ltd., Hyderabad, India, eMail engrahmed786@gmail.com

Keywords: Cable-stayed bridges, Extradosed Bridge, Dynamic analysis, Creek Bridge

1. INTRODUCTION

During the past decade, Extradosed bridge construction has experienced an upsurge in India. Extradosed bridge range from spans 125m to 250m. As navigation is compulsory through the Creek. Four creek bridges namely at Dighi (2.875 km), Dabhol (1.204 km) and Jaigad (2.650) on the western coast of India have been proposed with extradosed span. Each on the creek bridge have been given extradosed span of 160m in the middle of the bridge.

The pylon height above the deck level is 36m. The difference between the bed level and the normal water level throughout the year is 15m -17m, a vertical clearance of minimum 12.5m is required for navigation of ships. The bridges are provided with pile foundation and are falling under India's second highest seismic zone i.e. Seismic Zone IV. The soil strata upto a depth of 20m is completely sand.

The bridges are designed with cantilever construction method. The structural behavior response spectrum analysis, eigen value analysis, deflections, cable stay forces are compared.

An Extradosed bridge, which is intermediate to Girder Bridge and a cable stayed bridge, adds substantial prestress to the deck because of the shallow pylon, are found to be economical for spans upto 250m. Dynamic response prediction has been the matter of research for many authors, in particular as the structural design of many structures is governed by the earthquake load cases or combinations thereof.

The intrados is defined as the interior curve of an arch, or in the case of cantilever-constructed girder bridge, the soffit of the girder. Similarly, the extrados is defined as the uppermost surface of the arch. The term 'extradosed' was coined by Jacques Mathivat [1] to appropriately describe an innovative cabling concept he developed for the Arrêt-Darré Viaduct, in which external tendons were placed above the deck instead of within the cross-section as would be the case in a girder bridge. To differentiate these shallow external tendons, which define the uppermost surface of the bridge, from the stay cables found in a cable-stayed bridge, Mathivat[1] called them 'extradosed' prestressing.

Some features of extradosed bridge as given below:

- External appearance resembles cable-stayed bridge – but structural characteristics are comparable to those of conventional girder bridge

- The Girder Depth are lesser than that of conventional girder bridges
- The stay cables (prestressing tendons outside the girder) need no tension adjustment necessary for cable-stayed bridges, and can be treated as usual tendons as in girder bridges
- The height of pylon is half as that of cable-stayed bridge and hence easier to construct
- With small stress fluctuation under live load the anchorage method for stay cables can be same as that of tendons inside girder and thereby achieve economy.

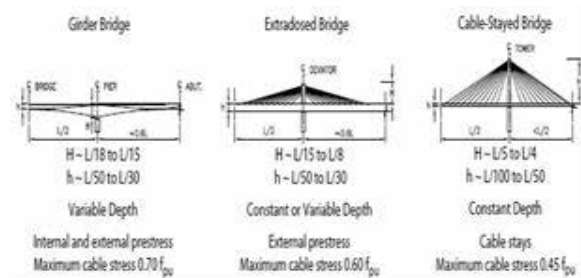


Figure 1: Figure showing cable arrangement for Girder, Extra-dosed and cable stayed bridge

The reduced cable inclination in an extradosed bridge leads to an increase in the axial load in the deck and a decrease in vertical component of force at the cable anchorages. Thus, the function of the extradosed cables is also to prestress the deck, not only to provide vertical support as in a cable-stayed bridge. Extradosed bridges are characterized by a low live load stress range in the stay cables.

With the rapid increase in span length, combined trend and also trend of using high strength materials have resulted in slender structures and a concern is being raised over dynamic behavior of such structures, in case of cable supported structures it is more pronounced as this further includes vibrations of cable elements also. An accurate analysis of natural frequencies is fundamental to the solution of its dynamic responses due to seismic and wind and traffic loads.

2. HIGHLIGHTS ON STATIC BEHAVIOUR

The basic difference between cable stayed bridge and Extradosed Bridge is its tower height. As per [2] For the span to tower height ratio is generally kept at 4-5, whereas for Extradosed Bridge it is 5-8, which means Extradosed bridges The stiffer the tower will enable the use of the full range of effective depth of

cross-section. Since the short towers act as cantilevers, effectively prestressed by the dead load of the girder acting through the cables, they require relatively little reinforcement to resist bending due to live load. Neither a flexurally stiff girder nor backstays are required in order to provide adequate system stiffness to control deformations due to live load. With short towers, larger stay cables are required, but the towers are more economical than the tall towers normally found in cable-stayed bridges. The methods of providing stiffness in cable supported structures are shown in figure 2

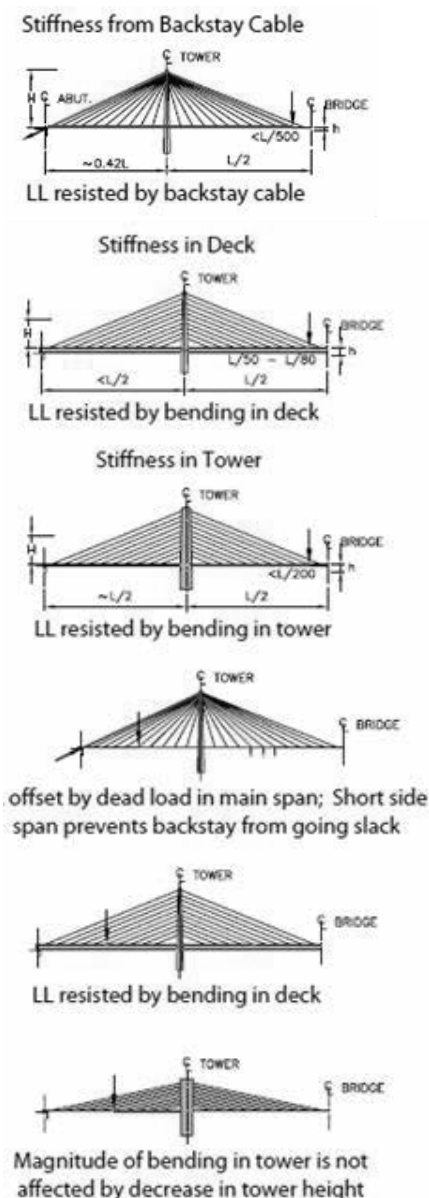


Figure 2: Response of cable supported bridge to live loads

SETRA [3] published recommended allowable stress limits that cover the full range of external cables. In that document, external prestressing tendons are defined as being subjected to a stress range of up to 15 MPa under live load while stays for cable-stayed bridges are subjected to a stress range of around 100 MPa and above. Extradosed cables are characterized as being subjected to

a live load stress range between 30 MPa and 100 MPa and are not sensitive to wind vibrations. These specifications resulted from a need for design recommendations for bridges that do not fall into distinct categories, and they propose design limits and approximations based on rational principles. This explains use of 0.6fu allowable stress in the Extradosed cables, which leads to material economy.

3. FREE AND FORCED VIBRATION ANALYSIS

Research methodology:

To study dynamic behaviour of Extradosed Bridge, 3 numbers of models with variable parameters are prepared. Basic span configuration as applicable for Extradosed span is selected to be 125, 150 and 260m main span, the side span is about 0.5 of main span. The pylon height is varied from 5.7 to 6.2 to account for the effect of varying cable inclinations. The cable inclination varies from 17 to 30 degrees. The requirement of cable area and prestressing is as per preliminary design. Box beam superstructure is adopted with solid rectangular pylon designed by Limit State Design as per IRC 112:2011[4]. For details of model refer table-1.

Table 1: Details of Extradosed Bridge used in study

S.no	Span(L)/ configuration(m)	Pylon ht (H) (m)	Remarks
1.	62.5+125+62.5 (Concrete deck)	22	On pile foundation, 21m wide deck
2.	75+150+75 (Concrete deck)	36	On pile foundation, 21m wide deck
3.	110+260+110 (steel deck)	45	On pile foundation, 21m wide deck

The dynamic response of structure for free vibrations as well as forced vibration has been studied. Software Midas 2018 [5] has been verified and used in the study. Deck is modelled as Euler Bernoulli Beam and the stay cables have been modelled as single truss elements in static/ dynamic analysis.

4.0 Free Vibrations of Extradosed Bridge

With the rapid increase in span length, combined trend and also trend of using high strength materials have resulted in slender structures and a concern is being raised over dynamic behaviour of such structures, in case of cable supported structures it is more pronounced as this further includes vibrations of cable elements also. An accurate analysis of natural frequencies is fundamental to the solution of its dynamic responses due to seismic and wind and traffic loads. The modal shapes and frequencies for above listed models are presented below;

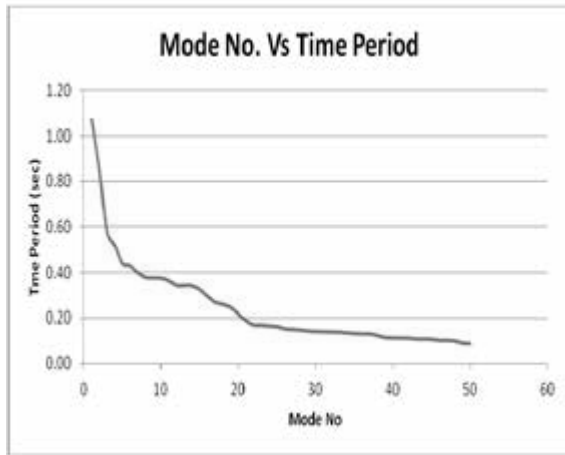


Figure 3: Mode no vs. time period in sec for 62.5+125+62.5 extradosed bridge

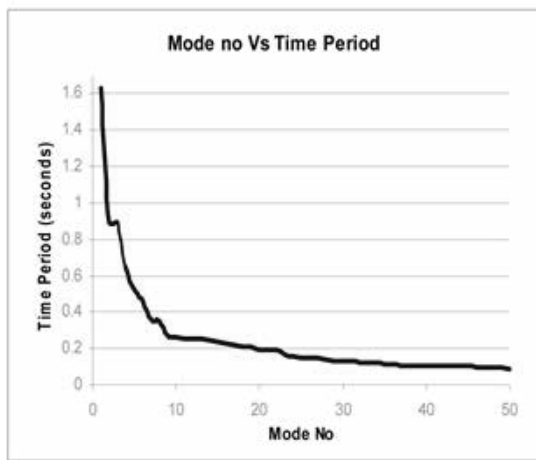


Figure 4: Mode no vs. time period in sec for 75+150+75 extradosed bridge

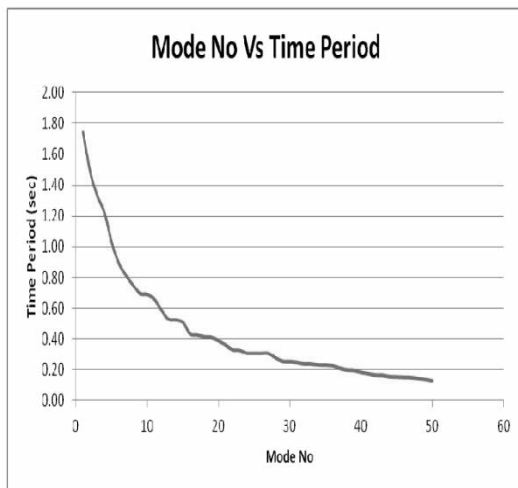


Figure 5: Mode no vs. time period in sec for 110+260+110m extradosed bridge

The first 5 mode shapes are presented below for one of the model



Figure 6: Mode 1 for span 75+150+75, T=1.09s



Figure 7: Mode 2 for span 75+150+75, T=0.87s

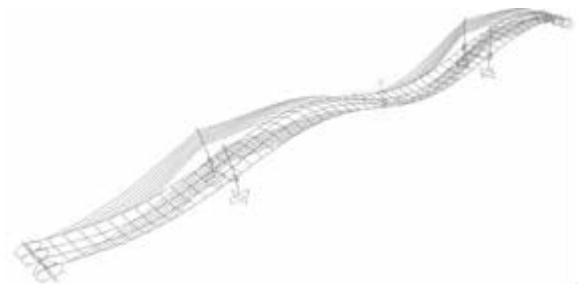


Figure 8: Mode 3 for span 75+150+75, T=0.58s

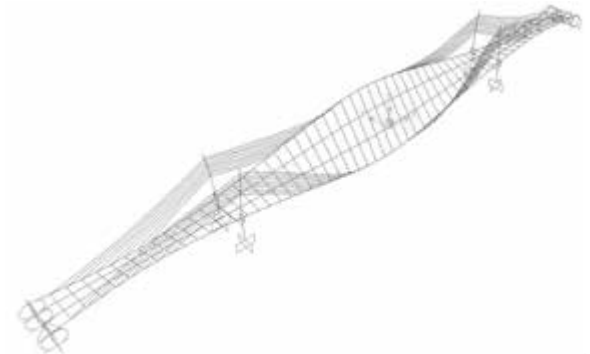


Figure 10: Mode 4 for span 48+120+48m, T=0.52s

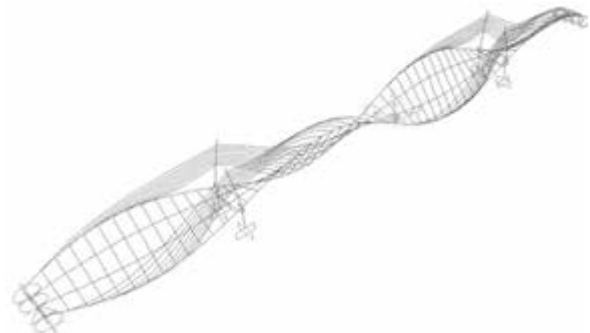


Figure 10: Mode 5 for span 75+150+75, T=0.43s

5.0 Free Vibrations of Extradosed cables

Each stay cable is analyzed as an inclined stay cable fixed & pinned at both ends to evaluate the natural frequencies of local vibrations. It is noted however that the real situation is slightly different, as the end anchorages themselves are movable. The first symmetric and anti-symmetric in-plane transverse vibration frequencies are computed considering pinned and fixed end conditions. The results are summarized in fig 11 and fig 12.

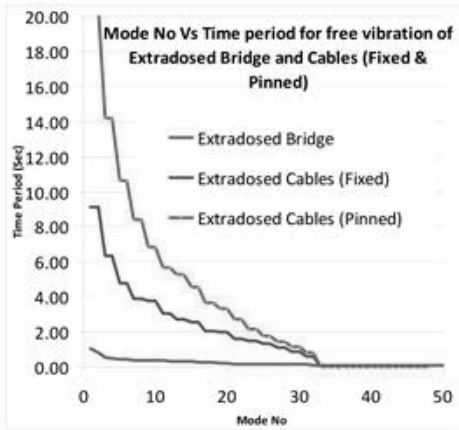


Figure 11: Mode no Vs Time period (s) for structure and cables for 62.5+125+62.5m Extradosed bridge

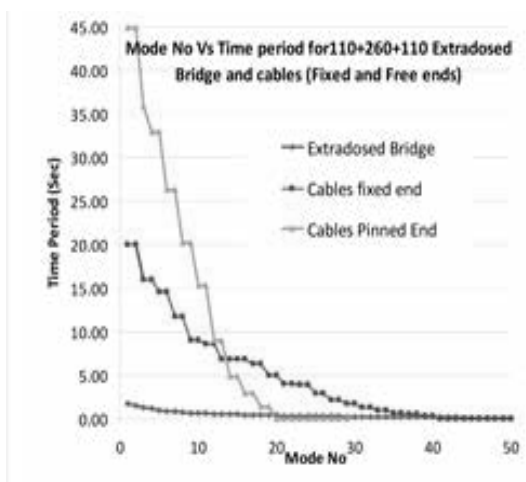


Figure 12: Mode no Vs Time period (s) for structure and cables for 110+260+110m Extradosed bridge

By looking at the mode shapes of the stay cables, it is possible to relate these natural frequencies of the “fixed/free end” cables to those obtained by analyzing the whole bridge using the finite element method. The results are shown in fig 12 & 13. Apart from those natural frequencies that are obviously outside the range under consideration, all local cable vibrations can be reflected by finite element analysis with multiple-element modelling of stay cables. In addition to those pure local vibrations of stay cables, some new frequencies are also discovered indicating strongly the existence of coupled vibration modes. Obviously, these

coupled vibration modes cannot be predicted by Equations. For investigating the possibility of coupled mode of vibration the time periods for various modes of vibration are superimposed for structure and cables

6.0 Forced Vibrations of Extradosed Bridge

Forced vibration is studied for selected earthquakes; the earthquakes selected were having different characteristics as given in table 1

Table 2: Details of Earthquakes time histories

Name	Magnitude	Duration (sec)	PGA Value (g)	Time for PGA Value(sec)
Koyna	6.5	7.02	0.49	2.60
Bhuj	6.9	120	0.30	39
El-	7.2	40	1.61	2.48

The time history analysis for these was performed on selected models and force effects at various points were recorded

7.0 Non-Dimensionalizing of parameters

Forced vibration analysis for three earthquake time histories having different characteristics are undertaken. To compare the results all parameter have been non dimensionalised using equivalent factors as mentioned below;

$$V = \rho * g * A * L$$

$$M = \rho * g * A * L^2$$

Where, V & M are non dimensioning factors for shear force, bending moment.

Where, ρ = Mass Density,

g= Gravitational acceleration,

A= Cross section area of component and L= Half span length of the component.

Span and pylon height are non-dimensionalized by using parametric length. The results obtained from the time history analysis in terms of bending moment and shear forced in the structure are non-dimensionalised and superimposed and presented in Fig 13 to 18

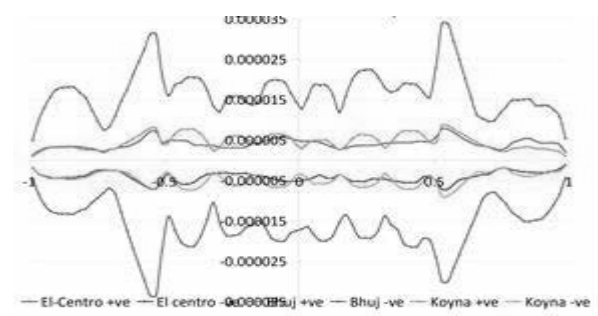


Fig 13. Variation of bending moment across span for 110+260+110m span (Non-dimentionalized)

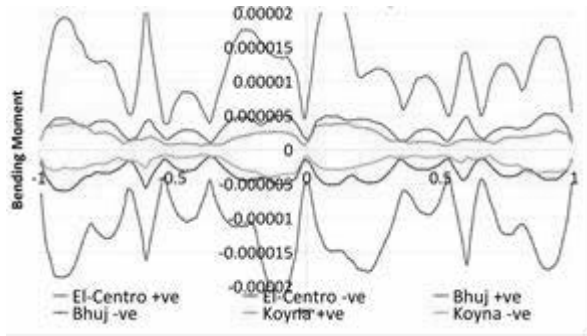


Figure 14: Variation of bending moment across span for 75+150+75 span (Non-dimensionalized)

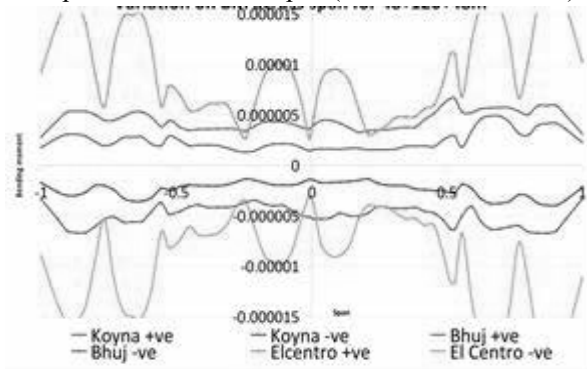


Figure 15: Variation of bending moment across span for 62.5+125+62.5 span (Non-dimensionalized)

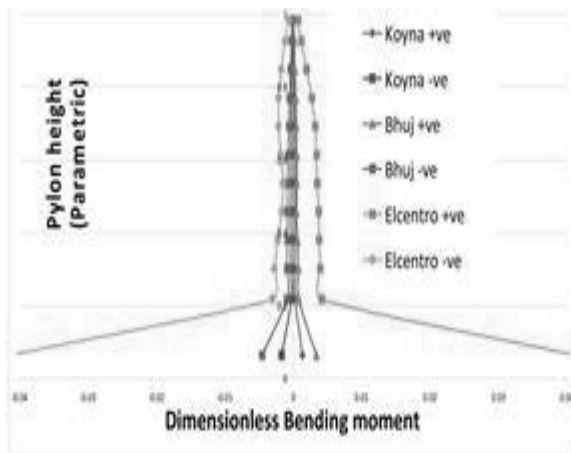


Figure 16: Variation of bending moment across pylon height for 110+260+110 span (Non-dimensionalized)

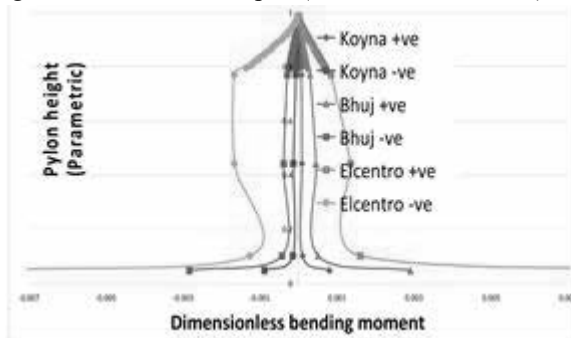


Figure 17: Variation of bending moment across pylon height for 75+150+75 span (Non-dimensionalized)

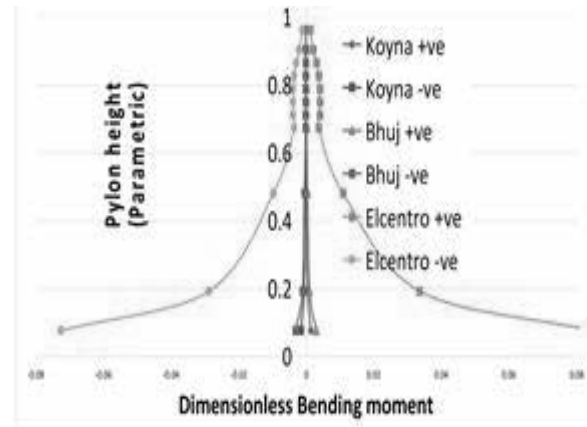


Figure 18: Variation of bending moment across pylon height for 62.5+150+62.5 span (Non-dimensionalized)

8.0 Forced Vibrations of Cables

Cable excitations can be caused by rain, wind, stochastic vibration due to plying vehicles or parametric vibrations

due to vibration of the deck. Due to the infinite number of damping values and angles of inclination that a cable may take, several values can be selected to represent typical cables. It is evident that zones of large-amplitude cable vibrations do tend to change with varying angles of inclination, when the geometric nonlinearity of the cable lessens, as the angle of inclination moves towards 90. Also, the onset of these regions of large-amplitude cable vibrations required higher amplitudes of cable end excitation as the damping of the cable increases.

It was considered important that the stochastic excitation or parametric excitations, which may occur due to various reasons, but the main reason being the vehicles plying on the bridge, which was to be imposed on the cables, be representative of a prototype stochastic time-history that might be imposed on a stay by a full-scale cable structure such as an extradosed bridge. Even though an approximation, cable structures, such as telecommunications masts and cable-stayed bridges, are subject to random wind forces, which have time-histories that are very similar to random normal distribution, for the low-frequency bandwidth under examination. An extradosed bridge or other similar structure will act as a signal filter, by filtering wind signals (or white noise signals) through its own structural characteristics. The resulting dynamic response input will be the actual response of the structure to the wind load. This filtered signal or structural response can then be used as a stochastic time-history (stochastic support excitation) for the examination of a cable's response to that time-history. As the wind will have varying characteristics, such as wind speed and wind direction, the force acting on the structure will also have varying characteristics. These will excite the structure at different frequencies with varying amplitudes of force.

9.0 DISCUSSIONS

Free Vibrations: - An accurate analysis of natural frequencies and mode shapes of cable supported structures such as Extradosed Bridge is fundamental to the solution of its dynamic responses due to seismic, wind and traffic loads. Now days, from economic considerations, the stay cables are often closely spaced, with the cable lengths and tensions gradually varying from position to position. The natural frequencies of their self-vibrations are therefore rather closely spaced. This may cause boundary-induced vibrations of the stay cables. This complicates the overall dynamic behavior of cable stayed structures. In addition to pure local vibrations of stay cables, some new frequencies are also present indicating strongly the existence of coupled vibration modes, these coupled vibration modes cannot be predicted by equations. The frequencies of cables with actual boundary conditions are expected to lie in-between those of with fixed and pinned ends. For investigating the possibility of coupled mode of vibration the time periods for various modes of vibration are superimposed for structure and cables. The intersection zone (intersection of stay cable vibrations and bridge vibrations) suggests the possibility of coupled vibrations.

Forced Vibrations: - Forced vibration studies of deck and pylon of three types of bridges reaffirms following facts for extradosed bridge:

- 1) Magnitude of bending moment / shear force is directly proportional to the magnitude of forcing function / PGA.
- 2) With increase in the distance between cables ssuupp-- ports the shear force in deck also increases.
- 3) Pylon stiffness does not have any effect on the deck moments/shear.
- 4) With increase in the pylon height/slenderness the shear force changes its sign in the upper part of pylon.
- 5) It is observed that only for cable stayed bridge with harp shape cable arrangement the shear force reduces at the junction of deck

REFERENCES

- [1] Katsuhiko Takami and Sumio Hamada (2005); Behavior of extradosed bridge with composite Girder; ASCE / Journal of Bridge Engineering.
- [2] H. Otsuka, T. Wakasa, J. Ogata, W. Yabuki and D. Takemura (2003); Comparison of structural characteristics for different types of cable-supported prestressed concrete bridges; Structural Concrete Mar-2002.
- [3] "External prestressing", Recommendations, SETRA, Bagneux, February 1990
- [4] IRC-112 2011 Code of practice for design of reinforced concrete bridges

[5]Midas Civil 2018 – Software for Bridge Structural Analysis
http://en.midasuser.com/product/civil_overview.asp

EFFECT OF ASPECT RATIO ON COLLAPSE MECHANISM OF RC STRUCTURES: COMPARING DAMAGE PATTERN USING STATIC PUSHOVER ANALYSIS

A.VIMALA¹ and R. PRADEEP KUMAR²

¹ Professor, Head Department of Civil Engg., AGI, Hyderabad, India, vimalace@cvsr.ac.in (corresponding author)

² Professor, Head, EERC, IIT Hyderabad, India, ramancharla@iiit.ac.in

Keywords: Aspect Ratio, Pushover analysis, Expended energy, Global damage

ABSTRACT

Reinforced concrete frame buildings have been widely constructed in seismic-prone regions Worldwide. Under a given earthquake, the level of damage to a structure is greatly influenced by nonlinear capacity of its members. Even when the nonlinear capacities are same, the overall damage is critically influenced by the structure's shape, size and geometry.

Present study assesses the nonlinear performance of the RC frames with different aspect ratios (3, 1 and 0.3). Performance assessments indicate that the structure with an aspect ratio (height to width) 3 shows ground floor mechanism and sudden failure observed after ultimate base shear. The structure with an aspect ratio of 1 shows first and second storey mechanism simultaneously and shows good ductile behavior in nonlinear state. The structure with an aspect ratio of 0.3 significantly changes the collapse mechanism of the frame structure, leading to a third story mechanism and also shows good ductile behavior after ultimate base shear. The results are compared in terms of damage, displacement and plastic hinge pattern.

1. INTRODUCTION

To study the damage profile by applying energy based damage methods, numerical study is carried out for three reinforced concrete structures. These structures are considered to represent low and medium rise RC buildings and the structures are chosen in such a way that their aspect ratio (height to width) is about 3, 1 and 0.3.

To quantify the damage many damage models are proposed in literature, they are classified broadly as local damage indices and global damage indices; the former quantify damage in individual members, at individual joints or at a particular cross section, and the latter damage in the whole structure [1]. A detailed review of damage indices is available in literature [2][3].

Pushover analysis is a simplified procedure for seismic performance evaluation of structures. The ATC-40 [4] and FEMA-356 [5] documents have developed modeling parameters, acceptance criteria and procedures of pushover analysis. Krawinkler and Seneviratna [6] pointed out that a carefully performed pushover analysis would provide insight into structural aspects that control performance during earthquakes. Pushover analysis methodologies are under continuous development. Gupta and Kunnath [7] presented an adaptive pushover method in which external force profile is adjusted in each analysis step taking into account the structure's current dynamic characteristics. Goel and Chopra [8] developed

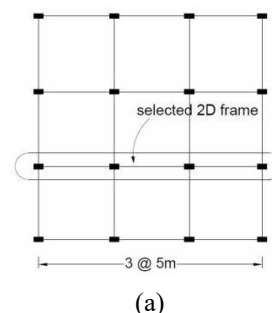
a modal pushover analysis (MPA) which accounts for the contribution of higher modes by conducting separate pushover analyses with external force profile proportional to the structure's significant modes. Mohamed Abdel-basset [9] proved that displacements and curvatures derived from non-linear static response can be used as good damage indicators even for a small amount of damage. Kotanidis and Doudoumis [10] proved that the area under the classic pushover curve (base shear Vs roof displacement) could lead to incorrect estimation of the amount of energy which the structure is able to dissipate.

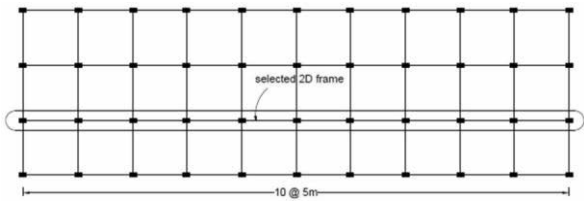
2. DETAILS OF STRUCTURES

Both, 11 and 4 story buildings are 15 m by 15 m in plan (Figure 1). Their typical floor-to-floor height is 4m. The interior frame, as shown in figure 1(a), represents 2-D models of these buildings. The other 4 storey building is 50 m by 15 m in plan (Figure 1) and its floor to floor height is 4 m. The interior frame, as shown in figure 1(b), represents a 2-D model of the buildings.

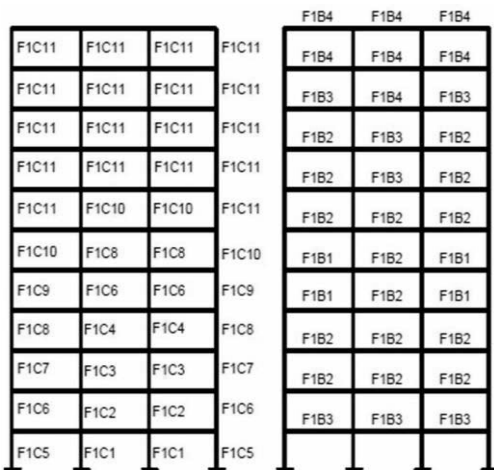
Buildings are designed according to Indian codes of practice for plain and reinforced concrete, IS: 456 and earthquake resistant design IS: 1893. The buildings are assumed to be situated in seismic zone V of IS: 1893–2002, with an intensity of 0.36g ground acceleration. Material properties are assumed to be 20 MPa for the concrete compressive strength, and 415 MPa for steel yield strength, for both, longitudinal and transverse reinforcements.

The 11 storey-3 bay frame is 44m in elevation (Figure 2). Beam, column dimension, amount and arrangement of longitudinal and transverse reinforcement are shown in figure 2. The 4 storey-3 bay frame is 16m in elevation (Figure 3). Beam, column dimension, amount and arrangement of longitudinal and transverse reinforcement are shown in figure 3. The 4 storey-10 bay frame is 16m in elevation (Figure 4). Beam, column dimension, amount and arrangement of longitudinal and transverse reinforcement are shown in figure 4.

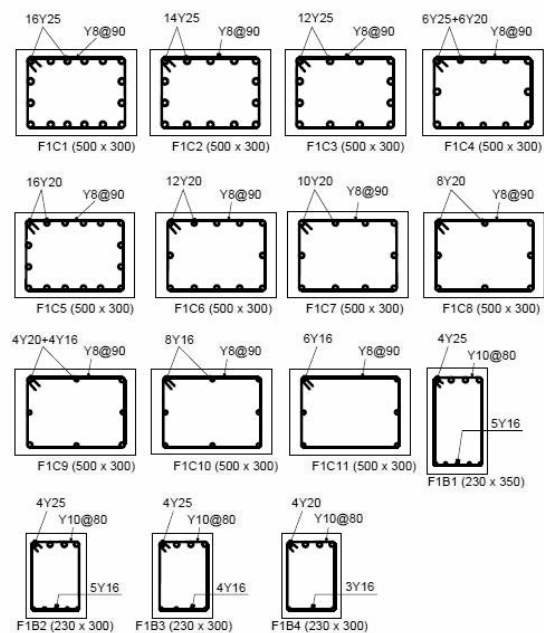




(b)
Figure 1: (a) Plan view of 11 and 4 storey buildings
 (b) Plan view of 4 storeys 10 bay building

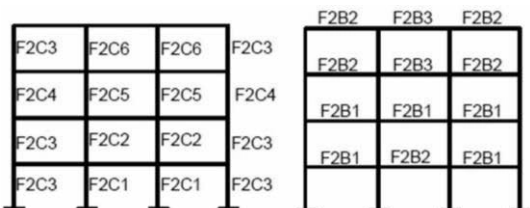


(a) Column labeling (b) Beam labeling

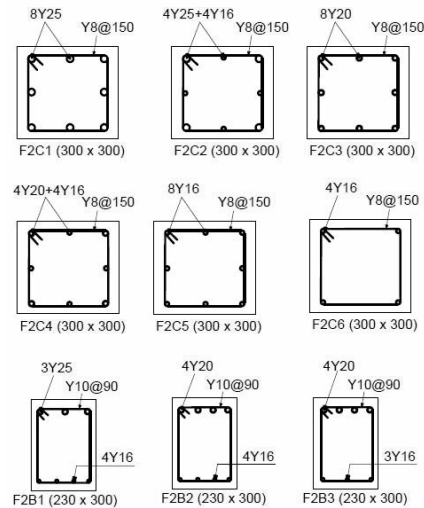


(c) Beam-Column reinforcement detail

Figure 1: Properties of frame-1 (11 storey-3 bay)

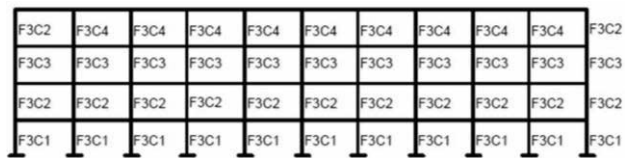


(a) Column labeling (b) Beam labeling

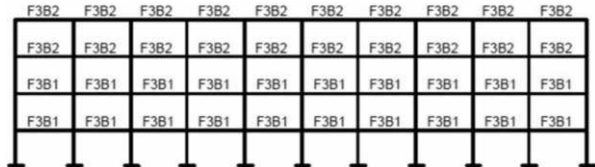


(c) Beam-Column reinforcement detail

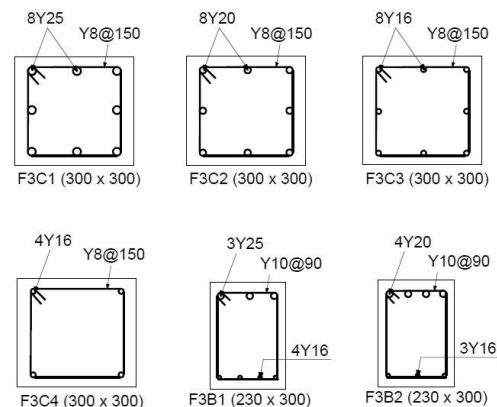
Figure 2: Properties of frame-2 (4 storey-3 bay)



(a) Column labelling



(b) Beam labeling



(c) Beam-Column reinforcement detail

Figure Ошибка! Текст указанного стиля в документе отсутствует.: Properties of frame-3 (4 storey-10 bay)

3. MODELING AND ANALYSIS

A two-dimensional model of each structure is created in SAP2000 to carry out non-linear static analysis. Beam and column elements are modeled as non-linear frame elements with lumped plasticity by defining plastic hinges at both ends of beams and columns. Torsion effect in the structure is neglected.

As shown in figure 5, five points, labeled A, B, C, D, and E define the force–deformation behavior of a flexure plastic hinge. In the present study, failure of each member is considered in two ranges, as shown in figure 5, the first range is load control region in which the member strength carrying capacity increases and it falls in range B to C, the second range is the displacement control range in which the lateral strength carrying capacity decreases drastically, and the member is unreliable in supporting lateral load.

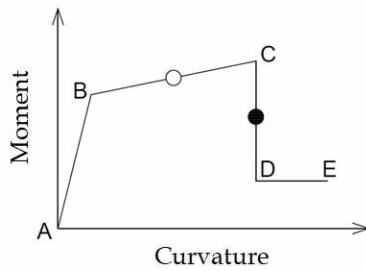


Figure 3: Force–deformation relationship of a typical plastic hinge.

Once the structure is modeled with section properties, steel content and the loads on it, hinges are assigned to the elements, PM hinges for columns and M3 hinges for beams. The structure is subjected to incremental lateral forces with IS1893 load distribution along the height of the structure and the lateral force at any story is calculated from the following formula:

$$F_i = V_b \frac{w_i h_i^2}{\sum_1^n w_i h_i^2}$$

where:

- V_b = Base shear
- w_i = Seismic weight of floor i
- h_i = Height of floor i measured from base
- F_i = Lateral force at floor i

External force profile ratio is shown in figure 4.6 for one of the pushover steps. The Pushover curve, base shear versus displacement at the centre of gravity of external force profile (Figure 6) are plotted to calculate the energy. At any deformation, the area under the curve, represents the total energy absorbed by the structure for particular deformation, which is equal to the work of external loads acting on the structure.

The area under the curve base shear versus displacement at C.G of external force profile, unlike classic pushover curve (base shear versus roof displacement), represents the total input energy dissipated/absorbed by the structure. During elastic response, all input energy is consumed by elastic deformation of structural members.

During elastic deformation, if the structure is unloaded, it returns to its unstressed condition without any remaining deformation and there is no damage to the structure. When external loads exceeds the structure’s yield strength, input energy is being consumed through plastic deformation of yielded structural members, and through elastic deformation of the rest of the structural members, and damage initiate in the structure.

In the expended energy based method, the total energy dissipated by frame in each incremental load step of the

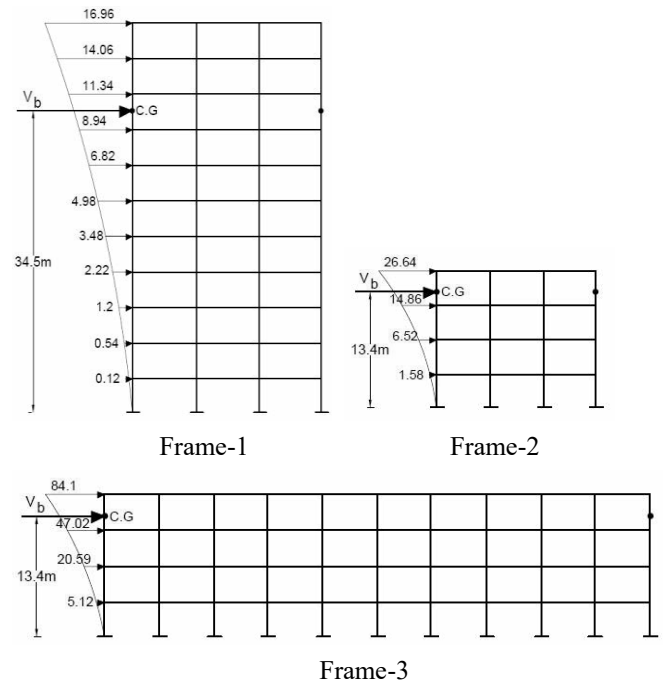
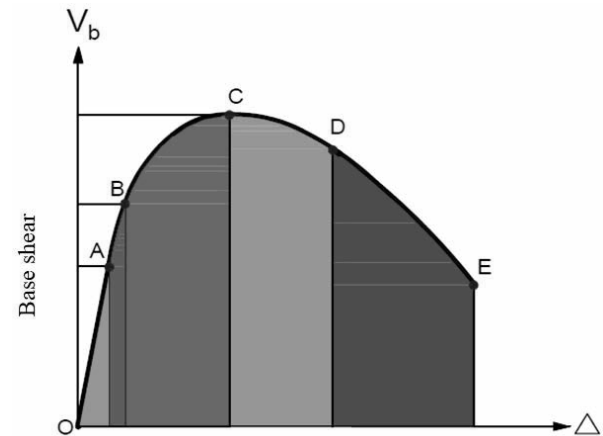


Figure 4: C.G of external force profile for three frames.



Displacement at C.G. of external force profile

Figure 7: Damage estimation critical points

pushover analysis (Figure 7) is calculated as the area under the curve, base shear versus displacement of the frame at the centre of gravity of the external force system, which gives the real meaning of external work done or total energy dissipated by the structure. The damage state of a structure in each incremental load step of the pushover analysis is calculated using energy function. Based on the capacity curve of the structure, the damage state of the structure can be represented as five stages, as shown in figure 7.

Point A indicates the elastic state of the structure, point B indicates the point at which the initial tangent of the curve deviates by 15%, point C indicates the ultimate strength of the structure, point D represents the stage of the structure at which the ultimate strength drops by 15%, point E indicates the collapse stage. The total pushover curve is divided into two parts one is positive slope curve

i.e O to C and named as load control region and another is negative slope curve i.e. C to E and named as displacement control region. Possible damage ranges are shown in table 1.

Table 1: Damage ranges

Range of deformation	Behaviour	State
OA	Elastic	No damage
AB	Strain hardening	Light damage
BC	Ultimate strength	Moderate damage
CD	Strength reduction	Severe damage
DE	Imminent collapse	Extreme damage and collapse

Damage method- 1

The damage index (D_i) is expressed as the ratio of expended energy which is responsible for damage to the total energy capacity of the structure. Figure 4 represents the damage parameters used in the model. The initial elastic energy (E_{ie}) is calculated as the area under the curve up to point 'ie' which is the first yield point of the structure (Figure 8a). E is the energy absorbed by the structure, up to any point 'i', where the damage is to be calculated (Figure 8b). The total energy capacity (E_T) of the structure is calculated as the total area under the pushover curve (Figure 8c).

$$D_1 = \frac{(E - E_{ie})}{(E_T - E_{ie})} \times 100 \quad [1]$$

Where:

- E - Represents the energy dissipated by the structure at any displacement, where the damage is to be estimated.
- E_{ie} - Represents the energy absorbed by the structure under linear displacement.
- E_T - Represents the total energy dissipation capacity of the structure.

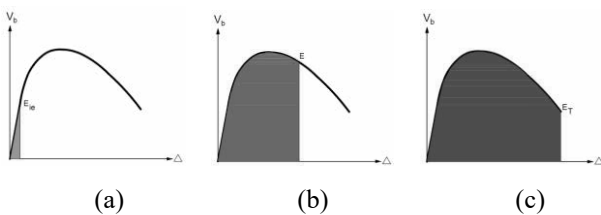


Figure 8: Damage estimation parameters for Method-1

Damage method-2

In this method, the damage parameters are E, E_c , E_T and E_{ie} , where E_c represents restored elastic energy at point i, all other variables are same as damage Method-1. The damage index (D_i) is expressed as the ratio of expended energy at any point i, to the total energy capacity of the structure.

In this method, the instant elastic energy (E_c) at any point i, is the area of the triangle as shown in figure 9. When the damage is to be calculated at the displacement i, at this point when the structure is unloaded, it is assumed that the structure comes back to static position by moving parallel to the initial tangent.

$$D_2 = \frac{(E - E_c)}{(E_T - E_{ie})} \times 100 \quad [2]$$

Where E_c - Represents the instant elastic energy when the structure attains static position.

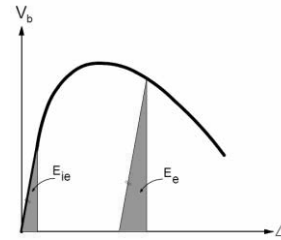


Figure 9: Damage estimation parameters for Method-2

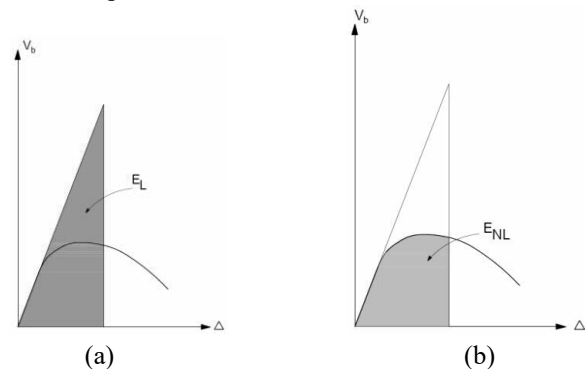
Damage method-3

In this method, damage parameters are energy dissipated under linear response (E_L) and energy dissipated under non linear response (E_{NL}). At any point i, the damage index (D_i) is expressed as the ratio of the expended energy to cause damage at point 'i', to the total energy capacity of the structure to resist damage (Figure 10)

$$D_3 = \frac{(E_L - E_{NL})}{(E_{LT} - E_{NLT})} \times 100 \quad [3]$$

Where

- E_L - Energy under linear response at a displacement where the damage is to be estimated.
- E_{NL} - Energy under non-linear response at a displacement where the damage is to be estimated.
- E_{LT} - Energy under linear response at maximum displacement of the structure.
- E_{NLT} - Energy under non-linear response at maximum displacement of the structure.



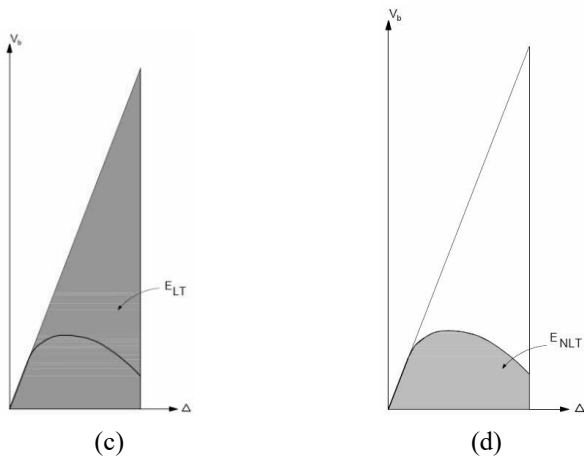


Figure 10: Damage estimation parameters for Method-3

4. RESULTS AND DISCUSSION

To carry out displacement based pushover analysis, target displacement needs to be defined. The target displacement for 11 storey frame is defined as 4% of drift i.e 1.76 m. The structure reached an unstable state at a displacement of 0.92 m i.e at a drift of 2%, where all base columns failed and entered the displacement control region, in which the structure is not reliable enough to support lateral loads any more. In this case, neither structure reached 4% of the drift or 2/3 of the ultimate strength. So the damage state of the structure was assumed to be 100%, at structural instability. For this structure, D and E points (Figure 11) were located at the same point, which depicts that the structure became unstable even before the ultimate base shear reduced by 15%. The damage profile of method-1 is almost linear; method-3 profile resembles the deflection profile of the structure. The profile of damage method-3 clearly depicts, the curve becoming almost straight after point C, this means that the damage increases rapidly from point C to D, which depicts the real behavior of the structure. At point C, where the strength degradation starts, one of the bottom storey columns entered to displacement control region, at which the member cannot be relied upon, to support lateral loads. When any member enters to displacement control region, the strength carrying capacity of the structure start decreases. After crossing point C, the structure attained an unstable state by entering all bottom storey columns into the (Figure 12)displacement control region.

The four storey 3-bay frame attained an unstable state at a displacement of 0.33 m i.e., at a drift of 2.1%, where some columns of storey-2 and storey-3 failed, and entered into the displacement control region, in which the structure was not reliable enough to support lateral loads any more. For this structure, points D and E were located at the same point (Figure 13), which shows that the structure became unstable even before the ultimate base shear reduced by 15%. Hinge formation is shown in figure 14. At point B, where the stiffness of the structure reduce by 15%, some beam and column members yielded. After crossing point C, the structure attained an unstable state by entering a few other columns of the

second and third storey into the displacement control region and the structure attained an unstable state, without reaching 4% drift.

Frame 3 with an aspect ratio of 0.3, reached unstable state at a displacement of 0.4 m i.e, at a drift of 2.6% (Figure 15), where almost all columns of storey-3 failed and entered the displacement control region, in which the structure was not reliable enough to support lateral loads any more. Hinge formation is shown in figure 16. At point B, where the stiffness of the structure reduced by 15%, no member reached the displacement control region. At point C, the third storey columns entered the displacement control region. At point D, total instability for storey 3 was attained, which continued till point E. finally, the damage was concentrated at storey-3.

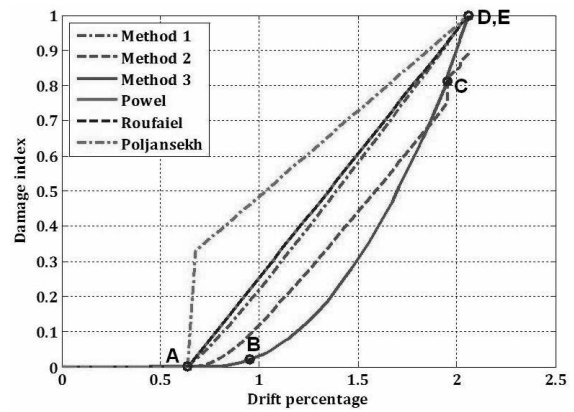


Figure 11: Damage profile for frame-1

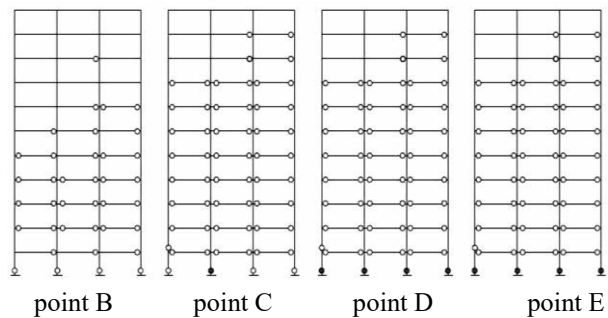


Figure 5: Hinge pattern for frame-1

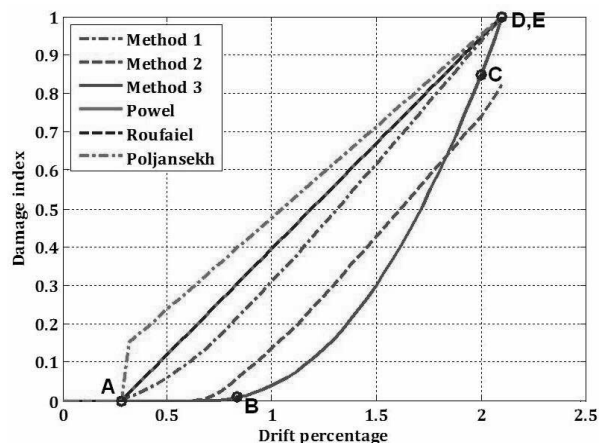


Figure 6: Damage profile for frame-2

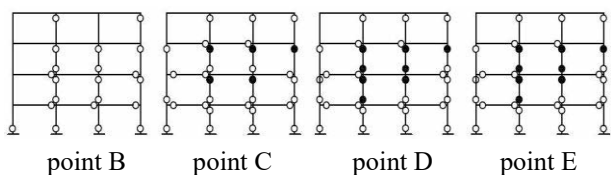


Figure 7: Hinge pattern for frame-2

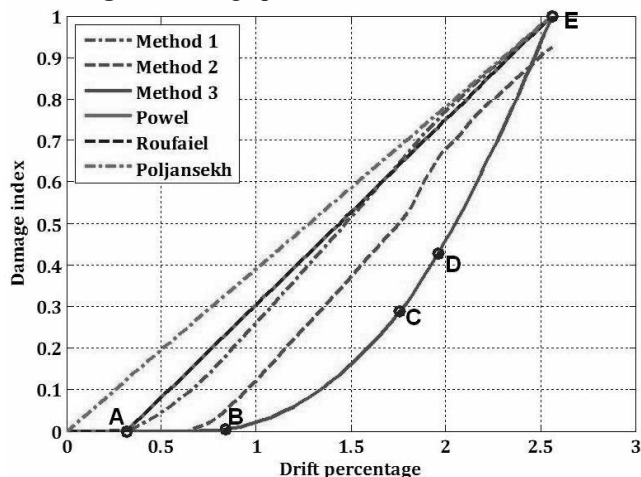


Figure 15: Damage profile for frame-3

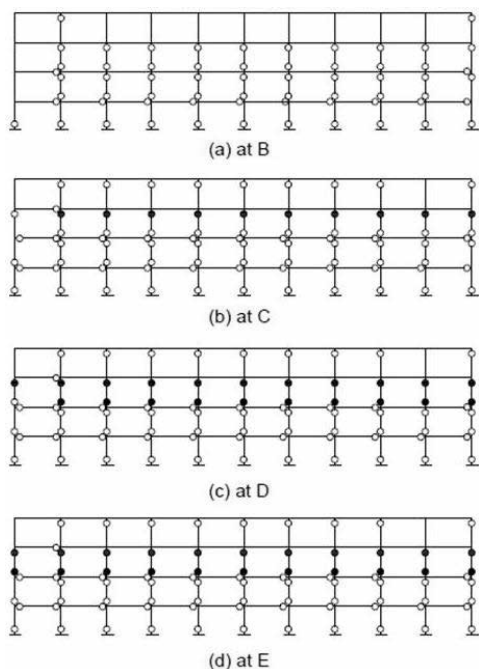


Figure 16: Hinge pattern for frame-3.

5. CONCLUSIONS

For all frames damage method-3 gave lower values where damage metho-1 gave higher values and method-2 gave unrealistic values. Among three methods method-3 gave accurate and realistic values. At any deformation method-3 clearly depicts, at what cost of energy damage has taken place unlike other methods includes linear members energy also in calculation of damage.

The 11 storey structure with an aspect ratio of 3 failed at 2% drift, and the four storey structure with an aspect

ratio of 0.3 failed at 2.6% drift, this shows, as aspect ratio decrease drift caring capacity increases.

And another observation from the results is that the 11 storey frame became unstable immediately after point 'C', but the later frame shown good ductility and has greater margin for total collapse this indicates that, increase of aspect ratio also decreases ductility capacity of the structure.

REFERENCES

[1] Kappos, A.J. (1997). Seismic damage indices for RC buildings: evaluation of concepts and procedures. *Progress in Structural Engineering and Materials*, 1(1), 78-87.

[2] Williams, M.S. and Sexsmith, R.G. (1995). Seismic damage indices for concrete structures: A State-of-the-Art Review. *Earthquake Spectra*, 11(2), 740-757.

[3] Padilla, D., and Rodriguez, M. (2009). A damage index for the seismic analysis of reinforced concrete members. *Journal of Earthquake Engineering*, 13(3), 364-383.

[4] Applied Technology Council (ATC), *Seismic Evaluation and Retrofit of Concrete Buildings*, ATC 40-1996, California.

[5] Federal Emergency Management Agency (FEMA), *Prestandard and Commentary for Seismic Rehabilitation of Buildings*, FEMA 356-2000, Washington D.C., USA

[6] Krawinkler H., Seneviratna G.D.P.K. (1998): Pros and Cons of a Pushover Analysis of Seismic Performance Evaluation, *Engineering Structures*, Vol.20, 452-464.

[7] Gupta B. and Kunnath S. (2000). Adaptive Spectra-Based Pushover Procedure for Seismic Evaluation of Structures, *Earthquake Spectra* 16(2), 367-390.

[8] Goel R. K. and Chopra A. K. (2002). Reversal in higher mode Pushover curves and its implications on implementation of the MPA procedure. Report distributed to participants in project ATC-55, Applied Technology Council, Redwood City, California.

[9] Mohamed Abdel-basset abdo (2012). Parametric study of using only static response in structural damage detection. *Engineering Structures*, 34, 124-131.

[10] Kotanidis C. and I.N. Doudoumis (2008). Energy-based approach of static pushover analysis. Proc. The 14th World Conference on Earthquake Engineering, October 12-17, 2008, Beijing, China.

[11] Powell GH and Allahabadi R. (1988). Seismic damage prediction by deterministic methods: concepts and procedures. *Earthquake Engineering and Structural Dynamics*, 16, 719-734.

[12] Poljansek K., and Fajfar P. (2008). A new damage model for the seismic damage assessment of reinforced concrete frame structures, Proc. The 14th World Conference on Earthquake Engineering, 12-17 October 2008, Beijing, China.

[12] Roufaiel MSL and Meyer C. (1987). Analytical modeling of hysteretic behaviour of R/C frames. *Journal of Structural Engineering (ASCE)*, 113(3), 429-444.

FIELD INVESTIGATION ON A SINKHOLE DEVELOPED IN LOOSE VOLCANIC SOIL

R. KUWANO¹, N. KOMINAMI², M. OTSUBO³, and I. SATO⁴

¹ Professor, Institute of Industrial Science, The Univ. of Tokyo, Japan, kuwano@iis.u-tokyo.ac.jp (corresponding author)

² Former graduate student, Dept. of Civil Engineering, The Univ. of Tokyo, Japan, naotokominami@gmail.com

³ Research associate, Institute of Industrial Science, The Univ. of Tokyo, Japan, otsubo@iis.u-tokyo.ac.jp

⁴ Graduate student, Dept. of Civil Engineering, The Univ. of Tokyo, Japan, i-sato@iis.u-tokyo.ac.jp

Keywords: Volcanic soil, Sinkhole, Field investigation, Piping

1. INTRODUCTION

Due to the typhoon on Sept.19, 2016, a large sinkhole occurred in a sweet-potato field of Miyakonojo, Miyazaki, leading to a soil outflow of 1500m³ to the road nearby through a piping hole, as shown in Figure 1. The size of sinkhole was 31m long, 13m wide and 7m deep. Fortunately, there were no human casualties, but sinkholes may lead to serious accidents depending on the time and place of occurrence. It is important to investigate the cause and take measures to prevent these accidents. The area is covered by the volcanic soil, called “Shirasu”, which generally has low density and high permeability. Surveys including dynamic cone penetration tests and surface wave surveys were conducted to identify the locations of cavities, water paths and loosened ground.

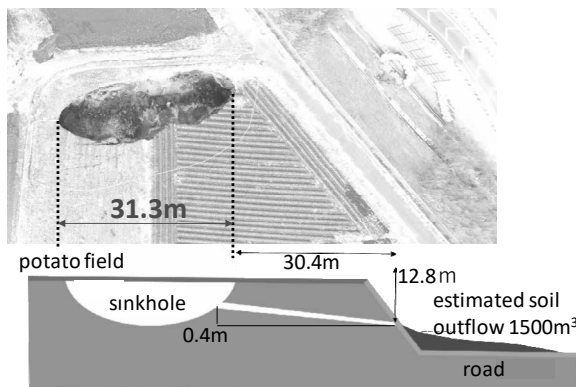


Figure 1: Outline of Miyakonojo sinkhole (2016)

2. FIELD INVESTIGATION

Some of the results of dynamic cone penetration test conducted around the sinkhole are shown in Figure 2. At points A, B, C and E, near the sinkhole, the N_d values were small, less than 10. At point B, a clear cavity ($N_d=0$) of about 2m was observed at 10m deep. While at point D, about 100m away from the sinkhole, N_d values increase at the depth of more than 6m. Further dynamic cone penetration tests indicated that the relatively stiff thin layer existed in the west side of the sinkhole at 4m deep. Surface wave survey was conducted on 6 lines as indicated in Figure 3 and ground structure was obtained. The results obtained from the surface wave survey showed reasonable agreement with those from dynamic cone penetration tests. Loosened ground was observed in the west side of the sinkhole and the presence of water pathway was suspected.

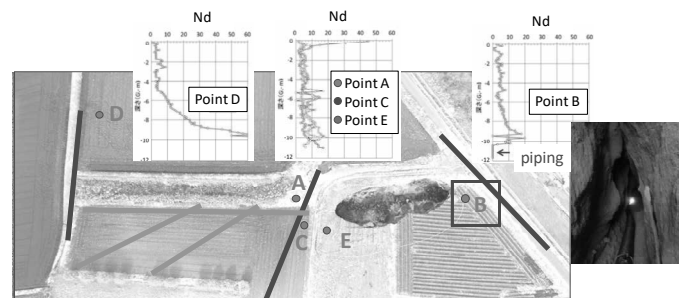


Figure2: Dynamic cone penetration test

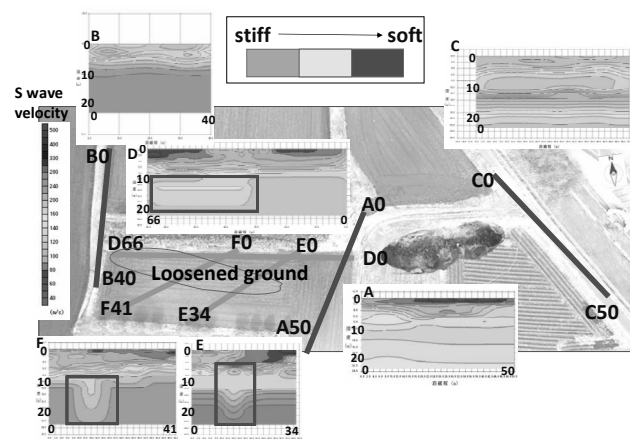


Figure3: surface wave survey

3. FORMATION OF SINKHOLE

Very loose Shirasu layer was identified above the impermeable clayey layer at the depth of about 12m. Water paths seemed to form within Shirasu layer and Shirasu was subjected to internal erosion. A relatively stiff layer was also found at a depth of 4m, below which the erosion seemed to be accelerated as schematically shown in Figure 3. Surface wave survey results indicated that water paths, the potential cause of sinkholes, were further extended. Judging from elongated shape of the sinkhole, two or three sinkholes simultaneously or successively occurred above the water paths.

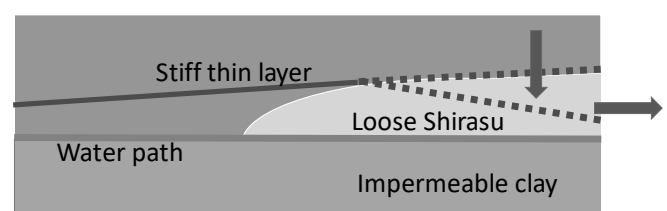


Figure4: Mechanism of sinkhole formation

SYSTEM FOR PREVENTING FLAKING OF LINING CONCRETE IN SUBWAY TUNNEL

Saki NEMOTO¹, Shinji KONISHI², Daisuke TANAKA³, Yuki ENOKIDANI⁴ and Naoki IMAIZUMI⁵

¹ Engineer, Infrastructure Maintenance Dept., Tokyo Metro Co., Ltd., Tokyo, Japan, s.nemoto.g3t@tokyometro.jp (corresponding author)

² Department Manager, Infrastructure Maintenance Dept., Tokyo Metro Co., Ltd., Tokyo, Japan, s.konishi.r4r@tokyometro.jp

³ Engineer, Infrastructure Maintenance Dept., Tokyo Metro Co., Ltd., Tokyo, Japan, d.tanaka@tokyometro.jp

⁴ Engineer, Infrastructure Maintenance Dept., Tokyo Metro Co., Ltd., Tokyo, Japan, y.enokidani@tokyometro.jp

⁵ Assistant Manager, Infrastructure Maintenance Dept., Tokyo Metro Co., Ltd., Tokyo, Japan, n.imaizumi@tokyometro.jp

Keywords: Subway tunnel, Flaking, Spalling, inspection, Visible Image, Infrared Thermography

1. GENERAL INSTRUCTIONS

Tokyo Metro Co., Ltd. (“Tokyo Metro”) currently operates nine subway lines over 195.1 km of track (532.6 km of track if through services are included) and transports roughly 7.24 million passengers per day; Tokyo Metro is an integral part of the massive railway network of the metropolis of Tokyo. However, by 2020, the year of the Tokyo Olympics, 52.6% of Tokyo Metro’s tunnels will be at least 50 years old, a fact that heightens the importance of daily maintenance toward continuing to provide services into the future while ensuring safety and security for passengers. Tunnels comprise 85%, or 166.8 km, of the subway lines operated by Tokyo Metro. Nonetheless, safe and consistent operation is provided through appropriate maintenance that complies with Maintenance Standards for Railway Structures.^{1,2}

When fragments of concrete peel away from the lining of railway tunnels, emergency inspections are normally conducted of entire lines to check whether peeling is occurring in other locations, and locations that appear to be at risk for peeling are determined and then treated. The work of determining locations is extremely physically demanding, and the fact that it is also urgent means that there is a risk of peeling being overlooked. Therefore, a highly precise, efficient method of determination is desirable.

In light of these circumstances, Tokyo Metro used inspection data, visible image data (digital data) (Figure 2), and infrared thermography data from all tunnel sections under our ownership to research and develop a system that can automatically determine spalling and peeling on the basis of statistical analysis and image analysis technology. This report summarizes the four methods that were used, and describes Tokyo Metro’s system for preventing peeling.

2. SYSTEM for DETERMINING SPALLING and PEELING LOCATIONS USING VISIBLE IMAGES

Tokyo Metro presently has visible image data from all nine subway lines, and a digitized database of the records

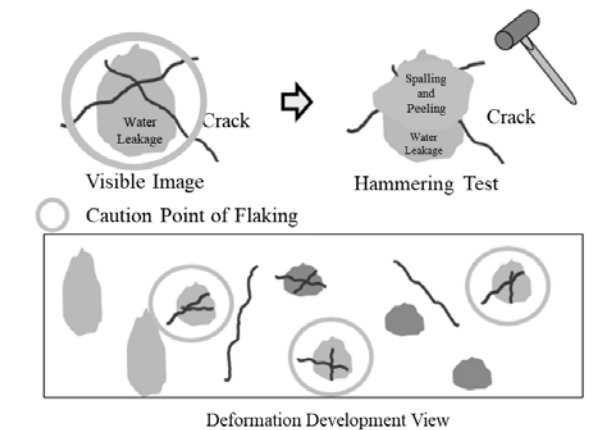


Figure 1. Revealed Rules Image

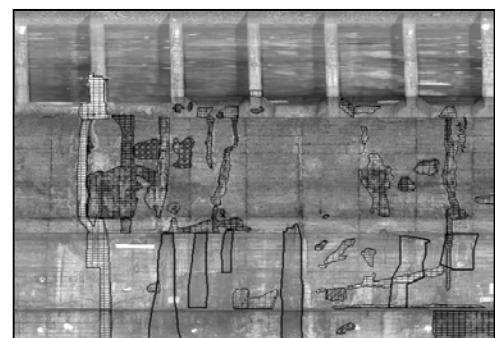


Figure 2. Visible Image (Database)

of cracks, leakage and other forms of deterioration revealed by the data. This database is being used to develop a system for detecting the locations of spalling and peeling. When components peel away and fall off of structures on railway lines, total inspections are conducted to check for similar locations. This is extremely difficult to carry out in a short period of time given the vast number of cases of structural deterioration occurring over long distances in the tunnels. Thus, a system is being developed that uses image recognition technology to determine locations that closely resemble the previous states of locations where concrete peeled and fell off.

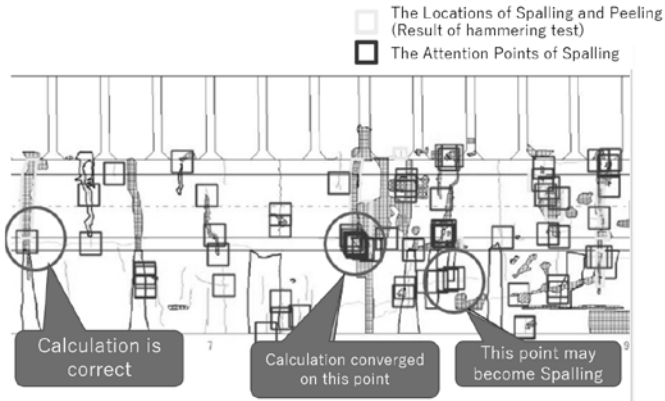


Figure3. Calculation Image Using Visible Images

Development and testing is continuing on a program for critical deterioration patterns (the pattern in which two instances of deterioration cross and the pattern where they develop in parallel), and in test zones 98% of spalling and peeling locations detected in general inspections have been successfully detected.

However, using only visible images resulted in over-detection due to the way the deteriorations were grouped and for other reasons. In addition, it is obviously impossible to detect potential spalling or peeling when locations show no surface deterioration on visible images. Therefore, infrared thermography projections of spalling and peeling locations, as detailed below, were added to increase the precision of the detection system.

3. INFRARED THERMOGRAPHY

The surfaces of tunnel walls are warmed by heat from passing trains during operating hours. The surfaces are quickly cooled at night once cold, outdoor air circulates through the tunnels after last trains, but locations where spalling exists cool more easily, resulting in temperatures that differ from those of healthy locations. Ways to use infrared cameras to detect these differences are currently

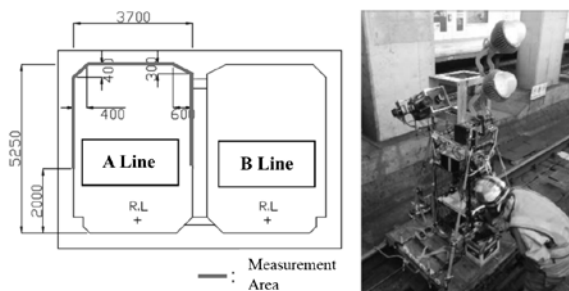


Figure 4. How to Measure Using Infrared Thermography

being considered. The evidence gathered from actual tunnels over the past three years has taught us the following:

(1) Temperature differences of at least 0.03°C between the concrete in healthy parts and in places where spalling exists can be detected

(2) The differences described in (1) occur when the temperature difference between the air inside tunnels and the concrete is at least 0.35°C

(3) Cold winter days are ideal for taking measurements because the differences described in (2) often occur when the outside air temperature is 5°C to 10°C or lower

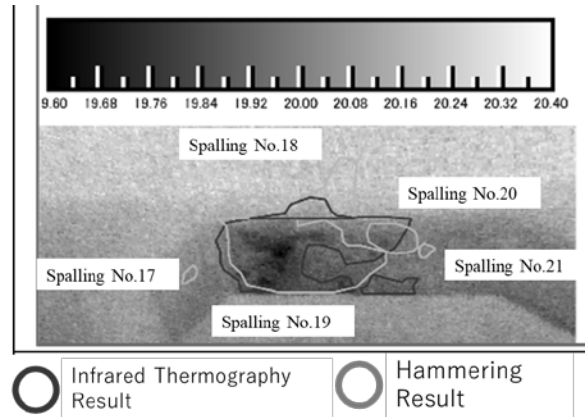


Figure 5. Calculation Image Using Infrared Thermography

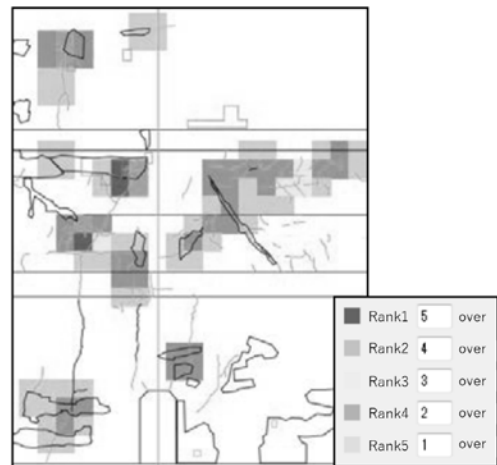


Figure6. Calculation Map of Flaking

Now that measurements are taken under these conditions, it has become possible to detect roughly 95% of spalling and peeling discovered during general inspections in shield tunnels, and roughly 80% in open-cut tunnels.

In addition, in some sections infrared thermography was used after general inspections to detect problems other than those detected in the inspections, and further hammering tests were conducted in those locations. As a result, it is now understood that spalling and peeling actually exists in roughly 55% of locations where the use of infrared predicted spalling and peeling not detected in general inspections. Essentially, spalling and peeling was successfully detected in locations where it could not have been discovered visually.

In addition, hammering tests were conducted over entire surfaces in some of the areas where analysis was conducted to investigate the extent to which problematic

locations that general inspections failed to reveal were being detected. It was found that 22% of the instances of deterioration newly discovered by hammering tests of entire surfaces could be detected. The simplest way to detect spalling and peeling in locations with no visible surface deterioration is to conduct hammering tests over entire surfaces; however, since this is physically impossible to do over entire lines, the infrared thermography method holds promise as an effective inspection tool.

However, while it has been shown that inspections are highly precise near stations, ventilation openings and other locations where air circulates through underground spaces and where temperature changes occur easily, they are not as precise between stations, where there are no ventilation openings and where temperature changes are slight. It is imperative to further increase the number of verifications to carefully examine the threshold in the second of the three environmental conditions described previously (when the temperature difference between the air inside tunnels and concrete is at least 0.35°C) in order to expand the scope of application for this method.

In addition, as explained in Section 2, work is under way to improve the accuracy of predictions of spalling and peeling by combining these efforts with the system for determining spalling and peeling locations using visible images. As part of the consideration toward implementing this technology in the field, a heat map like the one in Figure 5 was used to visualize the combination of the two methods of prediction so that a single glance is all it takes to establish the priority of locations to hammer and eliminate locations that do not require hammering. However, the lack of landmarks in tunnels makes it difficult to conduct hammering tests in the field using heat maps. Therefore, ways to reproduce this method in the field are continuously being considered.

4. BAYESIAN NETWORKS

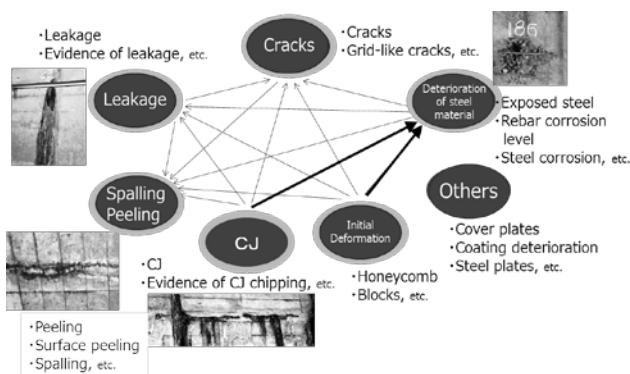


Figure 7. Image of Bayesian Networks

Tokyo Metro is working on the development of a method based on statistical methodology to determine locations that may have been overlooked during inspections.

This method uses causal relationships between deterioration types to predict the locations of these deteriorations. For example, given the two deterioration types of

cracks and leakage, and the conditional probabilities that leakage also occurs where cracks have occurred, and that cracks also occur where leakage has occurred, it is apparent that the causal relationship is stronger where the observation probability is higher. This probabilistic model that efficiently calculates conditional probabilities between variables is called a Bayesian network.

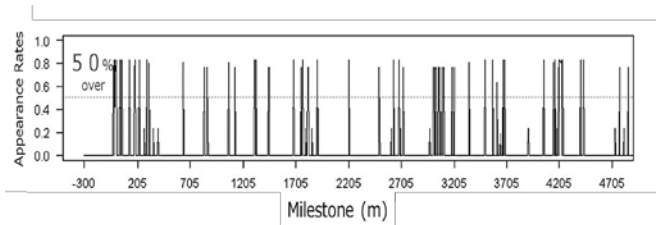


Figure 8. Calculation Image of Bayesian Networks

For example, while leakage may not have been observed in a particular location to date, the presence of spalling, peeling, cracks and other forms of deterioration (as detected in inspections) should mark that location as a place where leakage could easily occur. In other words, it is possible to estimate locations where leakage has a high likelihood of being overlooked. This method can be used to discover locations where it is highly likely that spalling or peeling has been overlooked.

Figure 8 shows an actual subway line. Although it is highly probable that some locations may have been overlooked during inspections, hammering tests can be conducted in those locations to efficiently discover spalling and peeling not seen before. This method is straightforward for everyone because the results are expressed as probabilities. Therefore, verification of the validity of the models is under way, and the feasibility of implementing this method is being considered.

5. STATISTICAL ANALYSIS OF INSPECTION DATA AND STRUCTURE SPECIFICATIONS

#	Variable Name	Partial Regression Coefficient (Absolute Value)	Partial Regression Coefficient
1	Upper Floor Slabs × Leakage	0.09	0.09
2	Upper Floor Slabs × Repair	0.07	0.07
3	Upper Floor Slabs × Vertical Cracks	0.06	0.06
4	Upper Floor Slabs × Initial Repair	0.05	0.06
5	Lower Geological Features : Silt	0.05	0.06
6	Side Wall × Spalling & Peeling	0.05	0.05
7	Overburden's Amount of Change : Under 0.76m	0.04	-0.04
8	Upper Geological Features : Silt	0.04	0.04
9	Center Part Geological Features : Silt	0.03	0.03
10	Middle Wall × Slanting Cracks	0.03	-0.03

Figure 9. C-Line Discriminant Impact Results

In addition to inspections required by ministerial ordinance, Tokyo Metro conducts hammering tests of all subway lines at least once every four years. These tests—in particular, tests of upper floor slabs—require an immense amount of work to prepare the scaffolding and perform the other tasks in the limited amount of time

between the last train on one day and the first train on the next day. Therefore, the test frequency must be optimized and the sections selected wisely.

Toward that end, development is proceeding with the aim of streamlining hammering test work by predicting sections of upper floor slabs susceptible to deterioration via the analysis of specifications, environmental data, and inspection and test data.

Two methods are used to conduct this analysis. Under the first method, the aim is to fully understand statistical trends by using map visualization to confirm typical distributions of deteriorated locations in terms of geographical space, and histograms of numbers of deterioration cases in tunnels. Under the second method, statistical methods are used through cluster analysis, t-tests, relativity analysis, multiple regression analysis and the like (Figure 9).

Presently, various elements are analyzed such as construction years and completion years to determine and sort factors with the highest relativity to the occurrence of spalling and peeling. The results of this analysis have been used to identify sections susceptible to deterioration and create scatter diagrams to visualize the sections. (Figure 10)

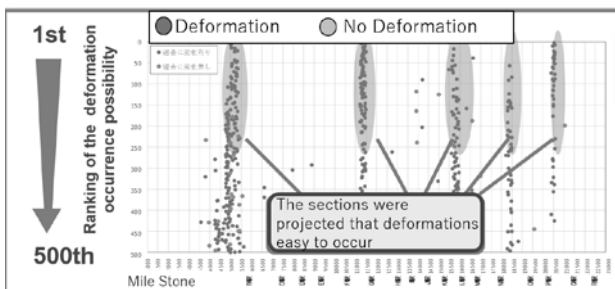


Figure 10. Example of Visualize Which Area Susceptible to Deterioration

The results of this statistical analysis were used to conduct interviews with actual inspectors as to whether they are satisfied with the factors (explanatory variables) with the highest relativity to the occurrence of spalling and peeling and the sections projected as susceptible to spalling and peeling. The inspectors expressed a high level of satisfaction with the analysis when it identified highly deteriorated sections that they recognized from their experience in the field. However, the inspectors were disappointed with the discriminant analysis when the results revealed variance in the distribution of lines that made trends difficult to interpret, or when the results failed to assign high priority to sections that they knew from experience to be deteriorated. In addition, because the same explanatory variables produced extreme differences in the level of satisfaction between respondents, new interviews are being conducted as to the discrepancies with engineering knowledge, and the results compared.

This model makes it possible to identify factors in line with objectives through the selection of discriminant properties while referring to two performance curves. (Figure 11) For example, it is estimated that using a

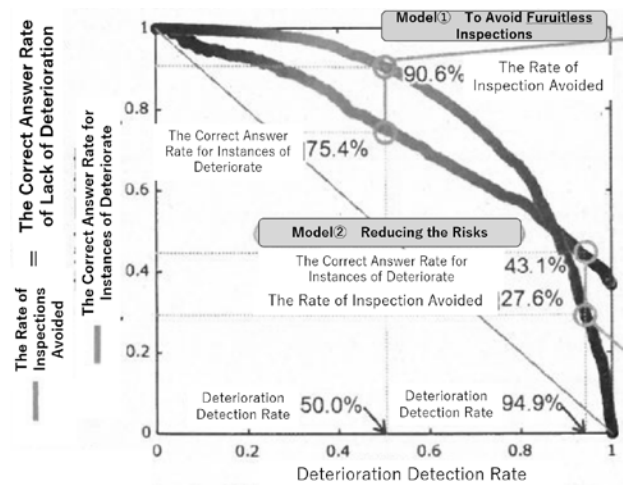


Figure 11. Two Performance Curves

model designed to avoid fruitless inspections by emphasizing the rate of inspections avoided (the correct answer rate for lack of deterioration) enables us to improve the correct answer rate for instances of deterioration (the probability of discovering structural deterioration via hammering) 2.06 times over hammering tests over entire sections, thereby reducing the work of fruitless inspections (hammering tests that result in no deterioration being found) by 90.6%; 50% of deterioration locations can be detected with 9.4% of the workload.

Or, if a discriminant model designed to emphasize risk reduction by emphasizing deterioration detection rates (the lack of unexpected results) is used, it is possible to reduce the workload by 27.6% while maintaining a deterioration detection rate of 94.9% (5% unexpected results). The plan going forward is to proceed with investigations into the selection of discriminant properties and setting of thresholds to serve as evaluation indices for different applications of the results of analysis.

6. PRACTICAL APPLICATIONS

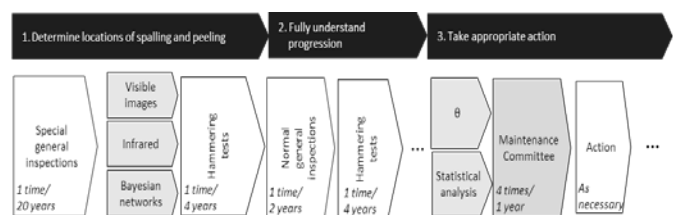


Figure 12. Proposed Flow of Operations for Preventing Concrete from Peeling Away and Falling Off

Figure 12 shows the process being considered for everything from detecting to taking action against spalling and peeling. Regular implementation of the guidelines in the three stages explained to this point can deliver excellent results over the short term as well as the long term.

For example, the ability to establish places to hammer (and places not to hammer) in the voluntary hammering tests that are being conducted once every four years not only introduces variation to these tests, but also enables



Picture1. Scenes from a Maintenance Committee Meeting

Section	Attention Rank
<p>Ex) OO Sta. ~ ▲▲ Sta. A5B Line * k*** m~* k*** m</p> <p>Write deformations which soundness were ranked up.</p> <p>● History * Ex) Because high level groundwater, it was difficult to construct this tunnel.</p> <p>● Carbonation * Ex) None</p> <p>● Salt Damage * Ex) None</p> <p>● Result of Levelling * O:None</p> <p>● Displacement of Inner Section * O:None</p> <p>● Information of Proximity Construction * Ex) B class * S/C/O Building Construction (20***~20**)</p> <p>Ex) Because of high groundwater level, there are a lot of water leaks.</p>	<p>None / Follow Up / Warning</p> <p>Survey Matter / Counter-Measure</p> <p>Ex) Follow up in the Next General Inspection.</p> <p>Ex) Take a visible image in this section.</p>
<p>Ex) Double track shield tunnel</p> <p>Ex) Because of water leakage, it has a risk of flaking caused by rebar corrosion.</p>	

Figure 13. Documents for a Maintenance Committee Meeting

the effective and efficient distribution of limited human and financial resources when drafting short-term maintenance plans (daily inspections).

In addition, Tokyo Metro has established an internal maintenance committee to provide a venue to discuss maintenance policy and other issues for each line. This committee discusses plans for short-term maintenance (daily repairs) and long-term maintenance (major repairs) that incorporate preventive maintenance in light of the results of various inspections, investigations, the statistical analysis described previously, past repairs and more.

In other words, analyzing the results of inspections and daily measurements in long-term maintenance plans makes it possible to identify sections potentially at risk of deterioration. As a result, highly explicit preventive maintenance and other maintenance plans can be drafted for each line, including plans to investigate root causes and propose countermeasures, as well as policy for major repairs and reinforcement. (Figure 13)

7. SUMMARY

Tokyo Metro has taken various approaches toward working to prevent concrete tunnel lining from peeling away and falling off. The effectiveness of the individual methods has been proven along the way; thus, our aim is to integrate them into overall maintenance operations, and to keep implementing these systems until they become a natural part of operations. By doing so, Tokyo Metro is striving to perform high-level tunnel maintenance that will contribute to the continuation of

secure, safe and consistent operation.

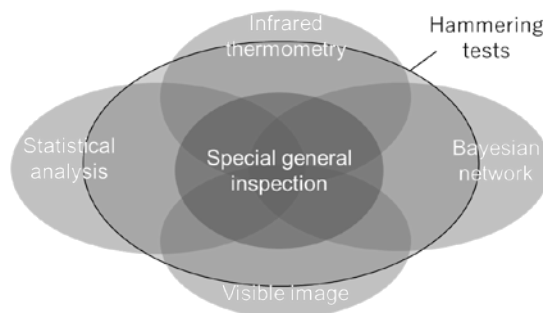


Figure 14. Conceptual Diagram of Method of Determining Potential Locations of Spalling and Peeling

8. REFERENCES

- [1] Railway Technical Research Institute: “Maintenance Standards for Railway Structures and Commentary (Structures): Tunnels,” Editorial Supervision by the Railway Bureau, Ministry of Land, Infrastructure, Transport and Tourism, Maruzen, 2007.
- [2] Kubo et al.: “Consideration toward Using Infrared Thermography to Improve Detection of Spalling and Peeling of Tunnel Concrete,” Summary of 72nd Annual Academic Lectures, Vol. VI, 6-939, 2017.
- [3] Wakuta et al.: “Prediction of Subway Tunnel Sections Susceptible to Upper Floor Slab Concrete Peeling and Falling Off Based on Multiple Regression Analysis,” Summary of 72nd Annual Academic Lectures, Vol. VI, 6-529, 2017.
- [4] Shinohara et al.: “Developing a System for Automatic Extraction of Locations Susceptible to Concrete Peeling Using Image Recognition Technology,” Department of Proceedings of the 26th Tunnel Engineering Committee Meeting, 2016.
- [5] Shinozaki et al.: “Analysis of Causal Relationship of Deterioration Occurrence via Bayesian Network Using General Inspection Results,” Summary of the 70th JSCE Annual Academic Lectures, Vol. VI, VI-343, 2015.

USMCA 2018

SESSION 8

DISASTER MANAGEMENT II

Dolomite rock sand as fine aggregate replacement for secondary construction activities: a comparative study

A.C Bharath KRISHNAA^{1*}, R Vineeth^{2*}, S Malavika Sasi^{3*}, C Prakash^{4*}, M Ananthkumar^{5*}

¹ Student, Civil Engineering, Amrita Vishwa Vidyapeetham, Coimbatore, India, bharathkrishnaa5@gmail.com

² Student, Civil Engineering, Amrita Vishwa Vidyapeetham, Coimbatore, India, vineethrengaraj538@gmail.com

³ Student, Civil Engineering, Amrita Vishwa Vidyapeetham, Coimbatore, India, malavikasdharan@gmail.com

⁴ Assistant Professor, Civil Engineering, Amrita Vishwa Vidyapeetham, Coimbatore, India, pen2prakash@gmail.com

⁵ Assistant Professor, Civil Engineering, Amrita Vishwa Vidyapeetham, Coimbatore, India, amritananth@gmail.com

KEYWORDS: DRS- Dolomite Rock Sand, M Sand, Compressive Strength, Fine Aggregates, Sustainable, Life Cycle Analysis, Coimbatore.

This paper attempts to study the use of Dolomite rock sand (DRS) as fine aggregate replacement to conventional manufacture sand (M sand) considering the increasing demand from construction industry and depleting M sand availability. DRS as fine aggregate (FA) replacement might be a sustainable option. DRS was chosen for this study, since it's locally available and is present in abundance in the region of Coimbatore. Further, its transportation within the region proves to be cost effective in comparison with river sand. Design mixes were prepared to achieve concrete grades of M20, M25 and M30 for FA replacement by 0, 20 and 30 % for each concrete grade. Tests were conducted to check the 28 day compressive strength of concrete. The results of the study showed that for all concrete grades, 20-30% of FA replacement by DRS was found to be suitable. Further, comparative analysis was performed between river sand and DRS replacement for considering the suitability of DRS replacement concrete for various secondary construction activities. DRS showed better performance in structures which are not subjected to heavy loads and thus could be a sustainable replacement for M sand.

Table 1 : Compressive strength of concrete with variation in DRS % for grades of 20 25 and 30.

Compressive Strength (N/ mm ²) after 28 days			
CONCRETE GRADE	10% REPLACEMENT	20% REPLACEMENT	30% REPLACEMENT
M20	19.7	19.6	18.9
M25	24.8	24.3	23.7
M30	30.2	29.5	28.6

Table 2 : Comparison of parameters for the two different Fine Aggregates

Parameters	M Sand	Dolomite Rock Sand
Specific Gravity	2.59	2.704
fineness modulus	3.1	2
Water Absorption	1.8%	1.3%



Figure 1: Cubes casted with Dolomite Rock Sand

Preliminary tests were carried out on the aggregates and the design mix was calculated based on the values obtained from Table 2. Specific gravity of cement used was 2.95.

Life cycle analysis was done on the basis of “Cradle to Grave “of processing of Dolomite Rock sand from its production to usage. By using DRS we are able to form a closed loop system. DRS which is a waste product of cement factory in Coimbatore proves to be cost efficient in its transportation.

Conclusion:

Based on the experimental data it was found that Dolomite Rock Sand proves to be efficient when combined with M sand in proper proportions and helps us achieve the desired strength. The result of the compressive strength test proves that it can also be used in structural elements. This report provides a platform to achieve sustainable development and prevents exploitation of river sand , reduces the usage M Sand. Thus, this can be implemented in places with abundant lime stone deposits and takes us a step closer to environmental sustainability and development.

References:

1. Ž. Rudžionis, E. Ivanauskas and M. Senkus, “The Analysis of Secondary Raw Materials Usage in Self-Compacting Concrete Production,” *Materials Science*, vol. 11, no. 3, pp. 272–277, 2005.
2. Viktor Vaganov, Andrey Kireev, Sergey Avdeev, Genādijs Šahmenko, Māris Šinka, "Prospects for Effective Use of Dolomite in Concrete Compositions", *Construction Science* 19 (1), 27-32, 2016.
3. “Building Construction” By Rangwala.

RECONSTRUCTION PROJECTS' COMPLETION SPEED AND DAMAGE CONDITIONS DUE TO THE GREAT EAST JAPAN EARTHQUAKE

O. MURAO¹ and M. NUMAYAMA²

¹ Professor, International Research Institute of Disaster Science, Tohoku University, Sendai, Japan,
 murao@irides.tohoku.ac.jp (corresponding author)

² Former Students, Graduate School of Engineering, Tohoku University, Sendai, Japan

Keywords: affected municipalities, tsunami, urban recovery, land use mitigation, recovery project, recovery process

1. INTRODUCTION

The Great East Japan Earthquake and Tsunami catastrophically struck the eastern part of Japan on March 11, 2011, especially the coastal areas of the Tohoku region. As of March 7, 2018, the number of casualty is 19,630, with 2,569 people still considered missing [1]. Seven years have passed since the event, and the reconstruction projects are underway in each damaged area. Affected municipalities can use and combine some reconstruction projects prepared by Reconstruction Agency after the event. However, the area where the reconstruction project is carried out ranges from 500 km north to south. It is very rare to simultaneously promote the reconstruction of a large number of wide areas with the common reconstruction system. There is no research focusing on the entire tsunami-damaged area by the disaster, especially about the relationship between the reconstruction plan and project and the transition of space.

It is meaningful to comprehensively understand the reconstruction mechanism from the Great East Japan Earthquake for future catastrophes. In this research, the authors organize a dataset of the reconstruction projects and the damage situation of the affected areas, and categorize the patterns of the reconstruction process from the disaster.

The authors gathered information on recovery project progress situation of 61 municipalities as of March 2017 for comparative analysis of their recovery processes. This research aims to quantitatively evaluate the reconstruction processes.

2. RECOVERY PATTERN OF AFFECTED DISTRICTS

MLIT [2] classified recovery plans, the residential districts would need, into five patterns based on the surveys for consideration of recovery patterns for the damaged residential districts above-mentioned. According to the damage and geographic conditions, those recovery patterns were classified into five categories: (A) Relocation, (B) Concentration, (C) Compacted terraces and berms, (D) Relocation and compacted terraces and berms, and (E) Reconstruction on the original site with facility reinforcement. The five patterns are illustrated in Figure 1.

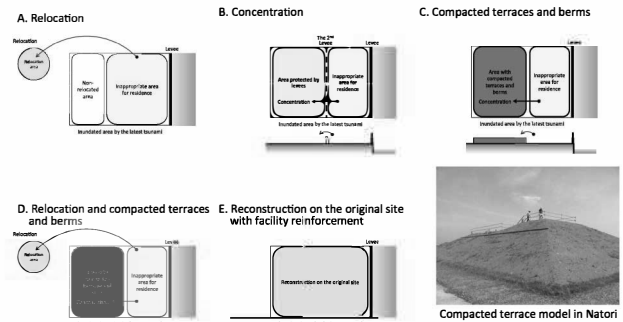


Figure 1: Recovery patterns after the Great East Japan Earthquake

3. METHOD

The research was carried out the following procedure.

(1) Target districts

The objective of this research is 379 districts seriously damaged by the tsunami in Iwate, Miyagi, and Fukushima prefectures.

(2) Data Collection

Related dataset for the target municipalities released by Reconstruction Agency are gathered from the progress report site.

(3) Data Analysis

Using the dataset, recovery progress conditions are compared in terms of adopted recovery projects, the number of constructed housings with construction period, and so on.

(4) Making recovery curves

Recovery curves of recovery project progress are demonstrated for the comparison.

4. COMPARISON OF RECOVERY PROCESSES

Finally, reconstruction processes from the 2011 Great East Japan Earthquake are compared in terms of project types and prefectures.

(1) Comparison of Recovery Processes by Project Types

Fig. 2 demonstrates recovery processes in terms of recovery projects constructed by the data collected from Reconstruction Agency. X-axis indicates time period from 2011, and Y-axis shows construction completion ratio out of the total number of objective districts.

The speed of Type (A), collective relocation, is the highest, followed by Type (B), enhancement of fishery settlements' function. The lowest is of Type (C), land

adjustment. The time period each construction ratio achieves 50% from 2012, the year construction commenced, is about 2 years for Type (A) and Type (B), 3 years for Type (D), construction of disaster public housings, and more than four and half years for Type (C). The difference between Type (A) and Type (C) is two and half years. This delay of construction situation of Type (C) is caused by difficulties of land arrangement on the original sites devastated by the 2011 tsunami.

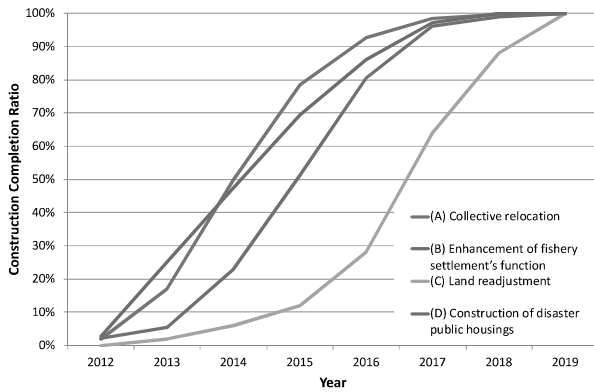


Figure 2: Recovery Curves in Terms of Projects' Type

(2) Comparison of Recovery Processes by Prefectures

Recovery processes in terms of prefectures, Iwate, Miyagi, and Fukushima prefectures together with a curve of total situation, are shown in Fig. 3. As well as Fig. 2, X-axis indicates time period from 2011, and Y-axis shows construction completion ratio out of the total number of objective districts.

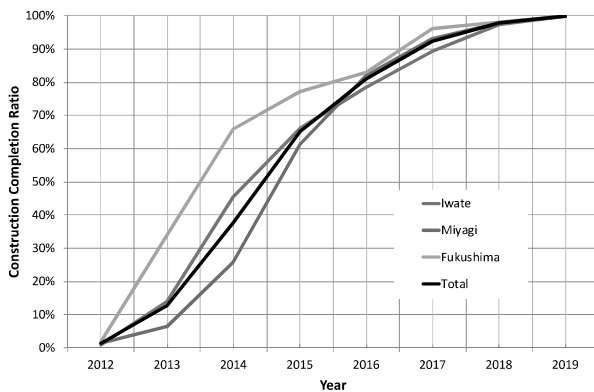


Figure 3: Recovery Curves in Terms of Prefecture

As of the end of fiscal year 2015, the final year of intensive construction period after the 2011 event designated by Reconstruction Agency, 66% of construction is completed in Iwate, 61% in Miyagi, and 77% in Fukushima. It indicates the recovery speed in Fukushima is the higher than the other two prefectures. It can be explained that some municipalities around the TEPCO's Fukushima No. 1 Nuclear Power Plant accident were eliminated, and the damage level of objective districts in Fukushima were less than other districts in Iwate and Miyagi.

(3) Relationship between Reconstruction Speed and Damage Conditions

Fig. 4 shows the relationship between the months of completion and the number of seriously damaged houses. Correlation coefficient is 0.76 and it suggests that the length of reconstruction completion time can be estimated by the damage conditions. It may be useful to estimate the necessary time for urban recovery from a future disaster.

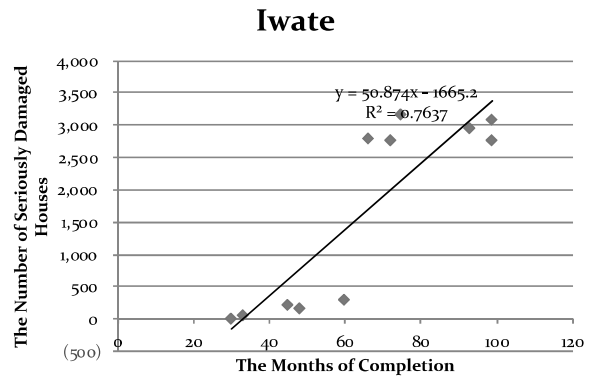


Figure 4: Recovery patterns after the Great East Japan Earthquake

ACKNOWLEDGMENT

This work is supported by the Japan Society for the Promotion of Science (JSPS) through the Grants-in-Aid for Scientific Research No. 25242036, "Resilience of the Urban Recovery System after the 2011 Great East Japan Earthquake and Regional Vulnerability Assessment to Tsunami," and No.18H03801, "Comprehensive Examination of Recovery from the 2011 Great East Japan Earthquake and Tsunami, and Urban Safety Induction Strategies Considering Natural Disaster Risk in the 21 Century."

REFERENCES

[1] Fire and Disaster Management Agency (FDMA), "Report on the 2011 Off the Pacific Coast of Tohoku Earthquake #157 (as of March 7, 2018), <http://www.fdma.go.jp/bn/157.pdf>. March 2018. (accessed August 18, 2018)
 [2] City Bureau, Ministry of Land, Infrastructure, Transport and Tourism (MLIT), <http://www.mlit.go.jp/common/000209868.pdf>, 2012.4.

EARTHQUAKE EARLY WARNING SYSTEM FOR SHINKANSEN AND ITS EFFECTIVENESS

S. UEMURA¹, H. SUZUKI², H. MIYAKOSHI³, T. NAGASAWA⁴, S. AOI⁵, W. SUZUKI⁶ and S. Yamamoto⁷

¹ Chief Researcher, R & D Center of JR East group, East Japan Railway Company, Saitama, Japan, s-uemura@jreast.co.jp (corresponding author)

² Director, R & D Center of JR East Group, East Japan Railway Company, Saitama, Japan, h-suzuki@jreast.co.jp

³ Researcher, R & D Center of JR East Group, East Japan Railway Company, Saitama, Japan, hi-miyakoshi@jreast.co.jp

⁴ Manager, Facilities Department, East Japan Railway Company, Tokyo, Japan, t-nagasawa@jreast.co.jp

⁵ Director-General, Network Center for Earthquake, Tsunami and Volcano, National Research Institute for Earth Science and Disaster Resilience, Tsukuba, Japan, aoi@bosai.go.jp

⁶ Chief Researcher, Network Center for Earthquake, Tsunami and Volcano, National Research Institute for Earth Science and Disaster Resilience, Tsukuba, Japan, wsuzuki@bosai.go.jp

⁷ Laboratory Head, Disaster Prevention Technology Division, Railway Technical Research Institute, yamamoto.shunroku.11@rtri.or.jp

Keywords: Earthquake Early Warning Systems, ocean bottom seismometer, Shinkansen

1. INTRODUCTIONS

Japan is one of the most earthquake-prone areas in the world, where the Pacific Plate, Philippine Sea Plate, North American Plate and Eurasia Plate all interact with each other. Japan often suffers serious damage from large earthquakes (Fig.1). Therefore mitigation of earthquake damage is an important issue for railway



Figure 1: Shinkansen derailed by earthquake

companies in Japan. The East Japan Railway Company (JR East) has been enforcing “hard” and “soft” countermeasures for greater safety in seismic situations. Anti-seismic reinforcement is representative of “hard” countermeasures, while train operation control in times of seismic activity and the Earthquake Early Warning (EEW) System, stopping Shinkansen trains quickly in the event of a large earthquake, are representative of “soft” countermeasures.

In this paper, we outline the principle and effectiveness of the EEW system. In addition, as a recent effort, we will describe the use and effectiveness of ocean bottom seismograph data in operation control of the Shinkansen.

2. OUTLINE AND EFFECTIVENESS OF EEW SYSTEM

In the EEW system, seismometers are located at 85 points Railside, 30 points inland, and 20 points along the

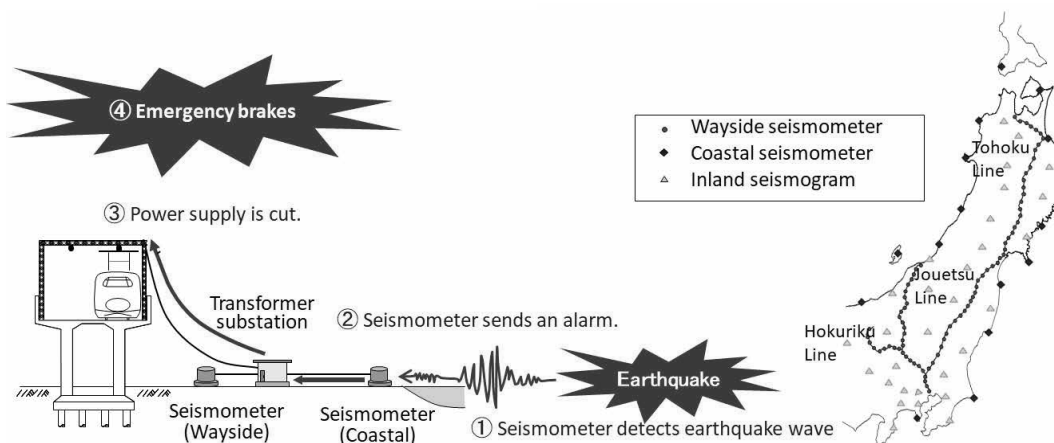


Figure 2: Overview of Earthquake Early Warning System in JR East

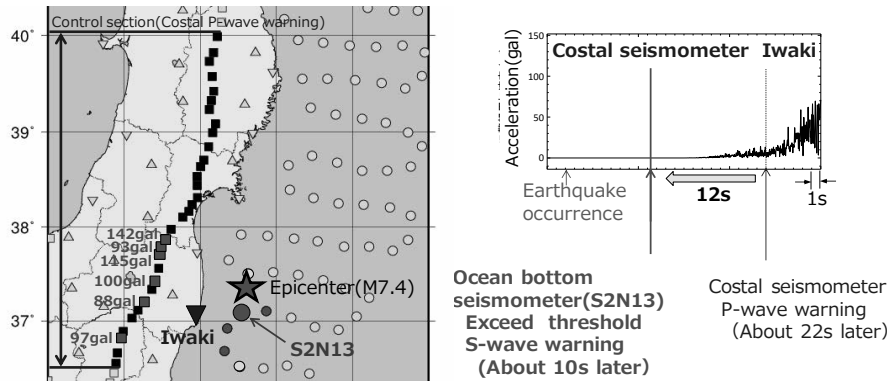


Figure 4: Verification of effect on the November 22, 2016 Earthquake Fukushima Prefecture Offshore

coast (Fig.2). RAILSIDE and inland seismometers detect mainly inland earthquakes, and seismometers along the coast detect mainly subduction-zone earthquakes. The EEW system issues P-wave and S-wave warning[1]. A P-wave warning is issued based on seismic magnitude and epicenter estimated by the initial part of P-wave. An S-wave warning is issued when acceleration exceeds the threshold. In a P-wave warning, warning can be issued earlier than an S-wave warning. When a warning is issued, power supply is cut, the Shinkansen emergency brakes are automatically applied, and trains stop. In the case of the Great East Japan Earthquake (Mw=9.0) occurring on March 11, 2011, the coastal seismometer closest to the epicenter issued an S-wave warning 12-22 seconds ahead of the “suspending operations” order based on lineside devices [2].

3. UTILIZING OCEAN BOTTOM SEISMOMETERS DATA IN EEW SYSTEM

The National Research Institute for Earth Science and Disaster Resilience (NIED) equipped 150 ocean bottom seismometers along the Japan Trench (S-net) in 2016 (Fig.3)[3]. JR East planned to incorporate data from these into the EEW system and began using data of a sub-network of 22 ocean bottom seismometers installed offshore on November 1, 2017[4]. This system issues an S-wave warning. Utilization data from the

remaining sub-networks will start in 2019.

There have been no instance of warning issued based on S-net data as of August 2018. Therefore, we verified the effectiveness of incorporating S-net into the EEW system based on past data. First of all, it was roughly estimated that by using S-net data for the Great East Japan Earthquake (2011), an S-wave warning would be issued about 25 seconds earlier than that of the conventional EEW system. Next, we verified effectiveness based on S-net archive data. Below is a case study of an earthquake occurring on 22 November 2016 offshore of Fukushima Prefecture with a magnitude of 7.4. In this earthquake, as shown in Fig. 4, a P wave warning was issued from the Iwaki coastal seismograph (▼ : epicentral distance 66km) closest to the epicenter 22 seconds after occurrence. On the other hand, the acceleration at the ocean bottom seismometer closest to the epicenter (● : epicentral distance 7 km) exceeded threshold value 10 seconds after the earthquake occurred. From the above, it is estimated that warning would be issued 12 seconds earlier than conventional EEW system if the ocean bottom seismometers of S-net are utilized.

4. CONCLUSIONS

In this paper, past and recent efforts related to the EEW system in JR East and their effectiveness were introduced. Though these efforts seem to have improved the safety in time of earthquake, we intend to continue to pursue further safety through new technologies and technological development.

REFERENCES

[1]H.Iwahashi.,N.Iwata., S.Saito., and K.Ashiya., (2004): "Practical Use of Earthquake Quick Alarm System" RTRI REPORT, Vol.18, No.9, pp.23-28.
 [2]S.Yamamoto., and M.Tomori.,(2013): "Earthquake early warning system for railway and its performance", Journal of JSCE, Vol.1, pp.322-328
 [3]K.Uehira., (2014) "Seafloor observation network for earthquakes tsunamis along the Japan Trench" Journal of the society of instrument and control engineers, Vol.53, No.6, pp.477-481
 [4]K.Mizuno.,H.Osawa.,and F.Aizawa.,(2018): "Utilization of earthquake information at JR East" Japan Railway Engineers Association, VOL.61, No.6, pp.23-26.

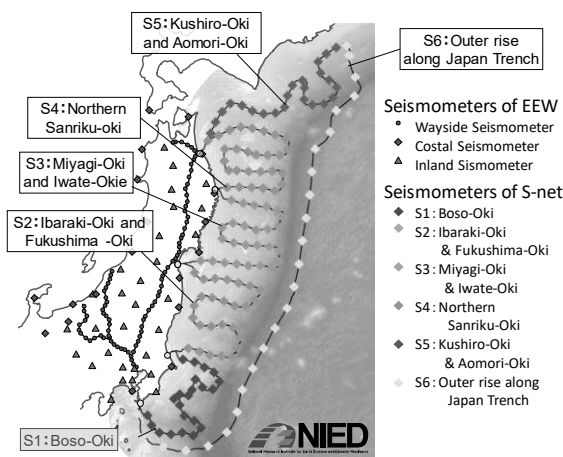


Figure 3: Ocean Bottom Seismometers arrangement in S-net

EVALUATING THE ROBUSTNESS OF NETWORKS REGARDING SPATIAL RELATIONSHIPS OF MULTIPLE ROUTES

Yudai HONMA¹, and Motoki TAJIMA²

¹ Associate Professor, ICUS IIS, The University of Tokyo, Tokyo, Japan, yudai@iis.u-tokyo.ac.jp (corresponding author)

² Former Student, Graduate School of Engineering, The University of Tokyo, Tokyo, Japan

Keywords: robustness, traffic network, spatial relationship, multiple routes

1. INTRODUCTION

In this research, we evaluate a robustness of transportation network assuming occurrence of simultaneous multiple events from huge disasters. By focusing on the spatial relationship between the routes in the transport network, we quantitatively analyze the influence of the shape characteristics of the transportation network on robustness.

Spatial movements of people and objects are achieved mainly by transportation networks which consists of roads, railways, waterways, airways etc. (Hereafter, we omit the word “transportation” and simply express as “networks”). Especially in developed countries including Japan, dense networks are formed, which contributes greatly to improving the convenience of our lives. On the other hand, there are many instances in which the network is interrupted due to natural disasters abnormal weather such as concentrated torrential rain and natural disasters such as earthquakes, concentrated torrential rain and eruptions, resulting in a great deal of damage. It is to say, the network is vulnerable to disasters.

Therefore, even if a disaster happens, it is important that a network maintains functionality without significant damage and the routes of evacuation behavior and distribution activities are secured. There are plenty of earlier studies on network assessment for disasters. There researches usually regard a disaster as a stochastic phenomenon, and evaluate a robustness/vulnerability of transportation abilities.

For example, Berdica et al. [1] defines vulnerabilities as susceptibility to incidents that could significantly reduce the serviceability of road networks. From such a point of view, some studies have focused on links that make up the network and evaluated its vulnerability. Taylor et al. [2] have defined various accessibility indicators from a socioeconomic point of view, and are searching for critical links that are greatly affected when a deficiency occurs. In addition, Jenelius et al. [3] introduces two concepts indicating the importance of importance for one link and the degree of exposure for scenarios including damage to multiple links. A geographical information system is essential for analyzing the damage of disaster, so there are also studies [4] that made large-scale computer experiments making full use of its features. They were trying to quantify damage based on actual data, and it seems to be useful for disaster damage estimation and disaster prevention plan formulation. However, such kind of GIS approaches generally have difficulty to obtain appealing conclusion

because these results tend to be complicated by assuming too many elements.

In this way, the robustness/vulnerability of the network against disasters have been studied from various viewpoints, and definitions are also various. In this research, we focused on the robustness of what quantified the remaining functions even if a disaster occurred. Meanwhile, we assume that the vulnerability is the quantified function which is lost due to a disaster. In this assumption, the sum of the value of robustness and the value of vulnerability is a quantified function of normal time, and we focus on the former robustness in the paper.

In this research, in order to quantify the robustness of the network, we treat events as a stochastic phenomenon and try to evaluate the influence of the event pattern on the network. We consider not only the network topology which lots of earlier studies focus on, but also the spatial relations of the network elements and the influenced area of events. By introducing the idea of spatial relations, one event would affect multiple links simultaneously. Since our model is based on pure formulation, it enables us to acquire broad perspectives about network robustness.

The structure of this paper is as follows. In Section 2, we will summarize the concept of network robustness in this research. In the following Section 3, we propose a new model which evaluate a robustness of the network assuming the occurrence of simultaneous multiple events. This model results to calculate an expected value which considers both the probability of event pattern based on the spatial Poisson distribution and the synthetic utility of the C-logit model [5,6]. In Section 4, we calculate the robustness value under various conditions and discuss its properties on an idealized network, which consists of 3 circular and 12 radial links. Finally, in Section 5, we state the summary and future development of this paper.

The following are main findings obtained in this research: (i) As for the circular-radial network, as the network scale becomes relatively smaller, hub of the network has a greater influence on robustness; (ii) robustness is also affected by the size relationship between the damage and the city block. As described above, using the mathematical model of this research, considering both the property as the network topology as in (i) and the property based on the spatial relation as in (ii), robustness It is possible to evaluate.

2. ROBUSTNESS OF NETWORKS

In this section, prior to formulation, we summarize the concept of network robustness in this research. As

mentioned above, in this study, it is assumed that simultaneous events are happened in various place. The following conditions are listed as preferred network characteristics against occurrence of such events.

- Many different alternate routes are remained.
- Each route must be spatially distributed so that it will not be disconnected at the same time due to one event.

There is certain that it is better to have multiple alternate routes from the viewpoint of robustness of the network. On the other hand, for the second condition, we should state actual case examples for better understanding. In the 1995 Great Hanshin-Awaji earthquake, several major arterial networks which were essential for domestic East-West traffics, such as National Highway No.2, Route 43, Hanshin Expressway 3 No.3 Kobe Line and the Chinese Expressway were damaged. As a result, there was a serious trouble to domestic east and west traffic, as well as difficulties of evacuation and rescue activities due to a decline in traffic capacity in the disaster region. One cause of such traffic confusion is the spatial relation of the above-mentioned networks. It has been pointed out that multiple arterial networks, which should originally be replaced, are spatially close to each other and passed through the afflicted regions, causing simultaneous damage and causing traffic disruption. This fact suggests that not only focusing on multiple routes as topology but also focusing on its spatial divergence when evaluating the robustness of the network against disasters. Based on the above idea, we propose a new evaluation model of network robustness considering both the network topology and the spatial relation of network links at the same time.

3. FORMULATION

3.1. ASSUMPTION

Suppose a network as a graph $G = (N, E)$ with vertex the set of node N and the set of link E . G is on the two-dimensional plane Z , and is a weighted graph in which the weight of each node is w_n and the length of each link is l_e . Also, the set of k_{\max}^{rs} th shortest paths from an origin $r \in N$ to a destination $s \in N$, the OD pair rs , is given by in ascending order of distance $K^{rs} = \{1, 2, \dots, k, \dots, k_{\max}^{rs}\}$. In addition, assume that A_k^{rs} is the link set of each route k .

Here, assuming a disaster phenomenon in which random simultaneous multiple events occur in several place and arbitral number, we consider the damage that the network receives (Fig.1). However, the event in this study is expressed as a circular area (hereinafter referred to as an “event disk”). If a link e is in the event disk, then it is cut off. We also assume that the size of the event disk is constant with the radius R . Also, if $e \in A_k^{rs}$ is disconnected, route k will be unavailable.

Descriptions of event disk assume, for example, catastrophic damage of a fertile area due to an earthquake. In Tokyo, there are scattered regions of about 6900 hectares in 28 areas (areas where particularly widespread

damage is assumed among wooden housing densely populated areas), and no huge bias is observed in the place and size. In addition, these areas would be damaged at the same time by fires, and in that case, the road passing through the damaged area cannot be used.

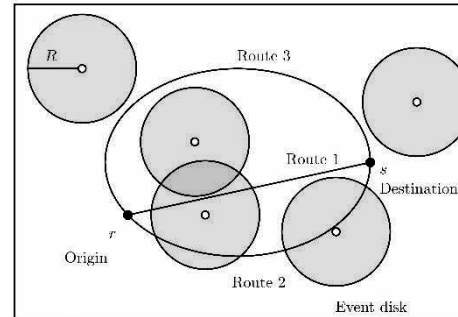


Figure 1: Example of events which randomly happen

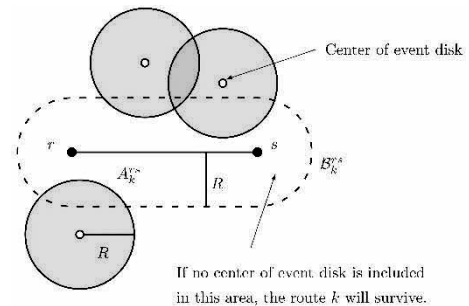


Figure 2: condition that a route survive

3.2. AFFECTED AREA

First, an affected area for sorting out the relationship between random event occurrence and disconnected route is described. Assuming that B_k^{rs} is the area where the distance from A_k^{rs} is less than R , the route k cannot be used only when the center point of the event disk is included in the area B_k^{rs} as shown in Fig.2. let us focus on B_k^{rs} and $B_{k'}^{rs}$, but $k \neq k'$. Specifically, we combine the common set of routes affected for all B_k^{rs} and express it by \mathcal{R}_I^{rs} ($I \in \Psi^{rs}$). The definition of \mathcal{R}_I^{rs} is as follows:

$$\mathcal{R}_I^{rs} = \bigcap_{k \in I} B_k^{rs} \cap \overline{\bigcap_{k \notin I} B_k^{rs}} \cap Z \quad (1)$$

$$\Psi^{rs} = \text{Power}(K^{rs}) - \{\phi\} \quad (2)$$

and its area is $|\mathcal{R}_I^{rs}|$. Here, Ψ^{rs} is obtained by removing the empty set from the power set of K^{rs} . In the example of Fig.3, since the total number of routes is 3, there are seven possible failure areas because $2^3 - 1 = 7$. However, in this case, there is no $\mathcal{R}_{\{2,3\}}^{rs}$.

As is clear from (1), \mathcal{R}_I^{rs} means a region where combinations of routes to be disconnected are the same when an event having a center point is included in the region. Even if a plurality of events occur in the same affected area, the situation does not change at all. Therefore, it is only important whether or not an event has happened within \mathcal{R}_I^{rs} . When points are randomly

distributed with a density ρ on the plane, the probability $q(v, S)$ that total v points are included in area S is given by the spatial Poisson distribution as follows:

$$q(v, S) = \frac{(\rho S)^v}{v!} \exp[-\rho S] \quad (v = 0, 1, 2, \dots) \quad (3)$$

Using (3), the probability that an event will happen within \mathcal{R}_i^{rs} can be determined as

$$q_i^{rs} = 1 - q(0, |\mathcal{R}_i^{rs}|) \quad (4)$$

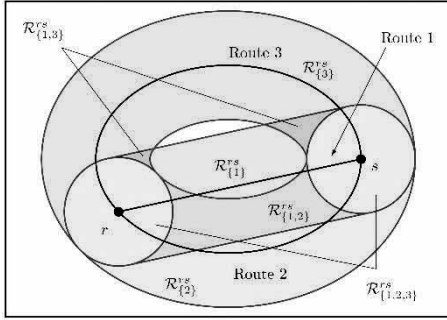


Figure 3: Relation between the route k and \mathcal{R}_i^{rs}

3.3. EVENT PATTERN

In this research, we assume that events happen randomly not only in places but also in numbers. In that case, for example, even if the route $\{1,2\}$ is disconnected as a result, various patterns can be considered as the event situation. For example, independent two events might happen in $\mathcal{R}_{\{1\}}^{rs}$ and $\mathcal{R}_{\{2\}}^{rs}$ respectively, and route 1 and route 2 may be disconnected. Meanwhile, an event happens in $\mathcal{R}_{\{1,2\}}^{rs}$, and route 1 and route 2 are disconnected at the same time. Therefore, it is necessary to enumerate all event patterns for how to disconnect routes. When the number of routes is 3 as shown in Fig.3, there are theoretically seven affected areas, and event patterns would be $2^7 = 128$ in total. Therefore, in order to classify whether or not an event has happened for all \mathcal{R}_i^{rs} , we consider the power set Ω^{rs} of Ψ^{rs} :

$$\Omega^{rs} = \text{Power}(\Psi^{rs}) \quad (5)$$

Note that $I \in J$ because I is an element of Ψ^{rs} and J is an element of Ω^{rs} . That is, if $I \in J$, it means that an event happens inside the corresponding \mathcal{R}_I^{rs} , and conversely if $I \notin J$, it means that no event has happened within \mathcal{R}_I^{rs} . Since the combination of all fault occurrence patterns is enumerated according to (5), each J shows different fault patterns. The probability p_J^{rs} that a certain event pattern J is happened can be calculate as (6):

$$p_J^{rs} = \prod_{I \in J} q_I^{rs} \prod_{I \notin J} (1 - q_I^{rs}) \quad (6)$$

This obviously satisfies $\sum_{J \in \Omega^{rs}} p_J^{rs} = 1$. For each event pattern J , the route that is damaged at that time is the union $\cup J$, so the relationship between the probability of event pattern and the route that is damaged has been sorted out.

3.4. EVALUATION OF REMAINING ROUTES

We now evaluate the remaining routes even when several events are happend. The route set \bar{K}_J^{rs} which is remaining under a certain event pattern J is given by

$$\bar{K}_J^{rs} = K^{rs} - \cup J \quad (7)$$

For this route set \bar{K}_J^{rs} , we use the log sum variable based on the C-Logit model considering the duplication rate of the route and define the inclusive distance \bar{L}_J^{rs} as follows:

$$\bar{L}_J^{rs} = -\frac{1}{\theta} \ln \sum_{k \in \bar{K}_J^{rs}} \exp[-\theta L_k^{rs} - c f_k^{rs}] \quad (8)$$

$$c f_k^{rs} = \ln \sum_{k' \in \bar{K}_J^{rs}} \left(\frac{\sum_{e \in A_k^{rs} \cap A_{k'}^{rs}} l_e^{rs}}{\sqrt{L_k^{rs}} \sqrt{L_{k'}^{rs}}} \right) \quad (9)$$

However, L_k is the total length of route k and is calculated by $L_k = \sum_{e \in A_k^{rs}} l_e$. Furthermore, $c f_k^{rs}$ is a term (commonality factor) expressing similarity of routes, and θ is a distance decay parameter.

Here, the mathematical properties of (8) and (9) are summarized. The C-logit model is a type of route choice model based on random utility model. In the case that routes are no overlapped, $c f_k^{rs} = 0$ in (9), and the inclusive distance of each route is equal to the inclusive distance calculated by a simple multinomial logit model. If there are n non-overlapping routes of length l^* , the inclusive distance is given by $l^* - \ln n / \theta$. Conversely, when assuming the existence of a plurality of perfectly matched routes, the inclusive distance obtained by the C-logit model is equal to the length of the matching route irrespective of the number of routes. As a result, the larger the number of routes, the shorter each route distance, and the more these routes do not overlap, the more the combined distance \bar{L}_J^{rs} is calculated to be shorter. In general, the shorter the distance between two points, the stronger the connection, so it can be considered that the robustness is high. Therefore, in this study, the evaluation value V_J^{rs} of the remaining path is defined as the reciprocal of \bar{L}_J^{rs} :

$$V_J^{rs} = \frac{1}{\bar{L}_J^{rs}} \quad (10)$$

Obviously when the inclusive distance is 0 (that is, when the origin r and destination s are the same point), the evaluation value becomes $+\infty$ and becomes maximum. Conversely, when the inclusive distance is $+\infty$, the evaluation value becomes 0, which is the minimum. That is, V_J^{rs} can also be interpreted as an indicator of proximity based on inclusive distance. Note that there is a possibility that \bar{L}_J^{rs} may become negative depending on the value of θ , so we need to set the parameter so that it becomes $\bar{L}_J^{rs} \geq 0$.

3.5. CALCULATION OF ROBUSTNESS

Based on the above preparations, this research gives the robustness $G^{rs}(\rho, R)$ between certain OD pair rs on the network as follows by using (6) and (10):

$$G^{rs}(\rho, R) = \sum_{j \in \Omega^{rs}} V_j^{rs} \cdot p_j^{rs} \quad (11)$$

As is apparent from (11), this is the expected value of V_j^{rs} based on the routes that still remain even under the condition that simultaneous multiple event has happened. As mentioned above, in this research, we assume that the value of robustness is “quantified the function still remaining even if it happens in a disaster”, and the proximity when the network is completely cut off is 0.

In addition, we can obtain the robustness $G^r(\rho, R)$ for each node by fixing the origin and calculating the weighted average for every destination. Similarly, robustness of the entire network $G(\rho, R)$ can be derived by calculating the weighted average for every OD pair:

$$G^r(\rho, R) = \frac{\sum_{s \in N} w_s \cdot G^{rs}(\rho, R)}{\sum_{s \in N} w_s} \quad (12)$$

$$G(\rho, R) = \frac{\sum_{r \in N} \sum_{s \in N} w_r w_s \cdot G^{rs}(\rho, R)}{\sum_{r \in N} \sum_{s \in N} w_r w_s} \quad (13)$$

Based on the above discussion, the robustness of the remaining network which maintains the function without being affected by the events is quantified under the assumption that a circular obstacle of radius R at a density of ρ pieces per unit area happens randomly for places and numbers. Note that comparing between networks of different scales is also possible because we calculate a weighted average rather than total. More remarkable feature of our model is that ρ and R are given as variables. By comparing these parameters in various ways, it is possible to evaluate robustness taking into account the difference in scale of disasters due to the magnitude of the disaster.

4. NUMERICAL EXAMPLES

4.1. NETWORKS AND PARAMETERS

On the infinite plane Z , let us assume an idealized network which has 3 circular and 12 radial links. We set that the radius of the network is 1. In this case, the number of nodes in the network is $|N| = 37$, and the number of links is $|E| = 72$. In addition to this (a) Basic network, we also prepare three types of derived networks; (b) No-core, (c) Three-quarters, and (d) No-core & Three-quarters (NC-TQ). There four networks are shown in Fig.4.

About parameters, we set the weight w_n of arbitrary nodes $w_n = 1$. Regarding the route set K^{rs} , in this numerical example, k -shortest paths [7] were calculated and set as follows:

$$K^{rs} = \{k | k \leq 8, L_k^{rs} \leq 1.5 \times L_1^{rs}\} \quad (14)$$

e assume that the total number of routes is 8 or less,

because Ω^{rs} increases dramatically according to the total number of routes ($|\Omega^{rs}| = 2^{(2^8-1)} \approx 5.79 \times 10^{76}$). It is nearly the limit of calculation. On the other hand, we set the upper limit of the deviation rate of 1.5 for practical reason of alternative routes. Finally, the distance resistance parameter θ was set to $\theta = 12.0$ so that the inclusive distance L_j^{rs} will not be negative. In order to calculate (11), it is necessary to derive $|\mathcal{R}_j^{rs}|$ in (4) but it is difficult to calculate analytically. Therefore, we uniformly arranging lattice points (representative points) at intervals of 0.02 on the target area, and numerically calculate $|\mathcal{R}_j^{rs}|$. On the other hand, all mathematical expression other than (4), including Ω^{rs} , were analytically calculated.

4.2. EFFECTS OF DISASTER SCALE

First, we focus on the how the robustness G of the basic network (Fig. 4 (a)) is affected when the event density ρ and the radius of event disk R are variously changed. Fig. 5 shows the results how R affects when the event density is set as $\rho = 0.25, 0.5, 1.0, 2.0$. Similarly, Fig.6 shows the result how ρ affects when the radius of event disk is set as $R = 0.1, 0.3, 0.5$.

From the results, it can be confirmed that robustness monotonically and exponentially decreases as the disaster scale such as ρ and R increases (when both ρ and R are 0, $G = 1.39$). These results are natural because it is apparent that the robustness finally converges to 0 as ρ and R increase. On the other hand, it is confirmed from Fig.6 that the robustness changes can be characterized by the value of R . Specifically, the decreasing process obviously differs between in the case of $R = 0.1$ and in the case of $R = 0.3, 0.5$. We consider that the size of the block surrounded by link is related. In this network, the interval of the circular link is $1/3$, so it is not so common that an event disk cuts multiple routes and in the case of $R = 0.1$. On the other hand, in the case of $R = 0.3, 0.5$, it almost corresponds to the size of two blocks, so it is easy to cut multiple routes at the same time. Fig. 6 is would be a result that shows the influence of block size.

4.3. EFFECTS OF THE HUB

Next, we calculate the robustness of the different four patterns of networks (Figure 4). The parameters are set to four conditions combining $\rho = 0.25, 1$ and $R = 0.1, 0.3$. The results are shown in Fig.7 to Fig.10. In the figure, robustness of each node G^r corresponds the color of the node and the total robustness G is shown numerically.

Let us compare Fig.7 with Fig.8, and Fig.9 with Fig.10 to consider the effects of the hub in the network. It is clearly confirmed that the nodes on the innermost circular road are more robust when the hub exists. Similarly, about the robustness of the entire network G , the difference of is 0.12 when comparing Fig.7 (a) with Fig.8 (a), which is about 10% better value. Furthermore, the difference is 0.26 when comparing Fig.9 (d) and Fig.10 (d), it is about 37% better. From this numerical example, we conclude that the existence of the hub greatly contributes to enhance the robustness of the network.

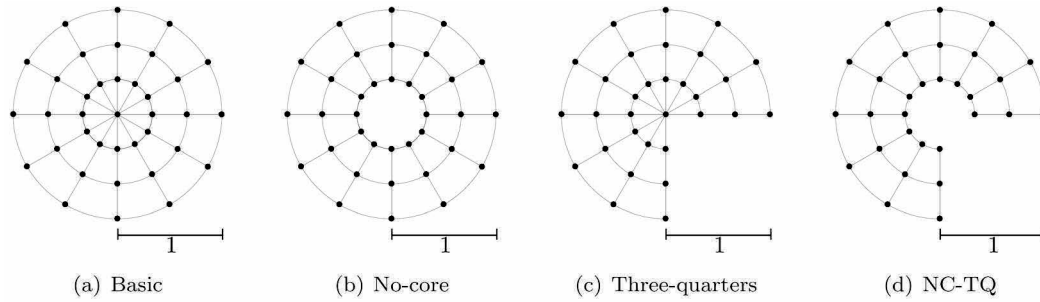


Figure 4: Examples of idealized networks

4.4. EFFECTS OF THE SHAPE

Finally, let us compare Fig.7 with Fig.9, and Fig.8 with Fig.10 to clarify how the shape of network affects to the results. Before observing the results, we should mention that that the relation between the size of network and the robustness is not simple in our model. As the network scale becomes smaller, the number of alternative routes that can be taken between OD will of course decrease and the inclusive distance will increase, which are factors that reduce robustness. On the other hand, the smaller the network scale, the smaller the total amount of disasters in the range of influence. In addition, as OD pairs with relatively long distances are also fewer, these would be the opposite factors that increase robustness.

Keeping this in mind, we now compare Fig.7 with Fig.9, and Fig.8 and 10. Then It is natural even if some nodes near center become robust in the case of three-quarters. The nodes which acquire greater value are away from the missing 1/4 part, so it results to a decrease in long distance OD pair. It means that the relative amount of the short distance pair increases, which results to the increase of the robustness. On the contrary, it is convinced that the robustness of the outer nodes, such as bottom or right end nodes of three-quarter type, are lower in robustness, because the short distance pair would be decreased. Moreover, when moving to the opposite region across the missing quarter part, it is necessary to bypass and the route concentrates around the center. This also contributes to reducing the robustness. In this way, we conclude that the model proposed in this research comprehensively considers not only the influence of the change in region shape on the route but also the distance distribution of OD.

5. CONCLUSIONS

In this research, we focused on the spatial relationship between multiple routes and proposed a mathematical model to quantitatively evaluate the robustness of the network. By considering not only the network topology mainly pursued in the previous research but also its spatial distributions at the same time, we could incorporate a phenomenon often observed, that is, a single events affects multiple routes. We discussed the average of the evaluation values of the remaining network assuming disaster-related events in which the number and location happen randomly by combining several mathematical tools such as power set, spatial Poisson distribution, and

inclusive utility. In addition, through numerical examples in the idealized network, we discussed from various viewpoints, such as the magnitude of disaster, the size of the block, the existence of the hub, the network shape, and the robustness of individual OD pairs. These knowledges about the robustness of the network must give us suggestions for disaster prevention plan in a real society.

REFERENCES

- [1] Berdica, K. (2002): An introduction to road vulnerability: what has been done, is done and should be done, *Transport Policy*, Vol.9, pp. 17–127.
- [2] Taylor, M.A.P., et al. (2006): Application of accessibility based methods for vulnerability analysis of strategic road networks, *Networks and Spatial Economics*, Vol.6, pp.267–291.
- [3] Jenelius, E., et al. (2006): Importance and exposure in road network vulnerability analysis, *Transportation Research*, Vol.40A, pp.537–560.
- [4] Sohn, J. (2006): Evaluating the significance of highway network links under the flood damage: an accessibility approach, *Transportation Research*, Vol.40A, pp.491–506.
- [5] Cascetta, E., et al. (1996): A Modified Logit Route Choice Model Overcoming Path Overlapping Problem. Specification and some Calibration results for Interurban Networks, *Transportation and Traffic Theory, Proceedings of the 13th International Symposium on Transportation and Traffic Theory*, Elsevier Science, Oxford, pp.195–207.
- [6] Cascetta, E., et al. (1998): Implicit Availability / Perception Logit Models for Route Choice in Transportation Networks, *World Transport Research : Selected Proceedings of 8th World Conference on Transport Research*, Pergamon, Oxford, Anversa, pp.15–24.
- [7] Yen, J.Y. (1970): Finding the k Shortest Loopless Paths in a Network, *Management Science*, Vol.17-11, pp.712–716.

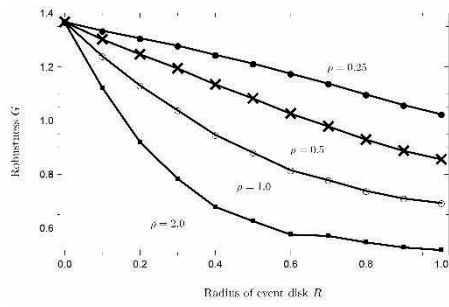


Figure 5: Relations between the radius of event disk and the robustness of networks

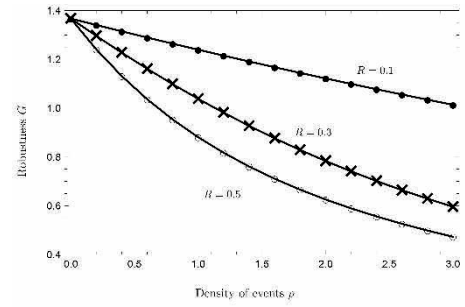


Figure 6: Relation between the density of events and the robustness of networks

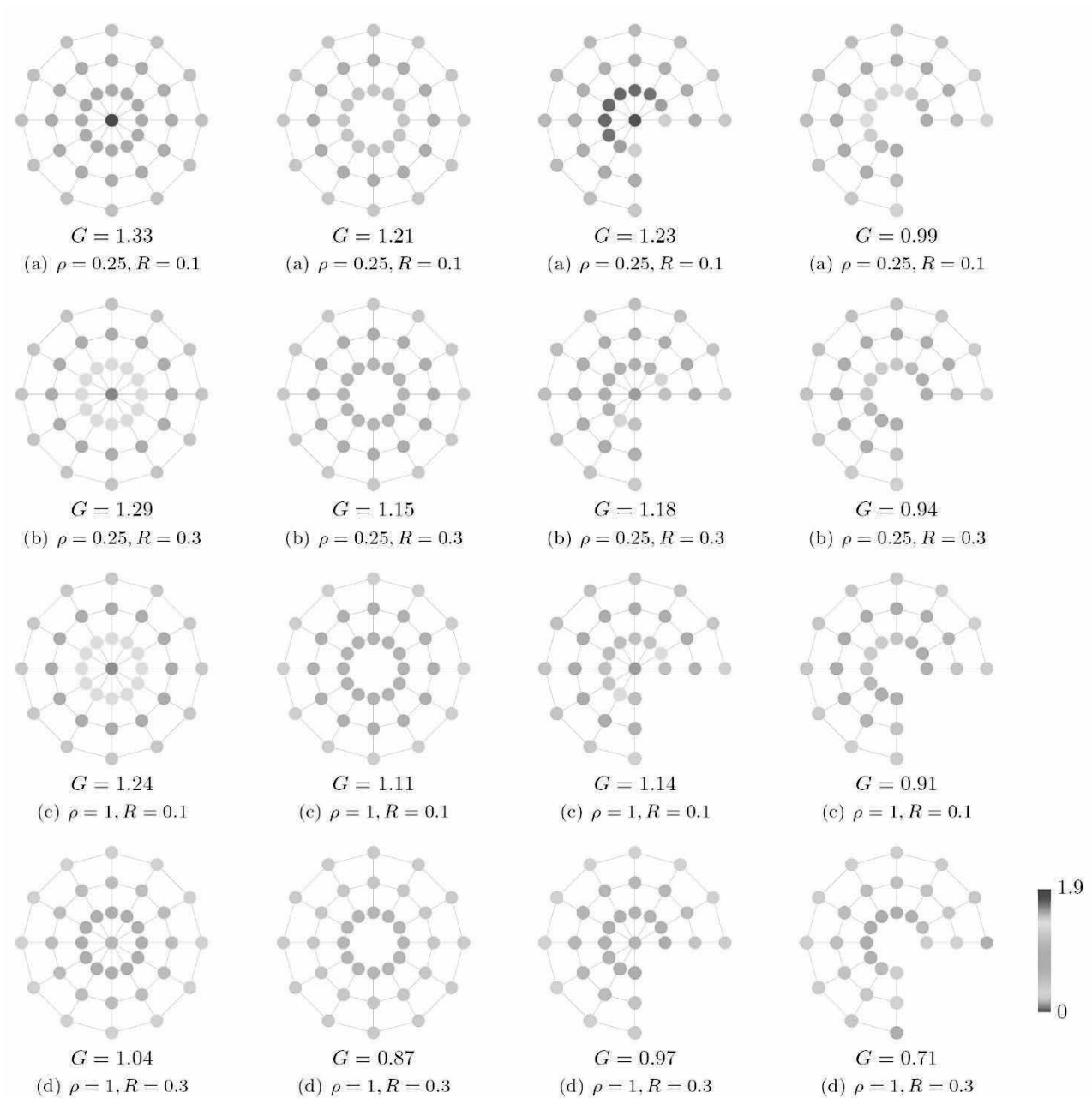


Figure 7: Robustness of each node (Basic)

Figure 8: Robustness of each node (No-core)

Figure 9: Robustness of each node (Three-quarters)

Figure 10: Robustness of each node (NC-TQ)

A MATHEMATICAL MODEL TO REPRESENT AN URBAN SYSTEM'S REGENERATIVE CAPACITY FOR COPING WITH NATURAL DISASTERS

Y. SHIOZAKI¹, and T. KATO²

¹ Project Researcher, Institute of Industrial Science, The University of Tokyo, Tokyo, Japan, yuto@iis.u-tokyo.ac.jp (corresponding author)

² Associate Professor, Institute of Industrial Science, The University of Tokyo, Tokyo, Japan, kato-t@iis.u-tokyo.ac.jp

Keywords: natural disasters, resilience, urban system, differential equation model

1. INTRODUCTION

In addition to disaster mitigation measures, the control measure of an urban system's ability to regenerate to a desirable situation in post-disaster phase should be considered. To control the capacity, the definition and mechanism of regenerative capacity needs to be clarified.

This study classifies the regenerative capacity into i) Stability, ii) Absorptive capacity, and iii) Adaptability as a result of review on the existing studies relating to urban system's regenerative capacity (e.g. [1], [2], [3]). Stability is defined as the ability of an urban system to return to the pre-disaster situation after a disaster. Absorptive capacity is defined as the ability of an urban system to absorb the damage and maintain the condition in which the system can recover. Adaptability is defined as the ability of an urban system to recover the damage and adapt the change of socio-economic environment.

The relationship structure (mechanism) between the Stability and its factors has been studied, and the disaster recovery model of an urban system is established to consider the measures to improve urban system's Stability ([1], [4]). On the other hand, regarding the Absorptive capacity and the Adaptability, the concepts are suggested ([2], [5]), but the mechanism is not sufficiently studied.

This study focuses on the Absorptive capacity and the Adaptability. A mathematical model to describe the dynamics of an urban system's state is established, which is then used to analyze the mechanism of Adaptability and represent the concept of Adaptability.

2. A MATHEMATICAL MODEL

This study assumes an urban system model the state of which is represented with labor population $x(t)$ and production capital $y(t)$. Figure 1 shows the whole picture of the model. In this model, there are only two cities: an object urban system and an outside system.

The dynamics of urban system's state is described by the following differential equations model:

$$dx/dt = r_x(A(x, y) - \omega)x \quad (1)$$

$$dy/dt = r_y F(x, y)/\varepsilon - \delta y \quad (2)$$

where $A(x, y) = a_I(x, y) + a_S(x, y) + a_C(x, y)$ (3)

$$F(x, y) = k_{max} \frac{(x^\alpha y^\beta)^\gamma}{(x^\alpha y^\beta)^\gamma + k_h^\gamma} \quad (4)$$

The dynamics of labor population $x(t)$ is described as proportional to the difference between the attractiveness

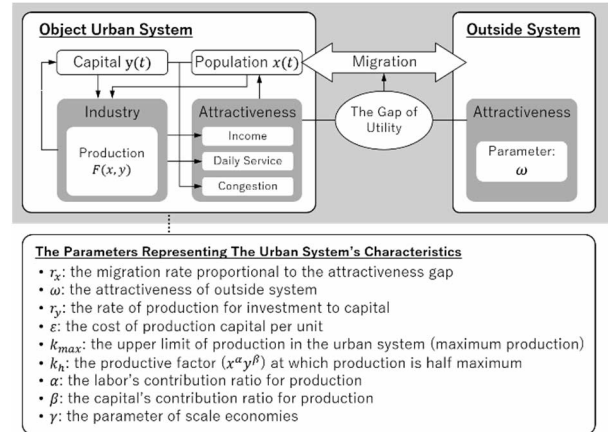


Figure 1: The whole picture of mathematical model

of object urban system and the one of outside system. The attractiveness $A(x, y)$ of object urban system is considered as the sum of three components: the attractiveness related to income per capita $a_I(x, y)$, the one related to daily service $a_S(x, y)$, and the one related to congestion $a_C(x, y)$. The attractiveness of outside system is exogenously given a parameter ω .

The dynamics of production capital $y(t)$ is decided by the difference between the increment and the decrement. The increment derives from the amount of investment to production capital, which the system allocates the production $F(x, y)$ into by the constant rate r_y . The remaining of the production $F(x, y)$ is allocated into labor population, and equally distributed among them. The decrement corresponds to the degradation of production capital.

In this urban system's industry, the amount of production $F(x, y)$ is decided by labor population and production capital. Scale economies operate in the industry, but the amount of production is not supposed to exceed the upper limit k_{max} .

3. ABSORPTIVE CAPACITY

The streamlines on the xy -plane, which are decided by the vector field based on equation (1) and (2), represent the dynamics of the urban system's state. Given a set of parameters to the equation (1) and (2), the streamlines and equilibria are obtained as Figure 2. Equilibrium Q_1 and Q_3 are attractors, and equilibrium Q_2 is a saddle point. The pale gray- and dark gray-colored area on Figure 2 is the basin of attractor Q_1 and Q_3 . The urban system's

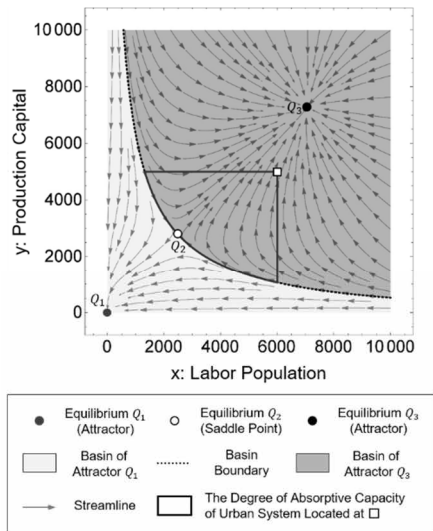


Figure 2: Streamlines, equilibria, basin of attractor, and the degree of Absorptive capacity ($k_{max} = 30000$)

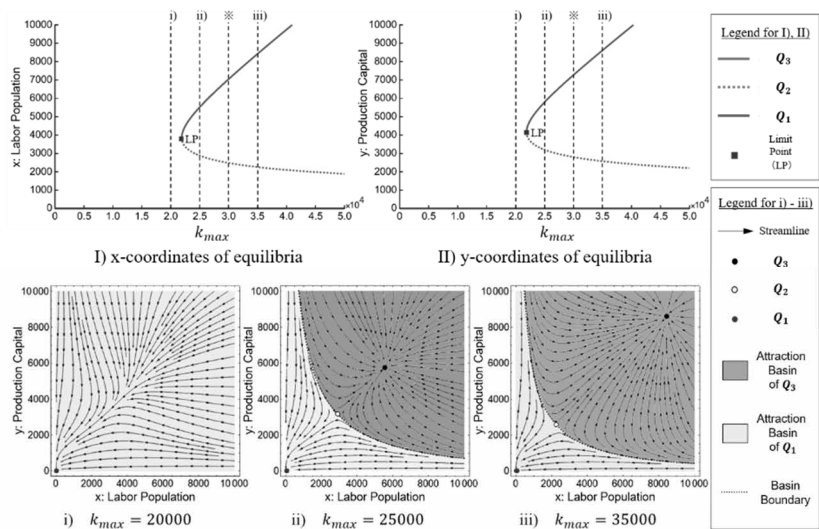


Figure 3: xy -coordinates of equilibria and basin of attractor by the change in the value of k_{max}

state, the initial value of which is located on a basin of attractor, will converge into the attractor. Varying the value of parameters, the shape of streamlines and the location of equilibrium is changed, and the equilibrium Q_2 and Q_3 can be disappeared depending on the value as shown on Figure 3.

The degree of Absorptive capacity of urban system, whose state is located at \square on Figure 3, is represented by the bold-black-lined area. Assuming that labor population would be moved out of the system and production capital would be decreased to a certain degree by a disaster, disaster damage would make the system's state move to left-lower direction on Figure 3. The devastated system can sustain if the state is still located in the basin of attractor Q_3 . Hence, the system's Absorptive capacity is reflected by the basin of attractor Q_3 . Analyzing how the Absorptive capacity is influenced by the change in parameter values relating to the characteristics of the urban system, the relational structure between the characteristics and the capacity is clarified.

4. ADAPTABILITY

Adaptability is necessary for an urban system when a disaster causes damage on the urban system, and the socio-economic environment of urban system is changing. Here, this study assumes an urban system whose industry is declining. In the above mathematical model, the declining industry is represented by the decreasing of production upper limit k_{max} in the urban system.

Attractor Q_3 is disappeared when the value of k_{max} is lower than a certain degree. At this time, the urban system's state is deteriorating, and the urban system will be eventually abandoned without disaster as shown in Figure 3 i). Moreover, if a disaster happens then, the deterioration will be accelerated.

In this situation, the urban system has to create a new industry with enough production upper limit k_{max} to make the attractor Q_3 reemerge. In addition, the urban

system's state needs to be located in the basin of attractor Q_3 when the attractor reemerges. Therefore, attractor Q_3 should be restored as soon as possible.

Adaptability can be considered as a capacity of urban system to restore an attractor where the system can be sustainable in case that the attractor is not existing.

5. CONCLUSION

First, this study builds up a differential equation model to describe the dynamics of an urban system state. Secondly, the model represents the degree of Absorptive capacity, and clarifies the mechanism of Absorptive capacity by the change in parameter values relating to the characteristics of the urban system in the model. Finally, this study explains the concept of Adaptability with the mathematical model.

REFERENCES

Reference to a journal publication:

- [1] M. Bruneau et al., (2003), "A Framework to Quantitatively Assess and Enhance the Seismic Resilience of Communities," *Earthquake Spectra*, Vol.19, No.4 pp.733–752
- [2] K. M. Bruijn, (2004), "Resilience and Flood Risk Management," *Water Policy*, Vol.6, pp.53-66
- [3] Y. Shiozaki et al., (2015) "The Concept of Urban System Resilience to Natural Disasters," *J. Japan Society of Civil Engineers*, Ser. D3, Vol.71, No.3 pp.127–140 (in Japanese)
- [4] S. B. Miles, and S. E. Chang, (2006), "Modeling Community Recovery from Earthquake," *Earthquake Spectra*, Vol.22, No.2, pp.439-458
- [5] F. H. Norris et al., (2008), "The meaning of system robustness for flood risk management," *Environmental Science & Policy*, Vol. 14, pp. 1121-1131

A SEAMLESS FRAMEWORK FOR INDOOR-OUTDOOR INTEGRATION OF BUILDING DATA FOR EMERGENCY EVACUATION

N. MAHESHWARI¹, K. S. RAJAN²

Lab for Spatial Informatics, IIIT Hyderabad, Hyderabad, India

¹ nishith.maheshwari@research.iiit.ac.in

² rajan@iiit.ac.in

Keywords: evacuation, indoor space, modeling, framework

1. INTRODUCTION

In case of an emergency in a building like fire, effective evacuation of people inside the building to a safe place is necessary. The steps involved is doing so starts from a room or hall (with furniture or other obstacles) to the connecting corridors leading to the exit from the floor and eventually exiting the building. After exiting the building the evacuees need to move to an evacuation site away from the building. This flow involves interaction of evacuees with multiple levels of building with different level of details.

A set of challenges are associated for a seamless flow of evacuees through these levels. One of the major challenges is regarding the data available for every level. For example a building may have only the floor plan layout available without the information about the elements comprising the space (obstacles like furniture). Even if the data is available, it may be in an incompatible format or with limited information to interact with an evacuation model. This brings us to the next challenge which deals with the processing and computation limitation of handling different types of data using a unified model. From the evacuee's perspective, initially only a local view of the space is needed and providing the whole view may lead to overload of information and cause confusion. As the scenario changes the detail of information should also change. So a need for proper information dissemination at different levels is needed.

Recent research works have handled evacuation modeling in various ways. Some works have focused on constructing a grid-based model to generate navigation routes for evacuation using 2D floorplans [1,2] and BIM IFC data [3] of the building. Others generate a graph network using the 2D floorplans [4] or by collapsing the 3D geometry of the building to 2D polygons [5,6].

But the major challenge remains that how can these different levels of data be incorporated in a framework and how we can have a seamless interaction between them.

Hence this work has focused on proposing a framework which defines the data in an hierarchical manner such that each level of hierarchy corresponds to

the type of information available and the kind of model to be used for computing navigation routes. It focuses on the 2D aspect mainly but has the flexibility to incorporate 3D data at floor and space level. The framework suggested here is a conceptual one and is a work in progress.

2. HIERARCHICAL FRAMEWORK

The framework has been defined in the following three levels of hierarchy -

Space level

The space level refers to a unit space (like room) with a dense amount of indoor information like the location of chairs, tables, shelves and other furniture available.

The data models that can provide data for this level are CityGML LOD4, architectural drawings with furnishing information and detailed BIM IFC models of the building.

In the context of evacuation, this level serves as the starting point for the evacuees. The navigation is done to exit the space, while avoiding the obstacles, to connect to other indoor spaces.

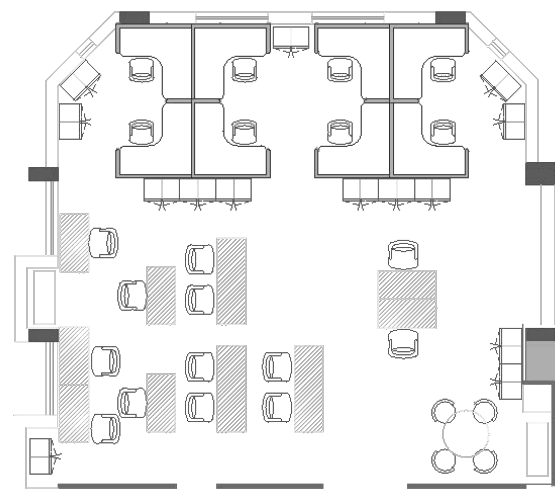


Figure 1: Example of a space with furniture

Floor level

This level of hierarchy considers a building floor level and focuses on navigation between the spaces on a floor and between multiple floors. The modeling is done based on the semantic model presented in [7].

During evacuation the goal is to exit the floor to move to a lower level (if on an upper floor) and eventually exiting the building. Using the semantics of the spaces a navigational network is generated which would be used for routing the evacuees.

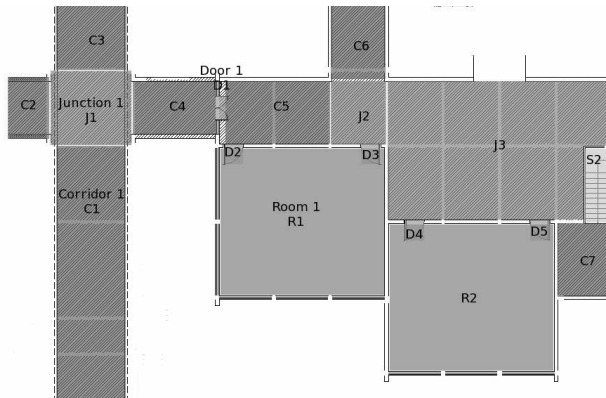


Figure 2: A floor plan with semantic labels.

Outdoor level

In this level, integration with the outdoor is explored. From an evacuation point of view even exiting the building may not be safe enough (as in the case of a fire) and the evacuees would need to be moved to a location away from the building. This level would also be able to incorporate managing the incoming first responders and other resources like hydrants around the building. The modeling of this level can be done using the existing GIS models for outdoors.

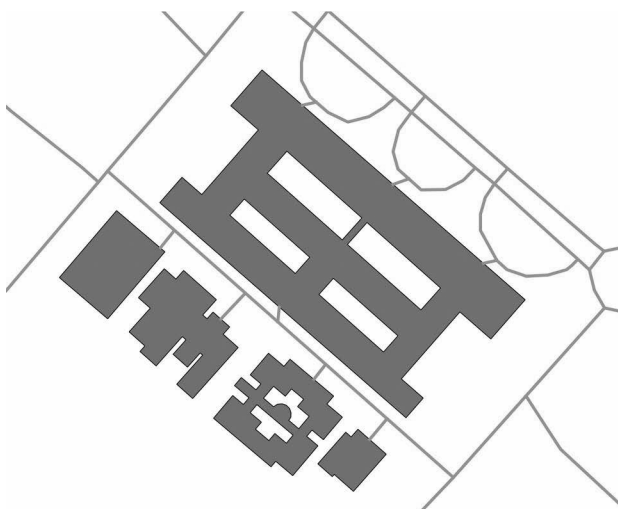


Figure 3: A set of buildings and the roads around them.

3. CONCLUSIONS

Each level of hierarchy handles data with a different level of detail (Space level: Spaces with the objects inside like furniture, Floor level: Floor-plan of each floor, Outdoor level: Building footprint and outdoor features). Such a framework would be able to provide the best functionality based on the type of data available in any given scenario by using the appropriate method for the task at hand.

REFERENCES

- [1] J. Sun and X. Li, (2011) "Indoor evacuation routes planning with a grid graph-based model," *19th International Conference on Geoinformatics*, Shanghai, pp.1-4.
- [2] L. Tan, H. Lin, M. Hu and W. Che, (2014) "Agent-based simulation of building evacuation using a grid graph-based model," *IOP conference series: earth and environmental science*, Vol.18, No.1
- [3] Y. H. Lin, Y. S. Liu, G. Gao, X. G. Han, C. Y. Lai and M. Gu, (2013) "The IFC-based path planning for 3D indoor spaces," *Advanced Engineering Informatics*, Vol.27, No.2, pp.189-205
- [4] S. Rai, M. Wang and X. Hu, (2015) "A graph-based agent-oriented model for building occupancy simulation," *Proceedings of the Symposium on Agent-Directed Simulation*, Society for Computer Simulation International, pp.76-83
- [5] L. Zhang, Y. Wang, H. Shi and L. Zhang, (2012) "Modeling and analyzing 3D complex building interiors for effective evacuation simulations," *Fire Safety Journal*, Vol.53, pp.1-12
- [6] M. Meijers, S. Zlatanova and N. Pfeifer, (2005) "3D geoinformation indoors: structuring for evacuation," *Proceedings of Next generation 3D city models*, Germany Bonn, Vol.6
- [7] N. Maheshwari and K. S. Rajan, (2016) "A semantic model to define indoor space in context of emergency evacuation," *International Archives of the Photogrammetry, Remote Sensing & Spatial Information Sciences*, Vol.41

A STUDY ON THE RESIDENT'S CONSCIOUSNESS OF TSUNAMI EVACUATION BEHAVIOR AFTER BUILDING THE TSUNAMI EVACUATION MOUND

K. MIYAUCHI¹, and K. TAKADA²

¹ Doctoral student, Graduate School of Advanced Science and Technology, Tokyo Denki University, Hatoyama, Japan

² Professor, Department of Architectural and Civil Engineering, Tokyo Denki University, Hatoyama, Japan, takada67@gmail.com (corresponding author)

Keywords: Tsunami Evacuation, Evacuation Mound,

1. BACKGROUND

In this study, evacuation method at Horikiri district in Tahara city, Aichi prefecture, was focused on since there would be hit by forthcoming Nankai trough earthquake with seismic intensity of 7 at maximum and also inundated with 2m depth within 18 minutes after the earthquake. There are 1,291 residents and 410 households as of 31 December, 2016. The ratio of elderly person with over 65 years is around 30%. This high ratio makes evacuation in this district more sever.

Meanwhile, this district is located in low flatland, as shown in the Figure 1, so that evacuation distance becomes longer. As shown in the Figure 2, Atsumi sport park, which locates on the slightly elevated hill and which is about 2 km away from residential area, is designated as tsunami evacuation place by the municipality. Since it is difficult to move to the evacuation place by foot before being inundated, the municipality set safety line as minimum goal in order not to give up their own evacuation and the safety line is marked on the road where 1.5m higher than estimated inundation level as shown by the picture in the in the Figure 2.

Considering such difficulty of the evacuation in this district, the municipality decide to build a tsunami evacuation mound on the site using the elementary school near the residential area. The top of the evacuation mound is 15 meters above sea-level which is higher than estimated inundation height with 11m-13m. The space of the mound is 850 square-meter as shown in the Figure 2, and 500 citizens can evacuate temporary.

In this study, influencing of the mound on the citizen's consciousness of tsunami evacuation was investigated by conducting questionnaire survey.

2. QUESTIONNAIRE SURVEY

In this study, a questionnaire survey was conducted to obtain the information mainly on (i) the implementation of disaster prevention and preparation measures in a household, (ii) the evaluation of the tsunami evacuation mound, (iii) the tsunami evacuation procedure (evacuation timing, evacuation place, moving means) and (iv) individual and household attributes. Outline of the survey is shown on Table 1.

3. EVALUATION OF THE EVACUATION MOUND



Figure 1: Landscape of the Horikiri district

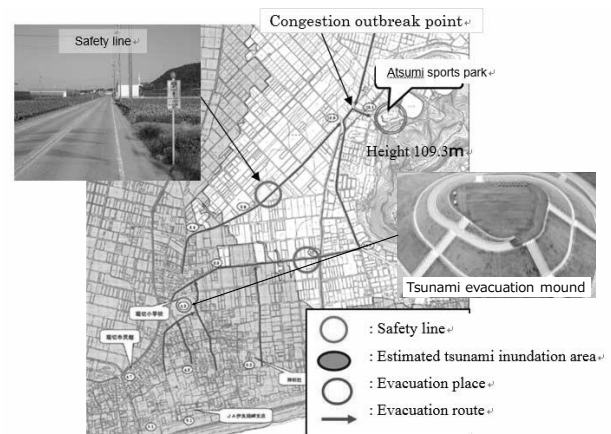


Figure 2: Location of the evacuation place and tsunami evacuation mound

Table 1: Outline of the survey

Households	378
Resident	1238
Number of surveys distributed	756
Number of surveys collected	303
Collection rate	40.1%

Figure 3 shows the evaluation of the tsunami evacuation mound. There are 10 question items from (a) to (j). The contents of the question is mentioned above the title of the figure. Evaluation results of each item is shown by age group. As shown in the figure (a), older age groups thinks that the mound will contribute to safer evacuation of older people. On the other hand, 40% of the older age group thinks that the mound cannot contribute to the safer evacuation. Meanwhile, as shown in the figure (b), all age groups think that the mound

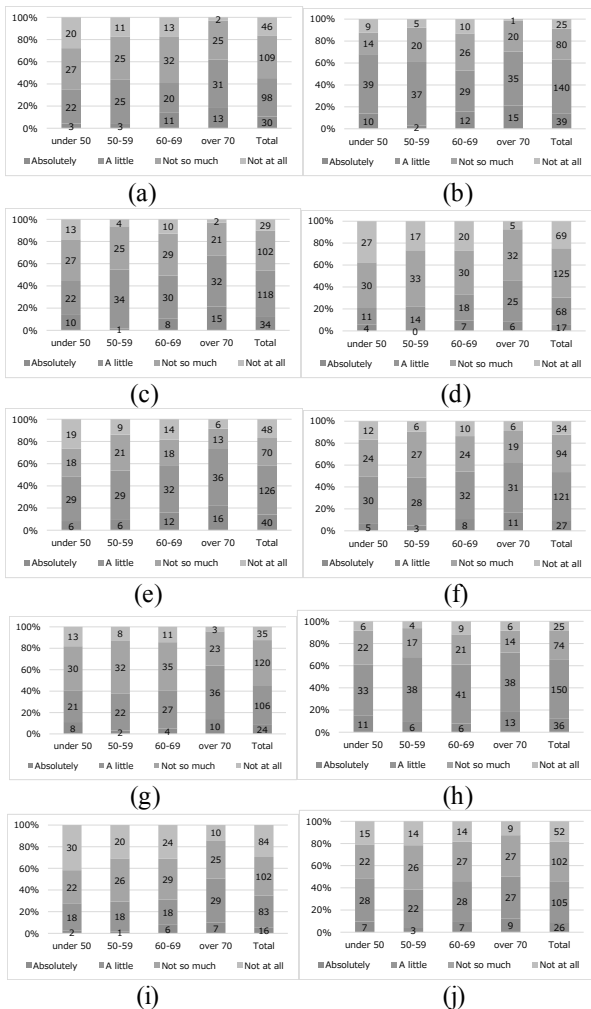


Figure 3: Evaluation of the tsunami evacuation mound

cannot contribute to safer evacuation for of support-needed person. Moreover, as shown in the figure (h), citizens think that there is existence effect to evoke tsunami evacuation routinely.

4. ASSUMED EVACUATION PROCEDURE

The respondents were requested to answer the considered evacuation procedure. Figure 4 shows the result of selected evacuation place during daytime and midnight. It shows that the evacuation mound locates at residential area is selected during midnight rather than during daytime. Meanwhile, Figure 5 shows the relation between evacuation place and moving means to the selected place during daytime and Figure 6 shows the relation during midnight. Comparing these figures,

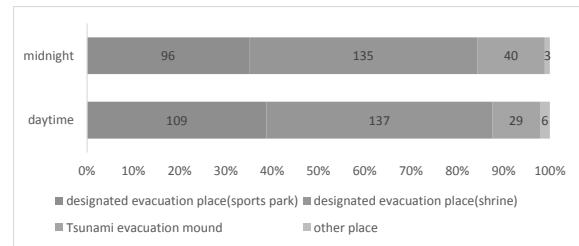


Figure 4: Selected evacuation place

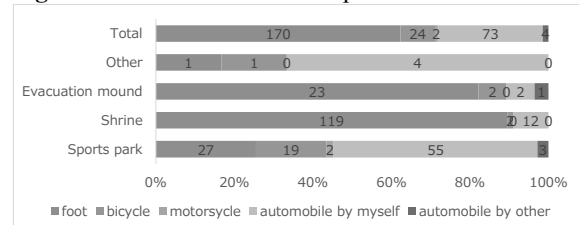


Figure 5: Evacuation place and moving means in case of daytime

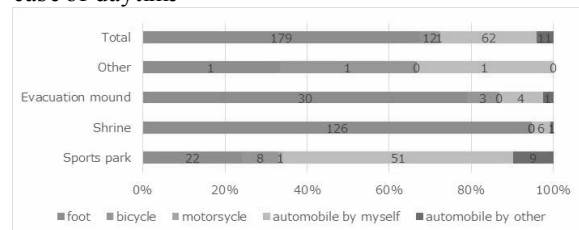


Figure 6: Evacuation place and moving means in case of midnight

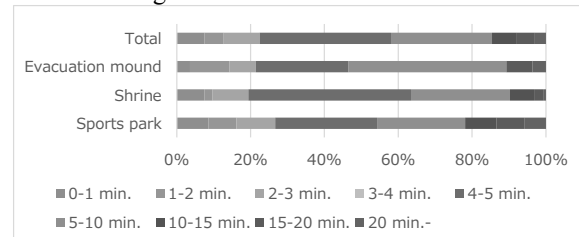


Figure 7: Evacuation place and evacuation timing in case of daytime

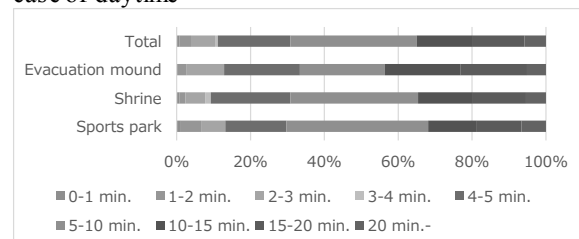


Figure 8: Evacuation place and evacuation timing in case of midnight

citizens tend to select foot as moving mode during midnight. Figure 7 and 8 show the relation between evacuation place and evacuation timing. It indicates that the evacuation timing during midnight is delayed and the timing of the citizen who choose the evacuation mound is especially delayed.

4. CONCLUSIONS

In this study, the citizen's evaluation to the tsunami evacuation mound and the considered evacuation procedure was examined. As the results, the influence of the mound on citizen's evacuation procedure was identified.

USMCA 2018

SESSION 9

DISASTER RISK & RESPONSE I

ANALYZING WIDE AREA POST SEISMIC EFFECTS OF THE GORKHA EARTHQUAKE USING PERSISTENT SCATTERER INTERFEROMETRY ON SENTINEL-1 IMAGES

A. TIWARI¹, A. B. NARAYAN¹, M. DEVARA², R. DWIVEDI², O. DIKSHIT¹

¹ Indian Institute of Technology, Civil Engineering - atiwari@iitk.ac.in

² Motilal Nehru National Institute of Technology- ([@mnnit.ac.in">rgi1703, ramjid](mailto:rgi1703,ramjid)) @mnnit.ac.in

¹ Indian Institute of Technology, Civil Engineering – ([@iitk.ac.in">avadhbn, onkar](mailto:avadhbn,onkar))@iitk.ac.in

ABSTRACT

Deformation events including landslides, flood and earthquakes occur frequently in the inhabited Kathmandu city in Nepal and surrounding mountains after the major Gorkha earthquake (8.1 M_w) in 2015. Information about the pattern and temporal rate of movement can be used as causative factors while developing rescue systems. In this study, a total of 21 Sentinel-1 Interferometric Wide Swath (IW) descending pass images of tracks 92 and 158, covering a time period of 27 months, are processed using the Persistent Scatterer interferometry (PSI) algorithm to estimate wide area post seismic effects of the Gorkha earthquake in 2015 and other deformation events in Nepal. The wide swath images provide a swath width of nearly 250 km divided in three sub-swaths. PSI algorithm was applied to two complete sub-swaths of the images corresponding to the two tracks, resulting in extraction of 360532 and 1177124 measurement pixels for the Mid-Western and Western Nepal regions respectively. In addition, a region containing the Kathmandu city and its surroundings was processed using 11 images of track 92. From the 1 dimensional Line Of Sight (LOS) displacement maps, it is evident that the Kathmandu city underwent subsidence at a rate of 200 mm yr⁻¹. Also, the hilly regions near to the Gorkha earthquake show southward downward movement (-200 to 250 mm yr⁻¹). Apart from subsidence, some hilly slopes show uplift ranging from 200 to 520 mm yr⁻¹. Analyzing the measurement pixels selected in by the PSI approach, it is found that pixels selected in the mountainous regions have larger topographic error contribution as compared to the urban area (Kathmandu and near surroundings), which constructed a bias in the displacement computation in case of hilly areas. From the time series displacement estimates generated from the processing of two tracks, it is observed that there are a number of regions showing large displacement magnitudes with a regular pattern, and can become cause of deformation events in near future. Regular time series monitoring using the Sentinel-1 IW data, along with GPS observations can provide information about the 3 dimensional displacement signature.

Keywords: *Keywords: Land subsidence, multi-temporal radar interferometry, Persistent Scatterers*

1. INTRODUCTION

Analysis of deformation events requires identification of study site, displacement measurement and interpretation of the displacement pattern. Deformation zones with a spread of less than a km or two, can generally be surveyed temporally using ground based geodetic surveying methods. Such field surveys involve the application of geodetic sensors like Global Navigation Satellite System (GNSS), Laser Scanning, Photogrammetry, Total Station and level network surveys. However, such surveys can become infeasible for analysis of deformation activities of very large areas e.g. area greater than 100 km, since geodetic surveys require locating sensors at various locations within the deformable zones and the surveys may get labour, cost and time intensive. Over the last decade, synthetic aperture radar interferometry (InSAR) has been successfully employed to retrieve one dimension line of sight (1D LOS) displacement velocities of relatively large areas. Each measurement pixel in a SAR interferogram acts a measurement point on the field and detects mm level movement of the surface. Processing a stack of SAR interferograms corresponding to images

acquired at different times can provide time series displacement estimates. During the last decade, multi-temporal SAR interferometry (MT-InSAR) algorithms are applied to detect displacement time series ([1], [2], [3], [4]). Information about the pattern and temporal rate of movement are used as causative factors while developing rescue systems.

The Himalayan region is predominantly affected by deformation events primarily comprising landslides, earthquakes and land subsidence. In this study, the Kathmandu city lying in Nepal and the surrounding mountains are investigated. Persistent Scatter Interferometry (PSI) based MT-InSAR approach is applied to investigate post seismic effects of the Gorkha earthquake (8.1 M_w) in 2015. The earthquake drastically affected the inhabited Kathmandu city in Nepal and surrounding mountains [5]. Next section describes the dataset used in this study, followed by the Methodology section. Results and discussions on the displacement maps are elaborated next, followed by Conclusions.

2. STUDY AREA AND SATELLITE DATASETS

Occurrence of the Gorkha earthquake (M_w 7.2) in 2015, along with subsidence activities associated with the Kathmandu city and areas lying in the Mid-Western Nepal encouraged deformation investigations of three different study areas for this research work. Subduction of the Indian plate beneath the Eurasian plate has caused uplift in the Himalayas, which is one of the prominent reasons for presence of tectonic events [5]. Gorkha lies in the Main Himalayan Thrust, an active deformation zone. Further, the densely populated Kathmandu city, lying in the lesser Himalayas, lies in an active seismic zone. The city has witnessed earthquakes nearly hundred years back, and is currently affected by subsidence activities [5]. Figure 2 shows the three study sites, covering Mid-Western and Western Nepal, and the city of Kathmandu. In order to see the effect of the earthquake, the other two areas were chosen on either sides of the earthquake. Kathmandu lies 82 km south east of the earthquake Hypocenter [7]. Other end of the earthquake lies in the Himalayan region and is prone to wide area deformation.

Two sets of 11 and 10 Sentinel-1 interferometric wide swath (IW) images corresponding to tracks 92 and 158 respectively, and covering a time period of 18 months were acquired. Since images of track 92 covered the region near to the Gorkha earthquake and the Kathmandu city, a single stack was used with different subsets and sub-swaths during the MT-InSAR processing. Since Sentinel-1 images have relatively reduced temporal and spatial baselines than the earlier missions, greater number of measurement points was expected. Table 1 shows the datasets used in this study and the relevant information required for MT-InSAR processing.

Table 1: Sentinel-1 datasets used to investigate deformation events in Nepal.

Parameters	Mid-Western Nepal	Western Nepal	Kathmandu
Track	158	92	92
#images	10	11	11
* B_{temp}	0 to 240	0 to 264	0 to 264
^s B_{perp}	0 to 180	0 to 160	0 to 160

#- No. of images

*- Range of temporal baselines (days)

^s - Range of perpendicular baselines (meters)

3. METHODOLOGY

In this study, multi-temporal SAR interferometry is applied on Sentinel-1 TOPS images. This required a stack of co-registered interferograms, which were generated by differential interferometric processing of a set of images belonging to same track and having the same ground coverage. The Sentinel-1 images contain three sub swaths, each sub swath covering a swath of about 80-100 km [6]. A specific sub-swath is selected based on the area of interest (AOI), and if the AOI lies in more than one sub swath, then more than one sub-swaths are processed together. This can be accomplished by processing individual sub-swaths and merging the sub-swaths later. Since three different study areas were chosen in this study, three set of images were used separately. Further, in all the three cases, the investigated site was covered in a single sub-swath, avoiding the requirement of merging the sub-swaths. A master image was chosen for each image stack, based on the criteria of minimizing the perpendicular and temporal baseline, while maximizing temporal coherence.

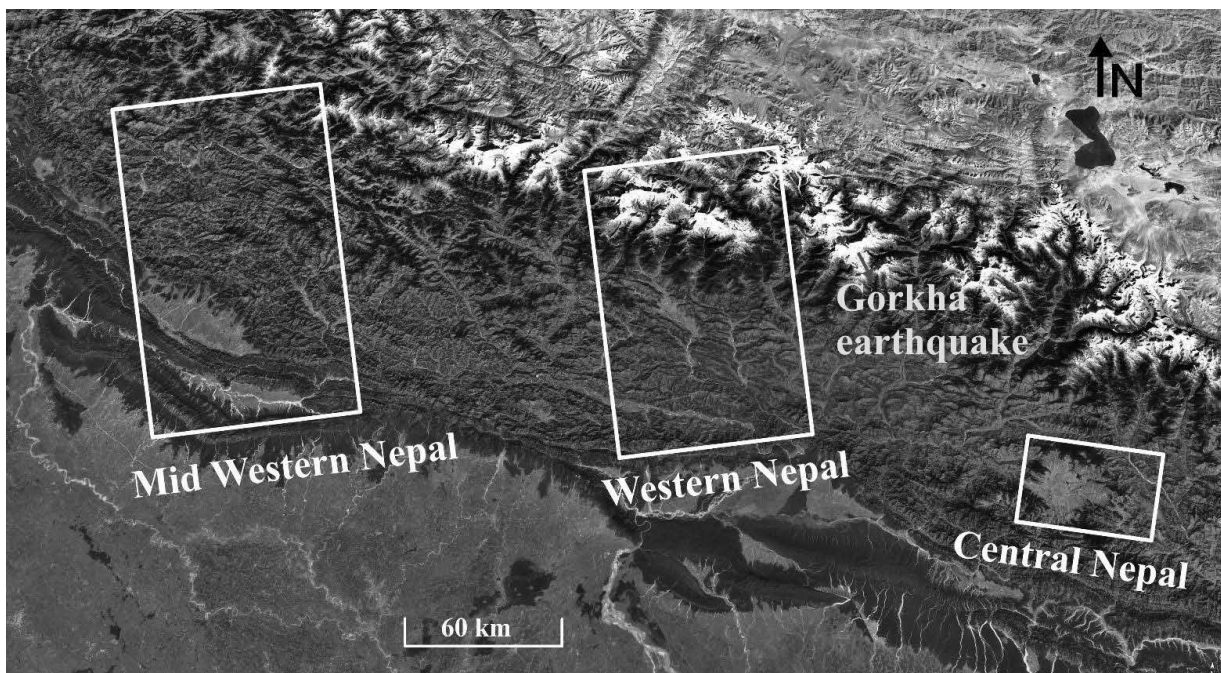


Figure 1. Google earth image of the study area. White rectangles show coverage of different set of Sentinel-1 image

The processing was divided into two steps, (i) generation of differential interferogram stack and (ii) MT-InSAR processing of the stack of differential interferograms. For stack generation, the Sentinels Application platform (SNAP) toolbox was employed. The stack was later exported to the Stanford method of Persistent Scatterer Interferometry (StaMPS) environment for MT-InSAR processing.

Each image in the stack was split into one sub-swath, such that it includes the same area ground coverage for all the images. Orbital corrections were applied to reduce the orbit related errors. The images were then co-registered with respect to the chosen master image, and resampled onto the grid of the master after co-registration. Once co-registered, each image was deburst to remove demarcation boundaries present in each sub-swath. The whole stack can now be cropped using the subset operation for selecting the AOI. Complex multiplication of each slave image with the master was then carried out, resulting in interferogram generation. A 3 arc second Digital elevation model (DEM) from SRTM was used for topography removal, finally producing a stack of differential interferograms [4]. Figure 2 shows the procedure followed for preparing a stack of differential interferograms. Using this procedure, three stacks of differential interferograms were generated, and exported to StaMPS environment for MT-InSAR processing.

MT-InSAR processing of the differential interferogram stack was performed using the Persistent Scatterer Interferometry (PSI) algorithm in StaMPS environment. The steps primarily involved selection of PS pixels, phase unwrapping and displacement estimation [4]. The MT-InSAR method followed in this study is shown in Figure 2. Initially, a set of candidate PS pixels were selected using the amplitude dispersion characteristics, *i.e.* the ratio of standard deviation and mean of the pixels in a time series. The candidate pixels were tested for phase stability using time series phase deviation. Pixels which passed the test of both amplitude dispersion and phase stability were selected as PS pixels.

The interferometric phase of these pixels contain components attributed to atmospheric error ϕ_a , surface displacement ϕ_{def} , topography ϕ_t , and noise ϕ_n , as shown in equation (1). The term k denotes the unknown number of phase cycles required to obtain the unwrapped phase value.

$$\phi_{int} = \phi_{def} + \phi_t + \phi_a + \phi_m + \phi_n + k.2\pi \quad (1)$$

Removal of terms other than ϕ_{def} from the interferometric phase could help in detection of temporal displacement. However, since the phase value is cyclic (wrapped to modulo 2π), the values need to be unwrapped. Hence, phase unwrapping was done to

unwrap the phase of the selected PS pixels. Once unwrapped, the unwrapped phase were converted to one dimensional line of sight (1D LOS) displacement. A 1D LOS velocity map generated from the above analysis showed time series velocity of each PS pixel over the period of study. The next section presents the results obtained by following the above mentioned methodology on the three study areas.

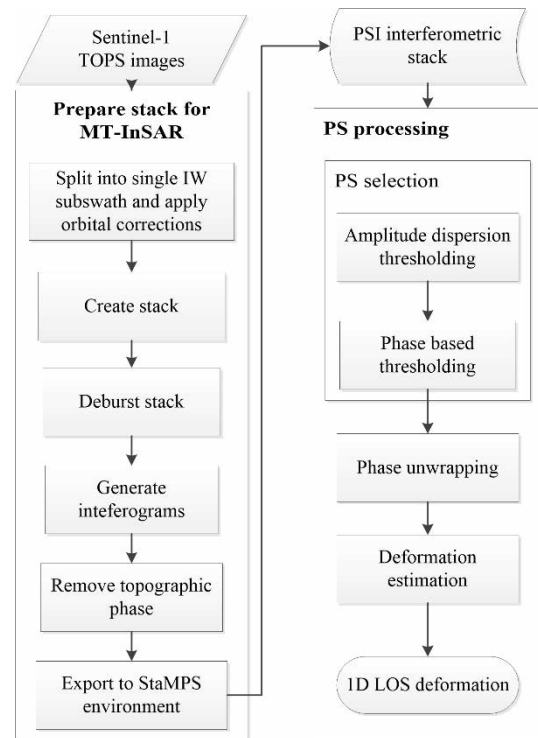


Figure 2. Multi-temporal InSAR processing chain for Sentinel-1 wide swath images.

4. RESULTS AND DISCUSSION

MT-InSAR processing of the Mid-Western and Western Nepal using the PSI algorithm resulted in the extraction of 360532 and 832939 measurement points respectively. Figure 3 shows the 1D LOS velocity plots of both the regions, with cold colours (blue) indicating movement towards the LOS and warm colours (red) showing movement away from the satellite LOS. In case of Mid-Western Nepal, it is observed that Khalanga and Damachaur regions had encountered subsidence at a rate of $\sim 100 \text{ mm yr}^{-1}$. For the western regions lying near to Gorkha, the higher magnitude subsidence is observed, with the complete displacement values ranging from -249.6 to 522.9 mm yr^{-1} . Pokhara, Besisar and Byas are the areas affected by subsidence. Mountainous regions near to Gorkha seem to have uplifted during the period of observations. Figure 4 shows the 1D displacement map of the Kathmandu city and near surroundings. It is observed that the city encountered subsidence at a rate of 200 mm yr^{-1} . Apart from Kathmandu city, a nearby region

named Tokha observed subsidence at a rate of $\sim 150 \text{ mm yr}^{-1}$.

Qualitative assessment of the displacement estimates was further carried out in order to find the accuracy of the deformation estimates. For this, error arising from different components of the interferometric phase was evaluated. Error estimates of the master related errors, orbit errors and phase noise had negligible magnitude. However, topographic error estimates showed high

magnitude. The topographic error can be attributed to errors associated with external DEM, which is used to remove topography from the interferometric stack. Furthermore, it is also noticed that the DEM elevation computations in case of hilly terrain is erroneous, with the errors reaching up to 50 meters in some cases.

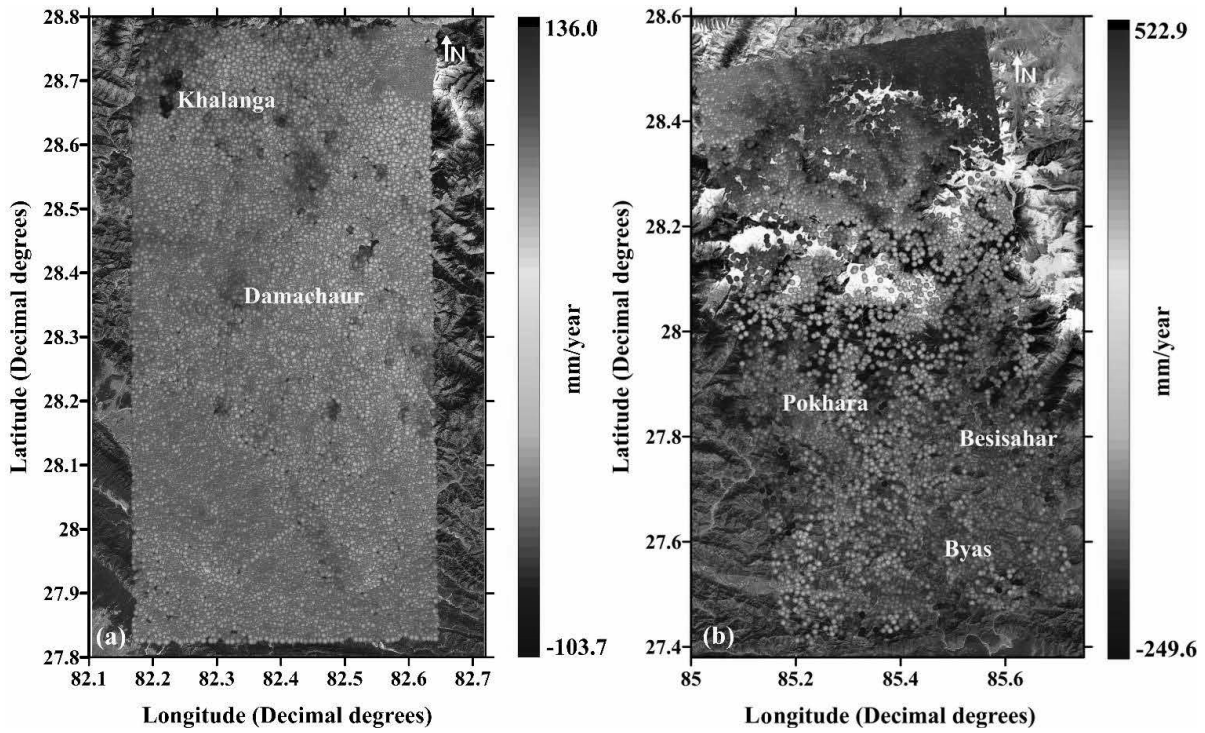


Figure 3. Time series velocity plots overlaid on Google earth images for the Mid-Western and Western Nepal regions.

(a) Mid-Western region and (b) Western Nepal.

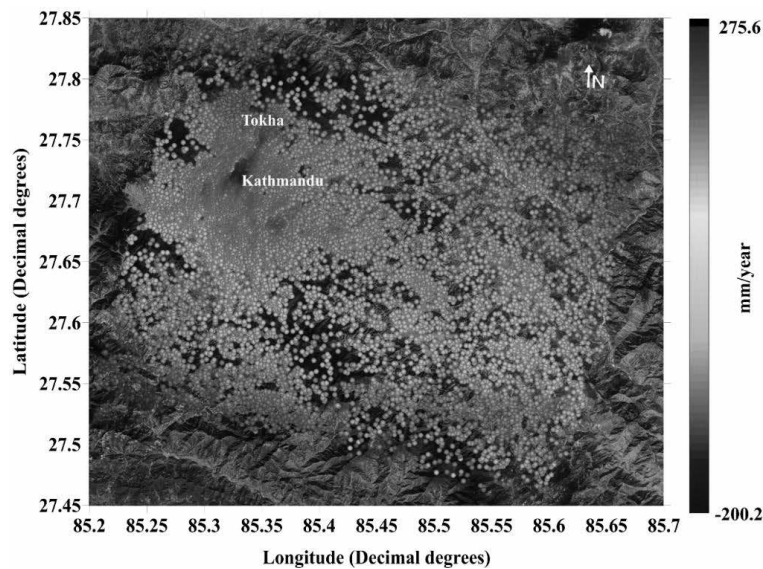


Figure 4. Time series velocity plot overlaid on Google earth image of the Kathmandu city.

Figure 5 shows the topographic errors plotted on the Google earth images of the Mid-Western and Western Nepal. It is revealed from the two plots (Figures 5 (a) and (b)) that the hilly areas have higher topography contribution. The error values ranged from -0.199 to 0.175 and -0.361 to 0.105 radians m^{-1} for the Mid-Western and Western Nepal respectively. The Western Nepal

region is near to the Gorkha, and is surrounded by mountains, which can be the reason for high magnitude of topographic errors. Moreover, for the Kathmandu city, which is situated at relatively less altitude, has lower values of topographical error, as shown in Figure 6. The error estimates in this case range from -0.101 to 0.102 radians m^{-1} .

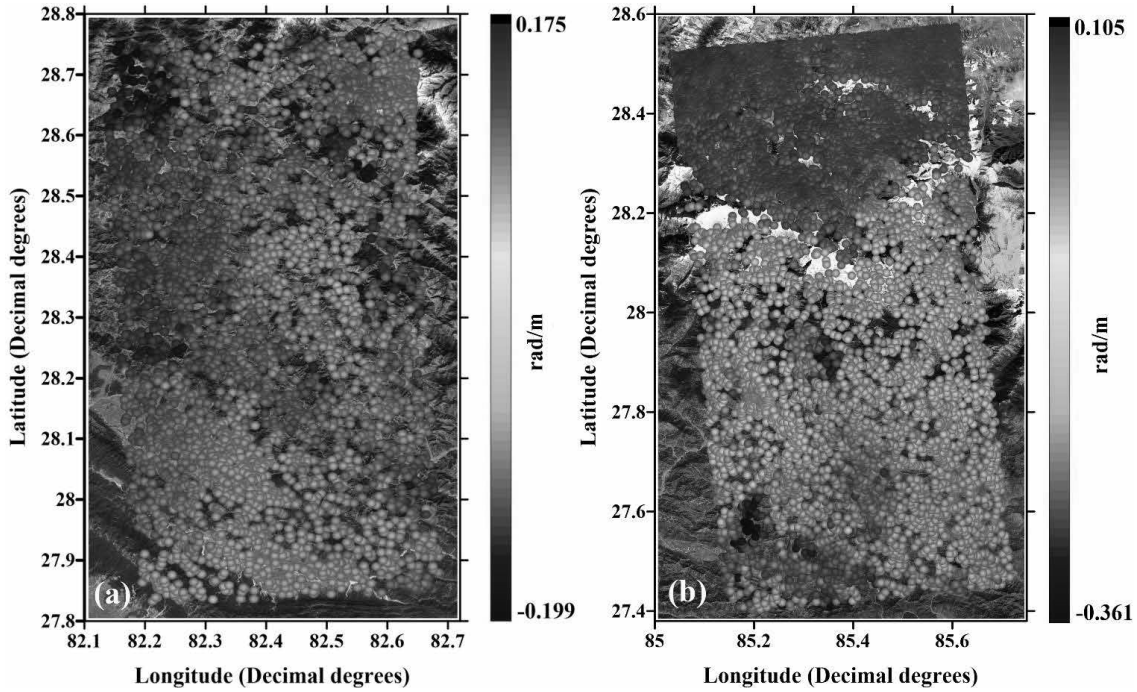


Figure 5. Plots of topographic errors for the displacement estimates of the Mid-Western and Western Nepal regions. (a) Mid-Western region and (b) Western Nepal.

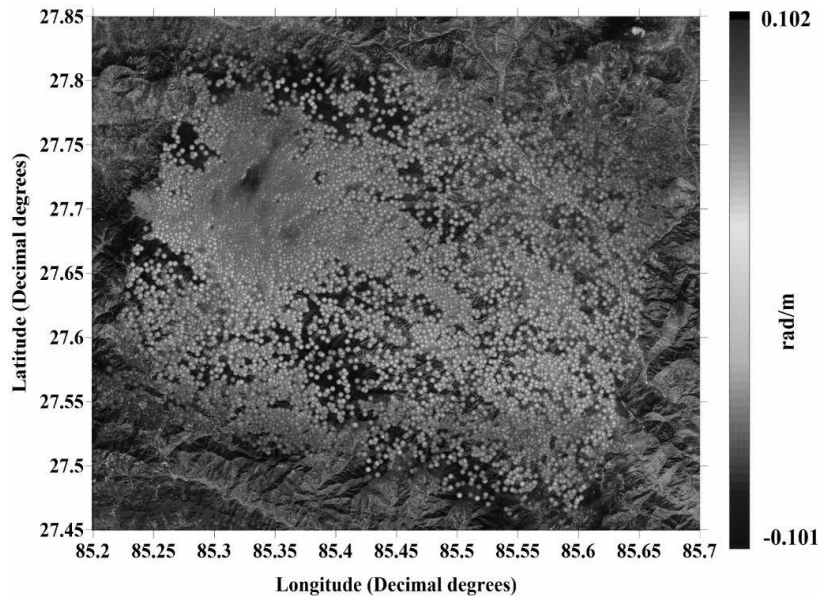


Figure 6. Plot of topographic error for the displacement estimates of the Kathmandu city.

5. CONCLUSION

Three wide areas covering the Mid-Western, Western and Central Nepal containing the densely populated Kathmandu city was investigated for presence of deformation events using the MT-InSAR approach on Sentinel-1 images. PSI based MT-InSAR approach extracted good number of measurement points in all the three areas, and detected large magnitude subsidence in areas lying close to Gorkha and in the city of Kathmandu. Regular monitoring of the detected deformation zones can help in early rescue operations. It is further revealed that the displacement estimates were affected by the topographical error estimates, which was higher in case of high mountains situated near to Gorkha while showing significant presence in the displacement estimation of all the sites. More time series observations, along with the improvement of topographical error estimation can provide better insight into the ongoing wide area deformation activity.

REFERENCES

- [1]. Crossetto, M., Monserrat, O., Gonzalez, M.C., Devanthery, N., Crippa, B., (2016). "Persistent Scatterer Interferometry: A review", *ISPRS Journal of Photogrammetry & Remote Sensing*, 115, 78-89.
- [2]. Ferretti, A., Prati, C., and Rocca F., (2000). "Nonlinear subsidence rate estimation using Permanent Scatterers in differential SAR", *IEEE Trans. GARS* Vol. 38, pp. 2202 – 2212, September 2000.
- [3]. Ferretti, A., Guarnieri, A.M., Prati, C., Rocca, M., (2007). *InSAR Principles: Guidelines for SAR Interferometry Processing and Interpretation, TM19*, The Netherlands.
- [4]. Hooper, A., Segall, P., and Zebker, H., (2007). "Persistent Scatterer InSAR for Crustal Deformation Analysis, with Application to Volcan Alcedo, Galapagos" *Journal of Geophysical Research*, 34.
- [5]. Krishnan P.V.S., Kim, D.J., Jung, J., (2018). "Subsidence in the Kathmandu Basin, before and after the 2015 Mw 7.8 Gorkha Earthquake, Nepal Revealed from Small Baseline Subset-DInSAR Analysis" *GIScience & Remote Sensing*, Vol. 55 (4), 604-621.
- [6]. Veci, L, 2015. *TOPS interferometry tutorial*, ESA Sentinel-1 toolbox, Array systems computing Inc.
- [7]. Sato, H. P., and Une, H., (2016). "Detection of the 2015 Gorkha earthquake-induced landslide surface deformation in Kathmandu using InSAR images from PALSAR-2 data" *Earth, Planets and Space*, 68-47.

A STUDY ON THE ASSESSMENT OF REGIONAL EVACUATION INFORMATION USING METEOROLOGY INFORMATION IN JAPAN

Kazuhiro NAGAKI¹, Yuma MORISAKI², Makoto FUJII³, and Junichi TAKAYAMA⁴

¹ Student, Kanazawa University, Department of Environmental Design, JAPAN, kazuhiro618@stu.kanazawa-u.ac.jp

² Bachelor(Eng.), Kanazawa University, Department of Environmental Design, JAPAN, yki20@stu.kanazawa-u.ac.jp

³ Ph.D., Assistant Professor, Kanazawa University, Department of Geosciences and Civil Engineering, JAPAN, fujiu@se.kanazawa-u.ac.jp

⁴ Dr., Eng., Professor, Kanazawa University, Department of Geoscience and Civil Engineering, JAPAN, takayama@se.kanazawa-u.ac.jp

Keywords: evacuation timing, information announcement, personal attribute, area, personal distribution

1. INTRODUCTION

Unlike sudden disasters such as earthquakes, flood damage caused by heavy rain can be predicted based on various data. However, in recent disasters caused by torrential rains frequently occurring in Japan, we have not been able to respond appropriately, such as issuing an evacuation order on the verge of levee of the embankment. Since flood damage is different from earthquake disaster etc. and the progress of disaster is relatively control, human damage can be minimized if early evacuation before the expansion of damage occur. Therefore, we think that provision of evacuation information at appropriate timing to local residents is important. In the heavy rain that occurred mainly in Hiroshima and Okayama prefectures shown as Figure 1, in July, 2018, (Heavy rain in July 2018), damage ranged to 221 deaths and 390 injured people [1]. More than 70% of the dead were over 60 years old [2], it was highlighting the fact that it was not possible to properly deal with persons who needed consideration in the event of a disaster. In the current information providing method, personal attribute such as age and physical condition of a resident is not taken into consideration, and planar information is provided. In order to reduce the damage of persons who need consideration in times of disasters, a new evacuation information providing method matching the area and personal attributes is necessary. Conventional research has many things that analyze changes in people's sense of crisis and evacuation awareness by changing the contents of information to be provided. In this study, we focused on the fact that there is a clear difference in the time required for evacuation between healthy people and those who need consideration, propose appropriate timings to provide evacuation information appropriate to the age and physical condition of the resident.

2. FLOW OF A STUDY AND USE DATE

We aim to examine how much damage can be reduced by considering the personal attribute and area attribute of the resident in the evacuation information and analyze with the four steps shown as Figure 2.

In step 1, examine of persons who need consideration in the event of a disaster. In the heavy rain in 2018,



Figure 1: District that was heavily damaged by heavy rain

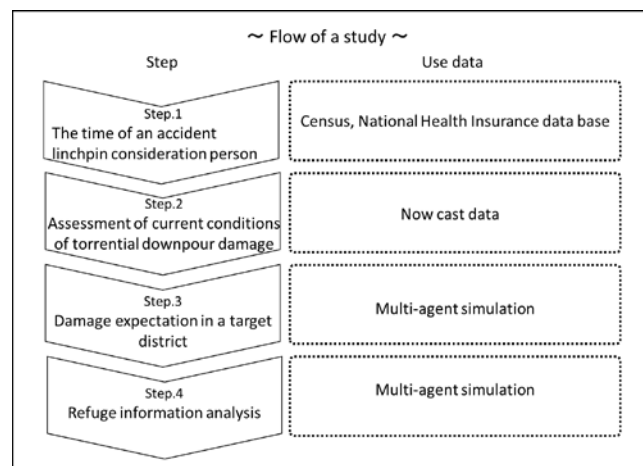


Figure 2: Flow of a study

70% of the dead are over 60 years old, and many elderly people are sacrificed due to heavy rain. Since it is indispensable to grasp detailed information of people who need consideration during disasters such as elderly people to reduce victims, we will examine those who are important in disasters using the census and the National Health Insurance database.

In step 2, we grasp the target district. As a basic examine of damage, understand the situation such as time transition of rainfall of heavy rain in Hiroshima prefecture and Okayama prefecture and time of evacuation information provision. To examine detailed rainfall conditions, use the data of Now cast shown as

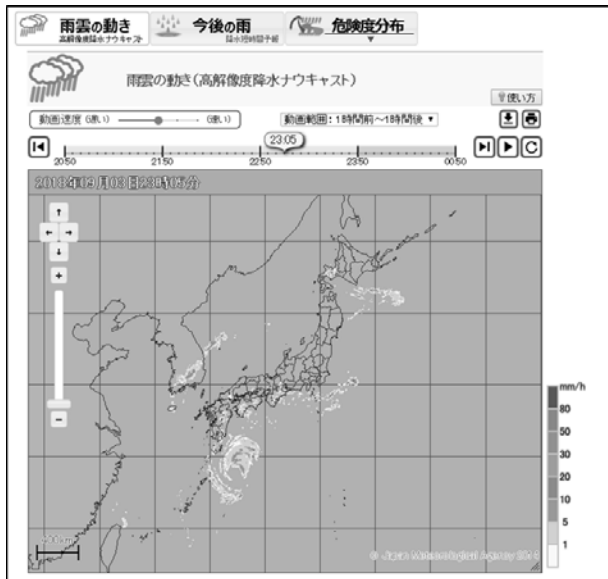


Figure 3: The data of Now cast

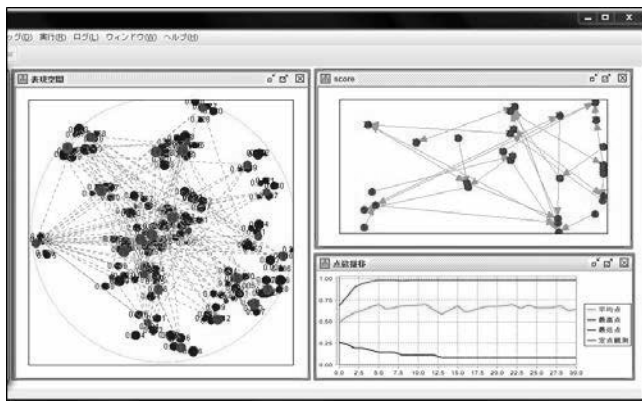


Figure 4: Multi-agent simulation

Figure 3. The data of Now cast accumulates what was observed and announced by the Meteorological Agency such as current situation and future prediction once every five minutes.

In Step 3, damage prediction of the target area is performed. It is necessary as a comparison target when examine the damage situation of the target district by present evacuation information provision and showing a new information provision method. Assuming that the torrential rain examined in Step 2 in the target area occurred in the target area, perform multi-agent simulation to predict damage, shown as Figure 4. By using multi-agent simulation, it is possible to simulate the settings such as walking speeds of healthy people and those who need consideration in times of disasters.

Step 4 conducts evacuation information analysis. In order to quantitatively evaluate the damage of new evacuation information provision method, we conduct multi agent simulation. Considering the information on persons who took care of during disasters examined in Step 1, we provide information separated by area rather than planar information and Compare with the current damage prediction in step 3.

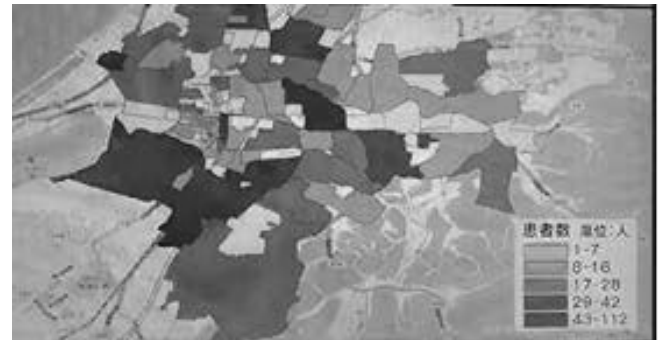


Figure 5: Disease distribution by medical big data

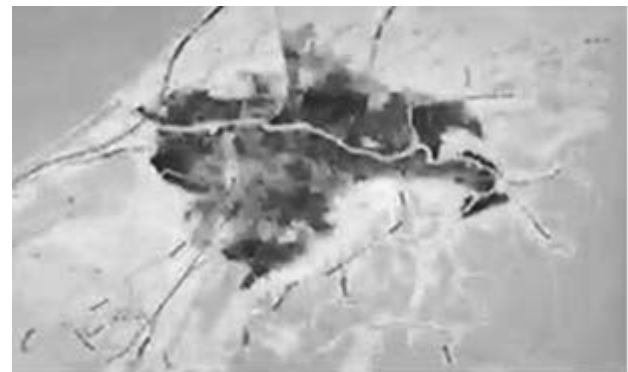


Figure 6: Depth of flood

3. UNIQUE DATA OF THIS STUDY

In this study, unique data use to analyze the distribution of disease which examine the vulnerable people during large scale disasters. That data has disease name, age, address, total amount of medical fee and so on. Figure 5 show that disease distribution has some characteristics. Figure 6 shows that depth of flood in target area. Maximum flood depth is about 5m, then two story houses are inundated by the flood. In this situation, aged person does not evacuate safety from their house due to inundate water by flood.

4. CONCLUSION AND FUTURE TASKS

In this research, we review current evacuation information provision method and propose new evacuation information providing method focusing on the timing and areas, attributes.

Future tasks include National Health Insurance Database, collection of census, and organization of Now cast data. In addition, we conduct a questionnaire survey to examine the present evacuation information provision law, conduct interview surveys to local governments and weather stations.

REFERENCES

- [1] Fire and Disaster Management Agency, Japan
<http://www.fdma.go.jp/bn/318b43ad8ead2c717087f45ff64a427e5cfc343d.pdf>
- [2] Asahi Shimbun Digital (2018)
<https://www.asahi.com/articles/ASL7D7FSZL7DPTIL01N.html>

EVALUATION OF REGIONAL HEALTH LEVEL DURING SUPER-AGING SOCIETY

Shizuka SANO¹, Junichi TAKAYAMA², Makoto FUJII³, Kiyoko YANAGIHARA⁴

Tatsuya NISHINO⁵, Masahiko SAGAE⁶ and Kohei HIRAKO⁷

¹ Bachelor (Eng.), Kanazawa university, Dept. of Environmental Design, osizu219@stu.kanazawa-u.ac.jp

² Dr., Eng., Professor, Kanazawa university, Geosciences and civil Engineering, takayama@staff.kanazawa-u.ac.jp

³ Ph.D., Assistant Professor, Kanazawa university, Geosciences and civil Engineering, fujii@se.kanazawa-u.ac.jp (corresponding author)

⁴ Ph.D., Associate Professor, Kanazawa university, Pharmaceutical and Health Sciences, kyana@mhs.mp.kanazawa-u.ac.jp

⁵ Ph.D., Associate Professor, Kanazawa university, Geosciences and civil Engineering, tan378@se.kanazawa-u.ac.jp

⁶ Ph.D., Professor, Kanazawa university, Human and Social Sciences, sagae.masahiko@gmail.com

⁷ Bachelor(Economics.), Project Assistant Professor, Kanazawa university, Organization of Frontier Science and Innovation, hirako@staff.kanazawa-u.ac.jp

Keywords: KDB, requiring long-term care, Komatsu city, regional characteristics

1. BACKGROUND AND PURPOSE

The average life span of Japan continues to grow year by year, the aging rate has reached 27.3%, and Japan has already entered into a super-aging society [1]. As a result, the number of care-need certificated persons has increased rapidly, and medical and nursing care problems will become more serious. In response to this problem, we will establish of a "Community-based integrated care systems" that enables elderly people to continue living in their home towns even if they come to need long-term care [2].

In Japan, which is a super-aging society, it is an urgent issue to build a community where elderly people can continue living at home, not nursing facilities, even if nursing care is needed. Therefore, in this study, 25 regions are classified into 6 groups with similar characteristics by cluster analysis using the National Health Insurance Data which is medical big data, and the questionnaire result. Then, clarify the living environment in the area where level of care dependency increases and where level of care dependency is maintained.

There have been few studies on factors that cause regional differences of changes in the level of care dependency. In addition, there is not much suggestion on how to utilize data on care-need certificated persons among the National Health Insurance Data. For this reason, the novelty of this study is to grasp the relationship between change in the level of care dependency and living environment using the National Health Insurance Data not fully utilized.

2. OVERVIEW OF ANALYSIS

Komatsu city, Ishikawa Prefecture, to be analyzed has a population of 108,582 people. There are 228 town, and it is divided into 25 elementary school districts. The aging rate of Komatsu city is 27.6%, which is higher than the national average of 26.6% [3].

We use data on care-need certificated persons in the National Health Insurance Data provided by Komatsu

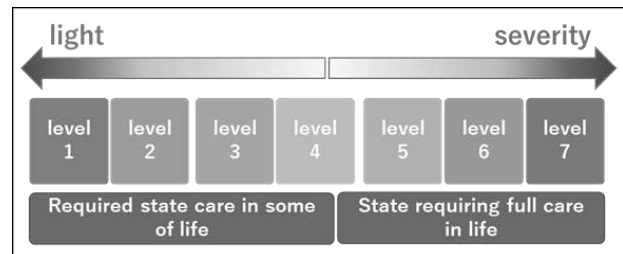


Figure 1: Level of care dependency

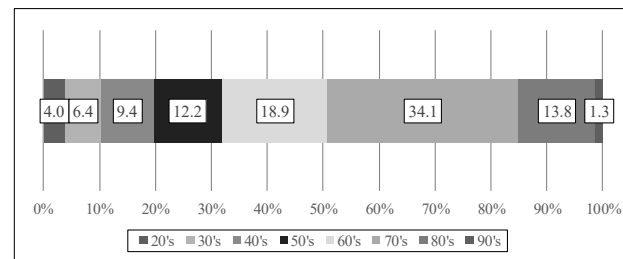


Figure 2: Percentage of respondents by age

city. This data includes personal attributes of late-stage elderly who certificated care-need, level of care dependency, content of nursing care service used, cost of care, etc. Depending on the physical and psychological state of the elderly, it is divided into seven level of care dependency. (Figure 1)

3. ANALYTICAL METHOD

For 25 elementary school districts in Komatsu city, we classify into six groups by agglomerative hierarchical clustering with the proportion of people who rose level of care dependency and the 17 variables representing the living environment.

For the proportion of people who rose level of care dependency, calculate for each elementary school district using the National Health Insurance Data. In this study, we refer to the proportion of people who rose level of care dependency as "State deterioration rate". State deterioration rate is the proportion of the people who

worsened to the level 3 to 7 (in 2015) to the people who certified the level 1 or level 2 (in 2012).

For the 17 variables representing the living environment, use the questionnaire for Komatsu resident. The questionnaire survey period was August 2017, and it was possible to collect 1523 samples. Figure 2 shows that more than half of respondents are elderly people; therefore, from the questionnaire result, we can grasp the living situation of elderly in Komatsu city. From the questionnaire, the response rate to the four kinds of question items are set as variables. The question items are divided into “Enhancement of living environment”, “Usual outing situation”, “Regional connection”, “Health awareness”.

4. RESULT OF ANALYSIS

Table 1 shows the average, unbiased variance, standard deviation of each of the 18 variables used for cluster analysis. It can be seen that the variable of “No smoking experience”, “Provision of commercial facilities”, “To go out 5 days a week or more” with large standard deviation greatly affects the classification result.

Table 2 shows the average value of 18 variables for each of the six clusters. The characteristics of cluster 3 with the largest State deterioration rate are unsatisfactory living environment, inconvenience go out, regional

Table 1: The average, unbiased variance, standard deviation of each of the 18 variables used for cluster analysis

Variable	Average	Unbiased variance	Standard deviation
State deterioration rate	42.65	97.07	9.85
Provision of commercial facilities	26.45	164.49	12.83
Provision of medical welfare facilities	26.97	91.15	9.55
Provision of public facilities	17.02	53.33	7.30
Provision of public transport	14.22	55.71	7.46
Enhancement of employment location	10.78	43.19	6.57
Sufficient greening maintenance	24.28	61.83	7.86
Safe sidewalk maintenance	32.86	119.99	10.95
To go out 5 days a week or more	64.10	158.78	12.60
Inconvenience is shopping	20.16	116.19	10.78
Inconvenience is attending a hospital	20.48	108.92	10.44
Intimate neighborhood relationship	11.05	64.38	8.02
Active participation in the neighborhood association	20.96	138.73	11.78
To exercise five days a week or more	18.66	52.92	7.27
Keep in mind a well-balanced meal	40.33	128.26	11.33
Keep in mind a regular life	48.13	125.72	11.21
No smoking experience	63.69	226.79	15.06
To get medical exams every year	84.35	50.07	7.08

Table 2: The average value of 18 variables for each of the six clusters

No	State deterioration rate	Provision of commercial facilities	Provision of medical welfare facilities	Provision of public facilities	Provision of public transport	Enhancement of employment location	Sufficient greening maintenance	Safe sidewalk maintenance	To go out 5 days a week or more	Inconvenience is shopping	Inconvenience is attending a hospital	Intimate neighborhood relationship	Active participation in the neighborhood association	To exercise five days a week or more	Keep in mind a well-balanced meal	Keep in mind a regular life	No smoking experience	To get medical exams every year
1	43.73	41.21	40.52	29.00	22.61	17.18	33.99	42.36	67.55	14.01	15.24	7.70	16.63	17.22	38.44	46.53	51.10	81.17
2	45.32	22.55	23.31	14.56	12.89	8.62	17.98	27.79	68.78	17.81	21.15	7.66	20.11	14.82	42.03	49.32	63.30	87.39
3	46.96	11.13	18.64	9.85	6.21	4.64	29.27	48.02	48.30	26.36	25.93	25.80	40.95	29.26	52.12	56.74	89.72	83.71
4	32.18	31.49	29.93	16.50	14.39	12.69	25.32	24.55	76.32	13.10	11.53	8.52	15.91	17.53	38.47	50.82	53.05	81.60
5	43.08	45.14	35.42	17.36	25.00	21.53	27.78	21.53	55.93	21.00	21.38	2.08	8.33	11.00	20.00	22.00	55.00	92.86
6	46.88	11.86	15.26	18.18	7.54	3.33	13.95	35.98	47.72	46.20	38.81	17.07	18.29	26.21	38.75	48.81	73.61	78.24

connections are intimate and high health awareness. Cluster 6 with second largest State deterioration rate is area where it is very inconvenient for usual outing and few people get medical exams every year. Cluster 4 with the smallest State deterioration rate is area where usual outings are very convenient and go out frequently. The characteristics of cluster 5 with second smallest State deterioration rate are satisfactory living environment and poor regional connections.

5. CONCLUSIONS

We divided 25 elementary school districts of Komatsu city into 6 clusters according to regional characteristics. As a result, it was revealed that common characteristics in areas where level of care dependency increases and where level of care dependency is maintained are convenience to usual outing. Level of care dependency is easier to rise in areas where usual outings are inconvenient, and conversely useful outing areas are less likely to rise in level of care dependency. Furthermore, in areas where level of care dependency increases, regional connections are intimate. In areas where level of care dependency is maintained, regional connections are poor.

In the future, we will clarify how each variable representing the living environment affects the proportion of people who rose level of care dependency and care-need certification rate.

REFERENCES

- [1] Cabinet Office, Government of Japan. (2018). *Annual Report on the Aging Society*, Retrieved Aug. 17, 2018, from http://www8.cao.go.jp/kourei/whitepaper/w-2017/zenbun/29pdf_index.html
- [2] Ministry of Health, Labor and Welfare. (2012). *References on Promotion of Healthy Japan 21 (second order)*, Retrieved Aug. 17, 2018, from http://www.mhlw.go.jp/bunya/kenkou/dl/kenkounippon21_02.pdf
- [3] Japan Medical Association. (n.d.). *Japan Medical Analysis Platform*, Retrieved Aug. 17, 2018, from <http://jmap.jp/cities/detail/city/17203>

LANDSLIDE DISASTER RISK FOR THE FUTURE POPULATION DECREASE IN JAPAN

TAKANORI KATO¹, MUNHEYOSHI NUMADA² and KIMIRO MEGURO³

¹Master student, Department of Civil Engineering, UTokyo, Japan, taka-kat@iis.u-tokyo.ac.jp (corresponding author)

²Associate Professor, IIS, UTokyo, Japan, numa@iis.u-tokyo.ac.jp

³Professor, IIS, UTokyo, Japan, meguro@iis.u-tokyo.ac.jp

Keywords: landslide disaster, relocation, population decrease, ArcGIS

1. INTRODUCTION

Every year in Japan, multiple natural disasters cause fatalities. To reduce the victims by the disasters, it is necessary to investigate the causes of deaths in each disaster [1]. By investigation of the kind of behavior in details, previous researches have analyzed how victims are lead to the death just before the disasters. The previous study of the authors identified the factors to reduce the deaths in each disaster [2]. Table 1 shows that landslide disasters and typhoons caused the most significant number of deaths by natural disasters in Japan in addition to the major earthquakes such as the 2011 Great East Japan Earthquake disaster. Especially, the major cause of death is that they did not evacuate and were staying at home even after an early warning (175 out of 437 people) as well as failed to evacuate (88 out of 437 people).

Table 1: Classification of causes by behavior before the death of disaster victims in Japan (2009-2017)

The pre-death behavior of disaster victims	Earth quake	Typhoon Flood	Snow storm
	people		
Actively approaching danger	0	17	0
Evacuation failure	50	<u>437</u>	122
Accident	0	17	244
Disaster-Related Death	194	7	0
Secondary disaster	5	8	1

Many people have no choice but to live in a vulnerable area while giving warning areas that are expected to suffer a landslide disaster in the future. The purpose of this research is to evaluate the number of people living in landslide disaster potential areas and high potential risk areas. The result showed the number of people in the landslide potential area would change due to the decreasing population, on the other hand, there are some areas where the risk of landslides will not change or increase even in the situation of decreasing population in Japan.

In addition, since the current municipal financial resources cannot provide people living in the landslide potential area with enough amount of relocation assistance, this research estimates how much economic loss would incur

if landslide disasters occur in the future and calculated the amount of financial support, which is desirable and feasible.

2. METHODOLOGY

The number of households living in the landslide warning area in the future and the amount of money of subsidies per household are calculated by the following procedure. First, the mesh data of the landslide disaster warning area provided by Kanagawa Prefecture was overlaid with the 500m × 500m mesh data of the population presumption until 2050, and the change of the population within the area is analyzed.

Next, the cost-effectiveness of each municipality by relocating households in the landslide disaster warning area is analyzed. At this time, we considered a scenario in 2050 that distributes subsidies to households who are still living within the landslide disaster warning area to evaluate the resident households to zero. In this case, it can be thought that the reduction of landslide disaster restoration cost and reduction of infrastructure maintenance and management cost are benefits of relocation. According to previous research [3], the infrastructures that can reduce the maintenance cost can be a municipal road, water supply system, sewage system, merger treatment septic tank. Based on this assumption, it is difficult to rerelease real estates to the market, so it is necessary for the administrative side to purchase it. Considering these differences as subsidies to households, we calculated subsidies per household.

3. RESULT

Kanagawa prefecture is set as the research target (Figure 1), because the number of landslide disasters in Kanagawa Prefecture happened in the past 10 years is largest in Japan.

Figure 2 and 3 show the mesh of the landslide disaster warning area and the mesh of predicted population. The sum of the landslide disaster warning area is larger in the southern area, but the population is concentrated in the northern area. As a result, it is shown that the resident population in the landslide disaster warning area of Kanagawa prefecture accounts for the majority in the municipality in the northern area including Yokohama-City.

Figure 4 shows the amount of subsidies for each municipality. 2 municipalities among 32 municipalities in Kanagawa prefecture can pay 10 million yen for one household. 10 municipalities (5.3% of the total population of Kanagawa Prefecture) can subsidize.

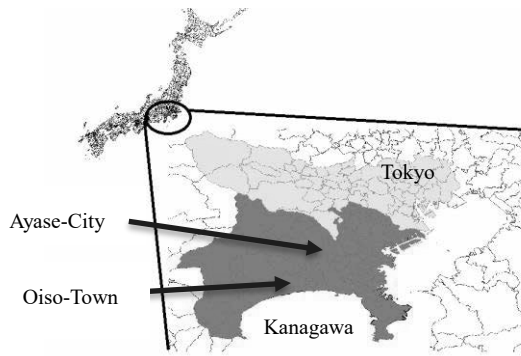


Figure 1: Location of Kanagawa prefecture

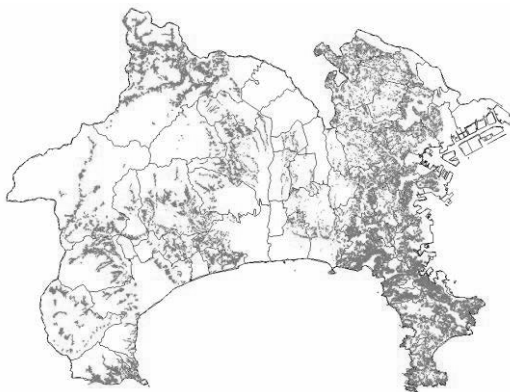


Figure 2: Mesh data of the landslide disaster warning area

The common point of two municipalities is that few households locate in the landslide disaster warning area, the cost of restoring damages at landslide disasters in the past is larger than other municipalities.

Other municipalities will become a deficit just by purchasing the land from the relocated households. Moreover, households that gain less than one million yen of the subsidies at the time of changing the residence will not relocate due to the lack of relocation. This research found that an enough relocation support cannot be provided merely by waiting for the anticipated population decrease.

4. CONCLUSION

First, the population in landslide disaster warning areas decreases due to the population decrease in Japan. However, the proportion of the total population in each municipality does not change drastically. Therefore, even if the policies such as relocation are delayed, the financial burden does not change so much. Municipal governments will need long-term policies by introducing guidelines for the residents to relocate to the outside of the warning area at the timing of changing residences.

Second, the cost-effectiveness analysis by the relocation turned out that there are considerably few local governments that can generate subsidies. Assuming that, if all the population relocate, even if supposing to induce such as a compact city and abandon maintenance of infrastructure, the number of municipalities that can subsidize will be about one third, 5.3% of the entire population of Kanagawa prefecture.

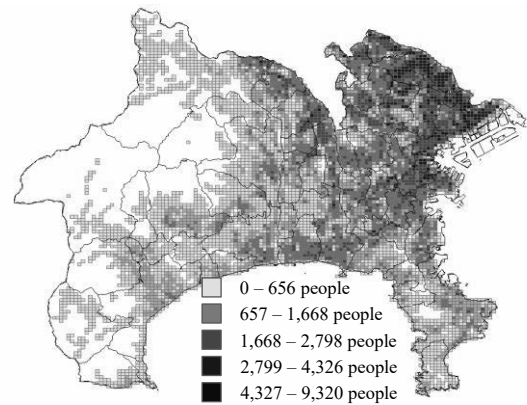


Figure 3: Mesh data (500m × 500m) of the population presumption in 2050

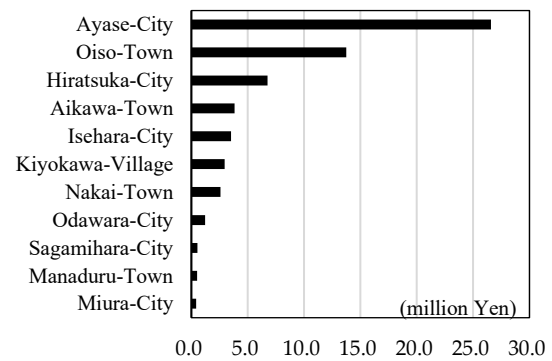


Figure 4: Subsidies per household in municipalities

Third, to reduce the risk of damage due to landslide disasters, it is necessary to induce people living in the landslide disaster warning area to move outside of the area before subsidizing financial support. It is important to minimize the financial burden of each municipality. It is very difficult for all the residents to provide financial relief assistance, reducing the residence within the warning area by methods other than relocation must be considered. For example, it is an unnatural system to secure these resources from residents living in areas with low disaster risk, so raising property tax of residents living in regions with high disaster risk need to be considered. In the future, it is intended to hypothesize these options and evaluate each option. In addition, it is necessary to consider all potential disasters with landslide disaster risk.

REFERENCES

[1] M. Ushiyama, Y. Takayanagi, (2010) “Characteristics of death or missing caused by heavy rainfall disaster events from 2004 to 2009” JJSNDS, No.29, Vol.3, pp. 355-363.
 [2] T. Kato, M. Numada, K. Meguro, (2018) “BEHAVIOR ANALYSIS BEFORE THE DEATH OF THE VICTIM AT DISASTERS”, JSCE Annual meeting, IV-159.
 [3] R. Kaijimoto, N. Kachi, K. Tsukahara, Y. Akiyama (2015) “FINANCIAL FEASIBILITY STUDY ON RELOCATION AT VILLAGE LEVEL FROM DISASTER DANGEROUS AREA”, JSCE, Vol.71, No.5, pp. 367-373.

UNDERSTANDING FATALITIES IN URBAN ROAD ACCIDENTS: A CASE STUDY

K. KALKAL¹, S. MISRA², and V. VASUDEVAN³

¹ Graduate Student, Department of Civil Engineering, IIT Kanpur, Kanpur, India, krutika@iitk.ac.in (corresponding)

² Professor, Department of Civil Engineering, IIT Kanpur, Kanpur, India, sud@iitk.ac.in

³ Associate Professor, Department of Civil Engineering, IIT Kanpur, Kanpur, India, vinodv@iitk.ac.in

Keywords: safety, fatalities, road accidents, safety performance, public transport, India

1. INTRODUCTION

Injuries and fatalities in road accidents are the 9th major killer in India, with around 1.4 lakh deaths in 2017. Improving the efficiency and safety record of public transportation systems is critical to increase their modal share and can contribute significantly to decongesting roads, especially in urban areas.

The effort in this paper is directed towards presenting the results of the analysis of data involving fatalities for the last four years from the public transport company of one of the metro cities of India. The aim of this work is to identify factors and physical conditions that contribute the most towards fatal accidents.

2. ANALYSIS AND RESULTS

Accidents are classified using accidents/bus, number of accidents occurring during monsoon season, and the distribution of accidents during the day. The results are discussed in the following paragraphs.

3.1 Fatal Accidents per Bus

A total of 24, 29, 21, and 21 fatal accidents occurred in 2014-15, 15-16, 16-17, and 17-18 respectively. When divided by the number of buses in operation in the different years, the ratio obtained is almost a constant, as visible in Figure 1.

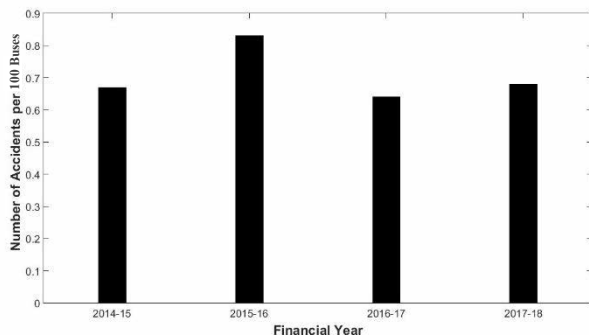


Figure 1: Number of Fatal Accidents per 100 Buses

3.2 Fatal Accidents during the Monsoon Season

To get an insight into the effect of rains on the number of fatalities, the data for the period of June-September, the known ‘rainy season’, was looked at separately.

It was found that the number of accidents in this 3-month period as a percentage of the total accidents in each year was 29%, 17%, 38% and 19%, which is not significantly different from 25% (i.e. for 3 out of 12 months, or 25% of a year).

3.3 Distribution of Fatal Accidents during the day

Data for all fatal accidents for the four-year period of 2014-18 was viewed in terms of hour-wise frequency of accidents. The results are plotted in Figure 2. Two peaks are observed – one from 11 am to 2 pm and another from 7 pm to 10 pm. There is a linear trend of increase in the number of fatal accidents as the traffic thins (and the corresponding vehicular speeds increase) both in the morning hours (7 am to 2 pm) and in the evening hours (4 pm to 11 pm).

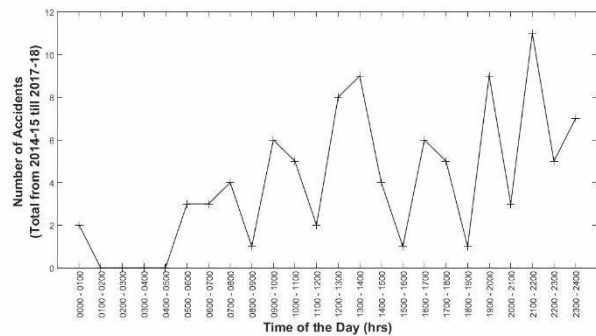


Figure 2: Distribution of Number of Total Accidents from 2014-15 to 2017-18

4. CONCLUDING REMARKS

The results from the preliminary analysis in terms of fatal accidents per bus and the effect of rains on fatal accidents are inconclusive. However, there is apparently a clear relation between the traffic density, speed and fatal accidents. This calls for further studies, including the collection of relevant data, to understand the effects of parameters such as driver training, road and bus condition.

REFERENCES

- [1] Ministry of Road Transport and Highways, *Physical Performance of SRTUs*, National Data Sharing and Accessibility Policy (NDSAP), Open Government Data (OGD) Platform India
- [2] W.A. Evans and A.J. Courtney, (1985) “An Analysis of Accident Data for Franchised Public Buses in Hong Kong”, *Accident Analysis and Prevention*, Vol. 17, pp 335–336
- [3] Somit Sen, (2018, May 2) 900 BEST Buses taken off roads in five years, *The Times of India*, Retrieved from <https://timesofindia.indiatimes.com/>
- [4] Sanchita Sharma, (2017, September 30) The top 10 causes of death in India, *Hindustan Times*, Retrieved from <https://hindustantimes.com/>

Is a change in land surface temperature treated as an early warning sign to predict earthquakes?

N. KAVYALAKSHMI¹, KAUSHAL KRISHNA TOTLA¹, M. VANI², and P. RAMA CHANDRA PRASAD²

¹ Department of Civil Engineering, Mahindra Ecole Centrale, Hyderabad-500043, India, nkavyalakshmi98@gmail.com, kaushal15238@mechhyd.ac.in

² Lab for Spatial Informatics, International Institute of Information Technology, Hyderabad-500032, India, m.vani@research.iiit.ac.in, rprasad@iiit.ac.in (corresponding author)

Keywords: surface temperature, earthquake, satellite imagery

1. INTRODUCTION

Recent advancements in space science reveals various processes associated with earthquakes like transformation of the earth surface, increasing surface temperature, variations in the atmospheric gases, aerosol expiration, and electromagnetic disturbances in the atmospheric column especially in the ionosphere. Analysis of these earths's processes carry prior information related to earthquake that serves as an indicator towards predicting the event of an earthquake. Land surface temperature (LST) is one such potential indicator linked with earthquakes. Information on the LST is derived from the thermal infra-red (TIR) band of the electromagnetic spectrum employed in sensors on-board satellites.

Scientific research has led to an observation of rise in the LST before the occurrence of an earthquake. A rise of 3-10°C has been observed before the event (Swapnamita Choudhury 2006, Adnan Barkat et al. 2018). This anomaly can be employed in forecasting earthquake. The rise in temperature can be explained by the tectonic stress built up around the epicenter of the earthquake.

2. STUDY AREA AND METHODOLOGY

This study attempts to analyze the thermal anomaly of eight events (Table 1) in and around India. The idea was to analyze the LST variations from 15 days prior and post the event of an earthquake; and existence of correlating patterns of earthquake magnitude and their corresponding variations in LST across locations.

Table 1: Study areas associated with earthquake event

Location	Magnitude	Date
Kashmir	7.6	08-10-2005
Hindu Kush, Afghanistan	7.5	26-10-2015
Imphal, Manipur	6.7	04-01-2016
Tripura	5.7	03-01-2017
Gujarat	5.5	06-04-2006
Jaisalmer	5.2	09-04-2009
Koyna Warna, Maharashtra	5.1	14-03-2005
Punjab	3.1	05-11-2015

The locations were chosen based on the availability of data and different earthquake classes (Major earthquake with potential to cause serious damage: 7.0 - 7.9

magnitude; Strong earthquake: 6.0 – 6.9; Moderate earthquake: 5.0 – 5.9; Minor earthquake: 3.0 – 3.9 with potential to cause minor damage) based on the magnitude. All the mentioned locations (except Koyna Warna, Maharashtra) lie close to the Alpide belt, which is very prone to earthquakes.

Analysis involve retrieval of the surface temperature from the thermal band of the Landsat series 5, 7 and 8 of satellite imageries using Mono-window algorithm developed after Qin et al. (2001). The bands corresponding to the NIR, red and TIR data were primarily used to retrieve LST of the locations. The LST is derived based on the parameters viz., ground emissivity, atmospheric transmittance and effective mean atmospheric temperature. The variations in the LST were analyzed by creating buffers at distances of 3 km, 6 km, 9 km, 12 km and 15 km from the epicenter. The analysis was done in two phase viz., variations in the intensity of LST: with the increasing distance from the epicenter and with time. The observed variations in the LST pattern were further linked to the Land Use/Land Cover (LULC) prevailing at the immediate vicinity of the epicenter.

3. RESULTS AND DISCUSSION

Three distinct patterns of surface temperature anomalies were observed as: (1) increasing surface temperature towards the event of an earthquake and reduction post the event; (2) higher temperature both pre and post an earthquake and lesser temperature at the event of earthquake; and (3) steadily increasing temperature prior to the earthquake that continues even post the earthquake event. A model plot of variations in the LST with increasing distance from the epicenter and time is shown in figures 1 and 2 respectively.

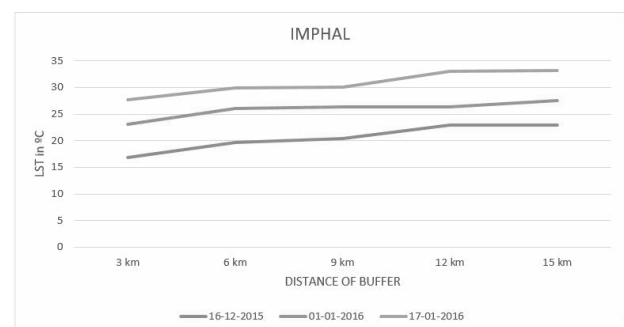


Figure 1: Distance of buffer vs LST

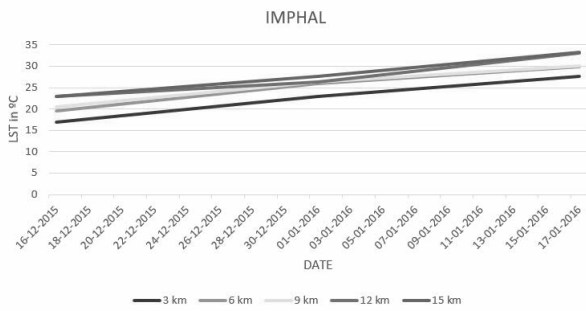


Figure 2: Date vs LST

While Hindu Kush and Koyna Warna witnessed an increase in the LST as we approach the event of earthquake and subsidence post the event; Gujarat, Kashmir and Punjab reported a gradual reduction in the LST towards the date of earthquake and an increase post the event. The LST in Imphal and Tripura have been observed to increase throughout the period of the study, i.e. before and after the earthquake event. Jaisalmer showcased a different pattern: a steady LST towards the event of earthquake and reduction later on. The complicated patterns observed at these locations intrigued to find out the possible reason behind the anomalies. Therefore LU/LC of the site at the epicenter was further investigated to find out if they could be the possible reason behind these varying patterns (Table 2).

Table 2: Observed LU/LC classes at the epicenters

<i>Locations</i>	<i>LU/LC</i>
Imphal	Forest
Gujarat	Open area
Kashmir	Open village area
Tripura	River Bank
Koyna Warna	Mountainous
Jaisalmer	Barren land
Hindu Kush	Mountainous
Punjab	Less density vegetation

The investigation on LU/LC identifies that the LST variations in the mountainous regions of Hindukush and Koyna Warna were similar following pattern (1); while low density settlements and vegetation as observed in Gujarat, Kashmir and Punjab reports a similar pattern (2) of LST variations. The potential cool areas forest and river bank observed at Imphal and Tripura respectively followed pattern (3) of the LST variations. It was inferred that a uniform pattern of surface temperature variations prevailed over similar LU/LC classes.

4. CONCLUSIONS

The changes in LST patterns vary according to the land use type and topography. This study is restricted only to the analysis of surface temperature and the land surface features and their efficiency in predicting an earthquake event. Further investigation needs to be done incorporating the soil parameters and sub-surface features of the earth that will enhance the results of this study to be more reliable to predict an earthquake event.

5. REFERENCES

- [1] Adnan Barkat, Aamir Ali, Khaista Rehman, Muhammad Awais, Muhammad Shahid Riaz, and Talat Iqbal (2018) “Thermal IR satellite data application for earthquake research in Pakistan”, *J of Geody.*, 116, 13-22
- [2] Swapnamita Choudhury, Sudipta Dasgupta, Arun K. Saraf and Santosh Panda (2006) “Remote sensing observations of pre-earthquake thermal anomalies in Iran”, *Int. J of Rem. Sens.*, TRES-PAP-2005-0503.R2
- [3] Qin Z., A. Karnieli, and P. Berliner (2001) “A mono-window algorithm for retrieving land surface temperature from Landsat TM data and its application to the Israel-Egypt border region”, *Int. J of Rem. Sens.*, 22:18, 3719-3746

USMCA 2018

SESSION 10

DISASTER RISK & RESPONSE II

DEVELOPMENT OF CAVE-IN POTENTIAL MAP OF FUJISAWA CITY

R. SERA¹, R. KUWANO², R. HIRATA³, M. HARIGAYA⁴, Y. YAMAMOTO⁵ and S. YONEMOTO⁶

¹ Manager, Operational Headquarter, GEOSEARCH Co.,LTD., Tokyo, JAPAN, r-sera@geosearch.co.jp (corresponding author)

² Professor, Institute of Industrial Science, The University of Tokyo, Tokyo, JAPAN, kuwano@iis.u-tokyo.ac.jp

³ Manager, Road and River Department, Fujisawa City, Fujisawa, JAPAN, fj0-kasensuuiro@city.fujisawa.lg.jp

⁴ Manager, Sewage Department, Fujisawa City, Fujisawa, JAPAN, fj2-gesui-ka@city.fujisawa.lg.jp

⁵ Senior chief, Road and River Department, Fujisawa City, Fujisawa, JAPAN, fj1-dorokasen-s@city.fujisawa.lg.jp

⁶ Chief, Tokyo Regional Office, GEOSEARCH Co.,LTD., Tokyo, JAPAN, s-yonemoto@geosearch.co.jp

Keywords: subsurface cavity, road cave-in, regional characteristics, factor analysis, evaluation of potential

1. BACKGROUND

Preventing road cave-in is key to keeping road traffic functions. A collaboration among Fujisawa city and IIS Univ. of Tokyo and GEO SEARCH started to develop effective solutions for prevention of road cave-in accidents in Fujisawa city in 2017. Fujisawa city is located in the central part of Kanagawa Prefecture adjoining western Tokyo. The south area faces the Pacific Ocean and the alluvial lowlands of the Shonan dunes lies. The intensive developments of infrastructure such as roads and sewers were during 1950's to 1970's. In recent years, deteriorate of infrastructures by the aging was obviously, and the handlings for them become a serious issue [1].

The development of "Cave-in Potential Map of Fujisawa City" is one approach to this collaborative study and this is the first attempt to evaluate the regional area based on cavity information. The purpose of development of the map is to understand the regional condition. For keeping road function against cave-ins, it is necessary to consider the road network around the cavities. The regional assessment of the potential of the cave-in and the map showing it give some benefits. It takes appropriate measures not only for regular situation but also for emergency situation such as large-scale natural disasters. In addition, these approaches will support discussion at other local governments that starting new measures for cave-in as experienced cases.

2. CAUSES OF CAVITIES

Road cave-in occurs suddenly with collapse and broken pavement. However the beginning is a small ground phenomenon. One of the factors forming cavities can be considered as washout of soil particles through a broken or joint failure of sewer pipe. Fig. 1 shows photos as actual examples of factor of cavities in Fujisawa city.



Figure 1: Photos of under cavities; left/ground water and joint failure of sewer, right/ broken sewer joint by aging

In addition, another main factors are consolidation settlement of soil particles in the subgrade, loosen soil around underground structure, and fluctuation of groundwater level. In many cases, some contributing factors influence each other forming cavities.

3. FINDINGS OF REGIONAL FACTORS OF CAVE-IN IN FUJISAWA CITY

The data of more than 430 cave-ins which covering Fujisawa city, the data of more than 230 cavities by passed investigation and the data of trial monitoring surveys on 10 roads in this study were analyzed for cave-in potential evaluation. And valuable data managed by Fujisawa city that sewage, groundwater, geological borings and so on were also used regional overlying and analyzing. In this collaborative study, detail condition around the cavities were surveyed to find out their factors [2] (Fig.1). In addition, the model tests were also conducted to clarify the process of expansion of cavity. The sand of the test was simulated as actual condition around a cavity where surveyed in detail [3] (Fig.2). Based on previous knowledges and regional findings from the study, four environmental factors: the oldness of sewage, the number of utilities, the level of groundwater, and the permeability of soils were selected as the regional potential factors.

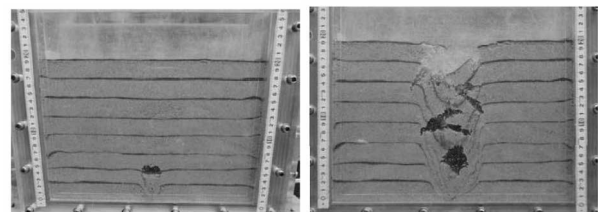


Figure 2: Model test of cavity occurrence in actual sand condition of Fujisawa city

4. A STUDY FOR POTENTIAL EVALUATION

Through the discussions about the effects and the evolutionary techniques, the cave-in potential of Fujisawa city were set by using four factors belonging to each divided grids. Fig. 3 shows the four maps of regional factors of cave-in in Fujisawa City, and an occurrence frequency of cave-in and cavity by sewer pipe classification into type and aged years as example.

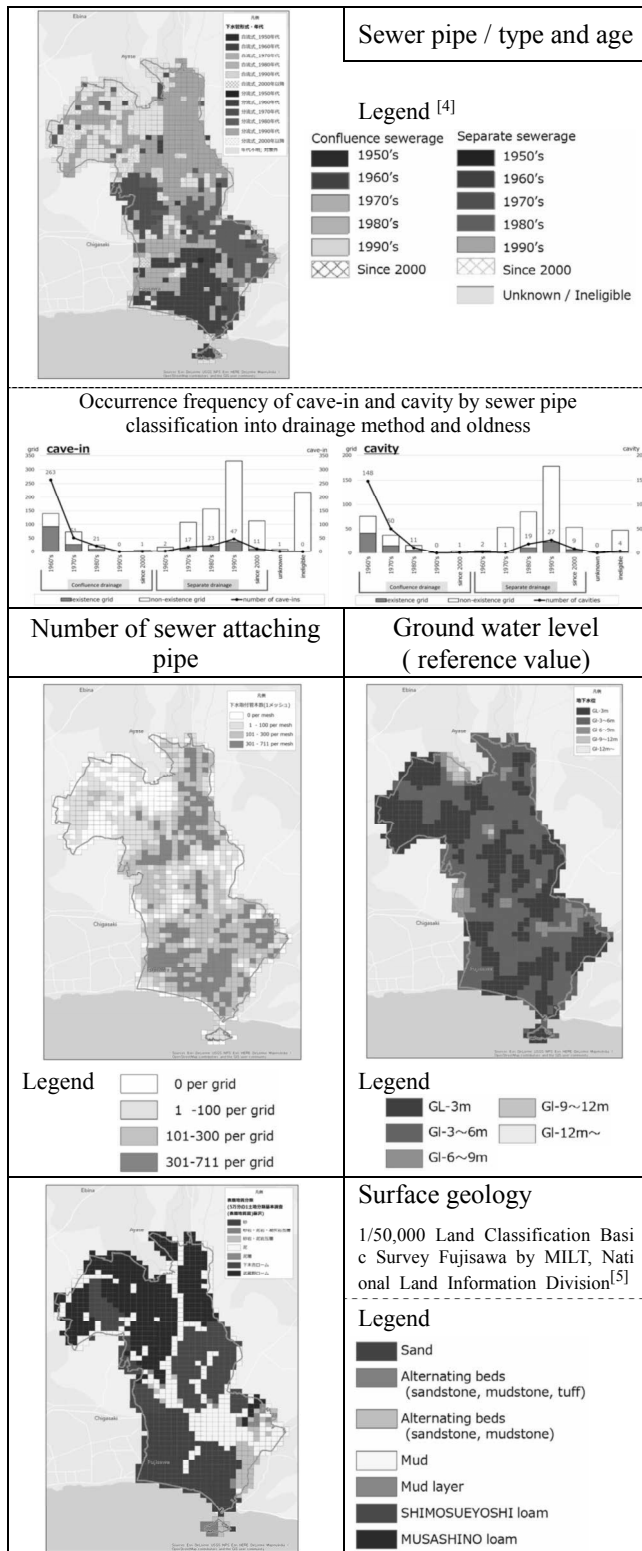


Figure 3: Four factor maps of cave-in in Fujisawa City

5. PROTOTYPE CAVE-IN POTENTIAL MAP OF FUJISAWA CITY

After making sure for appropriateness by sensitivity analysis of four potential factors in each, a knowledge that cavities often occur under overlapped multiple factors was reflected on this evaluation as a new attempt. Fig. 4 shows the prototype of cave-in potential map of Fujisawa city that evaluated based on the degree of overlap of multiple factors.

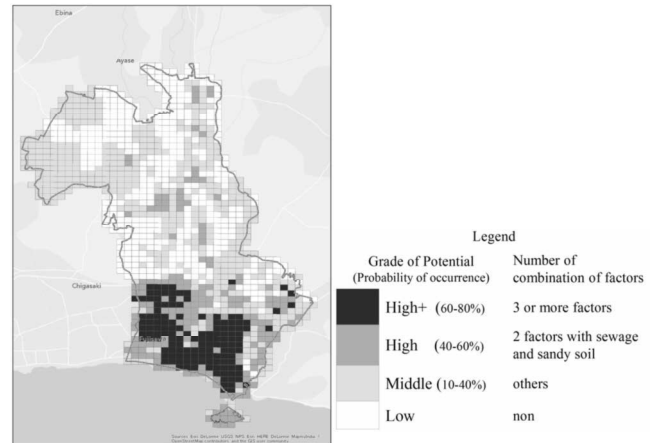


Figure 4: Prototype of cave-in potential map of Fujisawa City^[4]

Then the regional occurrence tendency of cave-ins was analyzed by overlaying the each four factor maps with the cave-in and cavity location map. Fig 3 shows

6. CONCLUSION

This is the first attempts to evaluate the area by the cavity information. And it was able to get the realistic result with the output named cave-in Potential Map. This was achieved by various data and regional findings form passed cavity survey data, actual cave-in information, precious managed sewer information, and several challenges in this collaborative study such as monitoring surveys and detailed investigations of cavity. Preventing road cave-in is key to keeping road traffic functions. And it is also a disaster-resistant system. These collaborative studies are most leading, advancing, and practical cases in the world. In the future, we would like to make effort to develop evaluation even more effective.

REFERENCES

[1] R. Hatakeyama., E. Nakamura., M. Harigaya., R. Kuwano., and H. Miki., (2018). *Development of Effective Technique for Prevention of Road Cave-in in FUJISAWA city*, 53rd Japan National Conference on Geotechnical Engineering, Takamatsu, pp. 1617-1618.
 [2] M. Okamura., M. Abe, K. Fujii., K. Kitamura., and R. Kuwano., (2018). *Development of Effective Technique for Prevention of Road Cave-in in FUJISAWA city*, 53rd Japan National Conference on Geotechnical Engineering, Takamatsu, pp. 1619-1620.
 [3] Y. Ohara., R. Kuwano., R. Sera., R. Hatakeyama., and H. Kageyama., (2018). *Development of Effective Technique for Prevention of Road Cave-in in FUJISAWA city*, 53rd Japan National Conference on Geotechnical Engineering, Takamatsu, pp. 1621-1622.
 [4] R. Sera., R. Kuwano., and M. Hotta., (2019). *Development of subsurface cavity potential map for prevention of road cave-in (in press)*, The 16th Asian Regional Conference on Soil Mechanics and Geotechnical Engineering (16ARC), Taipei.
 [5] <http://nrb-www.mlit.go.jp/kokjo/inspect/landclassification/download/index.html>

DEVELOPMENT OF SITE AND SCENARIO SPECIFIC DESIGN GROUND ACCELEROGRAMS USING RECORDED GROUND MOTIONS

C.K. GADAGAMMA¹, S.R. MENON², Y. ARAI³, S. SATO³, T. KATAGIRI⁴ and M. NUMADA⁵

¹ Project Assistant Professor, Institute of Industrial Science, Tokyo, Japan,

² Engineer, Kozo Keikaku Engineering, Tokyo, Japan,

³ Tokyo Metro Corporation, Tokyo, Japan,

⁴ Technical Director, Institute of Industrial Science, Tokyo, Japan

⁵ Lecturer, Institute of Industrial Science, Tokyo, Japan

Correspond to C.K. GADAGAMMA(chaitugk@iis.u-tokyo.ac.jp)

Keywords: Strong Motion, GMPEs, Attenuation, Strong Motion Prediction

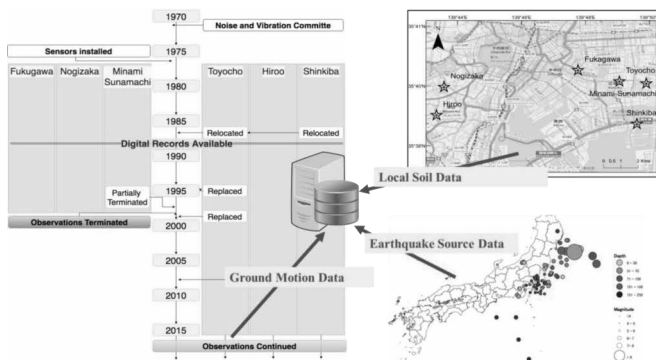


Figure 1: Background and development of the database

1 INTRODUCTION

In this research different methods have been established to generate a spectrum consistent earthquake design input motion, incorporating local site conditions using a database of strong ground motions, recorded by sensors buried at different depths at various locations in Tokyo since 40 years by Tokyo Metro Co., Ltd. as shown in 1, along with the source to site information and local site borehole data [1]. The distortions and shift in the axis and short and long period noises in the recorded ground motion records are initially processed with band-pass filtering of cut off frequencies of 0.02Hz and 20Hz, and baseline correction is done as shown in Figure 2. The source characteristics of each of the earthquake are obtained from the JMA repository. The borehole data for each of the station is further converted to engineering quantities using empirical relationships.

2 METHODOLOGY

The different strategies to obtain the target response spectrum are explained below as:

2.1 Method 1

Using the average normalised response spectrum at the surface depth [2]. The design response spectrum as prescribed by RTRI as L1 and L2 at engineering bedrock is taken for consideration. The values of peak

ground parameters, PGA, PGV and PGD are further extracted. In order to incorporate the local site effects, the design accelerogram is convoluted using equivalent linear analysis of ground tool, DYNEQ [3]. These peak ground parameters are then used to un-normalize the response spectrum to obtain a single target response spectrum. Applying Ohsaki method, the response spectrum is translated into an earthquake ground motion.

2.2 Method 2

In this method, a set of well tested GMPEs for Japan are considered and are validated using the ground motion database at different locations. Further, analysing the variations during the validation, applied corrections to obtain site-specific GMPEs. Utilizing recommended scenarios prescribed by J-SHIS [4], the deterministic demand in the form of peak ground parameters are estimated at the bed rock. An averaged normalized response spectrum is generated using the recorded ground motions at the bedrock. This is then un-normalized using the estimated demand parameters, to get the target spectrum. Using the local site conditions, a convoluted accelerogram is obtained at the tunnel site.

2.3 Method 3

In this method, the average normalized response spectrum at the surface is obtained from the recorded ground motions. The target response spectrum is obtained by using the probabilistic hazard prescribed at J-SHIS. This response spectrum is then deconvoluted to the tunnel location by using the local site conditions and DYNEQ.

3 RESULTS AND DISCUSSION

All three methods have been evaluated using the recorded data at Shinkiba station in Tokyo. The complete dataset of Shinkiba station measured at three different depths have been processed as mentioned earlier, an average normalized response spectrum, for method 1 is obtained as shown in Figure 4. The target response spectrum using RTRI design accelerogram peak ground parameters is shown in Figure 5 Further, a design accelerogram is

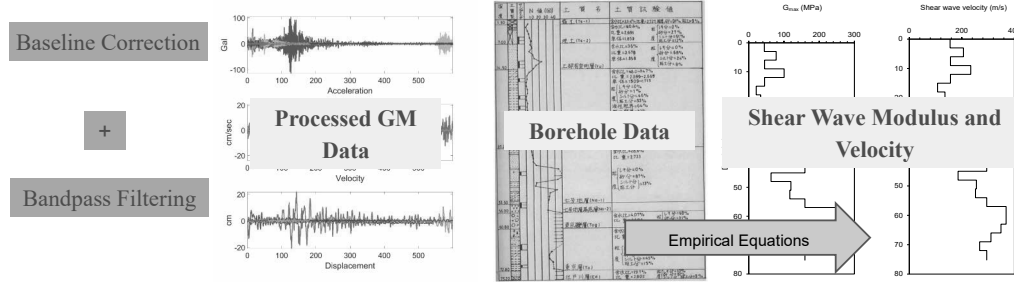


Figure 2: Data processing of ground motion records and conversion of borehole data to engineering parameters

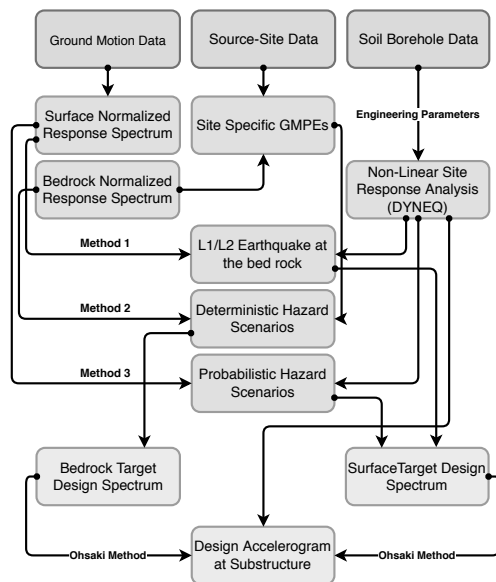


Figure 3: Flowchart of different methods in design accelerogram

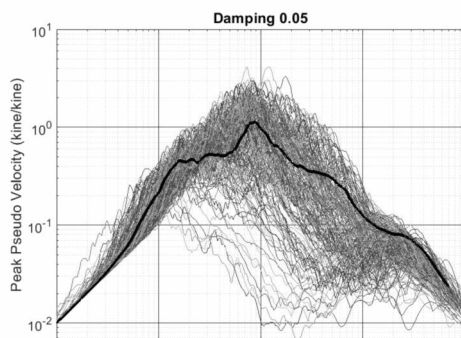


Figure 4: The normalized response spectrum in Method 1

developed using Ohsaki method as shown in Figure 6.

Further analysis is conducted on the accelerograms to evaluate the energy content and the frequency content.

4 CONCLUSIONS

A big data of ground motion, soil data and earthquake source information is compiled at different locations and depths to obtain design accelerograms. Multifaceted methods established and tested in the necessity of incorporating local site effects and accumulated data. The validation, sensitivities and aspects of applicability of these methods are a subject of future scope.

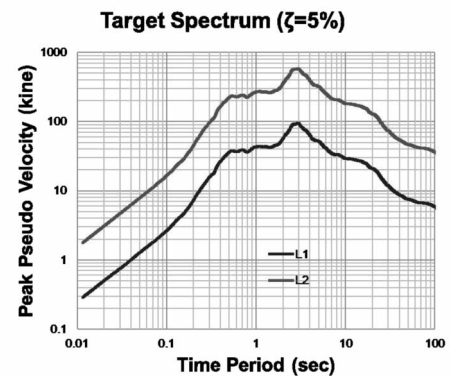


Figure 5: The target response spectrum in Method 1

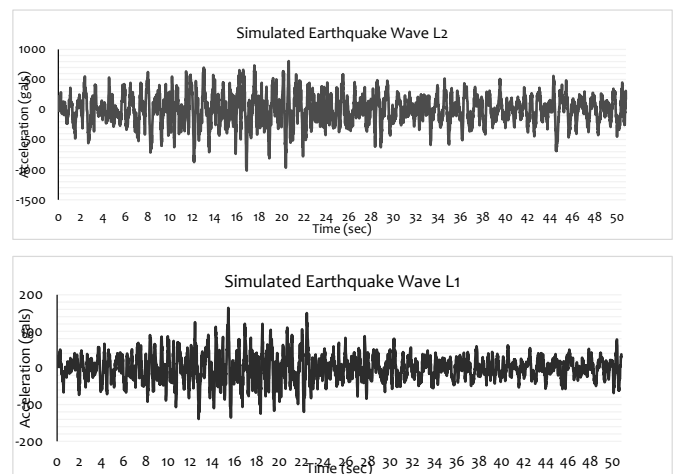


Figure 6: The simulated accelerograms in Method 1

REFERENCES

- [1] C. K. GADAGAMMA, S. M. RAJASEKHARAN, Y. ARAI, S. SATO, T. KATAGIRI, M. NUMADA, Observations of strong ground motion in tokyo metro stations at different depths, Seisan kenkyu 70 (4) (2018) 299–308. doi:10.11188/seisankenkyu.70.299.
- [2] P. K. Malhotra, Normalized Response Spectrum of Ground Motion, in: Annual Meeting of the Seismological Society of America, 2015.
- [3] N. Yoshida, I. Suetomi, DYNEQ: a computer program for dynamic analysis of level ground based on equivalent linear method, Reports of Engineering Research Institute, Sato Kogyo Co., Ltd (1996) 61–70.
- [4] J-SHIS (Japan Seismic Hazard Information Station). URL <http://www.j-shis.bosai.go.jp/en/>

COMMUTER AND ROAD SAFETY ON HYDERABAD CITY ROADS: TECHNOLOGY TRENDS

SVS KASTURI

Asst. Manager, IIIT Hyderabad, India. e-mail: vijay@iiit.ac.in (Corresponding author)

ABSTRACT

Human migration to urban cities is increasing day by day, world-wide. A prediction was that 2/3rd of world populace will settle down only in the cities by the year 2050 because of the better facilities that are available in education, health and employment etc. Contemplating the fact, the Government of India was focusing to set up decent urban infrastructure from the past three decades. Recently, an initiative - building 100 Smart Cities was started with an investment of Rs.96,000 crores to execute within five years (2015-2019). The aim of these cities is to meet the urban-centric citizen needs by adapting Information and Communication Technologies (ICTs). Yet, one question can remain is – are these cities are safer for the residents?

Safety of residents can be understood in two ways: (i) safety from natural disasters and (ii) safety from physical threats viz., thefts, robbery, road accident deaths etc. To protect from the physical threats, governments are making time bound solutions because safety of residents is a critical concern for them. According to the recent statistics, with the deployment of Close Circuit Television (CCTV) cameras, the number of threats and road accidents has come down in the city of Hyderabad which is the focus of this study.

Keywords: *Commuter Safety, Road Conditions, City Transportation, Smart Cities Mission, Technologies*

1. INTRODUCTION

The Hyderabad City is the 6th largest city in India with a population of about 7.75 million located in hilly and terrains. The city has approx. 40 lakh registered vehicles [3/4th are two wheelers] and the accident deaths are about 400 on average in a year, during 2013 to 2016. The number of road accident deaths is increasing due to the substantial growth of urbanization and loud boom of vehicles. However, after deployment of CCTVs, the number has come down to 288 in 2017 [1]. These cameras are integrated to a Command Control Centre

(CCC) to monitor real-time traffic incident management and, other civic issues on the roads. The CCC is a nodal office connected with electronic and network enabled devices such as Personal Digital Assistants, Tabs, Smart Phones and cameras. It enabled with on-line traffic management system to identify the chain-snatchers, traffic violators, signal jumping, vehicle parked at a wrong place etc. The camera recorded footage is helping to control anti-social elements and sensational crimes.

2. OBJECTIVES OF THE STUDY

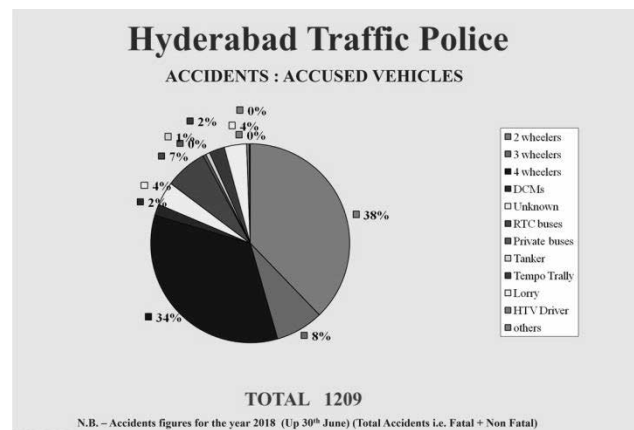
(i) To study the causes of road accidents in Hyderabad city. (ii) To understand the causes for road conditions and traffic congestions on the city roads. (iii) To analyze the various technologies deployed on the city roads to prevent the road accidents and deaths.

3. METHODOLOGY

The investigator interviewed about 30 senior police officers and, secondary data was collected from reliable web sources, reports and newspaper articles.

4. BACKGROUND

The city roads are covering with bicycles, scooters, autos, cars, trucks, buses, mini-vans and pedestrians etc. The recent traffic incidents data says two wheelers and four wheelers are causing more accidents on the city roads as shown in the below picture [2]. The cameras deployed are somewhat helping both the commuters and regulatory but a few more advancements are recently introduced for preventing the road accidents.



[Source: Hyderabad Traffic Police]

(i) *Technologies that are helping 'Regulatory Authority'*
mWallet, a free downloadable app act as a wallet to store licence related documents in the smart phones viz., driving licence, registration and insurance certificates that lessened both transport and police verification process. Earlier, *Collar mikes*, *body worn cameras* are in place for recording the interactions of an offender when he was caught by officers. *Online e-challan* is CCTV footage based penalty process, when traffic violation occurs it generates a challan and delivered to a violator postal address [3]. *HydCop* is another mobile app where the entire city police is connected and communicates with each other. With such exchange of information, incidents such as managing crowd, mob attacks are under control [4]. Other than the technologies, *Stone-pelting protection plates* and *blue colts* are safeguarding the police from the gangsters, decoit attacks and other civic agitations etc.

(ii) *Technologies that are helping 'commuters'*

MyGHMC is a mobile app where commuters can raise their grievances by capturing the photographs of any issues such as road conditions, hazards, street lightening, sanitation problems etc., *HawkEye* This GPS enabled mobile app that has SOS button is very useful for a women when she commutes in a private cab or on the city roads. *SHE Teams* is a special drive which is protecting the working women safety from the eve-teasers at bus stops i.e., safeguarding the women safety on the roads. *Integrated Voice Responsive System (IVRS)* toll free numbers *100, 101, 108 (24/7 Call Centres)* from where commuters can directly make complaints or report grievances to the authorities.

5. RESULTS

Other than these advancements, the study results have found some more distinguished features deployed for commuter safety and to create awareness towards traffic rules and the law. These are classified into three sections - Commuter Safety, Road Safety and Self Governance.

a. Commuter Safety [*Drive Safe and Stay Safe*]

The commuters, by taking an extra care while driving can safely reach their destination on the roads for which some technology advancements are introduced in the city.

Firstly, *Computer based tests* are deployed to take stringent steps while issuing driving licence [5]. It can be either learner licence or permanent licence. Recently, Insurance Regulatory and Development Authority of India (IRDA) had made mandatory that third party insurance to be enhanced to 3 years for cars and 5 years for two wheelers from 1st September 2018. Earlier it was only one year for both types of vehicle. Then, a *Twelve-point mobile based penalty system* was introduced to impose penalty for careless, license-less, speed and drunken driving etc. The majority commuter mobile numbers are linked and made mandatory when they purchase or register a new vehicle and while applying for the driving licences that eased the penalty system. *Hyderabad Traffic Live* is a mobile app that provides information on traffic conditions and details viz., nearby traffic police station address, concerned officer contacts and road safety tips etc. During any havoc or hazardous situations, commuters can approach the concerned officers for booking complaints. *Frequency modulation (FM) radio* and *social media (twitter)* alerts are also helping the commuters to manage the traffic congestions on the city roads. To control the vehicles speed - *laser guns, speed guns and breathalyzer tests for drunken driving* are in place. Recently, the police have also deployed *video analytics, face recognition* devices to identify the rowdy sheeters and perpetrator activities in public places viz., VIP bandobasth, political party meetings and railway stations etc., for better monitoring. A study led by the Rutgers University in New Jersey indicated that ordinary wi-fi could be used to detect weapons and explosives in public places in very near future [6]. These need to be explored and replicated on rapid basis for safety of commuters on the city roads.

b. Road Safety [*Accident brings tears – Safety brings Cheers*] A city road condition is another determining factor which avoid accidents but Indian road engineering varies among National highways, State highways, city, colony roads, footpath lanes, sub-ways, under-ground passages, flyovers, pedestrian and roads for cyclists etc. An extra care has taken while laying these different set of

roads by adopting the highest engineering standards. Especially, when a road has bumpy and potholes - the authority is overseeing the works in a time bound manner. Recently, a white topping technology was implemented on a pilot basis where cement concrete was overlaid on the damaged roads, which has 15 to 20 years of sustenance life [7]. The same technique was escalated to another 65 city roads that are accident prone junctions [ibid]. These junctions have black whole points (No Return Roads) and are safeguarding the traffic signals by converting them into a legal U-turns. The recently laid 158 kilometres Nehru Outer Ring Road with eight lane roads are avoiding heavy load vehicles on the city roads. *Light Detection and Ranging (LIDAR) Gun* is another device that estimates tailgating and speed of a vehicle on the cross roads but commuters are not much aware of this device. It is needed to create awareness on such devices to reduce the traffic violations on the city roads. Wayback in the year 2005, *Safety always for all roads (SAFAR)* was introduced to sensitize the commuters, drivers, school children and general public. The objectives of the program was somewhat met and need to reintroduce to meet the current trends of traffic violations. An *Advanced Driver Assistance System (ADAS)* which was in the pilot stages in European and Western countries that has an electronic stability control, autonomous emergency breaking system, anti-lock brake, lane departure warning, adaptive cruise control and blind spot features are yet to introduced on the Indian roads [8]. The existing number plate recognition devices, GPS enabled cabs and long fusion cameras are yet to sensitize the safety segment on the city roads. But with the currently available technologies and the effort of integrating several databases of commuters, road safety is reasonably in place. Notwithstanding the above means, it is also commuter responsibility to take extra care while commuting on the roads.

c. Self Governance [*Speed Thrills but Kills*]

Nearly, 75% of the road accidents occur due to the human error on the city roads viz., fatigue, drunken driving, over speeding and incompetent driving etc. It has to put on

record that safety of others is also important hence wearing helmets and seat belts are to be practiced in rigour. It is estimated that 30% accidental deaths and hazards are taking place only because of not having seat belts in the cars. It was also revealed that majority air-conditioned (AC) cars are meeting with the road accidents. Thus, the road accidents are manyfold especially, when it leading to a death, it can affect on the victim's family. The young generation aged between 18-35 years are causing more bike accidents due to the licence less driving [9]. The police are giving counselling to the parents who are giving costly and speed bikes to their children through *Community Policing (Nenu Saitham – meaning 'Me too')* campaign to prevent child riding [10]. Use of mobile phones and watching LCD television (distracted driving) are another reasons for the road accidents. Riding with more than one pillion, overloading cargo, outdated vehicles are some more causes [11]. It is impossible to cover all sorts of risks hence it is the discretion of commuters to govern themselves on the roads.

6. CONCLUSION

The Police department of Hyderabad city do not have sufficient budgets yet, they are managing the safety of commuters and roads mostly with the help of CCTV cameras, currently. But most of the time they are using outdated technologies (not updated) and not adequate to solve the real-time problems. The department has to sanction substantial budgets to purchase new (GPS, GIS enabled) vehicles and electronic gadgets so that those can be connected to command control centers for efficient patrolling. Though, Hyderabad is not chosen as a Smart city but the technologies adopted are commendable and can be replicated to any other cities. The road expansions, widening, dividers and speed controllers for the vehicles are to be enforced in regular intervals by the regulatory bodies. Road Safety Audit which regulates periodic maintenance of roads and standards is to ensure better and safe roads was difficult for the authorities to organize on the existing city roads. This limitation can be overcome while planning and designing of city roads in the future

green field cities. Due to the enormous growth in the number of vehicles, the number of risks and accidents are also equally increasing in the cities. Apart from that bus stops are also located near to cross road junctions which is causing more traffic jams and accidents i.e., close to the bus-bays. Many a times, these bus bays are occupied with the contract carriage vehicles which can be captured with the help of CCTV cameras to impose penalties. To identify the wrong path riders and to maintain the lane discipline on the roads, penalty through these cameras also another area that can be introduced. The currently available technologies are surely adequate to handle the current traffic conditions however there is a need to introduce more futuristic technologies to solve the future problems. The transport department has been imposing challans and penalties in substantial amounts compared to the old rates such additional income can be invested on building new infrastructure viz., multi-level complexes for car parking and double-decker fly-overs to control the traffic congestions. Integrating with the air quality sensors which are meant for predicting the pollution of a specific area on city roads is another feather that can be looked into. There were several incidents where the offenders escaped even from the CCTV images especially in the nights hence all the technologies can not guarantee fool-proof solutions but one has to have the will and passion to execute. Thus, the political and executive will is necessary in implementing the technologies in the administration process where Hyderabad police are far far ahead. Finally, new technologies will come and go but choosing and deploying the right one to the contemporary needs was the key to success.

7. REFERENCES

- [1] Donita Jose
<https://timesofindia.indiatimes.com/city/hyderabad/fatal-accidents-on-hyderabad-roads-drop-by-50/articleshow/62107205.cms> accessed on 12th Sep 2018
- [2] <http://hyderabadpolice.gov.in/Traffic.html> accessed on 8th Sep 2018
- [3] <http://www.htp.gov.in/> accessed on 9th Sep 2018
- [4] <http://www.thehansindia.com/posts/index/Hyderabad-Tab/2017-10-26/For-better-road-safety-use-Call-Ambulance-technology/335472>
- [5] Road Safety Strategy in the State, Transport Department, Government of Andhra Pradesh. Pg2
- [6] <https://www.bbc.co.uk/news/technology-45196164>
- [7] <https://india.smartcitiescouncil.com/article/hyderabad-adopts-white-topping-technology-gets-maintenance-free-roads>
- [ibid] <https://www.thehindu.com/news/cities/Hyderabad/technology-to-determine-quality-of-roads/article19862998.ece>
- [8] https://en.wikipedia.org/wiki/Advanced_driver-assistance_systems accessed on 30th September 2018
- [9] M. Bhagyaiah and B Shrinagesh. Traffic analysis and Road Accidents: A Case study of Hyderabad using GIS. IOP Conference Publishing. Pg.6. oi:10.1088/1755-1315/20/1/012026.
- [10] Harnam Singh and A D Aggarwal. Fatal Road Traffic Accidents among young Children. *J Indian Acad Forensic Med*, 32(4). ISSN 0971-0973. Pg.287.
[Ibid] <https://www.ncbi.nlm.nih.gov/pmc/articles/PMC3893966/>
- [11] Sanjay Kumar Singh. Road Traffic Accidents in India: Issues and Challenges. World Conference on Transport Research. Science Direct. Pg.4717.
[Ibid] <https://timesofindia.indiatimes.com/city/hyderabad/more-road-accidents-in-upscale-tech-corridor-than-highways-reveals-data/articleshow/63252115.cms>

BIBLIOGRAPHY

1. Guidelines for Road Safety Audit, A report by Govt. of Karnataka
2. Research Framework for Road Safety in the South-East Asia Region. A report by World Health Organization (WHO), 2015.
3. Road Safety – Impact of New Technologies: A report by Organization for Economic Cooperation and Development (OECD).
4. <https://sites.ndtv.com/roadsafety/5-technology-solutions-can-make-indias-roads-safer-2647/>

DEVELOPMENT OF QUICK INSPECTION SYSTEM FOR DAMAGED HOUSES AFTER THE EARTHQUAKE USING INFRARED CAMERA

**Yuki MATSUOKA¹, Makoto FUJII²,
Jyunichi TAKAYAMA³, Shinya SUDA⁴**

¹ Bachelor, School of Environmental Design, Kanazawa University, Kanazawa, Japan,

² Assistant Professor, Ph.D., School of Environmental Design, Kanazawa University, Kanazawa, Japan

³ Professor, Dr., Eng., School of Environmental Design, Kanazawa University, Kanazawa, Japan

⁴ President, SkyLink Japan, Kyoto, Japan

Keywords: earthquake, unmanned aerial vehicle, infrared camera, visible light camera, Microsoft Azure, AI

1. INTRODUCTION

The Kumamoto earthquake occurred at 1:25, April 16, 2016^[1]. There are many dangerous places in the affected area, restrictions are placed on the activities of the respondents of the victims in the affected area, the evacuation life of the victims in the affected area and the investigators of emergency risk determination performed after the earthquake disaster. In order for victims and investigators to work safely in disaster areas, it is important to grasp the hazards in advance. Therefore, in this research, we have machine-learned image data photographed in the disaster area using an infrared camera mounted on a small unmanned aerial vehicle (UAV), and identified and grasp the roof damage of the affected building by computer.

2. DATA

We selected the Miyazono area of Musashiro-machi, Kumamoto Prefecture, which was affected by the Kumamoto earthquake area. Masuki-cho is the area that observed the maximum seismic intensity 7 on the Kumamoto earthquake, the area most damaged in Kumamoto prefecture, where the building damage is noticeable. Therefore, we decided to obtain building damage data from the building in Miyagi-machi Miyazono area.

The building damage data was collected in Mashiki city on April 30, 2016. We flew a UAV equipped with an infrared camera up to about 50 m which does not interfere with obstacles such as electric poles and electric wires and the height does not become rough, and photographed the afflicted building in the Miyazono district from directly above. After that, we changed the camera to a visible light camera and shot at the same condition / place. The building damaged easily to compare the video taken with a visible light camera and infrared camera and to determine the roof damage, which is used as the subject of experiments in this study (Figure 1).

In this research, we use the image of the infrared camera to judge the damage of the roof of the building. The reason why the image of the infrared camera is used instead of the image of the visible light camera is that the amount of color information in the image of the visible light camera is too large, so it takes time to judge the damage. However, in the image of the infrared camera, since the information on the roof damage area is converted into the temperature information, the information amount is retained and the

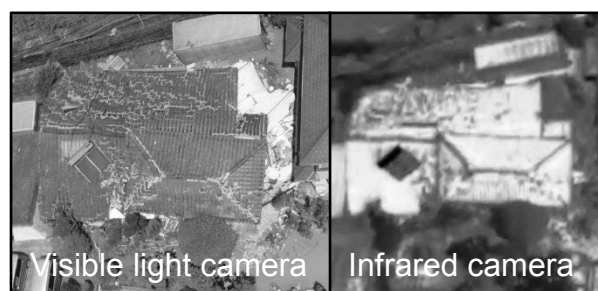


Figure 1: The building of experimental subject taken with a visible light camera and infrared camera

building can be recognized. Therefore, it is suitable for damage judgment.

4. BASIC ANALYSIS

First, it was confirmed visually the difference between how to appear the building damage in the visible light camera and the infrared camera. For example, from Figure 1 when the temperature of tile is high, the infrared camera indicate white color. And when the temperature of no tile is lower than the temperature of tile, the infrared camera indicate red color.

This color difference is determined using AI.

5. Outline of the AI system used in this research

In this research, in order to quickly judge the roof damage of a disaster-affected building in the affected area, we aim at automatic judgment by a computer, not visual judgment by a person. Therefore, I decided to use AI for that judgment.

We use Microsoft Azure's Cognitive Services For this analysis. This study used Custom Vision which is classified as vision in Cognitive Services,

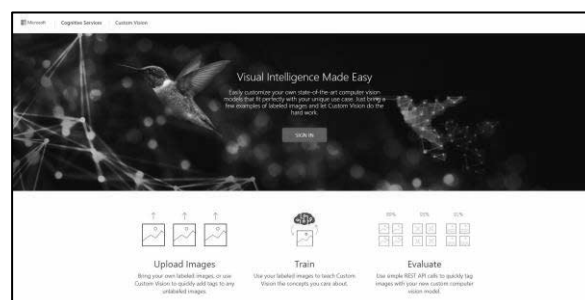


Figure 2: Microsoft Azure's Cognitive Services

6. Determination of damaged buildings from the infrared image using AI system

The Cognitive service is made to model by learning by AI. Therefore, the data for learning is necessary. In this analysis, we have learned infrared images of buildings with roof damage and infrared images of buildings without roof damage, in order to create a model to judge whether infrared images of buildings in affected areas have roof damage or not. In the infrared image of the building with the roof damage, tags of "building" and "roof damage" were tagged, and the infrared image of the building without roof damage was tagged with "building" and "no damage" and learned by AI. The accuracy of all tags was 100%, and when I recalled, the tags of "building" and "roof damaged" were 100% and the tag of "no damage" was 83.3% and the average was 94.4%.

We determined the building with roof damage and the building without damage using this created image recognition model. The results are shown in Figure 3 and 4. According to Fig. 3, the probability of "building" is 100%, the probability of "roof damage" is 99.9%, and the probability of "no damage" is 0% in the created image recognition model for buildings with roof damage. According to figure 4, the probability of "building" is 98.8%, the probability of "no damage" is 95%, and the probability of "roof damage" is 0% in the created image recognition model for buildings without roof damage.

Infrared images of two damaged buildings and two no-damage buildings were judged, and good results were obtained respectively.

From the above, it was suggested that the image recognition model created this time can judge the infrared image of the damaged building as "roof damaged" and "no damage".

7. CONCLUSIONS

2016 Kumamoto earthquake occurred at 1:25, April 16, 2016. It was taken of the building affected by the earthquake by the infrared camera mounted on UAV in Mashiki city on April 30, 2016. We visually confirmed that roof damage can be grasped from infrared image. In addition, Cognitive Services of Microsoft Azure was used to create a model to judge, whether or not the infrared image of the damaged building has roof damage.

As a result, it was possible to distinguish the damaged part from the non-damaged part, indicating the possibility of quickly judging the damage of a large number of buildings, and suggesting that it is possible to grasp the dangerous part in the afflicted region.

As a future prospect, we aim to learn and judge the building where the roof damage is caused and the blue sheet is put on the roof. Furthermore, we aim not only to judge the existence / nonexistence of the current damage, but also to create a model that classifies the damaged buildings according to the extent of the roof damage and allows them to learn and to judge the extent of the damage.

REFERENCES

Reference to a home page:

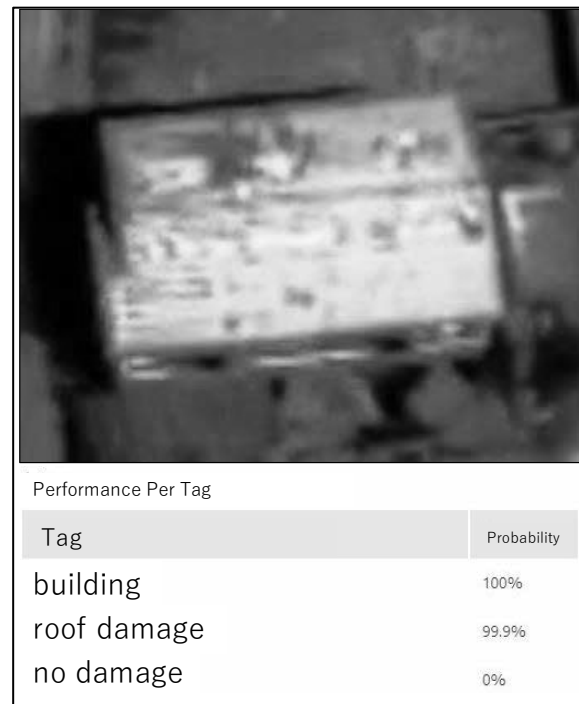


Figure 3: Determination result of building with roof damage

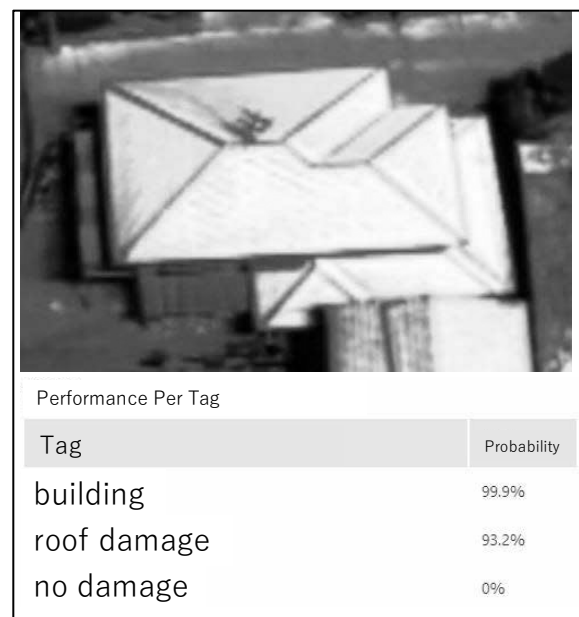


Figure 4: Determination result of building without roof damage

[1] Japan Meteorological Agency HP:
http://www.jma.go.jp/jp/quake/quake_local_index.html

Reference to an overview academic conference

[2]Yuki MATSUOKA, Makoto FUJIU, Jyunichi TAKAYAMA, Syoichiro NAKAYAMA, Shinya SUDA and Hiroki SAKAGUTI, (2016)
 “赤外線カメラを用いた地震発生直後の建物被害自動検出に関する基礎的研究”, 第36回地震工学研究発表会論文概要集

Notice : Part of the content of this paper is patent pending.

INFLUENCE OF CONTAINMENT REINFORCEMENT ON THE SEISMIC RESPONSE OF URM BUILDINGS CONSIDERING THE EFFECT OF FLEXIBILITY OF SOIL MEDIUM

S. R. VAIDEHI¹, P. NEETHU², and S.V. JISHA³

¹PG Research Scholar, Structural Engineering, Mar Baselios College of Engineering and Technology, Thiruvananthapuram, Kerala, India, vaidehisr781@gmail.com

²PG Research Scholar, Structural Engineering, Mar Baselios College of Engineering and Technology, Thiruvananthapuram, Kerala, India, neethusprakash94@gmail.com

³Assistant Professor, Department of Civil Engineering, Mar Baselios College of Engineering and Technology, Thiruvananthapuram, Kerala, India, jpn.nitk@gmail.com

Abstract: Un-Reinforced Masonry (URM) buildings represent one of the most seismically vulnerable building types, which are weak in resisting lateral loads. In most of the studies the seismic response of conventional URM buildings are evaluated without considering the effect of soil strata. The main objective of this study is to investigate the effectiveness of vertical containment in mitigating seismic vulnerability of URM buildings incorporating the effect of flexibility of underlying soil strata. Four URM buildings with dimension 6×3×3m are considered namely, (i) buildings without roof slab and lintel band (ii) building without roof slab and with lintel band (iii) buildings with roof slab and lintel band and (iv) buildings with roof slab, lintel band and containment reinforcement. Vertical containment reinforcement of 12mm diameter steel bars of Fe250 grade is provided on the surface of the walls on both faces with a spacing of 1m. Time history analysis is carried out by considering Bhuj (2001) ground motion. The effect of Soil-Structure Interaction (SSI) is evaluated by considering three different types of soil strata such as soft clayey sand strata, medium clayey sand strata and rock. Three-dimensional building-foundation-soil system is analysed using finite element method on the basis of direct method of SSI. Non-linear material behavior of underlying soil medium and linear behaviour of buildings is considered. The responses such as storey deflection and base shear of URM buildings with and without considering the effect of SSI are evaluated. It is found that responses such as storey deflection and base shear of the buildings increased by two times and nine times respectively for buildings with containment reinforcement than building without it due to the effect of SSI. Also, with lintel band, roof slab and containment reinforcement the deflection decreased by four times compared to building without it in mitigating seismic vulnerability in terms of deflection.

Keywords: Un-Reinforced Masonry buildings, Containment reinforcement, Time history analysis, Soil-Structure-Interaction

1. INTRODUCTION

Un-Reinforced Masonry (URM) construction is the most common type of construction in rural as well as urban areas due to its lower cost, ease of construction and good aesthetics. The damages observed in these structures depend on quality of materials and construction, structural layout and connections between structural elements.

Numerous experimental investigations were carried out on URM walls which shows the seismic behaviour of brick masonry walls [1-3]. Considering the influence of flanges on the in-plane behaviour of URM walls it is observed that for a diagonal tension-controlled wall, once a stair stepped crack is opened up, sliding can be expected to occur along the bed joints and deformation can be expected [4]. The seismic performance of URM with different types of failures such as in-plane failure [5], out-of- plane failure, lack of anchorage between

floor and walls, anchor failure when joists are anchored to walls were studied. A combined in-plane and out of plane effects showed that in-plane failure may not lead to collapse since the load carrying capacity of a wall is not completely lost by diagonal cracking, whereas, out-of-plane failure leads to unstable and explosive collapse [6]. The structural performance of URM buildings are improved by using containment reinforcement. This containment reinforcement is provided around masonry walls at an appropriate spacing. The reinforcements on the two faces are tied together through links or ties provided at a definite vertical spacing as shown in Fig.1. As the masonry wall bends, one face of masonry would be subjected to tension and the reinforcement on that side would bend to its profile. The reinforcement on the compression side would tend to become slack. The reverse happens as the wall bends the other way [7,8]. Here the reinforcement is intended to prevent the growth of flexural tensile cracks that lead to failure. The

containment reinforcement will prevent brittle failure due to tension cracks and permit larger deflections and hence a much higher absorption of energy without a substantial increase in strength.

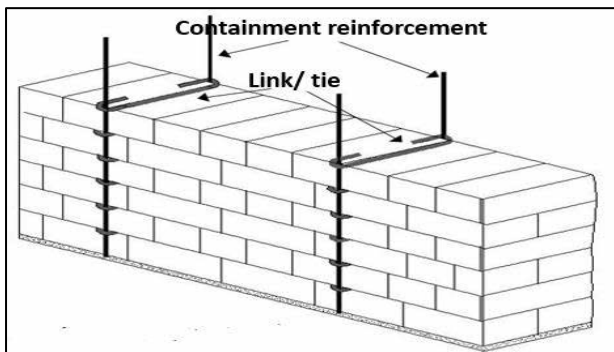


Fig. 1. Masonry with containment reinforcement and links [9]

From the studies it is understood that response of buildings depends on the response of the underlying soil medium and vice versa especially when considering the dynamic loads. The soil-structure interaction model can be used for a complete probabilistic study of the response of a corner section of a single storey masonry veneer house founded on an expansive soil [10]. The model has the potential for widespread applications for similar such studies [11-12]. The responses of various buildings on soft clay and hard rock have been performed by introducing the theory of SSI [13]. There are two different approaches for interaction effects namely, direct approach and indirect approach. In the direct approach, structure is modelled explicitly with soil strata and a complete solution is obtained in a single analysis. In the substructure method, the soil-structure system is analysed separately as two substructures; a structure which may include a portion of non-linear soil strata and the unbounded soil. If the structural foundations were perfectly rigid, the solution arrived by substructure approach and direct-method will be identical. The influence of SSI on elastic and inelastic range responses of low-rise building frames resting on shallow foundations shows that the base shear increases due to the effect of SSI. The seismic response of medium to high rise buildings generally decreases due to the influence of SSI [14,15].

Many of the previous researches focus on the numerical, analytical and experimental study on masonry building. Very few studies emphasis in the seismic behaviour of masonry buildings subjected to earthquake ground motion considering the effect of underlying soil medium. This study enumerates the effects of SSI on URM buildings using an integrated three-dimensional soil-structure system considering nonlinear behaviour of soil stratum.

2. METHODOLOGY

Idealisation of the building and foundation

In this study, single storeyed masonry buildings having masonry walls made of laterite blocks of 1:6 cement mortar is considered. For improving the seismic performance of URM buildings lintel bands, roof slabs and containment reinforcement are used. Four types of masonry buildings such as (i) building without roof slab and with lintel band (ii) building without roof slab and with lintel band (iii) building with roof slab and lintel band (iv) building with roof slab, lintel band and containment reinforcement are used. The designation used for the above four types of buildings are given in Table 1. Fig.2 shows the various building configurations used for the analysis. URM buildings with plan dimensions of 6m x 3m x 3m have been considered for the analysis. Provisions of openings in the buildings have been considered with one door of size 1 m x 2 m on front longer wall. The considered plan has one window in the front longer wall and two windows in the longer wall of backside. Each of the short walls is assumed to be provided with one central opening of dimension 1m x 1m for window. Fig.3 illustrates the plan dimension of the URM building with vertical containment reinforcement. Vertical containment reinforcement made of 12mm diameter steel bars of Fe250 grade is provided on the surface of the walls on both the faces at a spacing of 1 m. Roof slab of thickness 0.12m and lintel band of thickness 0.2m and width 0.2m with M25 grade concrete and Fe250 grade steel reinforcement is used.

Table 1. Types of single storeyed masonry structures

Designation	Building description
U	URM building without roof slab and lintel band
UL	URM building without roof slab and with lintel band
ULR	URM building with roof slab and lintel band
ULRC	URM building with roof slab, lintel band and containment reinforcement

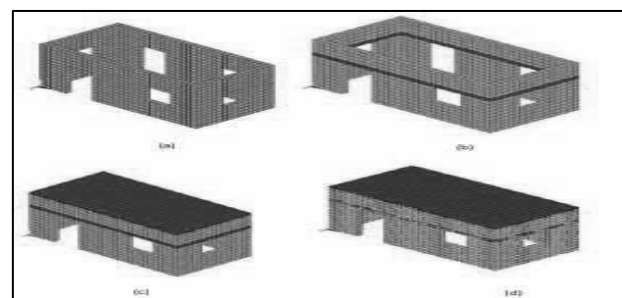


Fig.2. Configurations of URM buildings (a) U (b) UL (c)ULR (d) ULRC type [8]

Table 2. Material properties

Property	Masonry	RC (used in lintel band, Roof Slab)	Vertical Containment reinforcement
Modulus of Elasticity (kN/m ²)	1.20×10 ⁶	2.50×10 ⁷	2×10 ⁸
Poisson's Ratio (assume)	0.15	0.15	0.30
Mass Density (kg/m ³)	2100	2500	7850

Strip footing of random rubble masonry having width of 0.6 m and depth of 0.6m is provided. Table 2. provides the properties of masonry, RCC and vertical containment reinforcement bars. Fig.4 gives the sectional elevation of URM building giving the details of foundation.

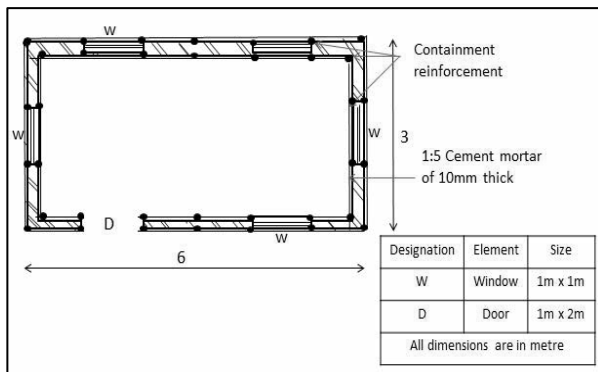


Fig.3. Plan of ULRC building [8]

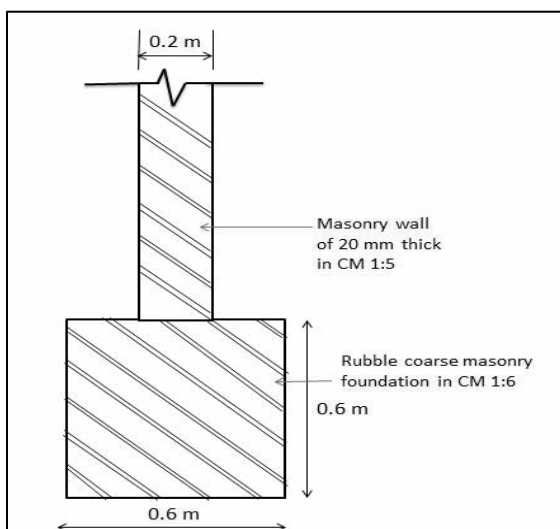


Fig.4. Sectional elevation of U building

Idealisation of soil strata

Three different soil strata considered in this analysis are Soft clayey sand strata (S), Medium clayey sand strata (M) and Rock (R) in which the flexibility decreases from rock to soft strata. Bedrock was assumed at a depth of 30m below the soil stratum. The lateral dimension of the soil stratum was taken as four times the lateral dimension of foundation [16]. The properties of soil strata are defined by its mass density, modulus of elasticity, poisson's ratio and angle of internal friction [17] as shown in Table 3. There are various types of soil models used to represent soil media. Here, Drucker-Prager (DP) model is used to define the non-linear soil stratum. DP model represents non-linear plastic failure of the soil and is simple as well as easy for numerical analysis. The DP yield criterion is a pressure-dependent model for determining whether a material has failed or undergone plastic yielding. The criterion was introduced to deal with the plastic deformation of soils and have been applied to rock, concrete, polymers, foams, and other pressure-dependent materials.

Table 3. Properties of soil strata [17]

Soil type	Poisson's ratio	Density (kg/m ³)	Elastic modulus (kN/m ²)	Angle of friction (θ)	Cohesion (kN/m ²)
S	0.20	16	50000	30	50
M	0.25	18	100000	34	100
R	0.30	20	250000	38	200

3. FINITE ELEMENT ANALYSIS

Finite element analyses of 3D integrated soil-structure system were carried out by using the finite element software. Different building components of a URM building under consideration are masonry, roof band, lintel band and vertical containment reinforcement. The URM building, foundation and underlying soil strata were modeled using eight noded brick element having three translation degrees of freedom at each node. Roof slab is modeled by using four noded elastic shell element. The element has six degrees of freedom at each node and has both bending and membrane capabilities. The vertical reinforcements were modeled using truss elements which is a uniaxial tension-compression element, also with three translational degrees of freedom at each node. All the masonry walls, lintel band, roof

slab, vertical containment reinforcement and foundation were discretized with mesh size 0.2m. The soil strata were discretized with mesh size of 1m upto a depth of 20m and with mesh size 2m for the remaining depth along the vertical direction. Along the lateral direction soil stratum is discretized with mesh size 1m. The finite element structure of building with and without soil medium is depicted in Fig.6 and Fig.7 respectively. The total discretized system, consisting of the structure and the soil was then analyzed. This system was analyzed based on direct method of SSI by assuming the linear behaviour of building and foundation and nonlinear behaviour of underlying soil strata.

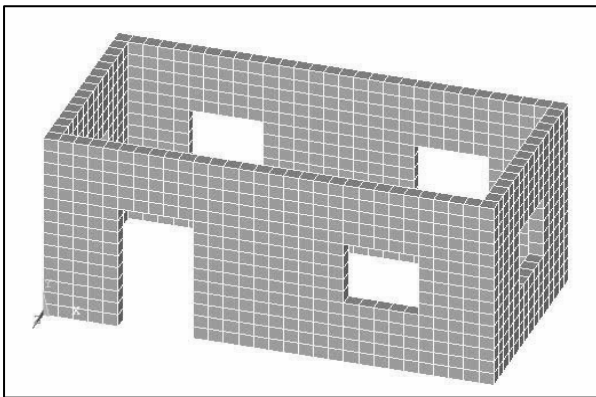


Fig.6. Finite element URM building

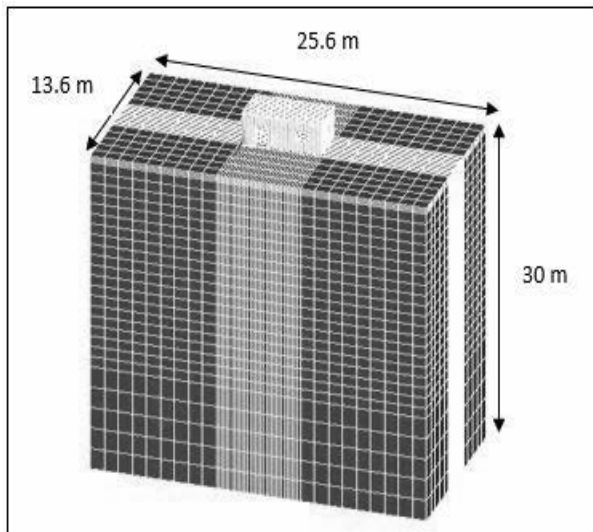


Fig.7. Finite element Soil-Structure system

4. GROUND MOTION

Time history analysis was conducted for URM buildings for Bhuj ground motion (2001). A part of the Bhuj ground motion acceleration recorded at Ahmedabad during earthquake which lasted over 135s is revealed in Fig.8 [18]. The peak ground acceleration is 0.11g at time

46.94s for Bhuj ground motion. The earthquake reached a magnitude of 7.7 M_w on the moment magnitude scale. The Fourier amplitude spectrum of Bhuj earthquake is revealed in Fig.9. Free vibration analysis is carried out to find the frequency and mode shapes of the U, UL, ULR and ULRC buildings with and without considering SSI. The responses such as storey deflection and base shear is also found out from the time history analysis considering their base fixity and base flexibility.

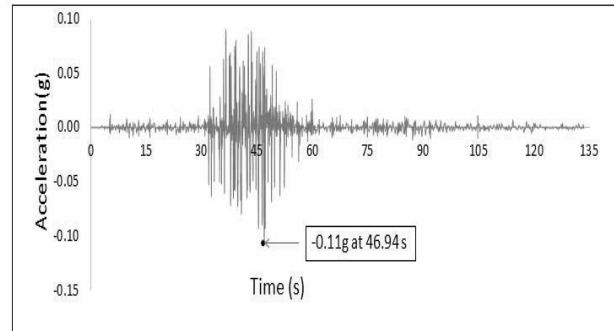


Fig.8. Acceleration time history of Bhuj earthquake [18]

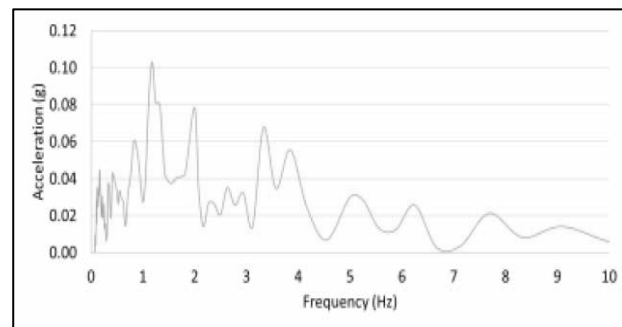


Fig.9. Fourier-amplitude spectrum Bhuj earthquake [18]

5. RESULTS AND DISCUSSIONS

All the four types of URM buildings were analysed to find their responses under Bhuj ground excitation. Frequencies were calculated. The absolute maximum responses such as deflection and base shear corresponding to fixed base buildings were evaluated.

Variation of Natural frequency

The natural frequency determined for URM building with and without the soil stratum is tabulated in Table 4. Fundamental natural frequency obtained from buildings with fixed base is higher than that obtained from SSI analysis. Increase in frequency of the buildings is due to the increase in stiffness of the building. Variation of fundamental frequency of building with flexible base from that of building with fixed base is more for U type building resting on soil type S and the maximum variation is about 47%.

Table 4. Comparison of natural frequency of building

	Fundamental Natural Frequency (Hz)			
	U	UL	ULR	ULRC
S	2.859	4.394	4.575	4.583
M	2.860	4.408	5.002	5.182
H	2.862	4.411	5.071	5.339
Fixed	4.950	6.904	11.058	12.397

Variation of deflection

The percentage variation of displacement of buildings with flexible base compared to fixed base is given in Table 5. The percentage variation of deflection for UL, ULR and ULRC buildings decreased by 43%, 95% and 96% respectively with respect to U building without considering the flexibility of soil strata. The percentage variation of deflection is 60% for U building supported on soft soil strata when compared with the same type of building with base fixed. The variation reduced to 40% and 20% for the same building supported on medium strata and rock respectively. The same is observed in UL, ULR and ULRC buildings. It is found that the deflection of the UL, ULR and ULRC building increases with decrease in stiffness of soil compared to U type building.

Table 5. Percentage variation in displacement

Designation	Displacement (Without SSI) (mm)	% variation of displacement (with SSI)		
		S	M	R
U	3.717	60.10	40.70	20.42
UL	2.109	78.97	73.37	40.25
ULR	0.160	96.47	93.31	87.40
ULRC	0.150	96.45	92.80	87.20

Variation of Base shear

Variation in base shear of low-rise buildings with flexible base is higher than buildings with fixed base. Table 6. displays percentage variation in the base shear of buildings. In the table given, there is an increase of 35% of base shear in ULRC type building than U type building. Therefore, base shear of a building with lintel band, roof slab and containment reinforcement are much higher than that of building without these. The building with more seismic weight has high base shear. Also, base shear got increased approximately about 94% for URM buildings due to the effect of SSI compared to masonry buildings without SSI.

Table 6. Variation in base shear of buildings

Designation	Base Shear (without SSI) (kN)	Variation of base shear of buildings (%)		
		S	M	R
U	179.98	87.78	92.17	93.49
UL	194.10	88.95	92.19	94.27
ULR	236.31	89.11	92.20	94.35
ULRC	243.06	89.75	93.57	94.85

6. CONCLUSIONS

The analysis of URM buildings considering the SSI effect is compared with buildings with fixed base. The major findings are shown below:

- (i) With lintel band, roof slab and containment reinforcement the deflection decreased by four times compared to building without it in mitigating seismic vulnerability in terms of deflection.
- (ii) The effect of SSI is significant while considering vertical containment reinforcement. The shear is increased by nine times and deflections increased by two times for buildings with vertical containment reinforcement than building without it when soft clayey sand stratum is account for.

REFERENCES

[1] Anthonie, A., Magonette, G. and Magenes, G., (1995) "Shear compression testing and analysis of brick masonry walls", *Proceedings of 10th European Conference on Earthquake Engineering, (Taylor and Francis)*, 657-1662

[2] Dolatshahi, K. M. and Aref, A. J., (2016) "Multi-directional response of unreinforced masonry walls: experimental and computational investigations", *Earthquake Engineering and Structural Dynamics, (Wiley Online Library)*, 45, 1427-1449

[3] Khanmohammadi, M., Behnamb, H. and Marefata, M. S., (2015) "Seismic behaviour prediction of flanged unreinforced masonry (FURM) walls", *Journal of Earthquake Engineering*, 18(5), 759-78

[4] Kalali, A. and Kabir, M. Z., (2012) "Cyclic behaviour of perforated masonry walls strengthened with glass fibre reinforced polymers." *Scientia Iranica, (Elsevier)*, 19(2), 151-65

[5] Singh, Y., Lang, D. H., Prasad, J. S. R. and Deoliya, R., (2013) "An analytical study on the seismic vulnerability of masonry buildings in India", *Journal of Earthquake Engineering*, 17, 399-422

- [6] Bruneau, M., (1994) "State-of-the-art report on seismic performance of unreinforced masonry buildings", *Journal of Structural Engineering, (ASCE)*, 120(1), 231-251
- [7] Unnikrishnan, S., Mattur, N. C., and Venkataramana, K., (2013) "Effect of containment reinforcement on the seismic response of box type laterite masonry structures – an analytical evaluation," *Earthquakes and Structures*, 5(1), 067-081
- [8] Jagadish, K. S., Raghunath, S. and Rao, N. K. S., (2002) "Shock table studies on masonry building model with containment reinforcement", *Journal of Structural Engineering*, 29(1), 09-17
- [9] <http://civil-online2010.blogspot.in/2010/02/earthquake-resistant-features-in-html> downloaded on 24/03/2018
- [10] Masia, M. J., Kleeman, P. W. and Melchers, R. E., (2004), "Modeling Soil of Structure Interaction for Masonry Structures." *Journal of Structural Engineering, ASCE*, 130, 641-649
- [11] Masia, M. J., Totoev, Y. Z., and Kleeman, P. W., (1999), "Modelling reactive soil movements for the study of cracking in masonry structures." *Proceedings of 16th Australian Conference on the Mechanics of Structures and Materials, Sydney, Australia*, 685–690
- [12] Saliba, J. E., Al-Akkad, R. S. and Sawaya, G. E., (1996), "Use of finite elements in masonry structures." *Masonry Society Journal*
- [13] Suyehiro, K., (1932) Engineering seismology notes on American lectures, *Proc. ASCE*, 58, 4, 1-110 (1932).
- [14] Dutta, S.C. and Roy, R. (2002). "A critical review on idealization and modelling for interaction among soil–foundation–structure system." *Computer and Structures*, 80, 1579-1594
- [15] Luigi, C., Sebastiano, R. and Giulia, M. B. V. (2013), "Soil–structure interaction for the seismic design of the Messina Strait Bridge", *Soil Dynamics and Earthquake Engineering, (Elsevier)*, 52, 103-115
- [16] Jisha, S. V., Jayalakshmi, B. R. and Shivashankar, R., (2015) "Response in piled raft foundation of tall chimneys under along-wind load incorporating flexibility of soil", *Frontiers of Structural and Civil Engineering, (Springer)*, 9(3), 307-322
- [17] Bowles, J. E., (1997) *Foundation analysis and design*, McGraw-Hill International Editions, Singapore.
- [18] <http://www.strongmotioncenter.org/vdc/scripts/event.plx?evt=785>
- [19] IS: 1893 (Part 1) :2016, Criteria for Earthquake Resistant Design of Structures, Bureau of Indian Standards, New Delhi, India
- [20] IS: 1080:1985, Code of Practice for Design and Construction of Shallow Foundation in Soils (other than raft, ring and shell), Bureau of Indian Standards, New Delhi, India

REJUVENATION OF AMANISHAH NALLAH – A CASE STUDY

N.K. HARANATH PINNAMARAJU¹, SHAIK MAHAMMAD JABEED², MOHAMMED.ARBAAZ PARVEZ³,

K. HARIHARANATH⁴

¹Senior Manager, TATA Projects Limited Hyderabad, haranathpnk@tataprojects.com

²Manager, TATA Projects Limited Hyderabad, shaikjabeed@tataprojects.com

³Deputy Manager, TATA Projects Limited Hyderabad, arbaazm@tataprojects.com

⁴Deputy General Manager, TATA Projects Limited Hyderabad, hariharanath@tataprojects.com

Keywords: Amanishah Nallah, Rejuvenation, Urban Safety.

1. INTRODUCTION

Dravyavati River which is now called as Amanishah Nallah is the major drainage system in the western outskirts of Jaipur City. It flows in a length of 47.5Km originating in the Amer Forest Nature Reserve and flow through the central part of Jaipur city and drains into Dhund River. It has the catchment area of 240 Sq.Km and maximum flood discharge of 1700 cumecs and the width of the river varies from minimum 50m to 300m. Due to adverse effect of urban Sprawl this river had been converted into Nallah which mainly undertakes drainages of rains from the catchment areas that includes banks and other branches, wastewater drainage and agricultural irrigation along the river. The Nallah being dry in most of the seasons, heavy encroachments have created a danger floods during Monsoons. The pollutants in the Amanishah Nallah are also rising causing health hazards and destroying the ecological system. This paper deals with, how we had transfigured Amanishah Nallah into a magnificent and attractive place to attract people and make Jaipur city clean and crowd pleaser.

2. KEY ISSUES

To rejuvenate back it into the cleaner, clearer, odorless flowing water which will be suitable for survival of aqua life and in creation of river front with better aesthetic surrounding, the following key issues should be resolved.

(1) Flood Problem: -

Amanishah Nallah is the main drainage channel in the city of Jaipur, which suffers from

- Serious water and soil erosion on the hills in Upstream area
- Illegal construction of building alongside the river occupying the river bed swathes.
- Growing of vegetables and commercial crop on the riverbed with polluted water.
- Unchecked use of the Banks and the Bed of the water channel as garbage dumps.

The above issues severely restrict the drainage capacity of river channel, making the area susceptible to floods, and thus threatening the safety of life and assets. Further, rapid urbanization increases hardened ground and reduces agricultural land which damages natural drainage mode. Moreover, in the rapid process of urbanization, the construction of drainage system in Jaipur now adding to the risks of floods. It has become

necessary to construct flood prevention system in accordance with design standards by undertaking river rehabilitation.

(2) Water pollution:

Presently, the areas adjoining Amanishah Nallah lack a sound wastewater management network. This wastewater is generated by the human habitation alongside the river, including hotels/commercial establishments. Industrialization process in the city and the surroundings impact and deteriorate the water seriously. Amanishah Nallah carries dirty stinking water, which fosters the growth of mosquitoes which is severe health and sanitary risks for the locals. In addition, the direct polluted water used for irrigation or infiltration of polluted water into the ground increases water pollution risks, leading to a potential health risk to agricultural products.

(3) Water resource:

Jaipur is facing serious water resource shortage. Being in semi-arid climate zone, Jaipur experiences an average annual rainfall of 650 mm, with 90% rainfalls during Jun.-Sep. The rains fail to supplement the ground water sufficiently. At the same time, water deterioration, shortage of water management infrastructure and rapid increase in population, aggravate this phenomenon. Therefore, we have to consider effective rainwater preservation/conservation measures to address the problem of water shortage. Further, the polluted water of the Nallah is being used for agriculture and thereby leading to health hazards with the production of toxic-infected food grains/vegetables.

(4) Ecology

Limited green spaces, disorderly constructions, encroachments and unauthorized industrialization along the Nallah have damaged the ecology. The water and soil erosion in the upstream is serious. Drainage of polluted water with domestic and industrial garbage is being dumped in Nallah. All of this has adversely affected the ecology along Amanishah Nallah which is does not complement the development plans of Jaipur.

(5) Value Creation and Economic Boost

Water is lifeline of any city's economic growth and development. Development of Amanishah Nallah will for sure add a significant factor to accelerate the business activities around some of the most valuable pockets of the Jaipur. While in current state Amanishah Nallah and its surrounding land have diminishing value due to adverse conditions. It is expected that this project will

give a significant fillip to the business activities around Nallah, starting with sky rocketing of the price of land holdings around Nallah. It is expected that this value enhancement will be multiple time of the proposed cost of the Nallah development work.

3. REJUVENATE OF NALLAH

To rejuvenate back it into its earlier form, construction of sewage treatment plant have been taken place at 5 different strategic Locations with advance treatment techniques like Sequential batch reactors, vortex grit chambers, turbo blowers etc. The present sewage that is being generated and joining the river is collected through underground pipes on the both banks. The collected sewage is taken to the sewage treatment plants totalling to 170MLD and the treated water is discharged into the river for the continual flow. After a proper examination of the flow and the length of the flow, Amanishah Nallah is dissect into 13 reaches

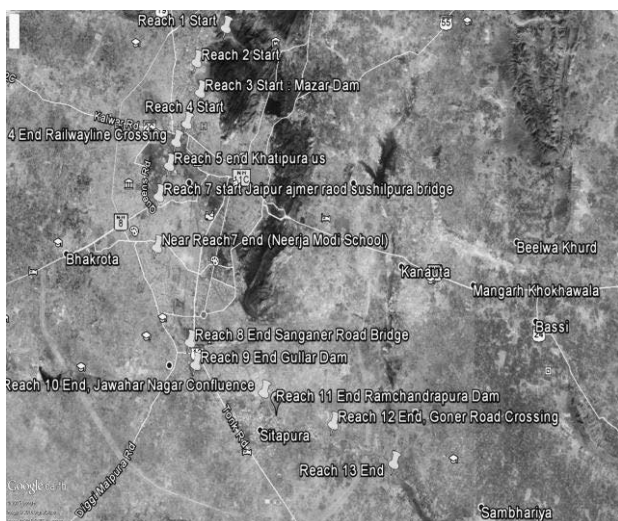


Figure 1: Maps Showing Amanishah Nallah Path (Source: Google Maps)

S.No	Reach	Reach Description	From (km)	To (km)	Length (km)
1	R1	Nahargarh Hill - Bhuteshwar Mahadev	0.00	2.80	2.80
2	R2	Bhuteshwar Mahadev-Mazar Dam	2.80	5.10	2.30
3	R3	Mazar Dam - Sikar Road Crossing	5.10	7.65	2.55
4	R4	Sikar Road Crossing-Jaipur jhotwara Railway line	7.65	9.60	1.95
5	R5	Jaipur jhotwara Railway line-N.B.C(Jaipur Khatipura road)	9.60	11.35	1.75
6	R6	N.B.C(Jaipur Khatipura road)-Ajmer Road	11.35	13.95	2.60
7	R7	Ajmer Road-Neerja Modi school crossing	13.95	17.65	3.70
8	R8	Neerja Modi school crossing-Sanganer Airport crossing	17.65	25.30	7.65
9	R9	Sanganer Airport crossing-Gullar Dam	25.30	26.55	1.25
10	R10	Gullar Dam-Confluence of Jawahar Nagar	26.55	32.75	6.20
11	R11	Confluence of Jawahar Nagar-Ramchandrapura Dam	32.75	34.80	2.05
12	R12	Ramchandrapura Dam-Goner Road Crossing	34.80	41.30	6.50
13	R13	Goner Road Crossing-End	41.30	47.50	6.20

Table 1: Showing Reach locations.



Figure 2: Present Photos

4. CONCLUSION

- The river rejuvenation has been designed to deliver value to the Pink city, Jaipur in multiple forms by Creating clean river front, recharging ground water, increasing green cover, creating community spaces, providing clean air to breath, adding beauty to the urban landscape.
- Increasing the economy by attracting tourists.
- As this project is one of its kind in India, Project experience center was built to understand the project profoundly

5. REFERENCES

- [1] CPHEEO Manual
- [2] Waste water engineering reference manual Latest Manual by Metcalfe and Eddy by McGraw hill
- [3] Water and waste water handbook of Degremont
- [4] Manual on Sewage and Sewage treatment, MoUD, CHPEEO and Jica – November 2013
- [5] Central Pollution Control Board (CPCB) Manual
- [6] CWC Manual on flood

**A STUDY ON THE ASSESSMENT OF DAMAGE LEVEL
 DURING LARGE SCALE EARTHQUAKE DISASTER USING KDB DATABASE**

**Yuma MORISAKI¹, Makoto FUJII², Junichi TAKAYAMA³, Kiyoko YANAGIHARA⁴, Tatsuya NISHINO⁵,
 Masahiko SAGAE⁶, and Kohei HIRAKO⁷**

¹ Bachelor(Eng.), Kanazawa University, Department of Environmental Design, Japan, yki20@stu.kanazawa-u.ac.jp

² Ph.D., Assistant Professor, Kanazawa University, Department of Geosciences and Civil Engineering, Japan, fujiu@se.kanazawa-u.ac.jp (corresponding author)

³ Dr., Eng., Professor, Kanazawa University, Department of Geosciences and Civil Engineering, Japan, takayama@se.kanazawa-u.ac.jp

⁴ Ph.D., Associate Professor, Kanazawa University, Department of Pharmaceutical and Health Sciences, Japan, kyana@mhs.mp.kanazawa-u.ac.jp

⁵ Ph.D., Associate Professor, Kanazawa University, Department of Geosciences and Civil Engineering, Japan, tan378@se.kanazawa-u.ac.jp

⁶ Ph.D., Professor, Kanazawa University, Department of Human and Social Science, Japan, sagae.masahiko@gmail.com

⁷ Bachelor., Project Assistant Professor, Kanazawa University, Organization of Frontier Science and Innovation, Japan, hirako@staff.kanazawa-u.ac.jp

Keywords: large scale earthquake disaster, damage assessment, KDB database vulnerability, vulnerable people

1. INTRODUCTION

In recent years, large-scale earthquake disaster such as The 2011 off the Pacific coast of Tohoku Earthquake and The 2016 Kumamoto Earthquake frequently occur in Japan. An earthquake with magnitude 6.7 and maximum seismic intensity (JMA) 7 occurred in middle eastern part of the iburi district of Hokkaido on September 6th, 2018, at 03:07(JST) [1]. This earthquake was named Hokkaido earthquake, 2018. As of 13:30 on September 13th, 2018, the number of dead and serious injury were 41 and 9[1]. The issue during large scale earthquake is respond to vulnerable people. They need care after earthquake disaster, such as rescue and evacuation. Specifically, aged person, injured person, pregnant person, infants and foreigner are considered vulnerable people. In Japan, establishing a support system for vulnerable people for large scale disaster is an urgent problem.

In order to achieve the establishment of support system for vulnerable people, it is important to examine the degree of weakness (Vulnerability) to the disaster. A lot of studies are being conducted about examination of vulnerability [2], [3], [4], [5]. Fujii et al [6] examined a comprehensive index on the vulnerability of the area integrating vulnerability of people and structures. In addition, Evaluation of disaster was conducted using the following equation (1) which is generally known as being able to examine quantitatively the disaster situation.

$$D = H \cdot V \tag{1}$$

D: Disaster
H: Hazard
V: Vulnerability

It is generally impossible to control the external force (Hazard) of disaster, and it is necessary to examine and control vulnerability in order to minimize disaster.

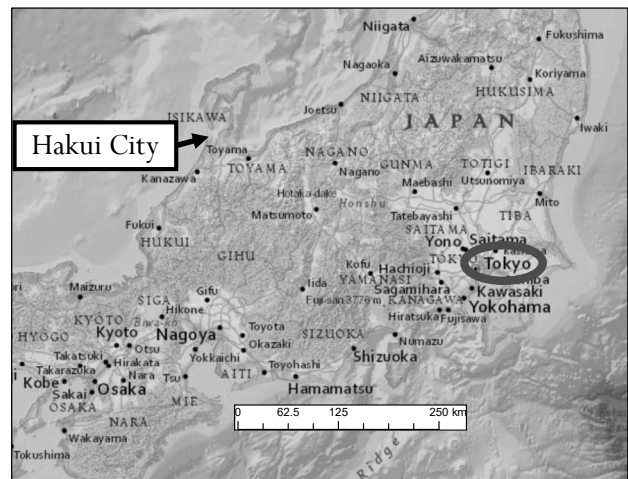


Figure.1 Location of Hakui-City, Ishikawa Prefecture

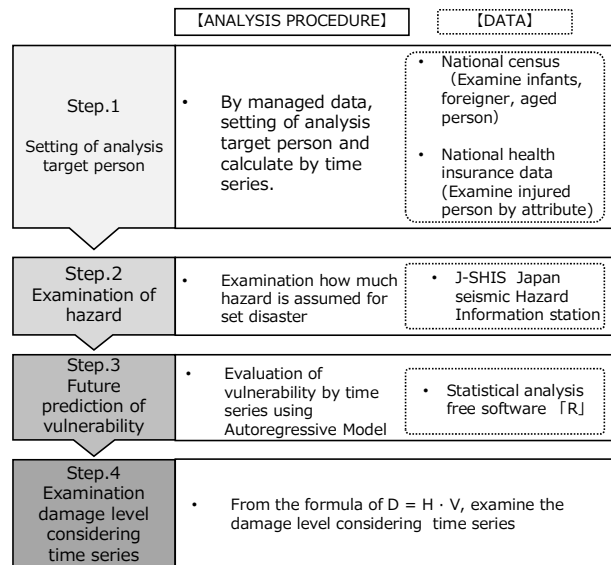


Figure.2 Analysis procedure of this study

Table.1 Example of KDB data

氏名	性別	年齢	生年月日	住所	住所	直近月レセプトの決定点数	糖尿病	インスリン	糖尿病性網膜病変	糖尿病性腎臓病	糖尿病性神経障害	糖尿病性高血圧症	高尿酸血症	虚血性心臓病	脳血管疾患	個人番号
						164.273										7747
						95.073										7747
						2.670										7747
						50.380	●	●	●	●		●			●	853
						39.084						●				7764
						96.090	●				●	●		●	●	1434
						65.183	●					●		●	●	1435
						49.493	●					●		●	●	735
						43.096	●	●				●		●	●	735
						2.956	●					●		●	●	726

Human vulnerability and physical vulnerability are mainly considered as vulnerability. As mentioned above, recent disasters, vulnerable people suffered huge damage. Therefore, the purpose of this study is to examine the human vulnerability and to estimate the future of human vulnerability considering large-scale earthquake disaster. By estimating human vulnerability, it is possible to simultaneously estimate the disaster situation, and it is also possible to examine detailed disaster situation considering time series data.

2. ANALYSIS PROCEDURE OF THIS STUDY

First, Hakui-City, Ishikawa Prefecture was set analysis field in this study. Hakui-City is a small city facing the Sea of Japan. Fig.1 shows location of Hakui-City, Ishikawa Prefecture. The analysis procedure of this study is as shown in Fig.2. Vulnerable people area examine using data on “population”. As mentioned above, aged person, injured person, pregnant, infants, and foreigner are considered vulnerable people. In this study, aged person, injured person, infants and foreigner is examined using national census. This census is large-scale survey focused according to attribution. In addition, this census is conducted every 5years. Injured person is examined using national health insurance data (KDB data). As shown in Table.1, KDB data can be comprehensively examined injured person. Those who have chronic renal failure, brain disease and cardiac disease are included as vulnerable people. By using national census, it is impossible to examine detailed injured person. However, by using national health insurance data, injured person can be examined. Both data have huge amount of information. National census is conducted every 5years from 1920, and national health insurance data has information since 2013 every 1 month. Therefore, using both data, vulnerable people can be examined considering time series data. Then, regarding degree of earthquake disaster (Hazard) by analysis target field, J-SHIS (Japan Seismic Hazard Information Station) is used. After that, future human vulnerability is estimated using Autoregressive Model. By evaluating future human vulnerability considering aged person, infants, injured person and foreigner using Autoregressive model, it is simultaneously possible to estimate future degree of disaster.

3. CONCLUSIONS AND FUTURE WORKS

This study is to estimated future human vulnerability of large-scale disasters by using census and national health insurance data in time series. As a future work of this

study, after evaluating future human vulnerability, we quantify the resilience having the opposite meaning to the human "vulnerability". After that, we would like to evaluate the region from two points of vulnerability and resilience. Moreover, Questionnaire survey is conducted to collect qualitative data for evaluation of resilience and future vulnerability.

REFERENCES

[1] Ministry of Land, Infrastructure and Transport, JMA, “https://www.jma.go.jp/jma/menu/20180906_iburi_jishin_menu.html”
 [2] Kunihiko AMAKUNI, Takahisa ENOMOTO, and Toshio MOCHIZUKI, (1999) “Research on Evaluation Methods for Vulnerability and Defense against Earthquake Disaster —A Case Study of Aomori Prefecture—” *Journal of social safety science*, Vol.1, pp.179–188
 [3] Zi YANG, Keiko INAGAKI, Satoshi YOSHIDA, and Satoru SADOHARA, (2015) “Regional Characteristics Analysis from the View of Community- Based Disaster Risk Management for People with Functional Needs in Times of Disaster” *Journal of social safety science*, Vol.27, pp.145–154
 [4] Makoto KOSUGI, Kenshi BABA, and Mitsuru TANAKA, (2017) “Resilience Index of Regional Communities to the Risks of Disasters—Comparison of Eight Regions through Questionnaire Survey Data—” *Environmental science*, Vol.30, No. 3, pp.225–237
 [5] Miwa ABE, Arinori YOSANO, (2013) “Social Vulnerability Analysis of Households in Kita ward, Osaka: Elucidating the Relationship between Residence Height and Elderly Demographics”
 http://hdl.handle.e.net/10112/7748
 [6] Makoto FUJII, Yuma MORISAKI, Junichi TAKAYAMA, Kiyoko YANAGIHARA, Tatsuya NISHINO, Masahiko SAGAE, Kohei HIRAKO, (2018) “Evaluation of Regional Vulnerability to Disasters by People of Ishikawa, Japan: A cross Sectional Study Using National Health Insurance Data” *Int. J. Environ. Res. Public Health*, Vol.15, No. 3, 507